

INFORMATION TO USERS

This manuscript has been reproduced from the microfilm master. UMI films the text directly from the original or copy submitted. Thus, some thesis and dissertation copies are in typewriter face, while others may be from any type of computer printer.

The quality of this reproduction is dependent upon the quality of the copy submitted. Broken or indistinct print, colored or poor quality illustrations and photographs, print bleedthrough, substandard margins, and improper alignment can adversely affect reproduction.

In the unlikely event that the author did not send UMI a complete manuscript and there are missing pages, these will be noted. Also, if unauthorized copyright material had to be removed, a note will indicate the deletion.

Oversize materials (e.g., maps, drawings, charts) are reproduced by sectioning the original, beginning at the upper left-hand corner and continuing from left to right in equal sections with small overlaps.

Photographs included in the original manuscript have been reproduced xerographically in this copy. Higher quality 6" x 9" black and white photographic prints are available for any photographs or illustrations appearing in this copy for an additional charge. Contact UMI directly to order.

**Bell & Howell Information and Learning
300 North Zeeb Road, Ann Arbor, MI 48106-1346 USA
800-521-0600**

UMI[®]

**Analysis, Detection and Early Warning Control of Dynamic Rollover
of Heavy Freight Vehicles**

Peijun Liu

A Thesis

in

The Department

of

Mechanical Engineering

Presented in Partial Fulfillment of the Requirements
for the Degree of Doctor of Philosophy at
Concordia University
Montreal, Quebec, Canada

January 1999

© Peijun Liu, 1999



National Library
of Canada

Acquisitions and
Bibliographic Services

395 Wellington Street
Ottawa ON K1A 0N4
Canada

Bibliothèque nationale
du Canada

Acquisitions et
services bibliographiques

395, rue Wellington
Ottawa ON K1A 0N4
Canada

Your file Votre référence

Our file Notre référence

The author has granted a non-exclusive licence allowing the National Library of Canada to reproduce, loan, distribute or sell copies of this thesis in microform, paper or electronic formats.

The author retains ownership of the copyright in this thesis. Neither the thesis nor substantial extracts from it may be printed or otherwise reproduced without the author's permission.

L'auteur a accordé une licence non exclusive permettant à la Bibliothèque nationale du Canada de reproduire, prêter, distribuer ou vendre des copies de cette thèse sous la forme de microfiche/film, de reproduction sur papier ou sur format électronique.

L'auteur conserve la propriété du droit d'auteur qui protège cette thèse. Ni la thèse ni des extraits substantiels de celle-ci ne doivent être imprimés ou autrement reproduits sans son autorisation.

0-612-43566-0

Canada

ABSTRACT

Analysis, Detection and Early Warning Control of Dynamic Rollover of Heavy Freight Vehicles

Peijun Liu, Ph.D.
Concordia University, 1999

The conceptual design of the early warning based roll instability enhancement system is realized through systematic investigations on static and dynamic roll behavior of the vehicles, identification of indicators for the onset of instability, and reliability analysis. The relative and absolute roll instability criteria are initially derived from the rollover mechanics of different heavy vehicle combinations. The relative roll instability conditions are evaluated under steady cornering maneuvers through development and analysis of static roll plane models. The sensitivity of the static rollover threshold (*SRT*) measure to variations in design and operating factors of the vehicle and suspension configurations is evaluated and the conditions of relative rollover for different vehicle configurations are identified. A constant velocity three-dimensional model is derived for relative roll instability analysis of articulated vehicles under dynamic directional maneuvers. Dynamic rollover threshold of articulated heavy vehicles is proposed on the basis of effective lateral acceleration (*ELA*) and relative rollover criterion. The absolute roll instability of heavy vehicles is further investigated using energy approach to derive the absolute rollover limits. A number of potential rollover indicators are identified and evaluated for a five-axle tractor semi-trailer combination using the constant velocity three-dimensional vehicle model in terms of their reliability and early warning capability for driver's actions.

The effectiveness of proposed indicators for the open-loop roll stability enhancement is investigated through development and analysis of a comprehensive vehicle model, incorporating braking dynamics. Time delays due to driver's reaction and the transportation lag of the braking system are characterized by a variable referred to as reaction delay. The rollover indicators are investigated for their effectiveness for open-loop roll stability control in various cornering and evasive maneuvers, road conditions, braking efforts, and reaction delays. The study revealed that the *RSF* is the most reliable indicator, irrespective of the vehicle configurations, while its measurability is relatively poor. The indicators based upon lateral acceleration, sprung and unsprung mass roll angles and steering velocity factor yield good correlation with *RSF*, but exhibit certain sensitivity to variations in design and operating factors.

ACKNOWLEDGEMENTS

The author wishes to express his sincere appreciation to his thesis supervisors, Dr. S. Rakheja and Dr. A.K.W. Ahmed, for initiating the study topic and providing continued guidance throughout the course of this investigation.

Thanks are due to the colleagues, faculty and staff at Mechanical Engineering Department, CONCAVE research center of Concordia University, for their contributions to this effort.

The financial support provided by the F.C.A.R doctoral scholarship funded by the Quebec Government, Canada, is gratefully acknowledged.

Finally, the author would like to express his special thanks to his wife and members of his family, for their encouragement.

TABLE OF CONTENTS

	<u>Page</u>
LIST OF FIGURES	x
LIST OF TABLES	xv
NOMENCLATURE	xviii
CHAPTER 1 LITERATURE REVIEW AND SCOPE OF THE DISSERTATION	1
1.1 Introduction	1
1.2 Review of Relevant Literature	4
1.2.1 Directional Dynamic Models	4
1.2.2 Roll Stability Analysis	10
1.2.3 Directional Stability Analysis	15
1.2.4 Detection and Control of Directional and Roll Instabilities	20
1.3 Scope and Objectives of the Dissertation	27
1.3.1 Objectives of the Dissertation	28
1.3.2 Organization of the Dissertation	29
CHAPTER 2 ROLL INSTABILITY CRITERIA AND MEASURES	32
2.1 Introduction	32
2.2 Classifications of Heavy Vehicles	33
2.3 Mechanics of Vehicle Rollover	36
2.3.1 Single Axle Representation	36
2.3.2 Multi-Axle Representation	43
2.4 Criteria for Heavy Vehicle Rollover	46
2.4.1 Definition of Roll Instability	46
2.4.2 Measures Based upon Relative Rollover Criterion	47
2.4.3 Measures Based upon Absolute Rollover Criterion	53
2.5 Summary	56

TABLE OF CONTENTS (Continued)

CHAPTER 3	DETECTION OF RELATIVE ROLL INSTABILITY IN STEADY TURNING MANEUVERS	58
3.1	Introduction	58
3.2	Development of Roll Plane Models of Different Combinations	59
3.2.1	Roll Plane Analysis of Straight Trucks and Full Trailers	60
3.2.2	Roll Plane Analysis of Tractor Semi-Trailer, B- and C-Train Doubles	70
3.2.3	Roll Plane Analysis of A-Train Doubles	82
3.3	Relative Rollover Conditions of Different Vehicle Combinations	83
3.3.1	Straight Trucks or Full Trailers	83
3.3.2	Tractor Semi-Trailer Combinations	86
3.3.3	B- and C-Train Doubles	96
3.3.4	A-Train Doubles	97
3.3.5	Roll Safety Factor	100
3.4	Summary	101
CHAPTER 4	DYNAMIC RELATIVE AND ABSOLUTE ROLL INSTABILITY ANALYSIS	103
4.1	Introduction	103
4.2	Development of a Constant Velocity Yaw/Roll Model	104
4.2.1	Equations of Motion	105
4.2.2	Suspension and Tire Forces	109
4.2.3	Constraint Equations	111
4.3	Dynamic Rollover Threshold of Articulated Freight Vehicles	114
4.3.1	Definition of Dynamic Rollover Threshold	114
4.3.2	Analysis of Dynamic Threshold of Articulated Freight Vehicles	117
4.3.3	Dynamic Rollover Initialization	128
4.4	Analysis of Absolute Rollover	134
4.4.1	Development of Absolute Rollover Vehicle Model	140
4.4.2	Modeling of Suspension Springs	146
4.5	Model Validation	149
4.6	Absolute Rollover Threshold	154
4.6.1	Absolute Roll Instability Indicators	154
4.6.2	Analysis of Absolute Rollover Threshold	156

TABLE OF CONTENTS (Continued)

4.7	Summary	161
CHAPTER 5	ANALYSIS OF IMPENDING ROLLOVER INDICATORS FOR OPEN-LOOP ROLLOVER CONTROL	162
5.1	Introduction	163
5.2	Identification of Potential Rollover Indicators	165
5.3	Measurability Analysis	170
5.4	Reliability Analysis	173
5.4.1	Estimation Error Analysis	173
5.4.2	Correlation Analysis with RSF	177
5.5	Early Warning Evaluation of Rollover Indicators	186
5.6	Feasibility of Rollover Early Warning Device	188
5.7	Summary	190
CHAPTER 6	EFFECTIVENESS ANALYSIS OF IMPENDING ROLLOVER INDICATORS FOR OPEN-LOOP ROLLOVER CONTROL	192
6.1	Introduction	192
6.2	Three - Dimensional Vehicle Model	194
6.2.1	Equations of Motion	195
6.2.2	Suspension Forces	197
6.2.3	Modeling of Tires	198
6.2.4	Steering System	208
6.3	Description of Input Variables	211
6.3.1	Time Delay due to Driver and Braking System	212
6.3.2	Vehicle Maneuvers	214
6.3.3	Road Adhesion Limit and Braking Intensity	218
6.4	Rollover Metric	220
6.5	Rollover Warning Threshold of Various Indicators	221
6.5.1	Rollover Warning Threshold in Cornering Maneuvers	223
6.5.2	Rollover Warning Threshold in Lane Change Maneuvers	228
6.5.3	Influence of Road Adhesion Limit and Braking Intensity on Open-Loop Rollover Control	237

TABLE OF CONTENTS (Continued)

6.6	Summary	243
CHAPTER 7 CONCLUSIONS AND RECOMMENDATIONS		245
7.1	Highlights of the Investigation	245
7.1.1	Development of Relative and Absolute Roll Instability Criteria	245
7.1.2	Development of Relative Rollover Condition and Roll Safety Factor	246
7.1.3	Dynamic Rollover Threshold Analysis	247
7.1.4	Development of Roll Plane Model for Absolute Rollover Analysis	248
7.1.5	Analysis of Potential Rollover Indicators	249
7.1.6	Feasibility Analysis of Open-Loop Rollover Control	250
7.2	Conclusions	251
7.3	Recommendations for Future Work	255
REFERENCES		259

LIST OF FIGURES

<u>Figure</u>	<u>Page</u>
2.1 Schematics of single drawbar A-dolly and double draw-bar C-dolly	34
2.2 Schematics of seven generic families of heavy freight vehicles	38
2.3 Lumped roll plane representation of a heavy vehicle before wheel lift-off	40
2.4 Lumped roll plane representation of the vehicle after the loss of wheel-road contact	41
2.5 Vehicle lateral acceleration and roll angle relationship during the course of rollover	42
2.6 Three composite axle representation of a multi-axle tractor semi-trailer vehicle	44
2.7 Roll moments versus roll angle for the three composite axle vehicle	44
2.8 Net roll moment versus roll angle for the three-axle vehicle representation	45
2.9 Path trajectory of a vehicle during a path change maneuver to assess <i>LRT</i>	49
3.1 Roll plane model of straight trucks or full trailers represented by two-composite-axle vehicles	62
3.2 Roll performance signature of a straight truck	68
3.3 Three-axle representation for the tractor semi-trailer combinations	70
3.4 Idealized representation of the tractor frame and the fifth wheel compliance	71
3.5 Static roll plane model of heavy vehicles	72
3.6 Four-axle representation for B-train or C-train doubles	73
3.7 Two independent roll units of an A-double	82
3.8 Lateral acceleration a_y - <i>LTR</i> signature of a P & D truck	84

LIST OF FIGURES (Continued)

3.9	Effect of total roll stiffness ratio on static rollover threshold and lift-off sequence	87
3.10	Effect of front/rear roll stiffness ratio on static rollover threshold and lift-off sequence	87
3.11	Force-displacement characteristics of suspension springs	89
3.12	Roll performance signature of a tractor semi-trailer combination	90
3.13	Roll performance signature of a tractor semi-trailer combination with reduced suspension rates on tractor rear and trailer axles	90
3.14	Force-deflection characteristics of different suspension springs	95
3.15	Roll performance signature of a B-train double	100
4.1	Axle system of the yaw/roll plane model	105
4.2	Representation of the conventional fifth wheel connection	113
4.3	Illustration of roll destabilizing moments	115
4.4	Cornering force properties of radial tires as a function of load and side-slip angle	120
4.5	Aligning torque property of radial tires as a function of load and side-slip angle	120
4.6	Lateral acceleration response and <i>RSF</i> of an articulated vehicle subject to two different maneuvers	122
4.7	Schematic of an eight-axle A-train double	126
4.8	The ratio of dynamic rollover threshold to static rollover threshold of a typical A-train double	128
4.9	Composite axle load transfer ratio of a five-axle tractor semi-trailer during a sinusoidal steering maneuver	130
4.10	Peak axle load transfer of a tractor semi-trailer as a function of vehicle forward speed	131

LIST OF FIGURES (Continued)

4.11	Axle load transfer characteristics of an A-train double in a 0.33 Hz sinusoidal steering maneuver	133
4.12	Groping of axles of different vehicle configurations for the development of roll plane models	136
4.13	Roll plane model of the vehicle prior to loss of tire-road contact	137
4.14	Roll plane model after the loss of tire-road contact	137
4.15	Typical tapered-leaf spring envelope with hysteresis loops	146
4.16	Simulation of a leaf spring property using numerical iteration	149
4.17	Comparison of the trailer lateral acceleration response of the roll plane model with that derived from the yaw/roll model	152
4.18	Comparison of load transfer ratio derived from the roll plane and the yaw/roll models	153
4.19	Dynamic rollover indicators in a rollover directional maneuver	158
4.20	Dynamic rollover indicators in a non-rollover directional maneuver	159
4.21	Prediction of the dynamic rollover limits using the <i>CDR</i> and <i>RPERF</i>	159
5.1	The relationship between the lateral acceleration response and the roll safety factor during different dynamic maneuvers	180
5.2	The relationship between the sprung mass roll responses and the roll safety factor	180
5.3	The relationship between the 5th axle roll angle, the steering velocity factor and the roll safety factor	181
5.4	Effects of semi-trailer c.g. height on rollover threshold of a_{y1} , a_{y2} and SVF	183
5.5	Effects of semi-trailer c.g. height on rollover threshold of φ_{u4} , φ_{u5} and φ_{s2} .	183
5.6	Effects of payload variation on rollover threshold of a_{y1} , a_{y2} and SVF	184

LIST OF FIGURES (Continued)

5.7	Effects of payload variation on rollover threshold of φ_{u4} , φ_{u5} and φ_{s2} .	184
5.8	Effects of different maneuvers on rollover threshold of a_{y1} , a_{y2} and SVF	185
5.9	Effects of different maneuvers on rollover threshold of φ_{u4} , φ_{u5} and φ_{s2} .	185
5.10	Rollover indicators in the time domain during a sinusoidal steering maneuver	187
6.1	Schematic diagram of an open-loop rollover control	192
6.2	Schematic of <i>DOF</i> of a tractor semi-trailer combination	197
6.3	A schematic representation of tire forces and moments at the contact patch	200
6.4	Magic formula simulation of longitudinal force of a truck tire as a function of slip ratio for five different loads	205
6.5	Magic formula simulation of lateral force of a truck tire as a function of slip ratio for five different loads	206
6.6	Magic formula simulation of aligning torque of a truck tire as a function of slip ratio for five different loads	206
6.7	Steering system model of heavy vehicles	209
6.8	A Schematic diagram of the elapsed time in braking sequence	213
6.9	Ramp steering inputs for cornering maneuvers	215
6.10	Definition of path trajectory for cornering maneuvers	216
6.11	Radius of path trajectories with different rates of path radius reduction	216
6.12	Schematic of typical single lane change maneuvers	217
6.13	Rollover warning given at different percentages of RSF^0	226

LIST OF FIGURES (Continued)

6.14	Relationship between RSF , a_{y1} , φ_{u1} and φ_{u5}	227
6.15	Relationship between RSF , a_{y2} , and φ_{u2}	227
6.16	Time history of lateral acceleration response of an articulated vehicle during a lane change maneuver	233
6.17	Time history of RSF amplification of an articulated vehicle during a lane change maneuver	233
6.18	RSF amplification factor during sinusoidal steer maneuvers	234
6.19	RSF amplification factor during a single lane change maneuver	234
6.20	Tractor lateral acceleration amplification during sinusoidal maneuvers	235
6.21	Semi-trailer lateral acceleration amplification during sinusoidal maneuvers	235
6.22	Tractor lateral acceleration amplification factor during a single lane change maneuver	236
6.23	Semi-trailer lateral acceleration amplification factor during a single lane change maneuver	236
6.24	Braking pressure on the left side wheels at 100% braking effort	239
6.25	Braking pressure on the right side wheels at 100% braking effort	240
6.26	Braking pressure on the left side wheels at 50% braking effort	240
6.27	Braking pressure on the right side wheels at 50% braking effort	241
6.28	Changes of vehicle forward speed during braking at different braking efforts	241
6.29	RSF signature at different braking efforts	242
6.30	Influence of braking on road-wheel steer angles	242
7.1	Flow chart of rollover warning based on monitoring of tire longitudinal slip ratio	258

LIST OF TABLES

<u>Table</u>	<u>Page</u>
2.1 Heavy vehicle units and coupling mechanisms	34
2.2 Generic families of heavy vehicles	36
2.3 Distribution of accidents involving heavy vehicles in Western Canada	39
3.1 Simulation parameters for a straight truck configuration	67
3.2 Conditions of relative rollover of straight truck or full trailer configurations	69
3.3 Simulation parameters for a pickup and delivery truck	84
3.4 Vehicle configurations with different roll stiffness distribution	85
3.5 Simulation parameters for a tractor semi-trailer combination	89
3.6 Parametric study: effects of auxiliary roll stiffness and roll compliance	92
3.7 Parametric study: effects of vehicle design and operating parameters	93
3.8 Parametric study: effects of tire elastic properties	94
3.9 Roll center and auxiliary roll stiffness of different suspension configurations	95
3.10 Parametric study: effects of different combinations of suspension springs	96
3.11 Simulation parameters for a B-train double	98
3.12 Parametric study on static rollover threshold and relative rollover condition of a B-train double	99
4.1 Simulation Parameters of the baseline 5-axle tractor semi-trailer	119
4.2 Range of variations in the design and operating factors of a tractor-semi trailer	119
4.3 Tractor rollover limits and rearward amplification factors of a tractor-semitrailer combination	124

LIST OF TABLES (Continued)

4.4	Dynamic and static rollover threshold values of a tractor-semitrailer at c.g. height of 1.78 m	125
4.5	Dynamic and static rollover threshold values of a tractor-semitrailer at c.g. height of 2.065 m	125
4.6	Rollover signature of a typical A-train double combination	127
4.7	Wheels lift-off sequence of a tractor semitrailer with different combinations of suspensions: trailer c.g. height 1.78m	131
4.8	Wheels lift-off sequence of a tractor semi-trailer with different combinations of suspensions: trailer c.g. height 2.06m	132
4.9	Wheels lift-off sequence of an A-train double with variations in c.g. height and steering frequency	134
4.10	Simulation parameters of a 5-axle tractor-semitrailer combination	151
4.11	Simulation parameters of a straight truck	160
4.12	Dynamic rollover threshold of the vehicle at different excitation frequencies	161
5.1	Potential rollover indicators of different vehicle combinations	169
5.2	Measurability of different rollover indicators	172
5.3	Classification of rollover indicators in terms of dependent parameters	174
5.4	Reliability analysis results in terms of estimation errors	176
5.5	Specifications of simulation vehicles and rollover indicators	179
5.6	Nominal simulation parameters of the baseline 5-axle tractor semi-trailer	179
5.7	Correlation coefficient and time delay between <i>RSF</i> and various rollover indicators	188
5.8	Proposal of a rollover early warning device	190
6.1	Simulation parameters for a 5-axle tractor semi-trailer combination	219
6.2	Static rollover limits in terms of different indicators	222

LIST OF TABLES (Continued)

6.3	Assessment of open-loop control in ramp steer maneuvers ($\mu = 0.8$, braking pressure: 700 kpa)	225
6.4	Open-loop rollover control on spiral paths with constant radius reduction rate ($\mu = 0.8$)	228
6.5	Amplification factors of various rollover indicators in sinusoidal steer and lane change maneuvers	232
6.6	Minimum warning threshold for different road friction and braking efforts	239

NOMENCLATURE

Symbol	Description
a :	distance between the front axle and sprung mass cg
a_{vi} :	lateral acceleration of sprung mass i
a_{uj} :	lateral acceleration of unsprung mass j
a_y :	vehicle lateral acceleration
A_i :	dual tire spacing of tires on axle i
A_{s1} :	peak lateral acceleration of lead unit
A_{s2} :	peak lateral acceleration of last unit
ART :	absolute rollover threshold
h_i :	vertical distance between i^{th} sprung mass c.g. to the top attachment point of the suspension spring
B_i ($i=x, y, z$):	stiffness factor in tire magic formula
c_u :	damping coefficient per tire on axle i
C_i ($i=x, y, z$):	shape factor in tire magic formula
C_{sw} :	compliance due to steering column
C_{tr} :	compliance due to tie-rod arm
CDR :	critical distance ratio
CSV :	critical sliding velocity
D_i ($i=x, y, z$):	peak value in tire magic formula
DRT :	dynamic rollover threshold
E_i ($i=x, y, z$):	curvature factor in tire magic formula
ELA :	effective lateral acceleration
F_c :	suspension coulomb friction force
F_{Ei} :	suspension envelop force at integration step i
F_x :	tire longitudinal force at combined cornering and braking

NOMENCLATURE (Continued)

F_{x0} :	tire longitudinal force at pure longitudinal slip
F_y :	tire lateral force at combined cornering and braking
F_{y0} :	tire lateral force at pure side slip
F_{zj} :	load on wheel j of axle i
FL, FR :	tire vertical load on the left and right tracks, respectively
FL_i, FR_i :	tire vertical load on the left and right sides of axle i
g :	acceleration due to gravity
G_{A1} :	tractor lateral acceleration amplification factor
G_{A2} :	semi-trailer lateral acceleration amplification factor
G_R :	gear ratio in the steering system
G_{RSF} :	<i>RSF</i> amplification factor
$G_{\phi 1}$:	tractor roll angle amplification factor
$G_{\phi 2}$:	semi-trailer roll angle amplification factor
$G_{\phi 5}$:	last axle roll angle amplification factor
h :	vehicle c.g. height above ground
h_{ci} :	roll center height of axle suspension i above the ground
h_s :	sprung mass c.g. height about the ground
h_{ui} :	cg height of unsprung mass i
h_R :	cg height of sprung mass from its roll center
h_s :	cg height of sprung mass from the ground
h_{si} :	cg height of sprung mass i from the ground
H_{ui} :	c.g. height of unsprung mass i
I_w :	polar moment of inertia of a spinning wheel
I_{xx} :	roll mass moment of inertia of a vehicle about its mass center

NOMENCLATURE (Continued)

I_{xx_u} :	roll mass moment of inertia of sprung mass i
I_{xx_u} :	roll mass moment of inertia of unsprung mass j
I_{xx0} :	roll mass moment of inertia of a vehicle about tire-road contact patch
I_{yy_u} :	pitch mass moment of inertial of sprung mass i
I_{zz_u} :	yaw mass moment of inertial of sprung mass i
k_t :	tire vertical stiffness
k_{ti} :	vertical stiffness of a tire on axle i
K_{ai} :	auxiliary roll stiffness of axle i
K_{ij} :	linear equivalent suspension spring constant on axle i and side j ($j=1, 2$)
K_u :	understeer coefficient of the vehicle
K_{ϕ} :	roll stiffness of axle suspension i
KF_1 :	torsional stiffness of tractor frame
KF_2 :	torsional stiffness due to compliance of fifth wheel and trailer structure
KF_3 :	torsional stiffness due to compliance of B- or C- dolly
KOT_{ij} :	overturning stiffness of tire i ($i=1, \dots, 4$) on axle j
KT_{ij} :	vertical stiffness of tire i ($i=1, \dots, 4$) on axle j
KYT_{ij} :	lateral stiffness of tire i ($i=1, \dots, 4$) on axle j
L :	wheelbase
L_g :	gate length to characterize lane change maneuvers
L_{MT} :	tire mechanical trail
L_r :	tire relaxation length
LTR :	lateral load transfer ratio
LTR_i :	load transfer ratio on axle i
m :	total vehicle mass

NOMENCLATURE (Continued)

m_s :	sprung mass
$m_{s,i}$:	sprung mass i
m_u :	unsprung mass i
M_{ybk} :	braking torque applied to a road wheel
M_z :	tire aligning moment in combined cornering and braking
$M_{z\theta}$:	tire aligning moment at pure side slip
n_s :	number of sprung masses in a complete roll unit
n_u :	number of unsprung masses in a complete roll unit
p_i :	suspension roll center displacement, perpendicular to axle i
p_{si} :	roll velocity of sprung mass i
p_{uj} :	roll velocity of unsprung mass j
P :	instantaneous braking pressure in the air chamber
P_0 :	air supply pressure in a air braking system
q_1, q_2 :	longitudinal cg location factor of sprung mass
q_{si} :	pitch velocity of sprung mass i
r_{si} :	yaw velocity of sprung mass i
R :	path radius
${}^{II}_{JJ}R$:	transformation matrix from coordinate system $JJ (X_{JJ} - Y_{JJ} - Z_{JJ})$ to coordinate system $II (X_{II} - Y_{II} - Z_{II})$
R_w, R_{wi} :	wheel radius on axle i
R_{bump} :	bump-steer coefficient
R_{roll} :	roll-steer coefficient
R_{wrap} :	wrap-steer coefficient
RAR :	rearward amplification ratio
$RPER$:	rollover prevention energy reserve

NOMENCLATURE (Continued)

$RPERF$:	rollover prevention energy reserve factor
RPM :	Rollover Prevention Metric
RSF :	roll safety factor
s_i :	half suspension spacing on axle i
$sign()$:	sign function
S_{hu} ($i=x, y, z$):	horizontal shift of tire forces and moments curves
S_{vu} ($i=x, y, z$):	vertical shift of tire forces and moments curves
SRT :	static rollover threshold
SSF :	static stability factor
SVF :	steer velocity factor
T :	half wheel track
T_{ci} :	distance between c.g. and roll center of unsprung mass i after wheel lift-off
T_i :	half wheel track on axle i
TC :	time constant of air braking systems
u_{vi} :	longitudinal velocity of sprung mass i
v_{vi} :	lateral velocity of sprung mass i
V_{ix} :	wheel lateral speed
V_{iy} :	wheel longitudinal speed
V_y :	vehicle lateral speed
W :	total vehicle weight
W_i :	static vertical load on axle i
w_{vi} :	vertical velocity of sprung mass i
w_{ui} :	vertical velocity of unsprung mass j
W_{ui} :	weight of unsprung mass i
W_5 :	load on fifth wheel

NOMENCLATURE (Continued)

$WAXL_i$:	dynamic axle load on axle i
y_i :	lateral displacement of tires on axle i
y_{un} :	lateral displacement of unsprung mass i
z_{Ri} :	distance between suspension roll center and unsprung mass roll center on axle i
z_{un} :	vertical displacement of unsprung mass i
α :	side-slip angle of tires
α_{si} :	Euler angle of sprung mass i in yaw
β_{si} :	Euler angle of sprung mass i in pitch
δ_{ul}, δ_{uR} :	left and right road wheel steer angles due to Ackerman steer
δ_h :	road wheel steer angle due to bump-steer effect
δ_{cL}, δ_{cR} :	left and right road wheel steer angle due to steering system compliance
δ_f :	average steer angle of the front wheels
δ_l :	effective left road wheel steer angle
δ_r :	effective right road wheel steer angle
δ_{roll} :	road wheel steer angle due to roll-steer effect
δ_w :	road wheel steer angle due to axle wrap steer effect
ε_{ij} :	backlash of suspension spring j ($j=1, 2$) on axle i
φ, φ_s :	roll angle of sprung mass
φ_{si} :	roll angle of sprung mass i
φ_{un} :	roll angle of unsprung mass i
φ_{ij} :	sprung mass roll angle at the wheel lift-off position
γ :	tire camber angle
κ :	longitudinal slip ratio of tires
$\kappa_{off}, \kappa_{on}$:	threshold values of longitudinal slip ratio to turn braking 'off' and 'on'

NOMENCLATURE (Continued)

λ :	suspension deflection constant
μ :	road adhesion coefficient
μ_0 :	adhesion coefficient of a reference road
Δ :	symbol put in front of a variable to represent variation of the variable
Δ_i :	suspension relative displacement at iteration step i
Δ_{ji} :	relative displacement of suspension j ($j=1,2$) on axle i
Δ_{vi} :	lateral displacement of sprung mass i
Δ_i :	dynamic deflection variation of tires
τ_n :	reaction delay due to driver and braking system
ω_w :	wheel spin velocity
0 :	superscript for rollover limits of indicators

CHAPTER 1

LITERATURE REVIEW AND SCOPE OF THE DISSERTATION

1.1 INTRODUCTION

Heavy freight vehicles, due to their excessive weights and large dimensions, exhibit lower directional stability limits and thus pose serious highway safety risks. A review of heavy vehicle accidents in the U.S and Canada revealed that heavy trucks were involved in 28% of single vehicle accidents, as compared with 19% for passenger vehicles [1]. Almost 23% of the heavy vehicle accidents were either associated with or resulted in rollover [2]. Highway accidents involving heavy vehicles cause a significant amount of property damage and human fatalities. Most heavy vehicle accidents result from instabilities, which may be classified into three types: (i) roll instability; (ii) yaw instability; and (iii) trailer yaw oscillation.

The roll stability limits of heavy freight vehicles are known to be considerably lower than those of the other road vehicles due to their excessive weights and dimensions, and high center of gravity (c.g.) location. The roll instability occurs when the centrifugal forces imposed on the vehicle during a maneuver exceed the rollover threshold of the vehicle, resulting in vehicle rollover. The yaw instability, caused by either braking or combined braking and steering maneuvers coupled with lock-up of axle wheels, can lead to vehicle jackknife. Jackknife is characterized by rapid and uncontrolled relative angular yaw motion between the tractor and the trailer. Jackknifing is one of the most frequent causes of serious accidents in which the articulated vehicle sweeps across the path of the

oncoming traffic. Unstable yaw response along with rapid corrective steering maneuvers of the heavy vehicle often leads to vehicle jackknife followed by a rollover. Heavy vehicle instability in terms of trailer yaw oscillation or snaking is characterized by periodic yaw motion of the trailer around the hitch.

The large weights and dimensions, high sprung mass center of gravity of heavy vehicles, and highly complex tire-road interactions yield reduced dynamic stability limits. The impending instability of the vehicle, in general, are averted by the corrective efforts of the driver, which in most cases, are limited to braking, acceleration and steering inputs. However, the driver is located at the front end of the vehicle and often remains unaware of the impending instability, which is mostly initiated at the rear end. Consequently, very little or no time is available for the driver to take appropriate corrective action upon perception of impending rollover. The impending instability is therefore often beyond the control of the driver. Almost all the drivers involved in rollover accidents felt that they had no warning of the impending rollover [3]. The lack of warning of the impending roll instability is due to excessive dynamic load transfer at the rearmost trailer axles where the rollover is initialized [4-5]. Tractor jackknifing instability is characterized by extremely rapid relative yaw motion caused by locked wheels at the tractor's rear axle, resulting in insufficient time for the driver to undertake corrective maneuvers. In the case of trailer swing, the driver usually retains control of the tractor while the semitrailer may exhibit large yaw oscillations [6]. Furthermore, in some cases the apparent corrective action such as braking may aggravate rather than alleviate the impending instability.

The highway safety risks associated with low dynamic stability limits of heavy vehicles can be minimized through early detection of an impending instability.

Appropriate control actions can then be undertaken to avert the potential rollover or jackknife. The directional control of the vehicle can be retained in an open loop manner, in which an early warning of impending vehicle instability is generated for the driver to take an appropriate corrective action. The early detection can further be utilized in a closed loop manner by activating control devices to take corrective actions automatically. An early detection feature, therefore, has significant potential to minimize the severity of instabilities, minimize vehicle damage and increase highway safety.

Roll stability and handling performance characteristics of heavy vehicles have been extensively investigated in the last two decades [7-9]. However, only a few attempts have been made towards identifying the vital motion cues associated with onset of vehicle instability [10]. While static instability measures have been proposed for on-line detection of instability and control, these measures are considered unreliable due to lack of consideration of directional dynamics of the vehicle. Alternatively, dynamic instability measures should be established by examining the dynamic response characteristics of the vehicle. This dissertation research is directed towards enhancement of handling and roll stability of heavy vehicles through on-line monitoring and early warning of a potential instability. The essential issues in this investigation include the study of dynamic performance measures through development and analysis of heavy vehicle models, and identification of a dynamic response vector directly related to the onset of vehicle instabilities. A brief review of the literature on dynamic models of heavy vehicles, directional and roll stability, as well as previous work on detection and control of heavy vehicle stability are presented in the following sections to formulate the scope of this dissertation research.

1.2 REVIEW OF RELEVANT LITERATURE

The detection and control of heavy vehicle instability is a complex issue involving: development of a realistic heavy vehicle model; analysis and evaluation of directional and roll instabilities; analysis and evaluation of response vectors to identify reliable and directly measurable control parameters; and the design of controllers. Extensive literature is available on heavy vehicle dynamics and stability analysis, which must be reviewed in order to draw from the experience and knowledge base that has been developed to date. The published works relevant to various aspect of this investigation are reviewed and grouped under different subjects in the following subsections to formulate the scope of the dissertation research.

1.2.1 Directional Dynamic Models

The handling and stability performance characteristics of heavy vehicles have been extensively investigated through development and analysis of varying complex vehicle models. A review of early works on the dynamic performance of articulated highway vehicles was published by Dugoff and Murphy [11]. Of their cited references, about one third related to directional dynamics and the remainder to braking performance. Vlk [12] conducted a more detailed review on the handling performance of commercial vehicle combinations based upon nearly 250 published studies. It is concluded that the problems associated with directional dynamics of truck-trailer combinations have been addressed in only few studies. The most recent survey of the studies on static stability of articulated commercial vehicles has been published by Fancher [13].

Jindra [14-15] and Ellis [16] developed articulated planar vehicle models in the sixties using the linear equations of motion. The bounce, pitch, and roll degrees of freedom were neglected in developing the vehicle models, and the tires were assumed to possess linear braking and cornering properties. While such simple models could predict the occurrence of trailer lateral oscillations, they did not yield information concerning the jackknifing and trailer swing. Schmid [17] conducted an analytical study on the directional stability of vehicle combinations, characterized by a linear dynamic system where each unit was considered to possess two degrees-of-freedom (*DOF*) of motion. The equations of motion were derived upon incorporating the influence of braking and acceleration, and the conditions of instability were derived from the characteristic equations. A special design of fifth wheel was proposed, which was claimed to improve the braking stability of the combination at the expense of larger pendulum movements.

In the seventies, the research efforts were directed towards development of increasingly sophisticated vehicle models including considerations of large number of degrees-of-freedom motion for each unit, multiple axles, and complex tire models. Strandberg [18] presented a model for vehicle combinations with four degrees-of-freedom (longitudinal, lateral, roll and yaw) for the leading vehicle unit, and described the performance characteristics in terms of overturning risk and rearward amplification factor. A comprehensive linear yaw plane model based on the work of Jindra et al [14-15], was developed by *UMTRI* (University of Michigan Transportation Research Institute) [19]. The model was extended to include multiple axles on the various units of the vehicle. The cornering forces and aligning moments generated at the tire-road interface were assumed to be linear functions of the side slip angle of the tire. Each unit

of the articulated vehicle was assumed as a rigid body, and the unsprung masses were assumed to be rigidly attached to their respective sprung masses. Mallikarjunarao [19] developed characteristic equations for the linear yaw plane model and investigated the vehicle stability using an eigenvalue analysis. Directional response characteristics of the Michigan double tanker were also investigated via computer simulation, and compared to those of other freight vehicles to demonstrate the performance potential of a modified hitch.

Leucht [20] presented a tractor-semitrailer model with nonlinear tire properties, which is frequently referred to as *TBS* model [21]. The lateral tire forces were expressed as a nonlinear function of slip angle and vertical load. The dynamic load transfer in both longitudinal and lateral directions had been taken into account in determining the normal load on each tire. Bernard [22] developed a vehicle model to analyze the directional response under steady turning and braking-in-a-turn maneuvers, while giving special considerations to tire modeling.

Heavy vehicles are more likely to rollover than most other vehicles due to their higher center of gravity (c.g.) height. The role of tire-road interaction in roll stability of heavy vehicles was investigated by Shapley [23] through development of a roll plane model, which incorporated pneumatic tires by lateral springs. It was indicated that the roll instability of a vehicle could arise from high c.g. location, and tire and suspension characteristics. All the displacements and rotations were assumed to be small and the study did not present numerical values for the roll limits. Miller and Barter [24] attempted a simple theoretical analysis of rollover of articulated vehicles, while neglecting the

contribution due to all dynamic forces. It was assumed that rollover occurs when the sum of the forces acting on the trailer c.g. falls outside of the trailer's outside wheels.

A sophisticated static roll model of articulated vehicles was developed by Mallikarjunarao et al. [25] to determine the rollover threshold of articulated vehicles during steady turning maneuvers. For multi-axle tractor-semitrailer combinations the axles with similar suspension properties were grouped together such that all axles on the vehicle were represented by a set of three composite axles: tractor front axle; an equivalent tractor rear axle; and an equivalent semitrailer axle. The sprung mass of the tractor was modeled as two sprung weights coupled through torsional stiffness of the tractor frame. The sprung weight of the semitrailer was coupled to the tractor rear weight by the torsional stiffness of the fifth wheel and semitrailer structure. Tires were modeled as linear springs, while the non-linear properties of suspension springs were included in this model. Extensive tilt table test results were used to validate the model [25]. An extensive parametric sensitivity analysis of the model was carried out by El-Gindy [26], where the vehicle design parameters were classified into three groups based upon their influence on the rollover threshold. The first group included the set of parameters that have no effect on the response, while the second group of parameters represented those which must be considered in the model. The last group represents the most important required input parameters, which need to be measured accurately. Piché [10] investigated static rollover thresholds of semi-trailers with different vehicle combinations using the static roll model developed in [25]. A compliance factor with a typical value of 0.72 was introduced to reflect the influence of the compliance of suspension springs and tires on rollover threshold.

The dynamic rollover of commercial vehicles has been studied using a nonlinear roll plane model developed by Verma [27]. The model, considered valid for large amplitude motion, is used to illustrate some of the dynamic phenomena associated with vehicle rollover, especially the interactive coupling between the roll and the vertical modes of motion. The study indicated that suspension backlash adversely influence the rollover threshold of the vehicle. It was shown that rollover of a vehicle could occur at lateral acceleration levels less than its static acceleration limit or rollover threshold due to roll mode resonance of the vehicle. Das et al [28] investigated maneuver-induced rollover threshold of commercial vehicles using this model. While computer simulation was carried out based on low speed experimental data, curve-fitting techniques were used to extrapolate for the threshold values of lateral acceleration and forward velocity.

A comprehensive three-dimensional directional dynamic model of commercial vehicle combinations, referred to as yaw/roll model, was developed for analysis of single and multiple articulated vehicles engaged in constant speed directional maneuvers [29]. The equations of motion of the vehicle were formulated by treating each of the sprung masses as a rigid body with motions along the five-degrees-of-freedom (lateral, vertical, yaw, roll and pitch), while each axle was treated as beam axle with two-degrees-of-freedom (roll and bounce). The yaw/roll model, however, does not adequately evaluate the rollover threshold of vehicles that exhibit yaw divergence at lateral acceleration levels lower than the rollover limit. A comprehensive three-dimensional vehicle model, refereed as the Phase 4 Model, was developed at *UMTRI* [30] for simulating the braking and steering dynamics of trucks, tractor-semitrailer combinations, doubles, and triple combinations. The dynamics of the vehicle combinations were represented by differential

equations that are solved by successive time increments and digital integration. The directional analysis can be performed using either directional maneuver, where the time history of front wheel steer angle is specified, or closed-loop driver path-follow maneuver, where the coordinates of the path are specified. The mathematical model incorporates up to 71 degrees-of-freedom, derived from the following:

- (1) The motion of sprung mass of the truck or the tractor is described by six degrees-of-freedom.
- (2) The motion of the semitrailer sprung weight is characterized by three rotational degrees-of-freedom, while the translational degrees-of-freedom are effectively eliminated by the dynamic constraints.
- (3) The motion of each full trailer is described by five degrees-of-freedom and up to two full trailers can be accommodated in the model.
- (4) The motion of each of the 13 axles allowed is characterized by two degrees-of-freedom (bounce and roll).
- (5) The motion of each of the 26 wheel allowed is described by one rotational motion.

El-Gindy and Wong [31] conducted a comparative study of various computer simulation models developed for directional analysis of heavy vehicles, including the linear yaw plane, the TBS, the yaw/roll and the Phase 4 models. The study concluded that a sophisticated simulation model did not necessarily guarantee a more accurate predication than a simpler one. It is however important to select a simulation model appropriate for a specific task on performance measures.

The majority of the analytical models reported in the literature and summarized above have been developed to analyze only certain measures of the directional performance. These models have been used to assess various measures including handling, static and dynamic roll stability, lateral dynamics, yaw oscillations, braking performance,

etc. The highlights of the reported models and their conclusions are thus further grouped under specific stability measures and discussed below.

1.2.2 Roll Stability Analysis

In view of the high rollover propensity of heavy vehicles, the roll stability of such vehicles has drawn considerable attention from the policy makers and the industry. The research efforts on roll stability analyses can be classified into two groups: static analysis and dynamic analysis. Static roll stability analyses yield a static rollover threshold, while dynamic analyses attempt to establish the dynamic rollover stability measures. Many theoretical and experimental investigations reveal that the likelihood of a vehicle rollover is strongly related to its Static Rollover Threshold (*SRT*), defined as the lateral acceleration level which the vehicle can sustain without suffering a divergent roll response [32, 33]. Vehicles with a low *SRT* are bound to be less safe than those with a high *SRT* [34]. The *SRT*, in general, depends on the vehicle geometry, suspension characteristics and tire properties, and can be evaluated experimentally and theoretically. The experimental methods include road test, side-pull test and tilt table test, of which the latter is extensively used to measure *SRT* of heavy vehicles. The tilt table attempts to simulate a lateral acceleration field, which the vehicle could experience during a steady cornering maneuver by inclining the test vehicle in the roll direction. The tilt table test is known to be simple with high degree of repeatability [35]. The tilt table used by Miller and Barter [24] was one of the earliest facilities developed to investigate the roll characteristics of articulated trucks. Preston-Thomas et al [33] investigated the rollover threshold of a selected number of heavy vehicles using the tilt table test. The *SRT* values

of the loaded 3-axle and 4-axle dump trucks range from 0.45 g to 0.5 g. The rollover threshold of a specified tractor-semitrailer approaches 0.34 g, when loaded. The tilt table test, however, has been criticized because it does not accurately represent a vehicle in a lateral acceleration field caused by steady state cornering. As the inclination angle increases, vertical force acting on the vehicle decreases. This will cause a change in the vehicle's c.g. height, and thus influence its rollover threshold [36]. Although there exist some drawbacks to the tilt table test, the Society of Automotive Engineers (SAE) has proposed to make it a standard device to measure *SRT* of heavy vehicles. Fancher and Mathew [37] proposed an "example target" *SRT* value of 0.38 g for tractor-semitrailers in the US. El-Gindy et al proposed the 0.4 g minimum *SRT* with a suggestion that a tolerance of $\pm 5\%$ be considered in Canada.

Miller and Barter [38] attempted a theoretical analysis of the articulated vehicle rollover ignoring all the dynamic forces and assuming that rollover occurs when all the wheels on one track of the vehicle experience lift-off. It indicated that the trailer c.g. height is the most important control parameter for rollover. The study concluded that speeds which drivers estimated quite safe are often quite close to the vehicle's rollover limit. Almost all the drivers involved in rollover accidents were surprised with the outcome and the lack of warning they had. A simple analytical treatment of the roll behavior of multi-axle vehicles has been outlined by Ervin et al [4, 32]. The static rollover threshold of a rigidly suspended vehicle is initially estimated as the ratio of half the effective track width to the c.g. height, referred to as *Static Stability Factor*. The contribution due to suspension and tire compliance are then considered by lumping various axle sets together to realize a single axle representation. Lumped compliant

suspensions and tires lead to a relatively lower value of static rollover threshold. For a multi-axle vehicle with different suspension properties, the three-axle representation of the vehicle would be required, which leads to even lower *SRT*. The semitrailer axles due to their relatively stiff suspension encounter larger load transfer than that experienced by the tractor's axles. This load transfer at the rearmost axles of the combination and the linear nature of the steering behavior up to the rollover limit implies that the driver is given very little or no warning of the impending rollover situation [3].

El-Gindy and Hosameldeen [26] published the results of a comprehensive parameter analysis of a tractor semi-trailer conducted using the *Static Roll Model*. It was concluded that, for the vehicle under consideration, the parameters of fundamental importance to the *SRT* include the c.g. heights of the sprung masses, the fifth-wheel separation moment, and the following parameters for the trailer and the tractor drive-axles: track width, suspension spring rates and spring-lash characteristics, vertical tire stiffness characteristics, auxiliary roll stiffness, and roll center heights. Rakheja et al. [39] investigated the roll stability of a partially filled tank vehicle for steady turning maneuvers with a modified *Static Roll Model* to reflect the influence of lateral movement of the liquid cargo. The study concluded that the rollover threshold levels of such vehicles are significantly lower due to lateral load shift, as compared to those of the vehicles carrying an equivalent rigid cargo. Influence of tank compartmenting on the steady turning roll response of the vehicle was analyzed and an optimal order of unloading a compartmented tank was proposed.

Significant research efforts have also been directed towards finding correlation between vehicle design parameters and rollover statistics from accidents databases. Jones

and Penny [40] conducted a statistical analysis to establish the influence of vehicle parameters on the rollover propensity. The study concluded that the *Static Stability Factor* was the strongest predictor of vehicle rollover for pickup trucks and utility vehicles. Statistical research was also carried out by NHTSA (National Highway Traffic Safety Administration, USA) [41] to evaluate several different metrics to determine their usefulness as indicators of likelihood of rollover of light vehicles. This research concluded that there exists a clear relationship between rollover stability measures and rollover propensity. Among the three basic roll stability metrics evaluated (tilt table ratio, static stability factor, and side pull ratio), the tilt table ratio appeared to provide the greatest explanatory power. As for heavy vehicles, no similar publication of statistical research can be found in the literature.

The prior works on the analysis of roll stability of heavy vehicles were primarily directed toward static roll phenomena that are applicable only under steady turning maneuvers. There exists a need to investigate the dynamic rollover characteristics of heavy vehicles. In general the dynamic rollover mechanism can be grouped into two classes: (i) tripped rollover; and (ii) maneuver-induced rollover. In evaluating a vehicle's rollover stability in a tripped rollover situation, three dynamic measures based on energy conservation have been proposed. Nalecz [42] developed an energy based function called Rollover Prevention Energy Reserve (*RPER*) to study the vehicle tripped rollover propensity. *RPER* is defined as the difference between the energy needed to bring the vehicle to its tip-over position and the vehicle rotational kinetic energy that can be transferred into gravitational potential energy to lift the vehicle. According to this definition, the value of the *RPER* function drops below zero before a vehicle reaches its

tip-over position in a rollover case, but always remains positive in a non-rollover case. Hinch et al [43] presented Rollover Prevention Metric (*RPM*) to predict tripped rollover stability, which is defined as the difference between the initial lateral translational kinetic energy and the rotational kinetic energy after the impact divided by the initial energy. The third measure is called Critical Sliding Velocity (*CSV*) [44], which is a measure of the minimum lateral velocity required to initiate a rollover.

El-Gindy [45] indicated two dynamic rollover stability measures for maneuver-induced rollovers in terms of Load Transfer Ratio (*LTR*) and Rearward Amplification Ratio. The *LTR* is defined as the ratio of the absolute value of the difference between the sum of right wheel loads and the sum of the left wheel loads, to the sum of all the wheels loads. The rearward amplification ratio is a frequency dependent measure, defined as the ratio of the peak lateral acceleration at the center of gravity of the rearmost trailer to the amplitude of lateral acceleration at the center of the tractor. A new proposed dynamic measure is called Yaw Damping Ratio, which describes how rapidly the lateral acceleration oscillations of the rearmost trailer of an articulated vehicle diminish after a pulse steer input [45]. This measure is evaluated at a vehicle speed of 100 km/h, by applying a steering wheel pulse input of 80° (half sine) over a 0.1s time interval. From the successive peaks of lateral acceleration decay of the rearmost trailer, a damping ratio is calculated using the standard logarithmic decrement procedure.

Winkler et al [46] investigated the phenomena of rearward amplification of articulated vehicles, and suggested a rearward amplification of 2.0 or less at 88 km/h for articulated vehicles. Macadam [47] investigated the relationship between directional and roll stability of heavy trucks. It indicated that yaw divergence will lead to rollover in the

absence of corrective steering action or reduced speed. It should be pointed out that most rollovers of heavy vehicles are maneuver-induced rollovers. This is because the static rollover threshold of most heavy vehicles in gravity level is well below the normal road adhesion factor 0.7 – 0.85. The lateral skid of the vehicle is thus not expected to be initialized before it rolls over.

1.2.3 Directional Stability Analysis

There exist three types of yaw instabilities for heavy vehicle combinations: trailing yaw oscillation, jackknifing and trailer swing. The early investigations on heavy vehicle stability were limited to trailer yaw oscillations only. Laurien [9] launched both experimental and theoretical investigations of directional stability of truck-trailer vehicles in the fifties. The most important conclusion was that the trailer yaw oscillations could be most effectively suppressed by the introduction of coulomb damping at the hitch and at the trailer steering mechanism. The trailers with Ackerman steering are more prone to lateral oscillations than the trailers with turnable (dolly) steering. Schmid [17] investigated the dynamic stability of tractor-trailer combinations through analysis of linear equations. Routh criteria were employed to distinguish between stability and instability, considering trailer yaw oscillation and jackknifing (aperiodic instability) separately. The investigation indicated that the following factors have positive influence on the directional stability of truck-trailer combinations: understeer behavior of the truck; large wheelbase of the truck; larger cornering stiffness of truck tires; the location of the dolly c.g. in front of the trailer's front axle; long drawbar; and large distance of turnable point from mass center of trailer body. A study conducted by Collins and Wong [48]

indicated that hitch loading, trailer length, mass, mass moment of inertia and small variations in the tractor tire pressure can influence the trailer stability. It was indicated that it is possible for a vehicle to exhibit a spinout response even in the absence of braking effort due to unfavorable balance in the lateral forces generated at the front and rear axle tires during cornering. An analysis conducted by Troger and Zeman [49] showed that the location of the c.g. of a semitrailer with respect to the fifth wheel location is one of the most critical parameters for the stability of tractor-semitrailer vehicle combinations.

Heavy vehicle dynamic stability analysis is often conducted using two principal methods: Routh-Hurwitz criterion and eigenvalue solution of the characteristic equation. Crolla and Hales [50] investigated the lateral stability characteristics of a tractor-trailer via an eigenvalue analysis. The study proposed the minimum damping and hitch load criteria to improve the yaw stability performance of the vehicles. Mikulcik [51] developed a set of algebraic equations to determine the stability boundaries of a car-trailer system. A general criterion governing both the oscillatory and aperiodic stability was derived using Routh's criterion. The graphical representation showed a stable region bounded by limits of oscillatory and aperiodic stability. A parametric sensitivity analysis was conducted to evaluate comparative stability and the relative effects of parameter changes. Mallikarjunarao [19] conducted eigenvalue analysis and computer simulation of double tanks. Root loci were plotted as a function of different parameters, such as vehicle forward speed, load distribution, trailer tandem axle location and fifth wheel location. The principal finding from the simulations was that there exists a very large amplification

factor between the lateral acceleration of the tractor and the lateral acceleration of semi-trailer in an obstacle avoidance steering maneuver.

Control of a truck-trailer combination during steady-steady cornering was carried out by Jindra [15]. Vlk [12] broadened the investigation of Jindra by examining the yaw stability of truck-trailer combinations during cornering. Ervin and Mallikarjunarao [52] investigated the yaw stability of tractor-semitrailer combinations. It was concluded that the combination was unconditionally stable when coupled with an understeer tractor. For any form of directional instability (jackknifing or trailer swing) to occur, the tractor must be oversteer. Jackknifing may occur when the semi-trailer is either understeer or oversteer. Trailer swing occurs for a vehicle combination when the semitrailer is oversteer and the ratio of the understeer coefficient of the semitrailer to that of the tractor is greater than the ratio of the semitrailer wheel base to that of the tractor. El-Gindy and Wong [53, 54] conducted a further study to analyze the steady state response of articulated vehicles to steering inputs.

Transient directional response characteristics of heavy vehicles are primarily investigated via computer simulations and scaled or full-scale tests using linear models. Vlk [55] investigated the transient turning behavior of articulated vehicles to evaluate the effects of variations in vehicle design parameters. The results showed that the directional dynamics of the vehicle are substantially affected by the vehicle velocity and damping between the units of the articulated combination. It has been further established that large yaw oscillations can be prevented by the application of hydraulic dampers between the two units of the articulated vehicle [56]. Vlk [57] further investigated the lateral stability of articulated buses using a three-dimensional nonlinear model. The directional stability

of articulated vehicles were investigated from the time history of the articulation angle response under an impulse steering input. The study revealed that articulated buses employing pusher type axles should be provided with additional damping between the front and the rear units to eliminate the possibility of jackknifing and trailing swing during acceleration or braking in a turn.

Dynamic stability characteristics of different vehicle combinations have been extensively investigated using full-scale experiments and computer simulations. Such studies were performed in Sweden for combinations of up to three articulations [58]. The dynamic stability characteristics were investigated by means of a double lane change maneuver, and the following design features were recommended to obtain desirable lane change behavior: long trailer wheelbase, short distance between dolly pintle hook and the first semitrailer rear axle, high tire cornering stiffness, low center of gravity height and high roll stiffness. The minimum performance requirements were proposed as follows: rearward amplification of side slip angles should not exceed 2; the side slip angles must not exceed 0.15 rad (8.6 degrees); the oscillatory damping must be such that all side slip angles are less than 0.02 rad (1.15 degrees) when the first axle of the combination has reached a point 75 m away from the entrance of the corridor. Singh [9] used a nonlinear model, assuming negligible roll and pitch motion, to investigate directional performance of a four-axle truck trailer during braking in a turn. It was indicated that the center of mass of the truck should be closer to the front axle than to the rear axle of the truck in order to reduce the jackknifing tendency. The distance from the center of mass of the truck to the front hitch should be large, and a full trailer should have a long drawbar to reduce the magnitude of trailer swing.

While there exists a large body of published studies on the development of various methodologies and computer simulation models for predicting the lateral dynamics of articulated vehicles, there appear to be relatively few published studies on the relative merits of different mathematical solution and simulation models. El-Gindy [59] developed a closed form solution of the transient and steady state directional response of a tractor semitrailer. The solution was then examined by two different computer simulation models. The study concluded that the closed form solutions of the linear mathematical model correlate very well with the results derived from the simulation models. Mashadi and Crolla [60] investigated the theoretical relationship between steady state and transient response properties of two-axle vehicles and concluded that the damping ratio of oversteered vehicle is always great than unity and only understeered vehicles can exhibit oscillatory response.

Braking performance of heavy vehicles is a very important factor as it directly relates to yaw and lateral instabilities. When the front wheels of the tractor experience lockup under sudden braking, the directional control of the vehicle is lost. The lockup of the rear wheels of the tractor can lead to rapid tractor spin with respect to the trailer, resulting in jackknife. On the other hand, when the trailer wheels experience lockup, the trailer may spin about the coupling point, resulting in trailer swing [61]. The vehicle combination may also exhibit instability, when all the wheels experience lockup at the same time, in the presence of a yaw disturbance at the beginning of the braking maneuver [62]. This directional behavior of articulated vehicles can be strongly attributed to the braking and cornering properties of the pneumatic tires. When the wheels experience lockup, the tires can not develop cornering forces necessary to maintain a desired path.

The cornering forces generated by the tires are nonlinear functions of the normal load, braking force and tire sideslip angles. Huston and Johnson [63] developed a relationship to estimate the cornering stiffness of tires and demonstrated that variations in cornering stiffness due to changes in normal loads significantly affect the critical speed of a vehicle combination. Segal and Ervin [64] investigated the influence of tire factors and distribution of roll stiffness on truck stability. The study concluded that the fore-aft roll stiffness distribution was the primary mechanism serving to aggravate the heavy truck yaw instability, and the shear-force properties of the truck tires cause the trucks to respond differently to parametric variations than the typical passenger cars.

The major factor that influences the directional stability of heavy vehicles is the braking force distribution. Schmid [17] concluded in his analytical study that the greater the proportion of the overall braking force of the combination upon the axles of the trailer, the less is the tendency for jackknifing. Load sensitive brake force distribution for the truck does not prevent the phenomenon of jackknifing, but certainly reduces jackknifing. The use of anti-lock braking system (*ABS*) has been strongly emphasized in many studies to achieve better braking performance and enhanced directional stability [65-67]. Those studies have demonstrated that *ABS* can prevent wheel lockup when braking, and provides directional stability, steer control and optimum stopping distances.

1.2.4 Detection and Control of Directional and Roll Instabilities

Tractor jackknifing, associated with the locked wheel at tractor's rear axle, is one of the dangerous directional instability scenarios of tractor semitrailer combinations. The development of tractor jackknifing is usually extremely fast, and thus prevents the driver

from taking effective corrective actions [68]. An automatic stabilizing technique to prevent tractor jackknifing is therefore needed to enhance stability. This technique includes the detection of the onset of jackknifing and the subsequent application of corrective actions. Trailer swing, on the other hand, occurs more slowly than tractor jackknifing due to the length of the trailer. In this mode of instability, the driver usually retains control of the tractor. Rollover of heavy vehicles poses another dangerous scenario to road users. Previous studies revealed that speeds estimated as safe by the drivers during a steady turn maneuver were often quite close to the vehicle's rollover limit [38]. Almost all the drivers involved in rollover accidents felt that they had no warning of the impending rollover. The lack of warning of the impending roll instability has been attributed to the large load transfer that first takes place at the rearmost axles of the vehicle.

Susemihl and Krauter [69-70] attempted to define the onset of jackknifing in a quantitative manner by using a nonlinear vehicle model. Local linearization was used to derive a stability matrix. The onset of tractor jackknifing was taken as the time at which the system, assumed to be originally locally stable, became locally unstable. However the above definition of the onset of tractor jackknife can not be used to develop a method for the detection of jackknife in a real vehicle. Instead, the relationship between the side force and the slip angle was examined to find a clue for tractor jackknifing. Tractor jackknifing is associated with saturation of the total side force produced by the drive axle tires. Such saturation is assumed to occur if the magnitude of the slip angle at either drive axle tire continues to grow when the rate of change of the total side force becomes zero. The locking of a wheel at the drive axle could, therefore, be taken as the indication of an

incipient tractor jackknife. The measurable motion parameters, describing the onset of vehicle jackknifing, have been established via computer simulation of a linear system [71]. The study concluded that an abrupt increase in tractor yaw angle, the trailer yaw velocity and tire skid at the tractor rear axles, can best describe the onset of jackknife. Rakheja and Piché [5, 10] investigated the tractor jackknifing stability limits using the three dimensional Phase IV model. It was concluded that the onset of vehicle jackknife could be detected via monitoring an approximated side force at the drive axle and the articulation angle. The necessary condition for tractor jackknifing is that the derivative of the approximated side force approaches zero, while the articulation angle continues to grow. The approximated side force can be derived from directly measurable response parameters such as tractor's lateral acceleration, forward velocity, yaw acceleration, yaw rate and lateral force at the fifth wheel constraint. In practice, it is generally accepted that in normal highway operations a jackknifing is imminent once the articulation angle exceeds approximately 15° [71]. This value, however, does not define a stability limit, but rather represents a value beyond which the driver has little opportunity to regain control of the vehicle and jackknifing follows.

Roll instability of heavy vehicles could occur during low speed cornering or high-speed directional maneuvers. The roll instability can be directly related to the normal load on the inside tires of the semitrailer and tractor rear axles. When the normal load acting on these tires approaches zero, the tires lose contact with the ground indicating the onset of a potential rollover. However, measurement of tire loads in a moving vehicle is quite intricate, and thus such a parameter may be considered infeasible to detect the onset of roll instability [5]. Alternatively, rollover during low speed cornering has been related to

the measurable parameter, namely, static rollover threshold (*SRT*) of the vehicle. The static rollover threshold is frequently used to rate vehicle's rollover propensity. It can not, however, be used as an indicator for the onset of vehicle rollover. It has been recognized that a vehicle rollover in a dynamic maneuver may occur at a lateral acceleration which is less than its static rollover threshold. Piché [10] proposed a safety factor of 1.1 for using the *SRT* as an indicator for onset of rollover, but provided no further explanation. The study further used the Yaw/Roll model to investigate the dynamic rollover properties of articulated vehicles, and concluded that the onset of vehicle rollover during high-speed directional maneuvers can be detected via on-line acquisition and monitoring of a semitrailer axle's roll angle. Allen and Rosenthal [72] illustrated that rollover instability can be simply identified using phase plane plots. A simultaneous increase in both body roll angle and roll rate may imply an unstable exponential divergence of roll motion.

Upon detection of onset of vehicle instabilities, the most important step is to prevent them from developing further. There are several different approaches used to prevent a jackknife. The first approach is the wheel anti-lock braking system. This method attempts to prevent a jackknife by retaining the tire side forces during the braking maneuver. Susemihl [69] investigated three forms of anti-skid braking and concluded that antiskid braking at all axles of the tractor appeared most desirable. The second approach is to balance the side force between the front and rear tractor wheels by locking the steering wheel at the same time the tractor and trailer wheels lockup, such as using a brake proportioning system. The third approach to prevent jackknifing is to control the articulation motion by applying damping, counter moment, or roll motion restrictions between tractor and trailer. Snelgrove [73] et al evaluated several jackknifing control

devices and concluded that the wheel anti-lock system provided the best anti-jackknifing property.

To stabilize the roll motion of heavy vehicles, a restoring moment should be generated by auxiliary anti-roll devices. However, few published studies have dealt specifically with the issue of roll control, especially for heavy vehicles. Dunwoody et al [74] presented an active roll control system to enhance roll stability of a semitrailer. The key components of the system are a tiltable fifth-wheel coupling, actuators to apply a moment to the trailer axles, a source of hydraulic power, sensors and a controller. It was claimed that the system could increase the rollover threshold of such a vehicle by up to 30% through control of the lateral shift of the vehicle's center of gravity during cornering. Actively controlled anti-roll bars can also be used to enhance roll stability of heavy vehicles [75]. The controlled anti-roll bar acts as a torsion spring when engaged, which introduces auxiliary roll stiffness between the axles and the vehicle body leading to reduced vehicle roll motion. Darling et al [76] examined an active anti-roll bar system based on "ideal roll cancellation". The ideal roll cancellation system did not address the hydraulic implications of an active device but applied a vertical force at each corner of the vehicle sufficient to overcome the roll moment generated by the action of lateral acceleration on the vehicle center of gravity. The ideal system was then modified to include a first order delay function to account for the dynamics of hydraulic actuators.

Constantine and Law [77] investigated the effects of roll control for passenger cars during emergency maneuvers. Based on the understanding of the effects of roll stiffness distribution on vehicle handling and braking performance, three types of roll controllers were proposed. The first controller was based upon a semi-active bang-bang

control concept, which varied the front and rear axle roll stiffness without providing any additional roll torque. This can be accomplished physically through variable state geared or clutched stabilizer bars (anti-roll bars). The stabilizer bars are engaged when the sprung mass roll angle exceeds certain limit. The second controller was based upon the concept of an active roll control with stability augmentation, which applies roll torque to the front and rear axles. The total applied roll moment is equal and opposite to the moment induced by the lateral acceleration on the sprung mass. The distribution of applied roll torque to the front and rear axles was estimated as inversely proportional to the ratio of front-to-rear corrected lateral acceleration in order to achieve increased understeer property during cornering. The last controller was referred to as active roll control with handling augmentation, which varied the roll stiffness and applied additional roll torque to improve lateral capability during avoidance maneuvers. A PID regulator with roll angle perturbations as the error signal was used to generate the required torque, and the gains were determined using pole placement techniques with Butterworth constraints. It demonstrated that the semi-active bang-bang roll control halves the roll angle during cornering. The other two controllers are quite effective in nulling out roll angle with no apparent oscillations. Hwang and Park [78] presented an anti-roll control algorithm for roll moment distribution based on predictive control to overcome the actuator's time lag.

It has been established that rollover of articulated vehicles is initialized at trailer's axles due to larger lateral acceleration at trailer's center of gravity. Various design approaches have been explored to reduce lateral acceleration of the semitrailer center of gravity. One such an approach is to introduce multiple steered axles to heavy articulated

trucks. The study conducted by Furleigh et al [79] concluded that active steering of the tractor rear axles could improve the directional response of articulated trucks. At higher speeds, the implementation of steerable rear axles can reduce the lateral acceleration response at the trailer center of gravity in an obstacle avoidance maneuver. At lower speeds, the tractor rear axle steering can improve performance for certain transient maneuvers by reducing the minimum turning radius of the truck and by limiting the offtracking. The influence of steered axles on the dynamic stability of heavy vehicles was also investigated by Auell and Edlund [80], and Sankar, et al [81]. The results from [80] indicated that active steering of the trailer rear axle could decrease the rearward amplification, and thus increase the roll stability of such vehicles. Watanabe, et al [82] investigated the effects of rear-axle steering on vehicle controllability and stability of a medium-duty truck in terms of yaw rate resonant frequency, difference between yaw rate steady-state gain and peak gain, phase lags of yaw rate, and lateral acceleration at specific frequency (0.5 Hz). A feed-forward controller was used to achieve the design targets, and it was concluded that the rear axle can yield increased yaw resonant frequency and damping ratio, and decreased yaw velocity phase lag.

Palkovics and El-Gindy [83] examined four different control strategies for directional and roll stability control of a tractor-semitrailer combination using *LQR* (Linear Quadratic Regulator) approach. The control strategies included: active steering of the tractor's rear wheels; active steering of the trailer's wheels; active torque control in the fifth-wheel joint; and active control of yaw torque acting on the tractor. The *LQR* controller was designed to minimize various vehicle response characteristics, including: the yaw rate of the tractor; the articulation rate; the side-slip angle of the tractor; and the

articulation angle. The control strategies considered for the tractor rear axle steering and yaw torque acting on the tractor resulted in improved performance of both the trailer and tractor. The strategy involving active steering of the trailer's wheels affected only the trailer's oscillatory behavior. The main problem associated with the LQR controller is that it does not compensate for the parametric uncertainties. To overcome the limitation of the LQR controller, a robust $H_\infty/RLQR$ controller was examined with a nonlinear vehicle model. The concept of an active braking system (unilateral braking) was proposed, which generates the desired directional torque based on the measured lateral accelerations of both the tractor and semitrailer. When the yaw rate and side slip angle of the tractor begins to increase, a torque of opposite sign is produced, which stabilizes the yaw motions of the vehicle.

1.3 SCOPE AND OBJECTIVES OF THE DISSERTATION

From the literature review, it is apparent that heavy vehicles are prone to various modes of instabilities due to their weights, dimensions and high location of c.g. Among the modes of instabilities, yaw instability and trailer yaw oscillations including jackknife have received significant attention, and have led to developments in *ABS* and auxiliary yaw dampers. Roll instability and its control and prevention on the other hand, is a difficult issue, where the drivers often remain unaware of the associated risk posed by the roll instability which mostly originates at the rearmost axle. The risk of vehicle rollover may thus be reduced by enhancing the driver's perception of onset of the instability, before it develops and propagates over the entire vehicle. In view of the lack of warning on the onset of roll instability, some form of early warning and implementation of timely

measures is vital to ensure the safety of the vehicle, driver and other highway users. In view of the need and potential for improvement, this dissertation research focuses on the analysis of dynamic roll instability of heavy vehicles, detection of onset of roll instability, and feasibility analysis of open-loop rollover control.

Establishment of potential measures for early detection of impending rollover under dynamic conditions and its subsequent use in control of the instability is a highly complex issue. A systematic study is therefore needed which will include: development of realistic vehicle models; analysis and evaluation of dynamic roll instabilities; analysis and evaluation of response vector to identify reliable and directly measurable control parameters; and the evaluation of effectiveness of open-loop rollover control. In view of limited investigations in open-loop rollover control in the literature, the major contributions of this dissertation research would be: (i) development of roll instability criteria, (ii) identification of rollover conditions of various configurations of heavy freight vehicles, (iii) identification and analysis of impending rollover indicators in terms of reliability, measurability, and through dynamic roll stability analysis, (iv) introduction of new roll stability measures in terms of dynamic rollover threshold and absolute rollover threshold, and (v) feasibility analysis of open-loop rollover control. The specific objectives in this investigation along with organization of the thesis are outlined in the following subsections.

1.3.1 Objectives of the Dissertation

The overall objective of the dissertation research is to contribute to the attainment of highway safety through systematic analysis of dynamic roll characteristics of freight

vehicles, and the application of the knowledge base in an open-loop roll stability enhancement system. The concept of an open-loop stability enhancement system is based upon detection of impending instabilities of the vehicle and generation of an early warning for the driver. The specific objectives of the dissertation research are:

- (1) Establishment of roll instability criteria and measures for heavy freight vehicles based on roll mechanics analysis.
- (2) Study of static rollover characteristics and identification of the relative roll instability conditions of heavy freight vehicles in steady cornering maneuvers.
- (3) Study of dynamic rollover characteristics through development and analysis of heavy vehicle models.
- (4) Identification of dynamic response vectors directly related to onset of vehicle roll instabilities.
- (5) Reliability, measurability and early warning capability analyses of the response vectors for a range vehicle design and operating conditions.
- (6) Feasibility analysis of open-loop roll stability enhancement through on-line monitoring and early warning generation through development of comprehensive three-dimensional heavy vehicle model and computer simulation.

1.3.2 Organization of the Dissertation

In chapter 2, various configurations of heavy freight vehicles are reviewed in terms of towing unit types, hitches, towed units, and accident occurrence rates. The rollover mechanics of heavy vehicles are analyzed for single-axle and multi-axle representations, respectively. The relative and absolute roll instabilities of heavy vehicles are defined and clarified in terms of roll severity for static and dynamic rollover analyses. Various measures of relative and absolute roll instability are defined for assessment of rollover propensity and their potential in detecting onset of rollover of heavy vehicles.

In chapter 3, a relative roll instability criterion is employed to investigate relative rollover conditions of articulated heavy vehicles in steady cornering maneuvers. Two-axle representation for straight trucks and full trailers is realized by grouping the front and rear axles into their respective single composite axle. Static roll equilibrium equations are derived by splitting overturning moments into the front and rear roll planes. An analytical relationship between the sprung mass roll angle and the lateral acceleration is derived for static rollover analysis of straight trucks and full trailers. Static roll plane models for tractor semi-trailers and B- or C-train doubles are developed for investigation of relative rollover conditions and static rollover threshold (*SRT*) of articulated freight vehicles. A parametric sensitivity study is conducted to identify the influence of an array of vehicle and suspension configurations on *SRT* and relative rollover conditions of tractor semi-trailer combinations, B- or C- train doubles.

In chapter 4, a comprehensive yaw/roll plane model is derived for investigation of dynamic roll response characteristics of articulated heavy vehicles. The concept of effective lateral acceleration (*ELA*) is proposed to characterize all the centrifugal forces of a complete roll unit. Dynamic rollover threshold is proposed based on *ELA* and relative rollover criterion. A roll plane model for the investigation of absolute roll instability of heavy vehicles is derived. The equations of motion are derived using the energy approach, which are considered valid until the vehicle approaches its tip-over position. Absolute rollover indicators are proposed and investigated for their effectiveness. Absolute rollover threshold of heavy vehicles, based on absolute rollover criterion, is analyzed using the proposed roll plane model.

In chapter 5, potential rollover indicators are identified through analysis of the lumped two-axle roll plane model developed in chapter 3. The potential rollover indicators are assessed in terms of measurability, reliability and time margin for driver's actions. Measurability analysis of the indicators is carried out based on current engineering practice. Reliability analysis is conducted in terms of parametric sensitivity analysis and linear correlation characteristics with *RSF*. The comprehensive yaw/roll model derived in chapter 4 is employed to assess its capability to provide an early warning of impending rollover with sufficient lead time for the driver's actions. Different designs of an early warning safety device are discussed.

In chapter 6, a sophisticated three-dimensional heavy vehicle model is developed for the investigation of effectiveness and feasibility of open-loop roll instability control. The steering system compliance, roll steer, bump steer, ackerman steer and wrap steer are incorporated in the vehicle model. The magic formula tire model is used to generate combined cornering and braking tire forces and moments with *ABS* algorithm. Time delay due to driver's reaction and the transportation lag of the braking system are characterized by a variable called reaction delay. The rollover indicators in terms of roll safety factor, tractor and trailer lateral accelerations and roll angles, and the rearmost axle roll angle are investigated for their effectiveness in open-loop roll stability control for various cornering and evasive maneuvers, road conditions, braking efforts, and reaction delays.

The highlights of the study and the conclusions drawn are summarized in chapter 7. The recommendations for further investigation of roll instability control of heavy freight vehicles are presented.

CHAPTER 2

ROLL INSTABILITY CRITERIA AND MEASURES

2.1 INTRODUCTION

One of the most important issues in the investigation of heavy vehicle rollover characteristics is the establishment of roll instability criterion under dynamic conditions. The mechanism for heavy vehicle rollover can be categorized under two distinct groups, namely: (1) tripped rollover, and (2) maneuver induced rollover. A tripped vehicle rollover may occur when the vehicle strikes a curb or an obstacle during cornering, and it often occurs in conjunction with lateral skid of the vehicle prior to the strike. A maneuver induced vehicle rollover occurs during a directional maneuver, and is primarily attributed to dynamic roll behavior of the vehicle, while the contributions from the tripping mechanism are absent. On very slippery pavements, however, lateral skid of the vehicle and strike with a curb may occur during a directional maneuver, resulting in tripped rollover of the vehicle.

The maneuver-induced rollovers are more likely to occur due to the poor rollover limits of the heavy vehicle combinations. The lateral acceleration rollover limits for most heavy vehicles have been reported to be in the 0.3g to 0.6g range [84], which is known to be well below the normal road adhesion factor of 0.7 - 0.85. Survey of highway accidents involving heavy vehicles in Canada revealed that nearly 77% of rollover accidents occurred on dry pavement, and could be classified as maneuver induced rollovers [85].

In this chapter, different types of heavy vehicles commonly used in Canada are reviewed. An analysis of rollover mechanics of heavy vehicles is conducted to derive roll

instability criteria of heavy vehicles in steady cornering and transient directional maneuvers. Roll instability measures defined on the basis of relative and absolute roll instabilities are presented.

2.2 CLASSIFICATION OF HEAVY VEHICLES

Commercial freight vehicles are designed with a wide range of weights, dimensions and design configurations ranging from straight trucks to triple trailer combinations, which in general consist of a towing or lead unit, hitches, and one or more towed units. Constraint forces and moments between the towing and towed units are transmitted through the hitches or coupling mechanisms. Table 2.1 illustrates different types of coupling mechanisms commonly used in articulated heavy vehicles. The towing unit can be a truck or a tractor. The connection between various units within a configuration is obtained through a hitch mechanism. Each of the hitch mechanism provides different constraints on the relative motions between the units. The fifth wheel permits relative yaw and pitch motions between the lead and trailing units, which exhibits stiff characteristics in the roll mode. The kingpin-type connection permits only relative yaw motions between the units. In the case of pintle hook connection, the trailing unit is permitted to roll, bounce, yaw, and pitch with respect to the lead unit.

Dollies are used for additional trailers in a double or triple combination. Commonly used dollies, referred to as A-dolly and C-dolly configurations, are illustrated in Figure 2.1. An A-dolly is a conventional single-drawbar dolly, which connects the first semi-trailer with a single pintle hitch to the second trailer with a fifth wheel (converted or turntable coupling). Thus an A-dolly permits yaw motion between the dolly and the first

trailer, and is considered as a weak roll-coupling mechanism. C-dollies, on the hand, practically eliminate relative yaw motion between the first trailer and the dolly through the use of rigid double drawbars and two pintle hitch connections. They also provide large roll stiffness between the first trailer and the dolly. Although there exists a variety of modified A- and C-dollies, their essential features remain the same. The towed unit in a heavy vehicle combination can be a semi-trailer, full trailer or B-type semi-trailer.

Table 2.1: Heavy vehicle units and coupling mechanisms.

Towing Units	Hitches	Towed Units
<ul style="list-style-type: none"> • Truck • Tractor 	<ul style="list-style-type: none"> • fifth wheel • Pintle hook • King pin • A-dolly • C-dolly 	<ul style="list-style-type: none"> • Semi-trailer • Full trailer • B-type semi-trailer

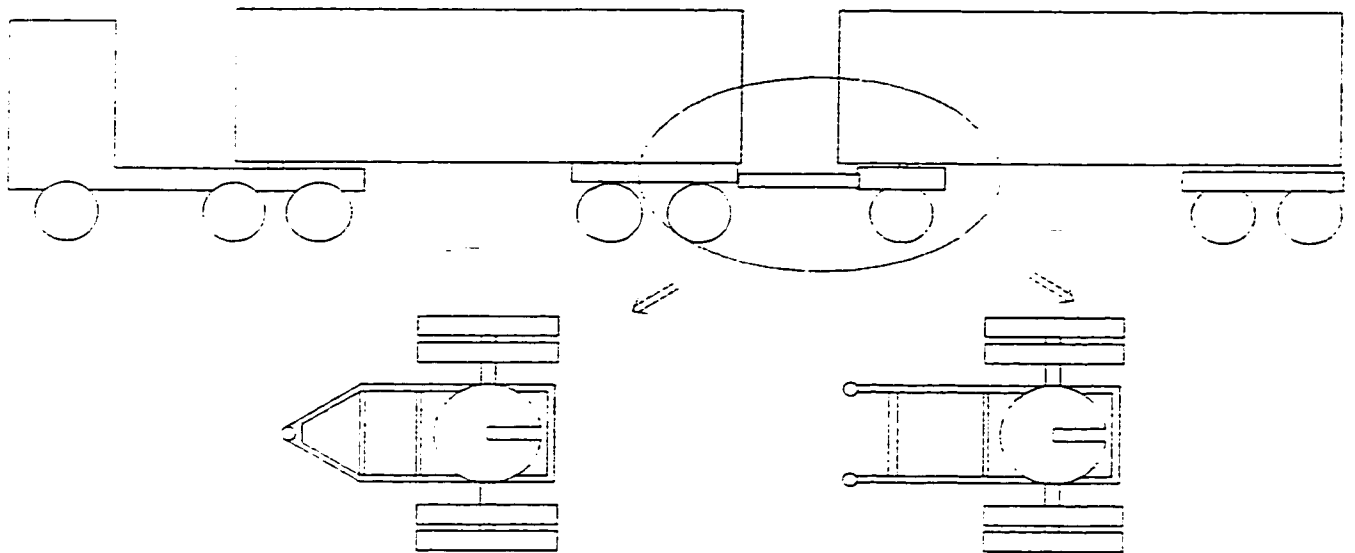


Figure 2.1: Schematics of single drawbar A-dolly and double draw-bar C-dolly.

A survey of the truck population in Canada revealed that seven generic families of heavy vehicles could be defined based on the number of trailers and coupling methods, as shown in Table 2.2 [86]. The schematic of each family of heavy vehicles is illustrated in Figure 2.2. The survey reported that approximately 77% of all heavy combination vehicles operating in Canada are tractor semitrailers, while 17% are A-train doubles, 5% are B-train doubles, and the remaining 1% are C-train triples. Among the types of heavy vehicles, only a straight truck has no articulation point involved, and can be considered as a single roll unit. For articulated heavy vehicles, articulation mechanisms have significant influence on directional response characteristics of such vehicles. It is thus very important to classify heavy vehicle combinations into complete roll units. A complete roll unit is a single unit or a combination of units that are not roll-coupled with other units. A tractor semi-trailer combination can thus be considered as an independent roll unit. An articulated heavy vehicle with A-dolly, however, should be considered as separated roll units due to weak roll stiffness of A-dolly. The rollover limits of articulated heavy vehicles are determined by the unit with the lowest roll stability limit. The last column in the table lists the number of roll units within a combination for the seven families of heavy freight vehicles.

A survey of rollover accidents involving heavy freight vehicles, conducted in western Canada, revealed that 17.6% of all tractor-semitrailer accidents were associated with vehicle rollover, and the corresponding percentages of accidents involving A-, B- and C-train combinations were reported as 34.2%, 9.0% and 31.3%, respectively [87]. Table 2.3 summarizes the distribution of highway accidents involving different vehicle configurations and cause factors. As shown, the highest percentage of single vehicle

accidents is categorized under rollover. It accounts for almost 23% of all heavy vehicle accidents. The accident data further reveal that A-train and C-train combinations roll over more frequently than other types of heavy vehicles. Although the rollover rate for tractor semitrailers is not as high as A-train and C-train combinations, the total rollover accidents involving tractor semi-trailer combinations can not be overlooked due to the large number in use in Canada. The roll stability analysis and open-loop rollover control is thus emphasized for the tractor semi-trailer combination in the later chapters.

Table 2.2: Generic families of heavy vehicles.

Combination	Towing Unit	Hitches	Towed Units	No. of roll units
Straight trucks	truck	N/A	N/A	1
Tractor semi-trailers	tractor	fifth wheel	semi-trailer	1
A-train doubles	tractor	fifth wheels, A-dolly	semi-trailers	2
B-train doubles	tractor	fifth wheels	B-type semi-trailer, semi-trailer	1
C-train doubles	tractor	fifth wheels, C-dolly	semi-trailers	1
A-train triples	tractor	fifth wheels, A-dollies	semi-trailers	3
C-train triples	tractor	fifth wheels, C-dollies	semi-trailers	1

2.3 MECHANICS OF VEHICLE ROLLOVER

2.3.1 Single Axle Representation

The mechanism of vehicle rollover during turning maneuvers can be illustrated through a static roll analysis of a suspended vehicle. Figure 2.3 illustrates a heavy vehicle lumped in a single roll plane prior to wheel lift-off. The combined weight of the sprung and unsprung masses is represented by W , at a height h above the ground. The roll angle ϕ is assumed small, and the vehicle is assumed to roll about a point on the ground plane. When the vehicle is subjected to a steering maneuver, the primary overturning moment is

caused by the lateral acceleration a_y that acts on the sprung mass. As the vehicle rolls about a point in the ground plane, the vehicle's center of gravity (c.g.) is displaced laterally thus gives rise to an additional moment due to the lateral displacement. In response to the overturning moments, a stabilizing moment is generated through transfer of vertical load from the inside tires to the outside tires. For small angle ϕ , the moment equilibrium equation can thus be written as:

$$(FR - FL)T = Wha_y + Wh\phi \quad (2.1)$$

where FR and FL are the vertical tire loads, which can be expressed in terms of tire vertical stiffness k_t :

$$FR - FL = 2k_t T \phi \quad (2.2)$$

Thus the relationship between the lateral acceleration and roll angle of the vehicle is derived as:

$$a_y = \left(\frac{2k_t T^2}{Wh} - 1 \right) \phi \quad (2.3)$$

Equation (2.3) reveals a linear relationship between lateral acceleration a_y and vehicle roll angle ϕ . This relationship can be considered valid as long as the tire-road contact is maintained. As the lateral acceleration increases, the stabilizing moment $(FR-FL)T$ increases until the tire load FL approaches zero, which is referred to as the wheel lift-off position. The maximum stabilizing moment is reached at this lift-off position and is equal to WT . Thus the maximum lateral acceleration the vehicle can sustain without suffering a

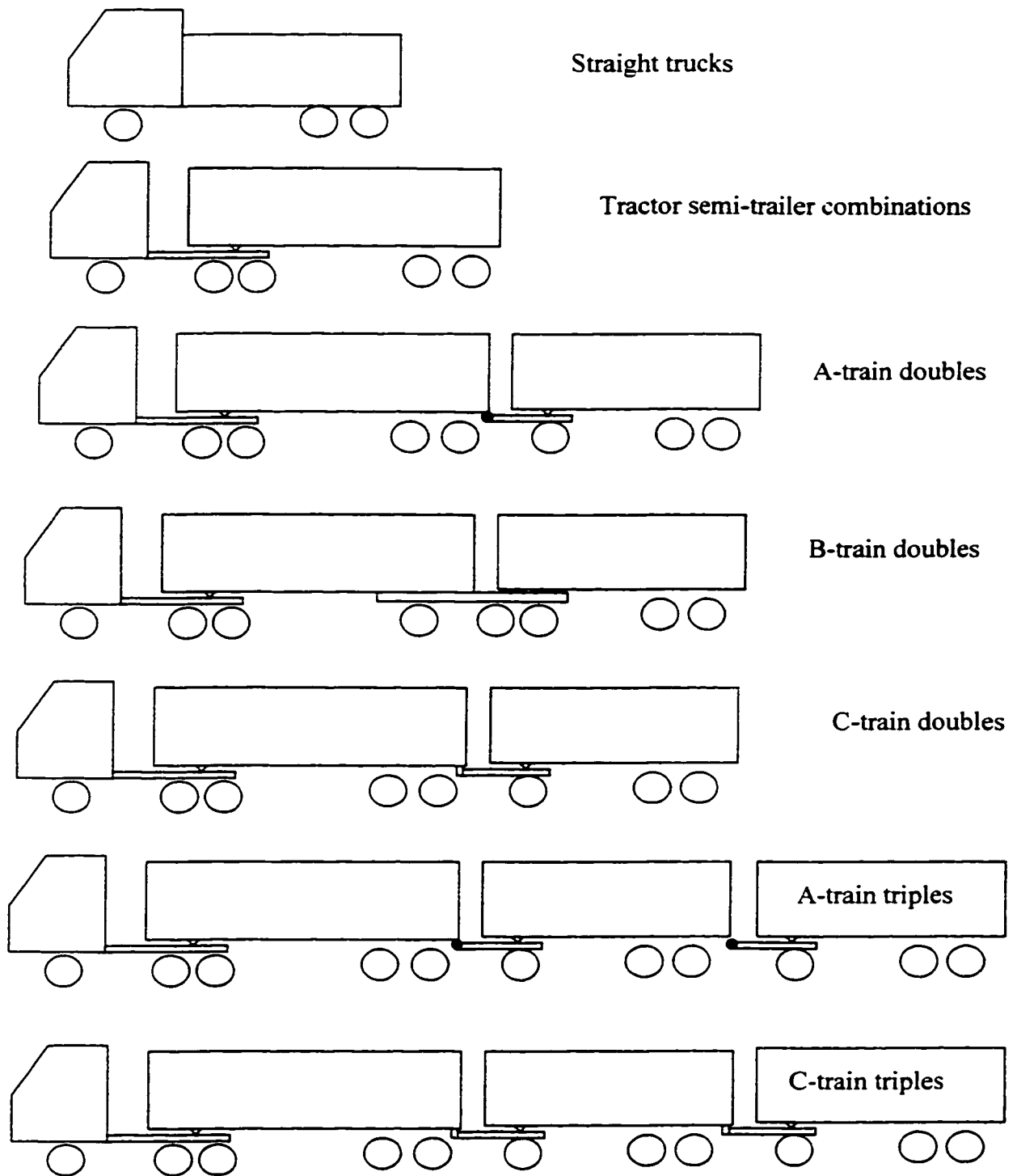


Figure 2.2: Schematics of seven generic families of heavy freight vehicles.

Table 2.3: Distribution of accidents involving heavy vehicles in Western Canada [87].

Configuration	Rollover		Hit Ditch		Third Party		Jackknife		Hit Animal		Driver Error		Equipment Malfunction		Total	
	#	%	#	%	#	%	#	%	#	%	#	%	#	%	#	%
Semi-Trailer	52	17.63%	29	9.83%	134	45.42%	20	6.78%	46	15.59%	10	3.39%	4	1.36%	295	100%
A-Train	80	34.19%	18	7.69%	82	35.04%	19	8.12%	29	12.39%	5	2.14%	1	0.43%	234	100%
B-Train	9	9.00%	14	14.00%	39	39.00%	9	9.00%	23	23.00%	2	2.00%	4	4.00%	100	100%
C-Train	10	31.25%	5	15.63%	8	25.00%	3	9.38%	4	12.50%	2	6.25%	0	0.00%	32	100%
Total	151	22.84%	66	9.98%	263	39.79%	51	7.72%	102	15.43%	19	2.87%	9	1.36%	661	100%

divergent roll response, which is frequently called as static rollover threshold (*SRT*) is obtained from Equation (2.1) as:

$$SRT = \frac{T}{h} - \varphi_0 \quad (2.4)$$

where φ_0 is the vehicle roll angle at the wheel lift-off position.

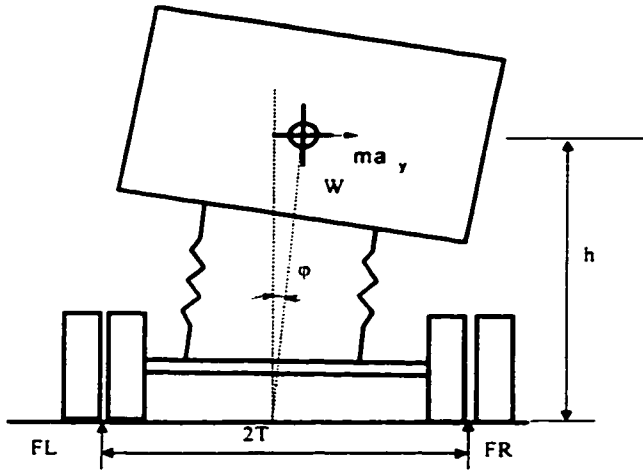


Figure 2.3: Lumped roll plane representation of a heavy vehicle before wheel lift-off.

The center of roll rotation of the vehicle model, considered near the center of vehicle track, can not be considered valid, when one of the wheels loses contact with the ground. As the inner tires of the vehicle lift off the ground, the rotation center of the vehicle is shifted to the contact area between the outer tires and the ground, as shown in Figure 2.4. Assuming that the vehicle has deflected along the roll axle by an angle α after the loss of contact, the moment equilibrium equation about the roll center is obtained as:

$$W a_y (T \sin \alpha + h \cos \varphi) = W (T \cos \alpha - h \sin \varphi) \quad (2.5)$$

where $\varphi = \alpha + \varphi_0$, is the total roll angle of the vehicle. The lateral acceleration can therefore be expressed as:

$$a_y = \frac{T \cos(\varphi - \varphi_0) - h \sin \varphi}{T \sin(\varphi - \varphi_0) + h \cos \varphi} \quad (2.6)$$

Equation (2.6) reveals that a_y decreases as roll angle φ increases in the form of a trigonometric function. The vehicle approaches its tip-over position when the mass center is aligned vertically with the tire-road contact patch. The vehicle roll angle at the tip-over position can be expressed as

$$\varphi = \cot^{-1}[(h - T \sin \varphi_0) / (T \cos \varphi_0)] \quad (2.7)$$

The corresponding lateral acceleration that the vehicle can sustain is reduced to zero.

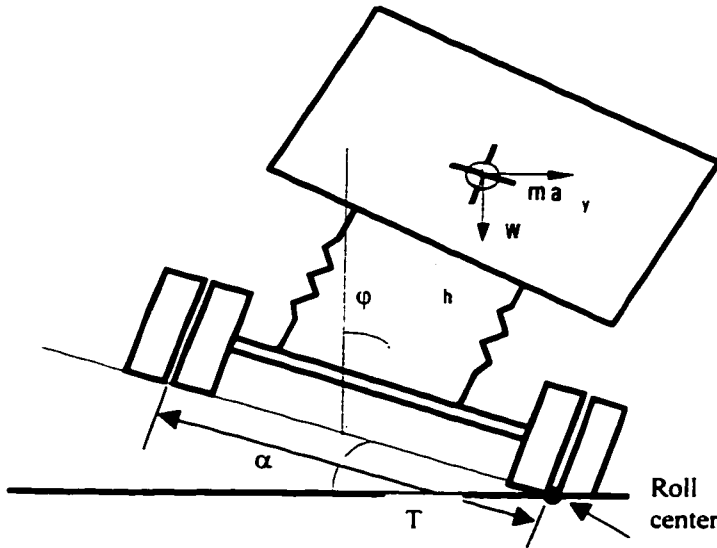


Figure 2.4: Lumped roll plane representation of the vehicle after the loss of wheel-road contact.

The relationship between the lateral acceleration a_y and roll angle φ during the course of static roll response, expressed by Equations (2.3) and (2.6), is illustrated in Figure 2.5. As roll angle φ increases from static position, the lateral acceleration

increases until wheels on a single track lose contact with the ground, which occurs at a roll angle φ_0 . The maximum lateral acceleration that the vehicle can sustain or its static rollover threshold (*SRT*) is derived as the acceleration achieved corresponding to roll angle φ_0 . After wheels lift off the ground, the lateral acceleration decreases with further increase in vehicle roll angle φ . When the vehicle approaches its tip-over position, the vehicle is in a critical equilibrium condition. The presence of a lateral disturbance or perturbation will cause an absolute rollover of the vehicle. The important states of the vehicle during a rollover are thus identified as:

- (1) Under the application of a centrifugal force, the wheels on one side of the vehicle lose contact with the ground surface, which corresponds to the maximum lateral acceleration that the vehicle can sustain without rollover.
- (2) With the continued application of the centrifugal force, the center of gravity of the vehicle approaches the tip-over position, which corresponds to the absolute rollover of the vehicle.

The above two states of vehicle rollover can be defined as *The Relative Rollover Instability*, and *The Absolute Rollover Instability*, respectively.

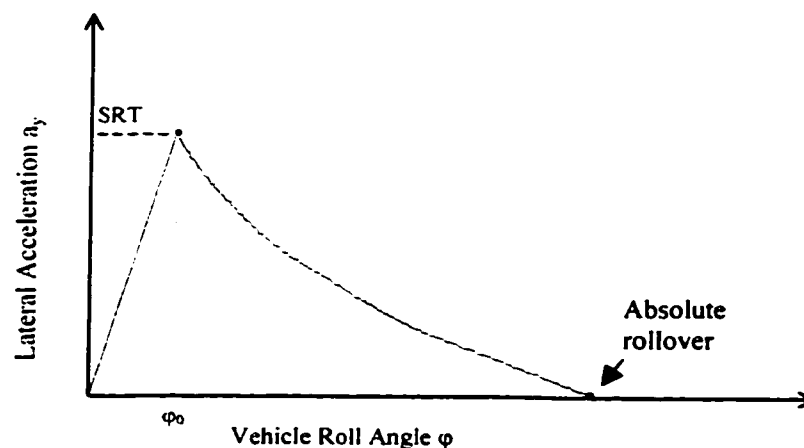


Figure 2.5: Vehicle lateral acceleration and roll angle relationship during the course of rollover.

2.3.2 Multi-Axle Representation

A single axle representation of the vehicle is not adequate for rollover analysis when the various axles possess different roll stiffness characteristics that are not proportional to the static loads supported by the axles [32]. A typical tractor-semitrailer configuration can be represented by a set of three composite axles based upon their suspension characteristics: tractor front axle; an equivalent tractor rear axle realized upon grouping the tandem drive axles; and an equivalent semi-trailer axle realized by grouping all the trailer axles with similar suspension characteristics, as shown in Figure 2.6. It is assumed that the roll axis of the total vehicle is located on the ground plane for analysis simplification. The combined weight of the sprung and unsprung masses is represented by W , with overall c.g. located at a height h above the ground level. The equilibrium equation in the roll plane of the vehicle subjected to a lateral acceleration a_y , can be written as:

$$\sum_{i=1}^3 (FR_i - FL_i) T_i - Wh\phi = Wha_y \quad (2.8)$$

where FR_i and FL_i are vertical loads acting on the tires of axle i ($i=1$ to 3), and T_i is half track width of axle i . Let W_i be the load carried by each of the three composite axles, the maximum roll resisting moment that is produced by each axle can then be derived as $W_i T_i$ ($i=1$ to 3). Depending upon the roll stiffness of each axle, the lift-off of tires on one side of the axles takes place at different roll angles. Figure 2.7 illustrates the roll resisting moment produced by each axle as a function of roll displacement of the vehicle. The lift-off of tires on the trailer axles occurs at a relatively small roll angle of the vehicle ϕ_3 , followed by lift-off of the tires on tractor rear axles (ϕ_2). The lift-off of the tires on the

front axle occurs at a relatively large roll angle (ϕ_1) of the vehicle due to its low roll stiffness. The overturning moment produced by the lateral shift of c.g. of the vehicle is also shown in the figure by a line with negative slope. The sum of all the roll resisting moments and the overturning moment represents the left side of Equation (2.8), referred to as net roll moment.

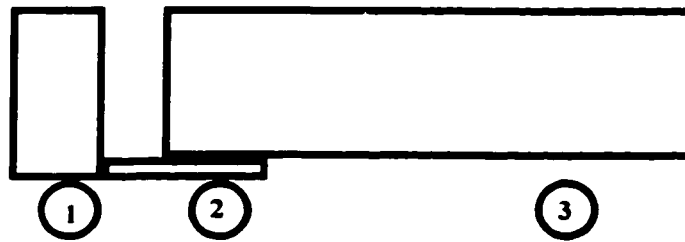


Figure 2.6: Three composite axle representation of a multi-axle tractor semi-trailer vehicle.

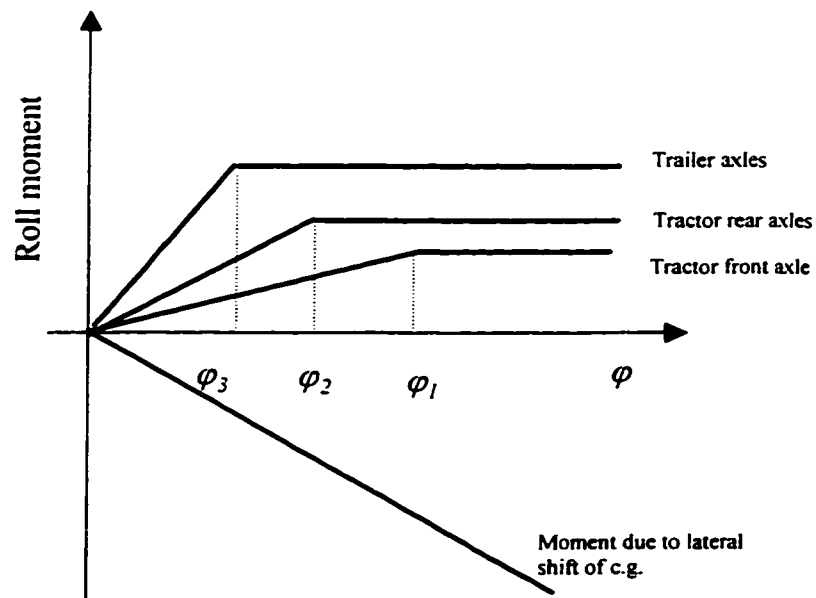


Figure 2.7: Roll moments versus roll angle for the three composite axle vehicle.

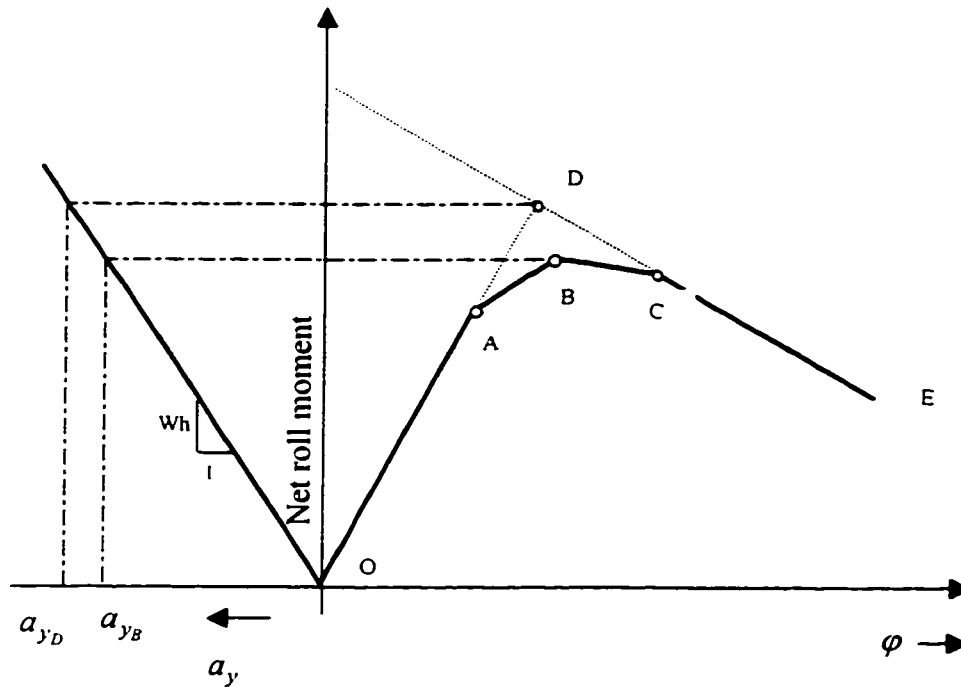


Figure 2.8: Net roll moment versus roll angle for the three-axle vehicle representation.

The net roll resisting moment versus the roll angle of the vehicle is shown in Figure 2.8. The points A, B, and C indicate the lift-off of tires on the trailer axles, the tractor rear axles, and the tractor front axle, respectively. The maximum value for the net roll-resisting moment is reached when the tires on the tractor rear axle lift off the ground (point B). The roll moment due to the lateral force is also illustrated in the left half of the figure as a function of a_y . The static rollover threshold of the vehicle as determined from the net moment diagram is a_{y_B} . Thus the relative rollover condition of the vehicle is reached as tires on the trailer and tractor's rear axles lift off the road surface. If the roll properties of all the axles were to be lumped together and represented by a single axle, the

net roll moment versus roll angle plot would follow the curve ODE, as shown in Figure 2.8. Such analysis for this vehicle will predict a rollover threshold a_{y_D} , which is greater than a_{y_B} . Thus the single roll plane representation tends to overestimate the anti-roll ability of multi-axle freight vehicles.

2.4 CRITERIA FOR HEAVY VEHICLE ROLLOVER

The analysis of rollover mechanics for a steady turning maneuver reveals that the roll instability of a heavy vehicle could be considered to occur in two different forms in terms of severity: (i) *Relative Roll Instability*; and (ii) *Absolute Roll Instability*. The relative roll instability is associated with maximum lateral acceleration which the vehicle can sustain without rollover in steady turning maneuvers. The absolute roll instability, on the other hand, is associated with the maximum roll angle of the vehicle where it has zero tolerance to lateral acceleration excitation. These rollover instability criteria along with measures corresponding to each criterion are discussed in the following subsections.

2.4.1 Definition of Roll Instability

Relative Roll Instability

When a vehicle can not remain stable under the action of a constant level of lateral force, the vehicle is said to be in a relatively unstable condition. The corresponding maximum lateral acceleration of the vehicle, realized during a steady turn maneuver, is referred to as the static rollover threshold. The relative rollover condition can be reached when tires on a single track of a vehicle lose road contact, as illustrated by the single-axle representation of heavy vehicles. For a multi-axle representation, the relative rollover

condition may be reached when tires on one or two axles lose road contact, depending on roll stiffness distributions of the vehicle. The existence of *Relative Instability* in a dynamic maneuver, however, does not imply definite occurrence of an actual rollover of the vehicle. Such relative instability can lead to an actual rollover, only if a sustained level of lateral acceleration is attained for a period of time, until an absolute instability is attained.

Absolute Roll Instability

The absolute roll instability of the vehicle occurs at tip-over, when center of mass of the vehicle aligns vertically above the effective contact region of the outer tires with the road. The existence of a lateral disturbance or perturbation will then lead to an actual rollover of the vehicle. Thus an actual rollover of a vehicle happens in the time sequence of first reaching the relative rollover condition, followed by an absolute rollover condition. Since the vehicle c.g. is considerably higher at tip-over than at lift-off, sufficient work must be done on the vehicle to bring the vehicle to its absolute instability position.

2.4.2 Measures Based upon Relative Rollover Criterion

Various measures describing both static and dynamic roll stability characteristics of heavy vehicles have been proposed [41, 42, 43, 45]. These measures proposed for assessment of rollover propensity and rollover detection can be classified on the basis of the above proposed roll instability criteria. Rollover measures based upon relative rollover criterion can be summarized as follows.

(1) Load Transfer Ratio (LTR)

Relative roll instability can be numerically evaluated using the non-dimensional overall load transfer ratio (*LTR*), defined as:

$$LTR = \frac{\left| \sum_{i=1}^n (FL_i - FR_i) \right|}{\sum_{i=1}^n (FL_i + FR_i)} \quad (2.9)$$

where FL_i and FR_i are normal loads acting on the left- and right- wheels, respectively, of the equivalent axle i , and n is the total number of axles used for a complete roll unit. The *LTR* has been proposed as a measure to assess dynamic roll stability of heavy vehicles in North America [45, 86]. It has been proposed that the relative dynamic roll stability of heavy vehicles can be assessed from the *LTR* evaluated during a path change maneuver conducted at 100 km/h, which yields a lateral acceleration response of approximately 0.15g at the c.g. of the towing unit. The trajectory of the path change maneuver is illustrated in Figure 2.9. The target value of load transfer ratio has been recommended as 0.6 [45].

The *LTR* during a directional maneuver approaches the unity value when all the wheels of the vehicle on a single track lose road contact. The overall *LTR* approaching 1 does not necessarily indicate the relative rollover condition, which may be realized with lift-off of one or more axles depending upon axle loading and axle suspension characteristics. Furthermore, variations in the design parameters of heavy vehicles may yield considerable variations in the overall *LTR* corresponding to relative rollover condition. Since there is no unique value of the overall *LTR* corresponding to relative rollover condition, the overall *LTR* is not considered as a good indicator of the relative roll instability.

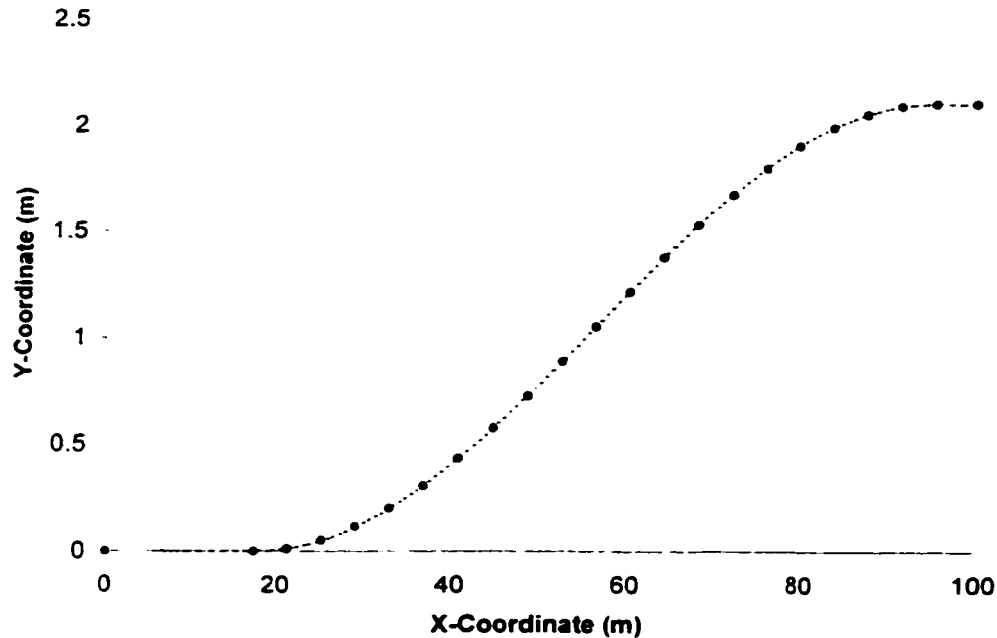


Figure 2.9: Path trajectory of a vehicle during a path change maneuver to assess *LRT*.

(2) Rearward Amplification Ratio (*RAR*)

Under high-speed evasive maneuvers, the articulated vehicles in general exhibit considerably larger lateral and roll motion response of the rearmost unit when compared to that of the lead unit. This phenomena is characterized by the rearward amplification ratio (*RAR*), defined as the ratio of the peak lateral acceleration response of the rearmost trailer to that of the lead unit [86-87]. This ratio describes the vehicle characteristics in amplifying the severity of the maneuver initiated at the lead unit. A large value of *RAR* portends an increased likelihood of rollover of the rearmost trailer. The *RAR* ratio may thus be considered as a measure of dynamic rollover. It has been proposed that the

rearward amplification factor of a combination vehicle subject to a path change maneuver, described in Figure 2.9 must not exceeded a value of 2.2 [45].

(3) Static Stability Factor (SSF)

This factor is proposed to estimate the rollover propensity of heavy vehicles by neglecting the compliance due to suspension and tires (rigid vehicle). The loss of wheel-road contact in such a rigid vehicle occurs at extremely low roll angles. The relative rollover condition can thus be satisfied when the vehicle roll angle is nearly zero. Let $\phi_0 \approx 0$, Equation (2.4) yields a measure of rollover propensity of a rigidly suspended vehicle referred to as Static Stability Factor (*SSF*), and given by:

$$SSF = \frac{T}{h} \quad (2.10)$$

The static stability factor is a function of effective wheel track width and c.g. height of the vehicle. While effective track width of the vehicle is mostly limited by the weights and dimension laws and designs, the c.g. height may vary considerably due to excessive variations in loading and load distributions. *SSF* is frequently employed to achieve a quick and conservative estimate of roll stability limit of a vehicle. A statistical analysis of vehicle rollover accidents conducted by Klein [41] reported that *SSF* closely correlates with actual rollover frequencies of road vehicles. Vehicles with lower *SSF* limits exhibit higher tendency of rollover. Heavy vehicles, however, possess highly complex compliant characteristics due to nonlinear force-deflection or moment-deflection properties of suspension, tire and structure. The heavy vehicles thus exhibit roll instability at a lateral acceleration considerably lower than *SSF*. Piché [10] investigated rollover limits of a tractor semi-trailer combination with different suspension and tire properties. A

compliance factor of 0.72 was proposed to account for reduction in the rollover threshold of the vehicle caused by compliance of different suspension springs and tires.

(4) Static Rollover Threshold (SRT)

The rollover propensity of a heavy vehicle is described quantitatively by its *static rollover threshold (SRT)*, defined as the level of steady lateral accelerations, which the vehicle can sustain without suffering a divergent roll response [32]. From various accident databases, it has been established that vehicles with low values of *SRT* are more likely to rollover than those with relatively high *SRT* [33]. A lower limit of 0.35g has been proposed for *SRT* of commercial freight vehicles to minimize the highway safety risks associated with potential roll instabilities. The recommended limit was further adopted as a performance measure by the Road and Transport Association of Canada (*RTAC*). Static rollover threshold can be evaluated in several ways, such as road, tilt-table and pull tests, and analytical methods.

Evaluations through road tests require full scale testing involving outriggers to ensure driver and vehicle safety. The road tests, however, are expensive due to requirements of extensive instrumentation, data acquisition and analysis, and installation of outriggers. Such tests exhibit poor repeatability and alter the inertial properties of the vehicle and compliant properties of the suspension due to added outriggers [44].

A tilt table test leads to a rollover measure defined as *Tilt Table Ratio*. The tests performed on a tilt-table attempt to simulate a steady lateral acceleration field which the vehicle could experience during a steady cornering maneuver by inclining the test vehicle in the roll direction. This causes components of the gravity force to act along the lateral as well as the vertical directions. The angle of table inclination (ϕ) is slowly increased until

the vehicle approaches relative rollover condition. The static lateral acceleration or rollover threshold in g units is then derived as $\tan\phi$. Tilt table tests do not require any additional measurements, and is known to be a highly efficient and inexpensive test method of assessment, which minimizes the risk of vehicle damage. The tilt table test method, however, has been criticized since it does not accurately represent a vehicle in a steady lateral acceleration field, caused by steady state cornering. As the table inclination angle increases, vertical force acting on the vehicle decreases. This results in variation in vehicle's cg height, and thus influences its "rollover threshold".

A side pull test may also be performed to assess static roll stability of a vehicle. A side pull simulates a cornering induced lateral acceleration field by applying a horizontal force at the total vehicle center of gravity. The rollover metric obtained is called *Side Pull Ratio*. The side pull test, however, requires a prior knowledge of the c.g. height of the vehicle, and poses relatively higher risk of vehicle body damage. Alternatively, relative roll instability or static rollover threshold (*SRT*) of a vehicle can be analyzed using analytical methods. A large number of analytical or computer simulation tools have been reported in the literature [25-34]. While all the test methods may be costly and time consuming, the computer simulation approach is widely recognized as an alternative in evaluation of rollover propensity of heavy vehicles. Simulation approach, however, poses many complexities associated with identification and characterization of nonlinear properties of several vehicle subsystems such as suspensions, tires and dollies.

2.4.3 Measures Based on Absolute Rollover Criterion

Three different measures defined on the basis of absolute roll instability criterion are proposed for analysis of rollover propensity of vehicles in dynamic tripped rollover situation.

(1) Rollover Prevention Energy Reserve (RPER)

Rollover Prevention Energy Reserve is proposed to study vehicle tripped rollover propensity, defined as the difference between the energy required to bring the vehicle to its tip-over position and the rotational kinetic energy of the vehicle, which can be transferred into gravitational potential energy to lift the vehicle [88]. From this definition, the *RPER* can be expressed as:

$$RPER = V_{tip} - T_k \quad (2.11)$$

where V_{tip} is the difference between gravitational potential energy with the vehicle in its present position, and gravitational potential energy of the vehicle corresponding to its tip-over position. T_k is total kinetic energy which can be transferred into gravitational energy. The value of the *RPER* function approaches a negative value before a vehicle approaches its tip-over position in a rollover case, but always remains positive in a non-rollover case.

Two different approaches are proposed to compute the total kinetic energy of the vehicle (T_k). In the first approach, kinetic energy associated with rollover motion consists of two terms associated with angular and lateral velocities:

$$T_{k1} = \frac{I}{2} \omega^2 + \frac{1}{2} m V_y^2 \quad (2.12)$$

where I_{cr0} is roll mass moment of inertia of the vehicle about the roll center located at the center of outer tire-road contact patch. I_{cr0} , corresponding to tip-over position, can be derived from:

$$I_{cr0} = I_{cx} + m(T^2 + h^2) \quad (2.13)$$

where I_{cx} is roll mass moment of inertia of the vehicle about its mass center, m is vehicle mass. ω is roll velocity and V_y is lateral velocity of the vehicle. T denotes half wheel track, and h represents vehicle c.g. height above the ground in static equilibrium condition. The first term in Equation (2.12) represents vehicle rotational energy, while the second term denotes the vehicle translational energy, which may be transformed into rotational kinetic energy during rollover motion.

In the second approach, vehicle kinetic energy is calculated in a more conservative fashion by excluding the translational energy:

$$T_{k2} = \frac{1}{2} I_{cr0} \omega^2 \quad (2.14)$$

The applications of total kinetic energy functions, presented in Equations (2.12), (2.14) yield two rollover prevention energy reserve functions, given by:

$$\begin{aligned} RPER_1 &= V_{tip} - T_{k1} \\ RPER_2 &= V_{tip} - T_{k2} \end{aligned} \quad (2.15)$$

The subscripts '1' and '2' in the above equation refer to the functions derived using two approaches based upon T_{k1} and T_{k2} . Reported experimental studies have concluded that $RPER_1$ could be employed to achieve reasonable prediction of tripped rollover of vehicles under mild-to-moderate impacts, while $RPER_2$ provides more reliable measure

of tripped rollover under the most severe impacts. The function $RPER_2$ is thus considered as a generally applicable rollover prediction function [88].

(2) Rollover Prevention Metric (RPM)

The rollover prevention metric is defined as the difference between the initial lateral translational kinetic energy before the impact and rotational kinetic energy after the impact divided by the initial energy, and expressed as:

$$RPM = \frac{T_0 - T_1}{T_0} \quad (2.16)$$

where:

$$T_0 = \frac{1}{2} m V_y^2; \quad \text{and} \quad T_1 = \frac{1}{2} \frac{m^2 V_y^2 h^2}{I_{xx0}} \quad (2.17)$$

Substituting for initial translational (T_0) and final rotational energy after the impact (T_1) into (2.16) yields:

$$RPM = 1 - \frac{m}{I_{xx} + m(SSF + 1)} \quad (2.18)$$

where $SSF = T/h$, as shown in Equation (2.10). Equation (2.18) reveals that RPM is a function of vehicle mass, roll mass moment of inertia and static stability factor (SSF). The results from Hinch [43] revealed that RPM has a very good correlation with rollover rates of light vehicles.

(3) Critical Sliding Velocity (CSV)

The critical sliding velocity is a measure of the minimum lateral velocity required to initiate a rollover in a tripped rollover situation. CSV is determined by equating vehicle energy prior to a tripped impact with the energy that is required to raise the vehicle c.g. to

its tip-over position [44]. Conservation of angular momentum about the tripped point can be written as:

$$mV_s h = I_{xx0} \dot{\theta}_0 \quad (2.19)$$

where V_s is the vehicle sliding velocity before impact, and $\dot{\theta}_0$ is the initial rotational speed of the vehicle about tripped point after the impact. The minimum rotational energy to bring the vehicle to tip-over position is given by:

$$\frac{I}{2} I_{xx0} \dot{\theta}_0^2 = mg(\sqrt{h^2 + T^2} - h) \quad (2.20)$$

Critical sliding speed (CSV) can thus be derived from Equations (2.13), (2.19) and (2.20) as:

$$CSV = V_s = \sqrt{2gh \left[\frac{I_{xx}}{mh^2} + SSF^2 + 1 \right] (\sqrt{SSF^2 + 1} - 1)} \quad (2.21)$$

Equation (2.21) reveals that critical sliding velocity is a function of mass, roll mass moment of inertia, c.g. height and static stability factor (SSF).

2.5 SUMMARY

Different configurations of heavy vehicles that are commonly used in Canada, together with their rollover propensity based on accident statistics are reviewed. The number of complete roll units for seven generic families of heavy freight vehicle combinations is identified on the basis of roll coupling mechanisms, which is essential for modeling and analysis of impending rollover of heavy freight vehicles in later chapters. Rollover mechanics of heavy vehicles are analyzed for single-axle and multi-axle configurations in order to derive criteria for relative and absolute roll instabilities of

heavy vehicles. The relative and absolute roll instability criteria are proposed and defined to characterize roll instability of different severity. The reported rollover measures in the literature are categorized on the basis of roll instability criteria such that their function scopes are clearly positioned. These measures are thoroughly examined in the following chapters to identify their potential for detecting an impending rollover under a wide range of operating conditions. Additional measures of rollover are further proposed to enhance the reliability and lead time of the rollover prediction.

CHAPTER 3

DETECTION OF RELATIVE ROLL INSTABILITY IN STEADY TURNING MANEUVERS

3.1 INTRODUCTION

Rollover of heavy vehicles frequently occurs during low speed cornering and high speed directional maneuvers. Detection and early warning of impending roll instability of heavy vehicles in such maneuvers is vital to ensure the safety of the vehicle, driver and the highway. The detection of roll instability for the generation of an early warning, however, cannot be realized upon absolute roll instability criterion, since sufficient lead time for driver actions cannot be ensured. Furthermore, the loss of tire-road contact during a directional maneuver may be considered undesirable in view of the need to maintain directional stability and control of the vehicle. Relative roll instability criterion may thus be considered appropriate for early detection of roll instability of heavy vehicles.

Freight vehicle combinations comprise different numbers of multi-axle units, where the suspension properties and loading conditions for each axle may differ considerably. The roll response characteristics of different unsprung masses of the vehicle subject to a directional maneuver may thus vary considerably. Under a severe directional maneuver, the loss of tire-road contact may initially occur with wheels on one of the axles, which may then be followed by the loss of contact between the road and wheels on another axle. The relative roll instability criterion does not necessarily imply that all the wheels on a single-track lift off the road surface. In typical designs of tractor semi-trailer

combinations. for example, the tractor front axle supports relatively less load than the tractor's rear and trailer axles. The effective vertical spring rate of the front axle suspension is also lower than those of the tractor's rear or trailer axles. The relative roll instability in general is initialized, when tires on the tractor's rear and semi-trailer axles lose contact with road surface, although the front wheels of the tractor may still retain the road contact. For straight trucks and full trailers, the sufficient condition for the relative instability may be reached when wheels on either all the axles or only one axle lift-off the ground, depending on the vehicle configurations, suspension designs and loading conditions. For evaluation of heavy vehicle roll stability performance, it is necessary to identify the relative rollover conditions, which may vary based on vehicle configurations.

In this chapter, relative roll instability conditions and static rollover threshold of different heavy vehicle configurations are evaluated under steady cornering maneuvers through development and analysis of static roll plane models. A parametric sensitivity study is carried out to identify the influence of an array of vehicle and suspension configurations on *SRT* and relative rollover conditions of tractor semi-trailer combinations, B- /C- doubles.

3.2 DEVELOPMENT OF ROLL PLANE MODELS OF DIFFERENT COMBINATIONS

The rollover propensity of heavy vehicle combinations is strongly dependent upon vehicle configuration, axle loads, weight distribution, vehicle roll stiffness, suspension properties, etc. Detection of impending vehicle rollover necessitates analysis of vehicle rollover propensity and relative rollover conditions for different configurations. While the

simplified roll plane models presented in Chapter 2 can qualitatively illustrate roll instabilities, they appear to be too coarse for the detection of relative rollover conditions of heavy vehicles with different suspension, tire properties, and hitch mechanisms. A large number of static roll analysis models have been proposed in the literature [25, 33, 34, 39], to derive the static rollover threshold limits of the vehicle. Such models, however, do not emphasize the dependence of rollover propensity on the configurations, and can not be employed to detect the relative rollover condition, and thus the onset of roll instabilities. Roll plane models for various configurations, such as straight trucks or full trailers, tractor semi-trailers, and A-, B-, and C- doubles are thus developed to evaluate their relative roll instability conditions. The analytical models together with the associated simplifying assumptions are discussed in the following sections.

3.2.1 Roll Plane Analysis of Straight Trucks and Full Trailers

Two-axle representation of heavy vehicles such as straight trucks and full trailers can be realized by grouping the front and the rear axles into their respective single composite axles, as shown in Figure 3.1. The roll center height of sprung mass h_R , measured from the c.g. location of the sprung mass, is considered to be constant and the roll center of unsprung mass i ($i=1, 2$) is assumed to coincide with its c.g. location. The destabilizing moments in the roll plane include those due to the centrifugal forces acting through the c.g. of the sprung and unsprung masses, and that due to the lateral displacement of the sprung mass center of gravity. The vertical load transferred from the inside to the outside tires during cornering generates a stabilizing roll moment. The rollover propensity of the entire vehicle can be derived from its roll plane model

illustrated in Figure 3.1. The roll moment equilibrium may be further analyzed to derive an analytical relationship between the sprung mass roll angle φ_s and the lateral acceleration a_y . Assuming small roll angles, the internal roll moment M_I between the sprung and unsprung masses can be written as:

$$M_I = m_s h_R (g \varphi_s + a_y) \quad (3.1)$$

which is balanced by the restoring moment M_R generated by the front and rear axle suspensions:

$$M_R = K_{\varphi 1} (\varphi_s - \varphi_{u1}) + K_{\varphi 2} (\varphi_s - \varphi_{u2}) \quad (3.2)$$

where φ_{ui} is the roll angle of unsprung mass i ($i=1, 2$), and $K_{\varphi i}$ is the roll stiffness of axle suspension i . Equations (3.1) and (3.2) yield:

$$\begin{bmatrix} K_{\varphi 1} + K_{\varphi 2} - m_s g h_R & -m_s h_R \end{bmatrix} \begin{bmatrix} \varphi_s \\ a_y \end{bmatrix} = \begin{bmatrix} K_{\varphi 1} & K_{\varphi 2} \end{bmatrix} \begin{bmatrix} \varphi_{u1} \\ \varphi_{u2} \end{bmatrix} \quad (3.3)$$

The moment equilibrium equations for the unsprung masses can be written as:

$$M_I + m_s q_1 h_{ci} a_y + m_{ui} h_{ui} a_y + m_s g q_1 z_{Ri} \varphi_{ui} = (FR_i - FL_i) T_i ; \quad i=1, 2 \quad (3.4)$$

where $q_1 = (L - a) / L$, $q_2 = a / L$, and h_{ui} is the c.g. height of the unsprung mass i . h_{ci} is the roll center height of suspension i . $z_{Ri} = h_{ci} - h_{ui}$, is the vertical distance between the suspension roll center and the unsprung mass roll center, and T_i is the effective half wheel track width of axle i . Assuming that the internal roll moment M_I is proportionally distributed between the axle suspensions in terms of their roll stiffness, the roll moment acting on axle i ($i=1, 2$) can be expressed as:

$$M_i = M_I K_{\varphi i} / (K_{\varphi 1} + K_{\varphi 2})$$

$$M_2 = M_I - M_I \quad (3.5)$$

The restoring forces due to tires on the right and left tracks of axle i (FR_i and FL_i) can be derived from effective vertical stiffness of tires. Assuming linear vertical force-deflection characteristics of tires about the operating point, the vertical forces developed due to tires are expressed as:

$$\begin{aligned} FR_i &= k_{ii} [0.5(m_s q_i + m_{ui})g / k_{ii} + T_i \varphi_{ui}] \\ FL_i &= k_{ii} [0.5(m_s q_i + m_{ui})g / k_{ii} - T_i \varphi_{ui}]; \quad (i=1, 2) \end{aligned} \quad (3.6)$$

where k_{ii} is the linear vertical stiffness of the tire on axle i . In case of dual tires, k_{ii} is the total vertical stiffness of the dual tires. Substituting Equations (3.1), (3.5) and (3.6) into (3.4), the following relationship between the roll angles and lateral acceleration can be established:

$$\begin{bmatrix} \varphi_{u1} \\ \varphi_{u2} \end{bmatrix} = \begin{bmatrix} a_{11} & a_{12} \\ a_{21} & a_{22} \end{bmatrix} \begin{bmatrix} \varphi_s \\ a_y \end{bmatrix} \quad (3.7)$$

where

$$\begin{aligned} a_{11} &= \frac{K_{\varphi 1} m_s g h_R}{(K_{\varphi 1} + K_{\varphi 2})(2k_{t1} T_1^2 - m_s g z_{R1} q_1)} \\ a_{21} &= \frac{K_{\varphi 2} m_s g h_R}{(K_{\varphi 1} + K_{\varphi 2})(2k_{t2} T_2^2 - m_s g z_{R2} q_2)} \\ a_{12} &= \frac{a_{11}}{g} \left[1 + \frac{(m_s h_{c1} q_1 + m_{u1} h_{u1})(K_{\varphi 1} + K_{\varphi 2})}{m_s h_R K_{\varphi 1}} \right] \\ a_{22} &= \frac{a_{21}}{g} \left[1 + \frac{(m_s h_{c2} q_2 + m_{u2} h_{u2})(K_{\varphi 1} + K_{\varphi 2})}{m_s h_R K_{\varphi 2}} \right] \end{aligned}$$

A direct relationship between a_y and φ_s can thus be derived from Equations (3.3) and (3.7) as:

$$a_y = \frac{K_{\varphi 1} + K_{\varphi 2} - m_s g h_R - K_{\varphi 1} a_{11} - K_{\varphi 2} a_{21}}{m_s h_R + K_{\varphi 1} a_{12} + K_{\varphi 2} a_{22}} \varphi_s \quad (3.8)$$

It should be noted that the above relationship can be considered valid until the restoring roll moment saturates. As the wheels of axle i ($i=1$ or 2) lose contact with the road, the restoring roll moment approaches its limiting value, $W_i T_i$. Under such conditions, the relationship between the lateral acceleration and sprung mass roll angle can be derived as follows.

Considering that the tires on one side of axle 2 lose contact with the road, the suspension roll moment acting on the axle can be derived from Equation (3.4):

$$M_2 = K_{\varphi 2}(\varphi_s - \varphi_{u2}) = W_2 T_2 - (m_s q_2 h_{c2} + m_{u2} h_{u2}) a_y - m_s g q_2 z_{R2} \varphi_{u2} \quad (3.9)$$

where $W_2 = (m_s q_2 + m_{u2}) g$. The roll moment due to first axle suspension can be derived from Equation (3.5):

$$M_1 = K_{\varphi 1}(\varphi_s - \varphi_{u1}) = m_s g h_R \varphi_s + (m_s h_R + m_s q_2 h_{c2} + m_{u2} h_{u2}) a_y + m_s g q_2 z_{R2} \varphi_{u2} - W_2 T_2 \quad (3.10)$$

Equations (3.9) and (3.10) are solved to yield the roll angles of unsprung masses as a function of the sprung mass roll angle and lateral acceleration, and expressed as:

$$\begin{aligned} \varphi_{u2} &= \frac{1}{K_{\varphi 2} - m_s g q_2 z_{R2}} [K_{\varphi 2} \varphi_s + (m_s q_2 h_{c2} + m_{u2} h_{u2}) a_y - W_2 T_2] \\ \varphi_{u1} &= \frac{1}{K_{\varphi 1}} [(K_{\varphi 1} - m_s g h_R) \varphi_s - (m_s h_R + m_s q_2 h_{c2} + m_{u2} h_{u2}) a_y + W_2 T_2] \\ &\quad - m_s g q_2 z_{R2} \varphi_{u2} \end{aligned} \quad (3.11)$$

As the tires on axle 2 experience lift-off, the equation of roll moment equilibrium for the entire vehicle can be derived as:

$$\begin{aligned} & (m_s h_s + m_{u1} h_{u1} + m_{u2} h_{u2}) a_y + m_s g h_R \varphi_s + m_s g q_1 z_{R1} \varphi_{u1} + m_s g q_2 z_{R2} \varphi_{u2} \\ & = 2k_{t1} T_1^2 \varphi_{u1} - W_2 T_2 \end{aligned} \quad (3.12)$$

where h_s is the sprung mass c.g. height from the road surface, which can be considered as a constant for small roll angles. Upon substituting for φ_{u1} and φ_{u2} from Equation (3.11) into Equation (3.12), a direct relationship between the lateral acceleration and sprung mass roll angle can be derived as:

$$a_y = \frac{1}{d} (c \varphi_s + e) \quad (3.13)$$

where the coefficients c, d and e are dependent upon the vehicle geometry and suspension parameters alone:

$$c = K_{\varphi 1} - m_s g h_R - m_s g q_2 z_{R2} (1 - f_1) K_{\varphi 2} / (K_{\varphi 2} - m_s g q_2 z_{R2}) - m_s g h_R f_1$$

$$\begin{aligned} d = & m_s h_R + m_s q_2 h_{c2} + m_{u2} h_{u2} + m_s g q_2 z_{R2} (m_s q_2 h_{c2} + m_{u2} h_{u2}) (1 - f_1) / (K_{\varphi 2} - m_s g q_2 z_{R2}) \\ & + f_1 (m_s h_s + m_{u1} h_{u1} + m_{u2} h_{u2}) \end{aligned}$$

$$e = W_2 T_2 + W_2 T_2 m_s g q_2 z_{R2} (1 - f_1) / (K_{\varphi 2} - m_s g q_2 z_{R2}) + W_2 T_2 f_1$$

$$f_1 = \frac{K_{\varphi 1}}{2k_{t1} T_1^2 - m_s g q_1 z_{R1}}$$

Equations (3.1) through (3.13) describe the roll equilibrium of a straight truck or full trailer vehicle represented by an equivalent two-axle vehicle model. The equilibrium equations are solved under small successive increments in the sprung mass roll angle to derive the lateral acceleration as a function of sprung mass roll angle. Equations (3.7) and

(3.8) are initially solved corresponding to each perturbation in the sprung mass roll angle φ_s , to determine the resulting unsprung mass roll angles (φ_{u1} and φ_{u2}) and lateral acceleration a_y . The corresponding tire loads are then evaluated from Equation (3.6). In the event of loss of contact between the tires on any axle and the road, the solutions based upon Equations (3.7) and (3.8) are considered invalid. Equation (3.11) is then solved to determine the unsprung mass roll angles, while the resulting lateral acceleration is derived from (3.13). The condition of relative roll instability can be established from the lateral acceleration - roll angle response characteristics of the sprung mass. The relative roll instability condition is realized, when the slope of $a_y \sim \varphi_s$ response approaches a negative value ($\partial a_y / \partial \varphi_s < 0$) due to insufficient restoring moment arising from suspension roll stiffness.

The roll performance signature of a straight truck configuration with parameters shown in Table 3.1, is presented in Figure 3.2. The $a_y \sim \varphi_s$ characteristics of the vehicle are shown for two different values of roll stiffness of the front axle suspension, indicated as $K_{\varphi 1}^a$ and $K_{\varphi 1}^b$. In case of a relatively soft front axle suspension (roll stiffness = $K_{\varphi 1}^a$), the lateral acceleration increases linearly with increase in the sprung mass roll angle. The peak lateral acceleration is achieved when wheels on the rear axle lift off the ground. A further increase in φ_s yields negative slope, which indicates that the roll stiffness due to front axle suspension is insufficient to generate adequate restoring moment. The relative rollover condition for such vehicles is thus realized when wheels on rear axle lose contact with the ground. It can be further shown that the relative roll instability of such vehicles is directly related to effective roll stiffness of front axle suspension. An increase in roll

stiffness to $K_{\phi l}^h$ can yield further increase in restoring moment and thus increase in the corresponding lateral acceleration. The static roll performance of the vehicle can be significantly enhanced by increasing the roll stiffness of the front axle ($K_{\phi l}^h > K_{\phi l}^u$). In this case, the relative rollover condition is established when wheels on both the axles lift off the ground, which results in increased static rollover threshold (SRT_b).

Table 3.1: Simulation parameters for a straight truck configuration.

Vehicle configuration	Symbol	Parameter values	
Wheel base (m)	L	6.096	
Distance between the front axle and sprung mass c.g. (m)	a	4.51	
Sprung mass c.g. height (m)	h_s	1.8	
Sprung mass (kg)	m_s	20884	
		front axle	rear axle
Unsprung mass (kg)	m_{ui}	545	1044
Suspension roll center height (m)	h_{ci}	0.508	0.737
Unsprung mass c.g. height (m)	h_{ui}	0.508	0.508
Wheel track (m)	T_i	1.087	0.9144
Tire vertical stiffness (kN/m)	K_{ti}	789	3156
Suspension roll stiffness (kNm/rad)	$K_{\phi i}$	156	1590

Since the distance from suspension roll center to the c.g. location of unsprung mass is considered small for most heavy vehicle suspensions, Equation (3.13) can be simplified by letting $z_{Ri} = 0$. The relationship between a_y and ϕ , may thus be expressed as:

$$a_y = \frac{[K_{\phi} - m_s g h_R (1 + f_j)] \phi + W_i T_i (1 + f_j)}{m_s h_R + m_s q_i h_{ci} + m_{ui} h_{ui} + f_j (m_s h_s + m_{ui} h_{ui} + m_{uj} h_{uj})} \quad (3.14)$$

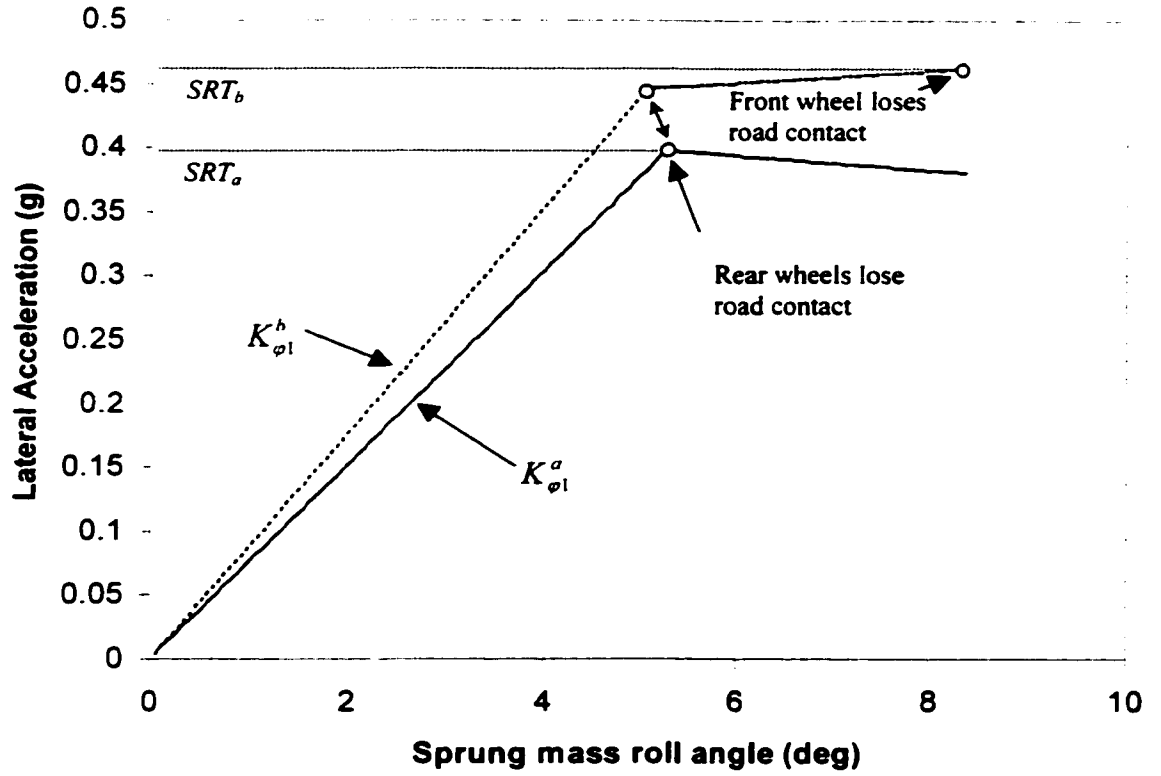


Figure 3.2: Roll performance signature of a straight truck.

In the above equation, i refers to the axle which experiences loss of tire-road contact and j corresponds to the axle which retains the tire-road contact. In the present case when $K_{\phi 1} = K_{\phi 1}^a$, $i=2$ and $j=1$. The relative roll instability condition, $(\partial a_y / \partial \phi_s < 0)$, requires that $K_{\phi} - m_s g h_R (1 + f_j) > 0$, which yields:

$$K_{\phi} > \frac{2k_y T_j^2 m_s g h_R}{2k_y T_j^2 - m_s g h_R} \quad (3.15)$$

The condition of relative roll stability of straight truck or full trailer configurations can thus be related to roll stiffness of the suspension and tires of the axle which continues to retain the road contact. If the roll stiffness of both the axle suspensions satisfy Equation (3.15), the relative roll instability is realized when wheels on both axles lose the road contact. The relative rollover condition for such vehicles thus depends upon the roll stiffness of the two axle suspensions, which satisfy Equation (3.15). Table 3.2 summarizes the different relative rollover conditions for the straight-truck or full-trailer configurations. In some particular vehicle suspension designs, the front axle roll stiffness may be considerably enhanced by using an anti-roll bar to achieve desired understeer performance. The front axle suspension may satisfy Equation (3.15), while the rear axle suspension does not. In this case, the relative rollover condition may be reached when wheels on the front axle lose road contact, as illustrated in Table 3.2.

Table 3.2: Conditions of relative rollover of straight truck or full trailer configurations.

Condition of relative roll stability	Suspension roll stiffness satisfying the condition		Condition of relative rollover Loss of tire-road contact of
	$K_{\phi 1}$	$K_{\phi 2}$	
$K_{\phi} > \frac{2k_{\phi} T_j^2 m_s g h_R}{2k_{\phi} T_j^2 - m_s g h_R}$	Yes	Yes	wheels on both axles
	No	Yes	wheels on axle #2
	No	No	wheels on axle #1 or #2
	Yes	No	wheels on axle #1

3.2.2 Roll Plane Analysis of Tractor Semi-trailer, B- and C- Train Doubles

A tractor semi-trailer combination can be characterized by a three-composite-axle vehicle, shown in Figure 3.3. The axles with similar suspension properties are grouped together such that all axles on the vehicle are shown by a set of three composite axes: tractor front axle, an equivalent tractor rear axle and an equivalent semi-trailer axle [25]. The sprung mass of the tractor is modeled as two sprung weights, supported by front and rear composite axes, coupled through torsional stiffness of the tractor frame KF_1 . The sprung weight of the semi-trailer is coupled to the tractor rear sprung weight by the torsional stiffness of KF_2 , which represents the compliance of the fifth wheel and the trailer structure. The friction existed in the tractor frame is assumed to be hysteretic, and the fifth wheel plate separation is modeled as an angular lash, as shown in Figure 3.4.

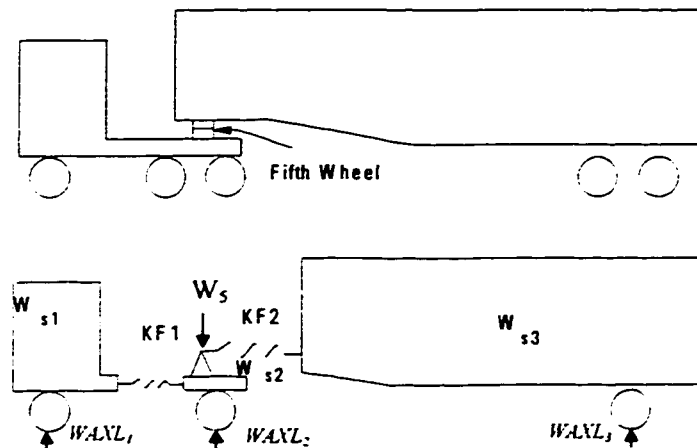


Figure 3.3: Three-axle representation for the tractor semi-trailer combinations.

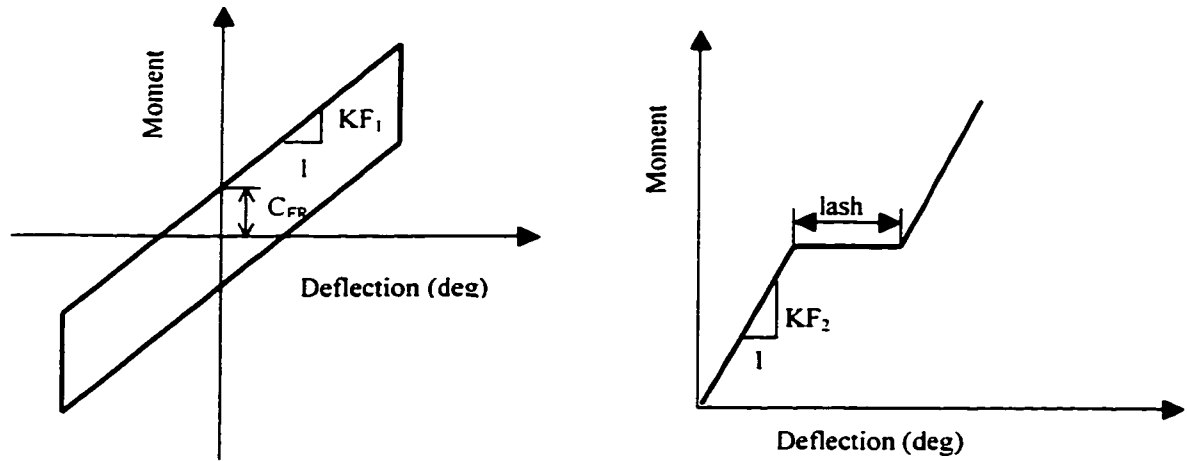


Figure 3.4: Idealized representation of the tractor frame and the fifth wheel compliance.

The static roll analysis of a tractor-semitrailer combination thus requires consideration of three-composite axle roll planes coupled through torsional compliance due to tractor frame KF_1 , and the fifth wheel and trailer's structure KF_2 . The roll plane model of the vehicle for each composite axle presentation is shown in Figure 3.5. The sprung masses are permitted to rotate about their respective roll centers, which are located at a fixed distance from the sprung mass center of gravity. The roll centers, however, are permitted to slide freely with respect to the axles along the \bar{k}_{u_i} axis. The suspension springs are assumed to remain parallel to the \bar{k}_{u_i} axis of the axles and transmit only elastic forces. Lateral forces between the sprung and unsprung masses are assumed to be transmitted through the respective roll centers. The vertical stiffness of the tires is assumed to be linear with spring constant k_{ij} , where $i = 1, 2, 3$ represents the axle, and $j = 1, 2, 3, 4$ represents the tires of each composite axle. The lateral forces developed by the tires on the inside of the turn are assumed to be negligible when compared to those developed by the tires on the outside of the turn. The articulation angles are assumed to

be small such that their influence on the roll response of the vehicle is neglected. The total vertical load carried by each composite axle is assumed to remain constant during the roll process. The pitch motion of the sprung masses, however, is incorporated by considering different vertical deflections of the sprung mass coordinates at each of the axle locations.

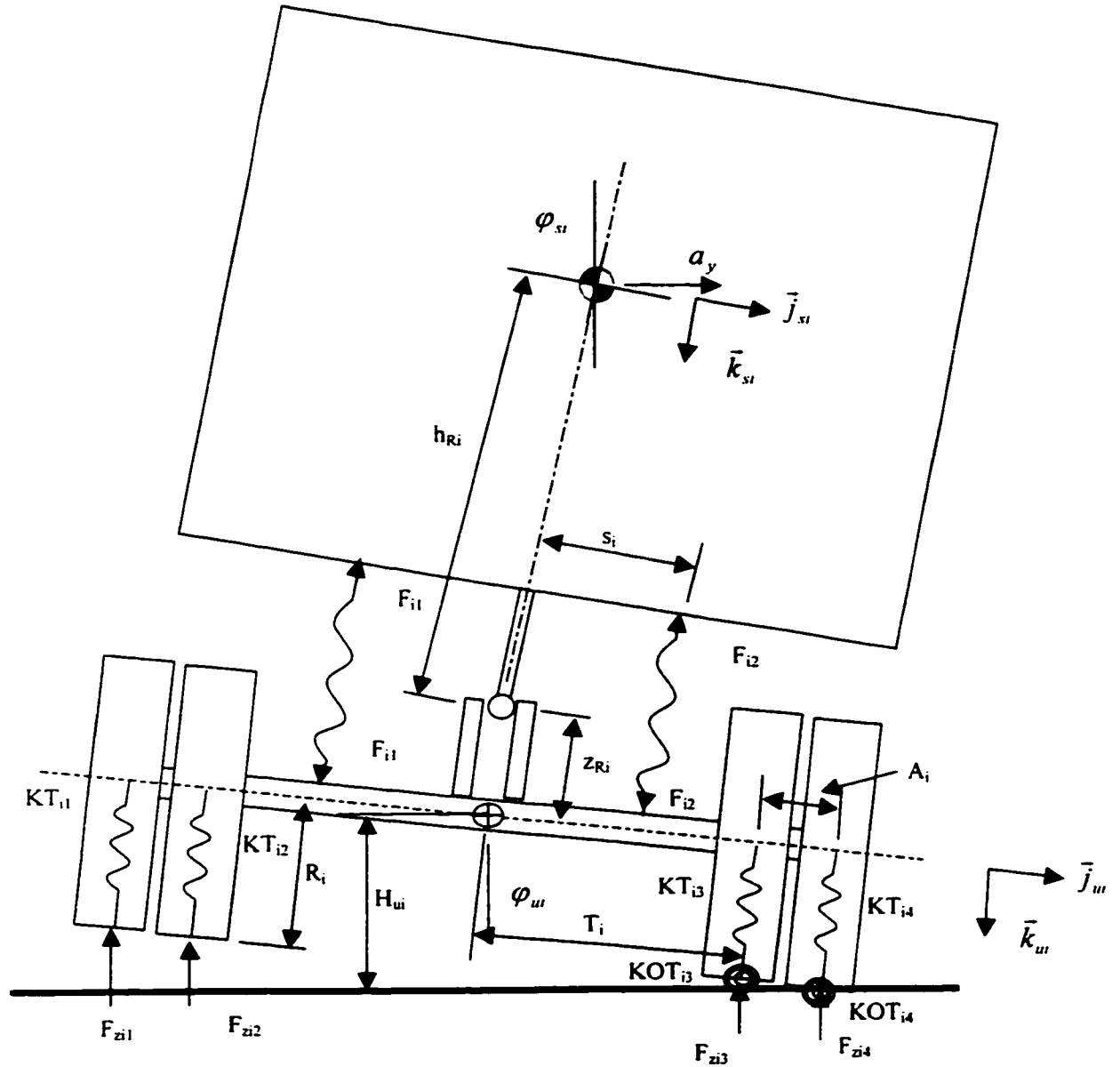


Figure 3.5: Static roll plane model of heavy vehicles.

B-train doubles are roll coupled combinations involving a tractor, a B-type semi-trailer, and a semi-trailer. C-train doubles are also roll-coupled combinations including a tractor, a semi-trailer, C-dolly, and a semi-trailer. These configurations can be represented by a four-composite-axle vehicle model, as illustrated in Figure 3.6. For each configuration, the first three axles represent the tractor semi-trailer combination, as illustrated in Figure 3.3, while the last axle represents the composite axle of the last semi-trailer. KF_3 denotes the compliance of B- or C-dolly and the second fifth wheel of the vehicle. The roll plane model of each composite axle is the same as that illustrated for the tractor semi-trailer vehicle and shown in Figure 3.5.

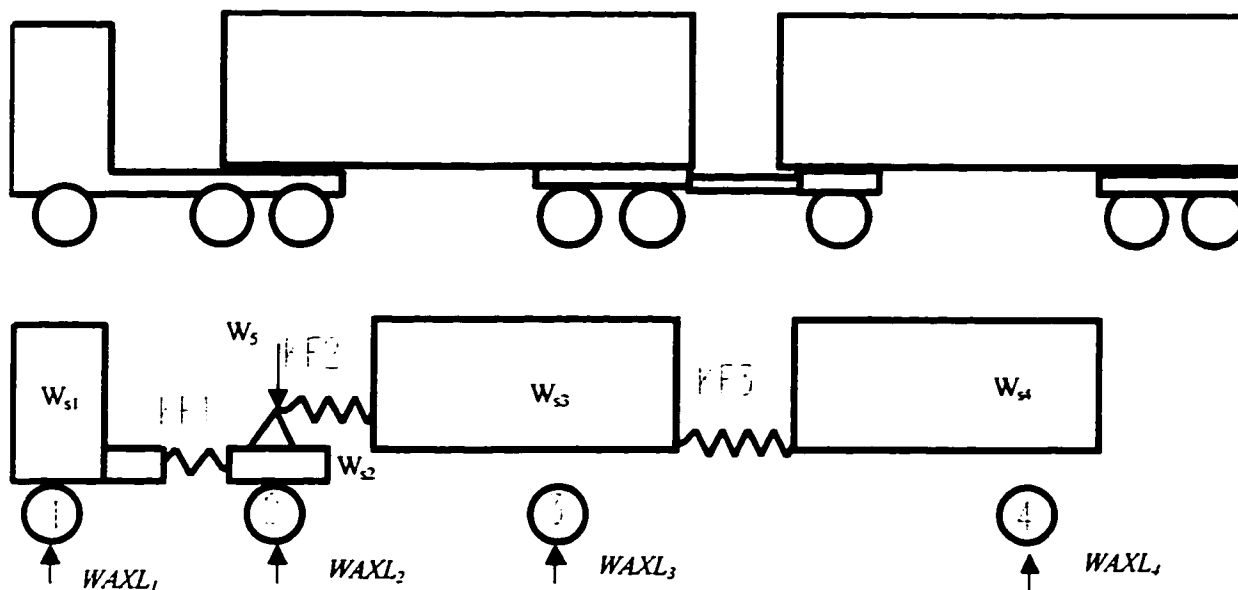


Figure 3.6: Four-axle representation for B-train or C-train doubles.

Static roll characteristics and conditions of relative roll instability of tractor-semitrailer, and B- and C- doubles can be evaluated upon consideration of static roll

equilibrium of n ($n=3, 4$) roll planes representing the combination. Generalized static roll equilibrium equations for the roll plane model of tractor semi-trailer combinations, presented in Figure 3.3, and for the B- and C- train doubles, presented in Figure 3.6, are derived as follows.

In a steady cornering maneuver, each mass of an articulated heavy vehicle is subjected to a static lateral acceleration a_y . The static roll characteristics of the vehicle in the roll plane for each axle presentation are expressed in terms of generalized variables: ❶ the sprung mass roll angle φ_{si} ($i=1, 2, 3$ for tractor-semitrailer, and $i=1$ to 4 for B- and C-doubles); ❷ the unsprung mass roll angle φ_{ui} ; ❸ the vertical distance from the axle c.g. to the suspension roll center z_{Ri} ; ❹ the vertical distance from the ground plane to the c.g. of the axle H_{ui} ; and ❺ the lateral displacement of tires on the outside of the turn y_i . A total of fifteen equations are needed to define the static roll equilibrium of a tractor semi-trailer combination; and a total of twenty equations are thus required to define the static roll equilibrium of a B- or C train double. The equations of static roll equilibrium are derived upon balancing the roll moments acting on the sprung and unsprung masses, lateral forces acting on the tires, and vertical suspension and tire forces.

Roll Moments Acting on the Sprung Masses

The roll moments acting on the sprung masses include moments due to suspension forces, torsional stiffness of the tractor and semi-trailer structures, lateral forces acting through the roll centers, and lateral components of the gravity forces. Summation of roll moments acting on each of the sprung weights yields:

$$F_{i1} [s_i \cos(\varphi_{si} - \varphi_{ui}) + h_{Ri} \sin(\varphi_{si} - \varphi_{ui})] - F_{i2} [s_i \cos(\varphi_{si} - \varphi_{ui}) - h_{Ri} \sin(\varphi_{si} - \varphi_{ui})] + M_i - F_{Ri} h_{Ri} \cos(\varphi_{si} - \varphi_{ui}) - K_{ai} (\varphi_{si} - \varphi_{ui}) = 0 \quad (3.16)$$

where F_{ij} is the force due to suspension springs on axle i ($i=1, \dots, 3$ for tractor semi-trailer or $i=1, \dots, 4$ for B- and C- doubles), and subscript j ($j=1, 2$) refers to left and right suspension springs, respectively. F_{Ri} is the lateral force transmitted between the sprung and unsprung masses on axle i , termed as the roll center force acting at the roll center. s_i is the half suspension spring track of axle i . K_{ai} is the auxiliary roll stiffness of axle i . φ_{si} and φ_{ui} are the roll angles of sprung and unsprung masses on axle i , respectively. M_i is the roll moment acting through different roll sections due to compliance of tractor frame and hitch mechanisms. Different expressions are derived for tractor semi-trailer combinations, and B-/C- doubles.

For tractor semi-trailer combinations:

$$M_i = \begin{cases} KF_1(\varphi_{s2} - \varphi_{s1}) + W_{FR}(a_y - \varphi_{s1})z_{FR1} & (i=1) \\ KF_2(\varphi_{s3} - \varphi_{s2}) - KF_1(\varphi_{s2} - \varphi_{s1}) - (W_{FR}z_{FR2} + W_5z_{52})(a_y - \varphi_{s2}) & (i=2) \\ -KF_2(\varphi_{s3} - \varphi_{s2}) + W_5z_{53}(a_y - \varphi_{s3}) & (i=3) \end{cases}$$

For B- or C- doubles:

$$M_i = \begin{cases} KF_1(\varphi_{s2} - \varphi_{s1}) + W_{FR}(a_y - \varphi_{s1})z_{FR1} & (i=1) \\ KF_2(\varphi_{s3} - \varphi_{s2}) - KF_1(\varphi_{s2} - \varphi_{s1}) - (W_{FR}z_{FR2} + W_5z_{52})(a_y - \varphi_{s2}) & (i=2) \\ KF_3(\varphi_{s4} - \varphi_{s3}) - KF_2(\varphi_{s3} - \varphi_{s2}) + W_5z_{53}(a_y - \varphi_{s3}) & (i=3) \\ -KF_3(\varphi_{s4} - \varphi_{s3}) & (i=4) \end{cases} \quad (3.17)$$

where $W_{FR} = W_{s2} + W_5 - WAXL_2$ is the vertical shear force acting through the tractor frame. Note that W_{s2} and W_5 are the sprung mass weight on tractor's rear axle, and load on the fifth wheel, respectively. $WAXL_2$ is the normal load on the tractor's rear axle. z_{FRi} ($i=1, 2$) is the distance from the tractor's front and rear suspension roll centers to the acting point of lateral force due to W_{FR} , respectively. z_{5i} ($i=2, 3$) is the distance from

the tractor's rear and trailer's suspension roll centers to the acting point of lateral force due to W_s . a_y is the steady lateral acceleration of the vehicle.

Assuming small roll angle, such that $\cos(\varphi_{si} - \varphi_{ui}) = 1$ and $\sin(\varphi_{si} - \varphi_{ui}) = \varphi_{si} - \varphi_{ui}$.

Equation (3.16) is simplified to:

$$(F_{i1} - F_{i2})s_i + [(F_{i1} + F_{i2})h_{Ri} - K_{ai}](\varphi_{si} - \varphi_{ui}) + M_i - F_{Ri}h_{Ri} = 0 \quad (3.18)$$

Differentiation of the above equation yields:

$$(\Delta F_{i1} - \Delta F_{i2})s_i + (\Delta F_{i1} + \Delta F_{i2})h_{Ri}(\varphi_{si} - \varphi_{ui}) + [(F_{i1} + F_{i2})h_{Ri} - K_{ai}](\Delta\varphi_{si} - \Delta\varphi_{ui}) + \Delta M_i - \Delta F_{Ri}h_{Ri} = 0 \quad (3.19)$$

with

For tractor semi-trailer:

$$\Delta M_i = \begin{cases} KF_1(\Delta\varphi_{s2} - \Delta\varphi_{s1}) + W_{FR}(\Delta a_y - \Delta\varphi_{s1})z_{FR1} & (i=1) \\ KF_2(\Delta\varphi_{s3} - \Delta\varphi_{s2}) - KF_1(\Delta\varphi_{s2} - \Delta\varphi_{s1}) - (W_{FR}z_{FR2} + W_s z_{s2})(\Delta a_y - \Delta\varphi_{s2}) & (i=2) \\ -KF_2(\Delta\varphi_{s3} - \Delta\varphi_{s2}) + W_s z_{s3}(\Delta a_y - \Delta\varphi_{s3}) & (i=3) \end{cases}$$

For B- or C-train doubles:

$$\Delta M_i = \begin{cases} KF_1(\Delta\varphi_{s2} - \Delta\varphi_{s1}) + W_{FR}(\Delta a_y - \Delta\varphi_{s1})z_{FR1} & (i=1) \\ KF_2(\Delta\varphi_{s3} - \Delta\varphi_{s2}) - KF_1(\Delta\varphi_{s2} - \Delta\varphi_{s1}) - (W_{FR}z_{FR2} + W_s z_{s2})(\Delta a_y - \Delta\varphi_{s2}) & (i=2) \\ KF_3(\Delta\varphi_{s4} - \Delta\varphi_{s3}) - KF_2(\Delta\varphi_{s3} - \Delta\varphi_{s2}) + W_s z_{s3}(\Delta a_y - \Delta\varphi_{s3}) & (i=3) \\ -KF_3(\Delta\varphi_{s4} - \Delta\varphi_{s3}) & (i=4) \end{cases} \quad (3.20)$$

The changes in the suspension forces at axle i (ΔF_{ij}) can be related to the variations in the deflections, $\Delta\varphi_{si}$, $\Delta\varphi_{ui}$, and Δz_{Ri} in the following manner:

$$\Delta F_{ij} = \frac{\partial F_{ij}}{\partial \varphi_{si}} \Delta\varphi_{si} + \frac{\partial F_{ij}}{\partial \varphi_{ui}} \Delta\varphi_{ui} + \frac{\partial F_{ij}}{\partial z_{Ri}} \Delta z_{Ri}; \quad i=1, \dots, 3 \text{ or } 1, \dots, 4; \text{ and } j=1, 2 \quad (3.21)$$

The partial differentials of suspension forces for the left-hand and right-hand side springs can be expressed in terms of local linear equivalent spring constants K_{ij} ($j=1,2$):

$$\begin{aligned}\Delta F_{i1} &= K_{i1} [\Delta z_{Ri} - s_i (\Delta \varphi_{si} - \Delta \varphi_{ui})] \\ \Delta F_{i2} &= K_{i2} [\Delta z_{Ri} + s_i (\Delta \varphi_{si} - \Delta \varphi_{ui})]\end{aligned}\quad (3.22)$$

The total suspension spring force developed along the \tilde{k}_u axis can also be expressed as:

$$F_{i1} + F_{i2} = (WAXL_i - W_{ui})(\cos \varphi_{ui} + a_y \sin \varphi_{ui}) \quad (3.23)$$

Assuming small angles, the variations in the total spring force can be derived from Equation (3.21):

$$\Delta F_{i1} + \Delta F_{i2} = (WAXL_i - W_{ui})(a_y \Delta \varphi_{ui} + \varphi_{ui} \Delta a_y) \quad (3.24)$$

The variation in the lateral force acting at the roll center F_{Ri} , can be expressed as:

$$\Delta F_{Ri} = (WAXL_i - W_{ui})(\Delta a_y - \Delta \varphi_{ui}) \quad (3.25)$$

Substitution of Equations (3.20), (3.22) - (3.25) into Equation (3.19) yields equilibrium of roll moments acting on the sprung mass supported by the front axle:

$$\begin{aligned}& \{ (WAXL_1 - W_{u1}) h_{R1} [(\varphi_{s1} - \varphi_{u1}) \varphi_{u1} - 1] + W_{FR} z_{FR1} \} \Delta a_y + [(WAXL_1 - W_{u1}) (1 + a_y \varphi_{u1}) h_{R1} \\ & - (K_{11} + K_{12}) s_1^2 - K_{F1} - W_{FR} z_{FR1} - K_{a1}] \Delta \varphi_{s1} + K_{F1} \Delta \varphi_{s2} + [(K_{11} + K_{12}) s_1^2 - \\ & (WAXL_1 - W_{u1}) a_y \varphi_{u1} h_{R1} + (WAXL_1 - W_{u1}) (\varphi_{s1} - \varphi_{u1}) h_{R1} a_y + K_{a1}] \Delta \varphi_{u1} \\ & + (K_{11} - K_{12}) s_1 \Delta z_{R1} = 0\end{aligned}\quad (3.26)$$

Similarly, the equations for the remaining sprung masses of a tractor semitrailer model can be derived as:

$$\begin{aligned}& \{ (WAXL_2 - W_{u2}) h_{R2} [(\varphi_{s2} - \varphi_{u2}) \varphi_{u2} - 1] - W_{FR1} z_{FR2} - W_5 z_{51} \} \Delta a_y + K_{F1} \Delta \varphi_{s1} + \\ & [(WAXL_2 - W_{u2}) (1 + a_y \varphi_{u2}) h_{R2} + W_{FR} z_{FR2} + W_5 z_{52} - (K_{21} + K_{22}) s_2^2 - K_{a2} - \\ & (K_{F1} + K_{F2})] \Delta \varphi_{s2} + K_{F2} \Delta \varphi_{s3} + [(K_{21} + K_{22}) s_2^2 - (WAXL_2 - W_{u2}) a_y \varphi_{u2} h_{R2} + \\ & (WAXL_2 - W_{u2}) (\varphi_{s2} - \varphi_{u2}) h_{R2} a_y + K_{a2}] \Delta \varphi_{u2} + (K_{21} - K_{22}) s_2 \Delta z_{R2} = 0\end{aligned}\quad (3.27)$$

$$\begin{aligned}
& \{ (WAXL_3 - W_{s3})h_{R3}[(\varphi_{s3} - \varphi_{u3})\varphi_{u3} - 1] + W_{s3}z_{s3} \} \Delta a_y + KF_2 \Delta \varphi_{s2} + \\
& [(WAXL_3 - W_{u3})(1 + a_y \varphi_{u3})h_{R3} - W_{s3}z_{s3} - (K_{31} + K_{32})s_3^2 - K_{a3} - KF_2] \Delta \varphi_{s3} \\
& + [(K_{31} + K_{32})s_3^2 - (WAXL_3 - W_{u3})a_y \varphi_{u3}h_{R3} + (WAXL_3 - W_{u3})(\varphi_{s3} - \varphi_{u3})h_{R3}a_y \\
& + K_{a3}] \Delta \varphi_{u3} + (K_{31} - K_{32})s_3 \Delta z_{R3} = 0
\end{aligned} \tag{3.28}$$

For B- or C-train doubles, the roll equilibrium equations for the sprung masses supported by the tractor front and rear axles are the same as Equations (3.26) and (3.27). The equations for the remaining sprung masses of B- or C-train doubles are derived as:

$$\begin{aligned}
& \{ (WAXL_3 - W_{s3})h_{R3}[(\varphi_{s3} - \varphi_{u3})\varphi_{u3} - 1] + W_{s3}z_{s3} \} \Delta a_y + KF_2 \Delta \varphi_{s2} + [(WAXL_3 - W_{u3})(1 + \\
& a_y \varphi_{u3})h_{R3} - W_{s3}z_{s3} - (K_{31} + K_{32})s_3^2 - K_{a3} - KF_2 - KF_3] \Delta \varphi_{s3} + KF_3 \Delta \varphi_{s4} \\
& + [(K_{31} + K_{32})s_3^2 - (WAXL_3 - W_{u3})a_y \varphi_{u3}h_{R3} + (WAXL_3 - W_{u3})(\varphi_{s3} - \varphi_{u3})h_{R3}a_y \\
& + K_{a3}] \Delta \varphi_{u3} + (K_{31} - K_{32})s_3 \Delta z_{R3} = 0
\end{aligned} \tag{3.29}$$

$$\begin{aligned}
& (WAXL_4 - W_{s4})h_{R4}[(\varphi_{s4} - \varphi_{u4})\varphi_{u4} - 1] \Delta a_y + KF_3 \Delta \varphi_{s3} + \\
& [(WAXL_4 - W_{u4})(1 + a_y \varphi_{u4})h_{R4} - (K_{41} + K_{42})s_4^2 - K_{a4} - KF_3] \Delta \varphi_{s4} \\
& + [(K_{41} + K_{42})s_4^2 - (WAXL_4 - W_{u4})a_y \varphi_{u4}h_{R4} + (WAXL_4 - W_{u4})(\varphi_{s4} - \varphi_{u4})h_{R4}a_y \\
& + K_{a4}] \Delta \varphi_{u4} + (K_{41} - K_{42})s_4 \Delta z_{R4} = 0
\end{aligned} \tag{3.30}$$

Equations (3.26) to (3.28) represent the equilibrium states of the roll moments for the three sprung weights supported by the composite axles of the tractor semi-trailer combination, while Equations (3.26), (3.27), (3.29), and (3.30) represent those of the four sprung weights supported by the composite axles of a B- or C- double.

Roll Moments Acting on the Unsprung Masses

The equation for the roll moment of the i th unsprung mass can be expressed as:

$$\begin{aligned}
& \sum_{j=1}^4 F_{zij} R_i \sin \varphi_{ui} + (F_{zi1} - F_{zi4})(T_i + A_i) \cos \varphi_{ui} + (F_{zi2} - F_{zi3})T_i \cos \varphi_{ui} - \\
& (F_{zi3} + F_{zi4})y_i \cos \varphi_{ui} - (F_{i1} - F_{i2})s_i + F_{Ri}z_{ui} + F_{yi}H_{ui} - MOT_i = 0
\end{aligned} \tag{3.31}$$

where F_{zj} is tire vertical force acting on tire j ($j=1$ to 4) of axle i , R_i is the effective radius of tires on axle i , T_i and A_i are half the inner tire track width, and dual tire spacing, respectively. F_{yi} is the lateral force developed at the tires of axle i , and y_i is the lateral displacement of tires on the outside of the turn. MOT_i is the roll-resisting moment produced at the tire-road interface. Applying the small roll angle assumption and differentiating the above equation, roll moment equilibrium is attained as:

$$\begin{aligned} & \sum_{j=1}^4 \Delta F_{zij} R_i \phi_{ui} + \sum_{j=1}^4 F_{zij} R_i \Delta \phi_{ui} + (\Delta F_{zi1} - \Delta F_{zi4})(T_i + A_i) + (\Delta F_{zi2} - \Delta F_{zi3})T_i \\ & - (F_{zi3} + F_{zi4})\Delta y_i - (\Delta F_{zi3} + \Delta F_{zi4})y_i - (\Delta F_{i1} - \Delta F_{i2})s_i + F_{Ri}\Delta z_{ui} + \\ & \Delta F_{Ri}z_{ui} + F_{yi}\Delta H_{ui} + \Delta F_{yi}H_{ui} + \Delta MOT = 0 \end{aligned} \quad (3.32)$$

The variations in normal forces acting on the four tires of a composite axle are expressed as a function of the linear stiffness coefficients and vertical deflections:

$$\begin{aligned} \Delta F_{z1} &= KT_{i1}[\Delta H_{ui} - (T_i + A_i)\Delta \phi_{ui}] \\ \Delta F_{z2} &= KT_{i2}(\Delta H_{ui} - T_i\Delta \phi_{ui}) \\ \Delta F_{z3} &= KT_{i3}[\Delta H_{ui} + (T_i - y_i)\Delta \phi_{ui} - \Delta y_i\phi_{ui}] \\ \Delta F_{z4} &= KT_{i4}[\Delta H_{ui} + (T_i + A_i - y_i)\Delta \phi_{ui} - \Delta y_i\phi_{ui}] \end{aligned} \quad (3.33)$$

The changes in the roll-resisting moment produced at the tire-road interface are more significant at outer side tires, and can be written as

$$\Delta MOT = (KOT_{i3} + KOT_{i4})\Delta \phi_{ui} \quad (3.34)$$

where KOT_{ij} is the linear overturning stiffness of tire j ($j=3, 4$) on axle i .

Upon substituting Equations (3.22), (3.25), (3.33) and (3.34) into Equation (3.32), the unsprung mass roll moment equations, as caused by small deviations from an equilibrium condition, are obtained as:

$$\begin{aligned}
& -[(WAXL_i - W_{ui})(R_i + z_{Ri}) + W_{ui}H_{ui}] \Delta a_y + (K_{i1} + K_{i2})s_i^2 \Delta \varphi_{ui} - [(K_{i1} + K_{i2})s_i^2 - \\
& WAXL_i R_i - (WAXL_i - W_{ui})z_{Ri} + KOT_{i3} + KOT_{i4} + KT_{i1}(T_i + A_i)^2 + KT_{i2}T_i^2 + \\
& KT_{i3}(T_i - y_i)^2 + KT_{i4}(T_i + A_i - y_i)^2] \Delta \varphi_{ui} + [(WAXL_i - W_{ui})(a_y - \varphi_{ui}) - \\
& (K_{i1} - K_{i2})s_i] \Delta z_{Ri} + [(KT_{i1} - KT_{i4})(T_i + A_i) + (KT_{i2} - KT_{i3})T_i + \\
& (KT_{i3} + KT_{i4})y_i + WAXL_i a_y] \Delta H_{ui} - \{F_{zj3} + F_{zj4} + [(KT_{i3} + KT_{i4})(T_i - y_i) + \\
& KT_{i4}A_i] \varphi_{ui}\} \Delta y_i = 0
\end{aligned} \tag{3.35}$$

Vertical Suspension Spring Forces

The small increment equilibrium equation for vertical suspension spring forces can be derived upon substituting Equations (3.22) into Equation (3.24) to yield:

$$\begin{aligned}
& -(WAXL_i - W_{ui})\varphi_{ui} \Delta a_y - (K_{i1} - K_{i2})s_i \Delta \varphi_{ui} + [(K_{i1} - K_{i2})s_i - \\
& (WAXL_i - W_{ui})a_y] \Delta \varphi_{ui} + (K_{i1} + K_{i2}) \Delta z_{Ri} = 0
\end{aligned} \tag{3.36}$$

Vertical Tire Forces

The vertical load carried by each composite axle is the sum of each wheel load, and can be simply expressed as:

$$WAXL_i = \sum_{j=1}^4 F_{zij} \tag{3.37}$$

Assuming constant axle load and small deviations about an equilibrium condition, Equation (3.37) can be written as:

$$\sum_{j=1}^4 \Delta F_{zij} = 0 \tag{3.38}$$

Upon substituting for vertical tire forces from Equation (3.33) into Equation (3.38), the vertical tire force equilibrium can be written as:

$$\begin{aligned}
& [(KT_{i4} - KT_{i1})(T_i + A_i) + (KT_{i3} - KT_{i2})T_i - (KT_{i3} + KT_{i4})y_i] \Delta \varphi_{ui} \\
& + \sum_{j=1}^4 KT_{ij} \Delta H_{ui} - (KT_{i3} + KT_{i4})\varphi_{ui} \Delta y_i = 0
\end{aligned} \tag{3.39}$$

Lateral Forces Acting on the Outside Tires

The lateral force equilibrium equation for axle i can be expressed in terms of outside tire lateral stiffness as:

$$WAXL_i a_y = (KYT_{i,3} + KYT_{i,4}) y_i \cos \phi_{ui} \quad (3.40)$$

Invoking the small roll angles assumption, the above equation can be rewritten for small deviations about an equilibrium condition:

$$WAXL_i \Delta a_y - (KYT_{i,3} + KYT_{i,4}) \Delta y_i = 0 \quad (3.41)$$

The equilibrium equations for the tractor semi-trailer combination, and B- and C-train doubles can be written in the matrix form as:

$$[A]\{\Delta x\} = \{b\} \Delta \phi_{ui} \quad (3.42)$$

where $[A]$ and $\{b\}$ are (15×15) and (15×1) matrices of vehicle parameters for tractor semi-trailers, and (20×20) and (20×1) matrices for B-train or C-train doubles, respectively. $\{\Delta x\}$ is the vector of vehicle response variables representing the increment of the lateral acceleration, roll angles of the sprung masses and the composite axles, vertical and lateral displacements of the composite axles, given by:

$$\{\Delta x\}^T = [\Delta a_y, \Delta \phi_{s1}, \dots, \Delta \phi_{s(n-1)}, \Delta \phi_{ui}, \Delta z_{ui}, \Delta H_{ui}, \Delta y_i] \quad i=1, 2, \dots, n \quad (3.43)$$

where n is the number of roll sections of the vehicle combination. $\Delta \phi_{ui}$ is the increment in roll angle of the rearmost or n^{th} sprung weight. The set of equations (3.42) are solved to determine the variations in lateral acceleration and roll angles of sprung and unsprung masses corresponding to an increment in roll angle of the last sprung weight ($\Delta \phi_{ui}$). Initially the vehicle is assumed to be in an upright position. The sprung mass roll angle

ϕ_{sn} is then increased by small increments, while the change in lateral acceleration is monitored. The relative rollover condition can be detected when the lateral acceleration exhibits a decrease ($\frac{\partial a_y}{\partial \phi_{sn}} < 0$) with the progressive increase in the trailer roll angle.

3.2.3: Roll Plane Analysis of A-Train Doubles

An A-train double consists of a tractor semi-trailer, an A-type dolly and a second semi-trailer. Due to weak roll stiffness of the A-dolly, an A-double can be considered as two complete roll units: a tractor semi-trailer; and a trailer, as discussed in Chapter 2. Roll plane model of an A-train double can thus be derived as the combination of those two units without roll coupling, as illustrated in Figure 3.7. The analytical models developed for tractor semi-trailers and full trailers can be used to predict the relative rollover condition and static rollover threshold of A-train doubles.

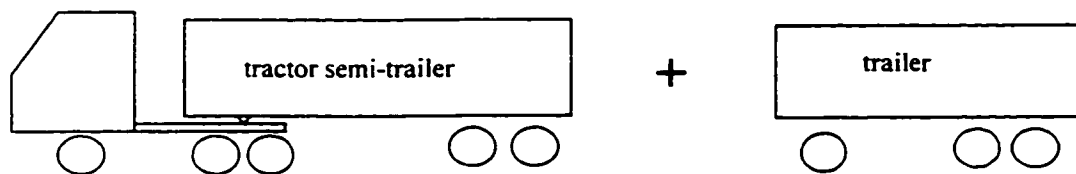


Figure 3.7: Two independent roll units of an A-double.

3.3 RELATIVE ROLLOVER CONDITIONS OF DIFFERENT VEHICLE COMBINATIONS

Relative rollover condition for straight trucks or full trailers can be analytically evaluated using Equations (3.8) and (3.13), while Equation (3.42) can be solved to derive the conditions for relative roll instability of tractor semitrailer, and B- or C- double combinations. The relative rollover conditions of tractor semi-trailer combinations, A-doubles, B- and C- doubles are investigated for an array of suspension configurations, and are presented in the following subsections.

3.3.1 Straight Trucks or Full Trailers

Analytical relationship between lateral acceleration a_y and vehicle roll angle ϕ_s has been derived in section 3.2.1 for straight trucks and full trailers, which can be used to attain static rollover thresholds and relative rollover conditions of such vehicles. The plot of lateral acceleration (a_y) as a function of front or rear axle load transfer ratio (LTR_i , $i=1, 2$) can provide further information on vehicle roll behavior. Single axle LTR_i is defined as $LTR_i = |FL_i - FR_i| / (FL_i + FR_i)$, where FL_i and FR_i are the normal loads on the left- and right-wheels of the axle i , respectively, calculated using Equation (3.6). A unity value of LTR_i indicates that wheels on one side of the axle lift off the road surface. The $a_y - LTR_i$ curve can thus provide information about LTR_i level at certain lateral acceleration, and wheels lift-off sequence. Figure 3.8 illustrates the signature of $a_y - LTR_i$ for a straight truck, whose parameters are illustrated in Table 3.3. The rear axle LTR_2 approaches a unity value faster than the front axle LTR_1 . Consequently, wheels on the rear axle lift off the road surface first, followed by wheels on the front axle. The slope

$d(a_y)/d(LTR_i)$ before wheels lift-off can thus be used to predict the lift-off sequence of road wheels.

Table 3.3: Simulation parameters for a pickup and delivery truck.

Vehicle configuration	Symbol	Parameter values	
Wheel base (m)	L	4.025	
Distance between the front axle and sprung mass c.g. (m)	a	2.14	
Sprung mass c.g. height (m)	h_s	1.461	
Sprung mass (kg)	m_s	4690	
		front axle	rear axle
Unsprung mass (kg)	m_{ui}	516	731.4
Suspension roll center height (m)	h_{ci}	0.4064	0.6858
Unsprung mass c.g. height (m)	h_{ui}	0.381	0.3937
Wheel track (m)	T_i	0.9906	0.8446
Tire vertical stiffness (kN/m)	K_{ti}	604	1208
Suspension roll stiffness (kNm/rad)	$K_{\phi i}$	322	281

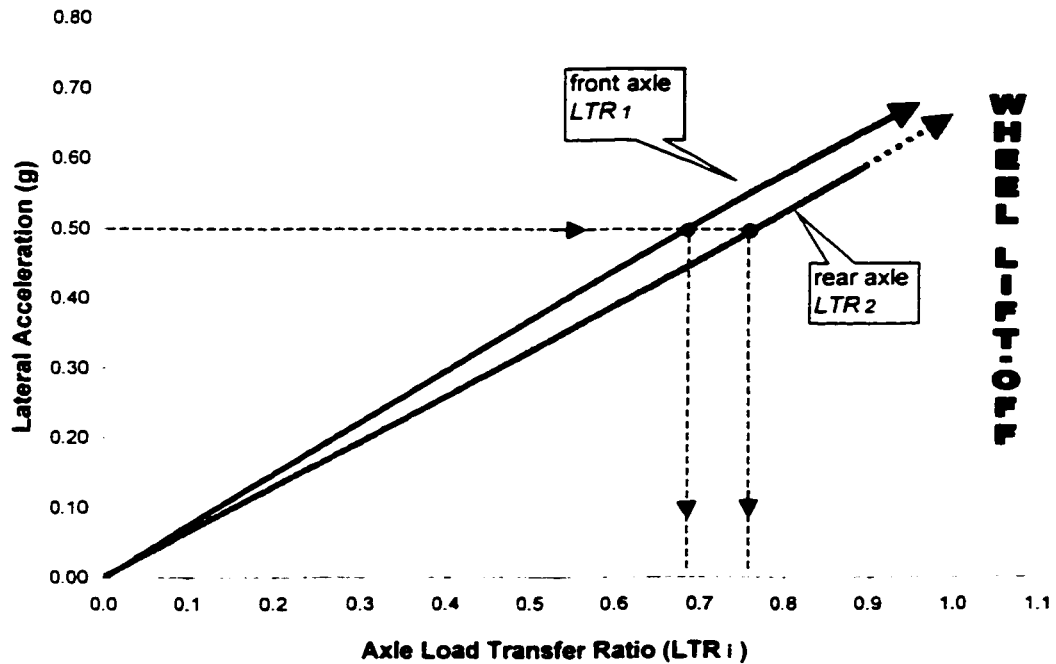


Figure 3.8: Lateral acceleration a_y - LTR signature of a P & D truck.

In view of the considerable influence of suspension roll stiffness on relative rollover condition and *SRT* as shown in Figure 3.2, further investigation about effect of roll stiffness on roll characteristics of straight trucks is conducted in a systematic manner. Table 3.4 illustrates eight vehicle configurations in terms of different combinations of front to rear axle roll stiffness distribution ratio KF_1 / KF_2 and overall roll stiffness ratio $(KF_1 + KF_2) / KF_{tot}$, where KF_{tot} is the total roll stiffness of the baseline vehicle, as listed in Table 3.3.

Table 3.4: Vehicle configurations with different roll stiffness distribution.

	configurations							
	①	②	③	④	⑤	⑥	⑦	⑧
KF_1 / KF_2	1.25	1.25	1.25	1.25	0.5	1.0	1.5	2.0
$\frac{KF_1 + KF_2}{KF_{tot}}$	0.75	1.0	1.25	1.5	1.0	1.0	1.0	1.0

Roll stability of the vehicle can be considerably improved by increasing the overall roll stiffness of the vehicle, as shown in Figure 3.9. Static rollover threshold (*SRT*) is increased from 0.65 g to 0.70 g when the total roll stiffness ratio is increased from 0.75 to 1.5. Since $d(a_y) / d(LTR_2)$ of the rear axle is less than $d(a_y) / d(LTR_1)$ of the front axle, wheels on the rear axle lift off first for the first four configurations listed in Table 3.4. If the total roll stiffness is kept as a constant, the increase of front to rear roll stiffness ratio first increases and then decreases static rollover threshold of the vehicle. The

maximum static rollover threshold is reached when wheels on a single track (front and rear wheels) lift off at the same lateral acceleration level, as shown by the cross point of the $d(a_y)/d(LTR_i)$ ($i=1, 2$) curves in Figure 3.10. The $d(a_y)/d(LTR_i)$ curves further reveal that wheels on the front axle lift off first when the front to rear roll stiffness is increased to 2.0. For all the eight configurations, relative rollover condition is reached when wheels on both the front and rear axles lift off the ground.

3.3.2 Tractor Semi-trailer Combinations

The simulation parameters of a typical tractor semi-trailer combination, comprising a three-axle tractor and a two-axle semi-trailer, are illustrated in Table 3.5. The three-axle representation for tractor semi-trailer combination is used for static roll performance analysis. The nonlinear force-deflection characteristics of typical suspension springs are incorporated using a lookup table, and linearization about the operating point is performed to identify a linear spring rate. The measured force-displacement characteristics of the suspension springs are illustrated in Figure 3.11. The figure reveals that the front suspension spring is considerably softer than the tractor rear and trailer suspension springs, which consists of pre-charge air springs. Equation (3.42) is solved for small increment in trailer's roll angle, while the wheel deflections on all the composite axles are monitored. The zero deflection of wheels indicates the lift-off of the tires.

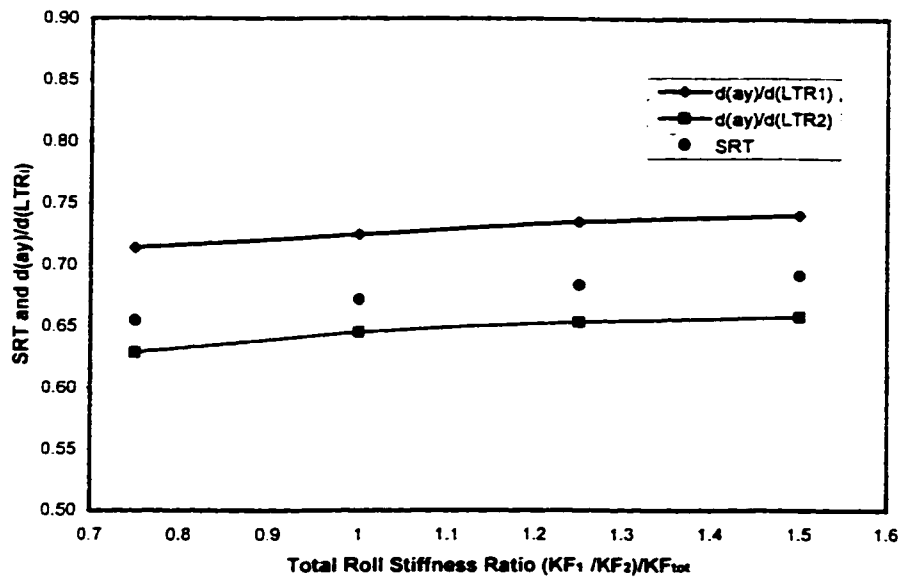


Figure 3.9: Effect of total roll stiffness ratio on static rollover threshold and lift-off sequence.

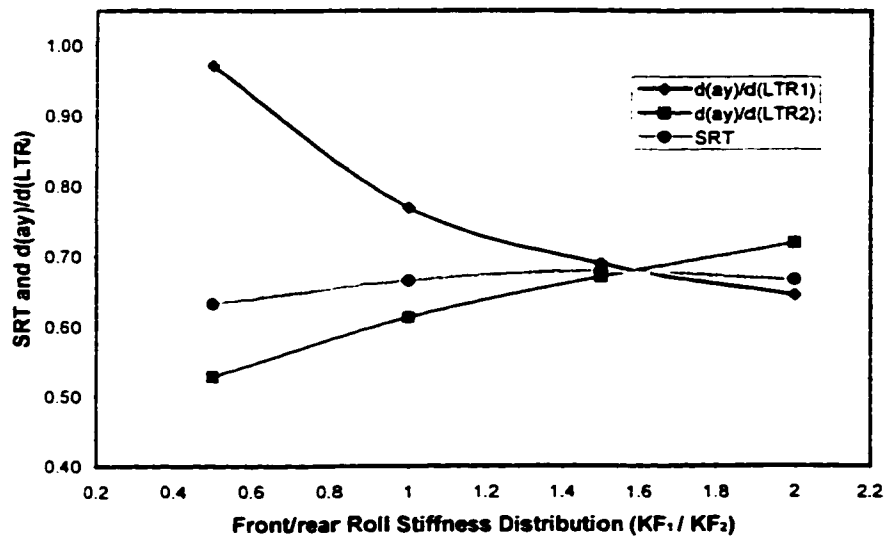


Figure 3.10: Effect of front/rear roll stiffness ratio on static rollover threshold and lift-off sequence.

The roll performance signature of the tractor semi-trailer combination, the relationship between lateral acceleration (a_y) and sprung mass roll angle (φ_m), is illustrated in Figure 3.12. The results demonstrate a negative slope ($\partial a_y / \partial \varphi_m < 0$), when wheels on both the second and the third composite axles lose contact with the ground. Thus the relative rollover condition is identified as the state when one side tires of the tractor rear axles as well as those on one side of the semi-trailer axles lose contact with the ground. A static rollover threshold of 0.42 g, denoted as SRT_a is obtained when the combination approaches its relative rollover condition, as shown in Figure 3.12. The corresponding roll angle of the trailer sprung mass approaches 5.3 degrees at the relative rollover condition. Figure 3.13 illustrates relative rollover condition and static rollover threshold of the combination when the suspension rates of the last two composite axles are reduced by 50%. While a lower static rollover threshold of 0.39 g is obtained, relative rollover condition is still approached when one side tires of the tractor rear axles as well as those on one side of the semi-trailer axles lose contact with the ground. The relative rollover condition, however, is approached at a relatively larger trailer roll angle of about 6.8 degrees. In order to conduct a parametric sensitivity analysis, the tractor semitrailer configuration, given in Table 3.5, is taken as a baseline vehicle. Each parameter is then changed by a reasonable percentage of its baseline value, while other parameters are kept unchanged. For each simulation run, the corresponding roll angle of the last sprung mass (φ_{s3}) is recorded when wheels on each axle lift off the road surface, which can be used to find out wheels lift-off sequence. Static rollover threshold (SRT) and relative rollover condition are determined from the roll performance signature ($a_y - \varphi_{s3}$).

Table 3.5: Simulation parameters for a tractor semi-trailer combination.

	Axle 1	Axle 2	Axle 3
Axle weight (kg)	548 (W_{u1})	2270 (W_{u2})	1362 (W_{u3})
Axle load (kg)	4404 ($WAXL_1$)	14365 ($WAXL_2$)	14365 ($WAXL_3$)
Distance from roll center to sprung weight c.g. (m)	0.656 (h_{R1})	0.282 (h_{R2})	1.328 (h_{R3})
Auxiliary roll stiffness (kNm/rad)	24.78 (K_{a1})	745.2 (K_{a2})	777.6 (K_{a3})
Half suspension spacing (m)	0.406 (s_1)	0.483 (s_2)	0.559 (s_3)
Wheel radius (m)	0.508 (R_1)	0.508 (R_2)	0.508 (R_3)
Half wheel track (m)	1.016 (T_1)	0.749 (T_2)	0.826 (T_3)
Dual tire spacing (m)	0 (A_1)	0.33 (A_2)	0.33 (A_3)
Tire vertical stiffness (kN/m)	847.6 (KT_{1j})	847.6 (KT_{2j})	847.6 (KT_{3j})
Tire overturning stiffness (Nm/deg)	113 (KOT_{1j})	226 (KOT_{2j})	226 (KOT_{3j})
Tire lateral stiffness (N/m)	876 (KYT_{1j})	1752 (KYT_{2j})	1752 (KYT_{3j})
Load on the fifth wheel (kg)	13620 (W_5)		
Roll stiffness of tractor frame (kNm/rad)	54.9 (KF_1)		
Roll stiffness of fifth wheel (kNm/rad)	5995 (KF_2)		

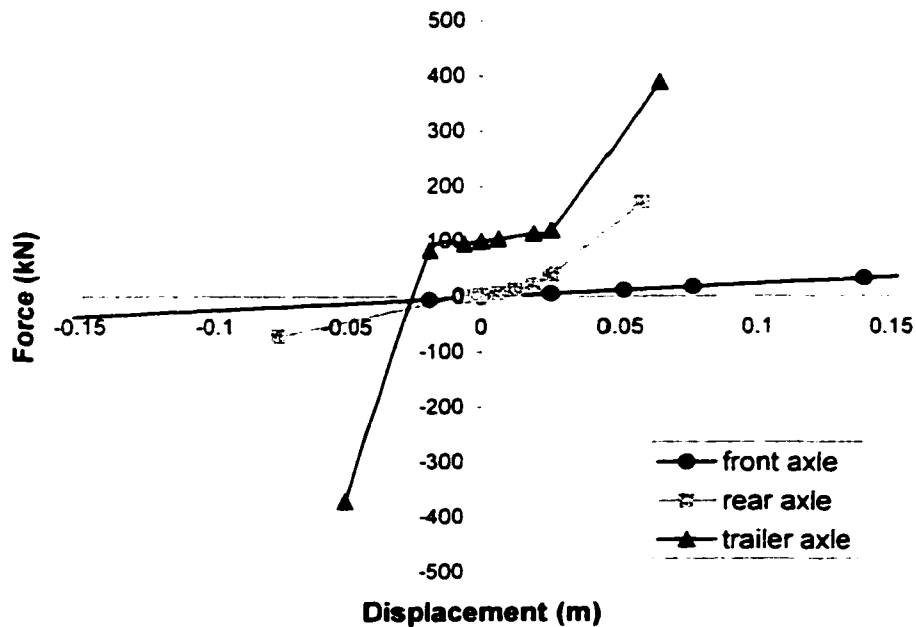


Figure 3.11: Force-displacement characteristics of suspension springs.

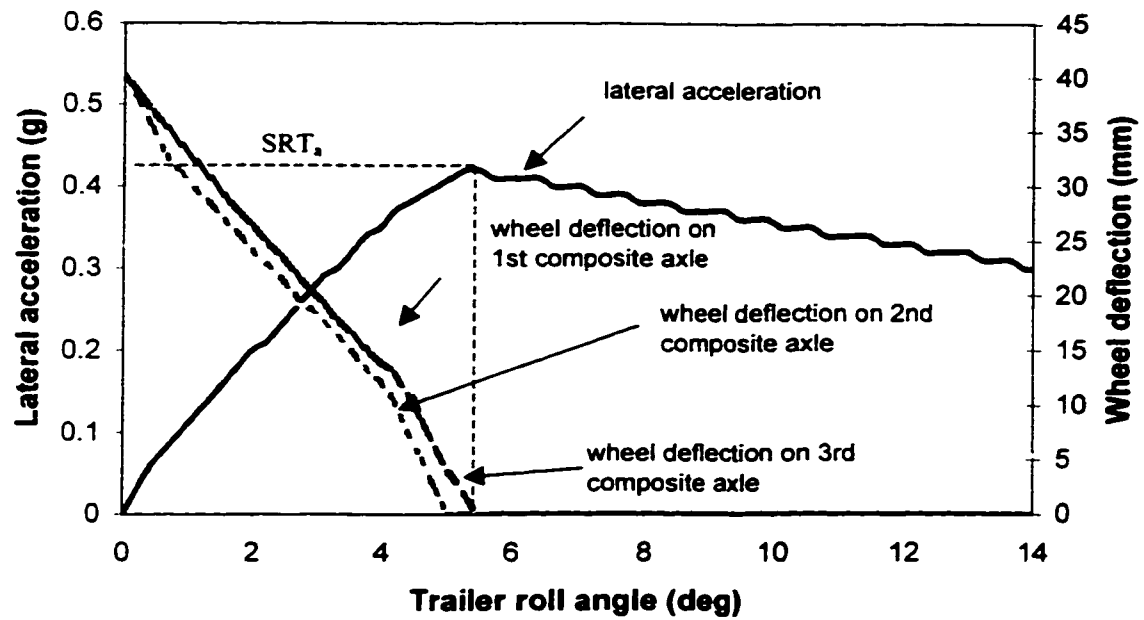


Figure 3.12: Roll performance signature of a tractor semi-trailer combination.

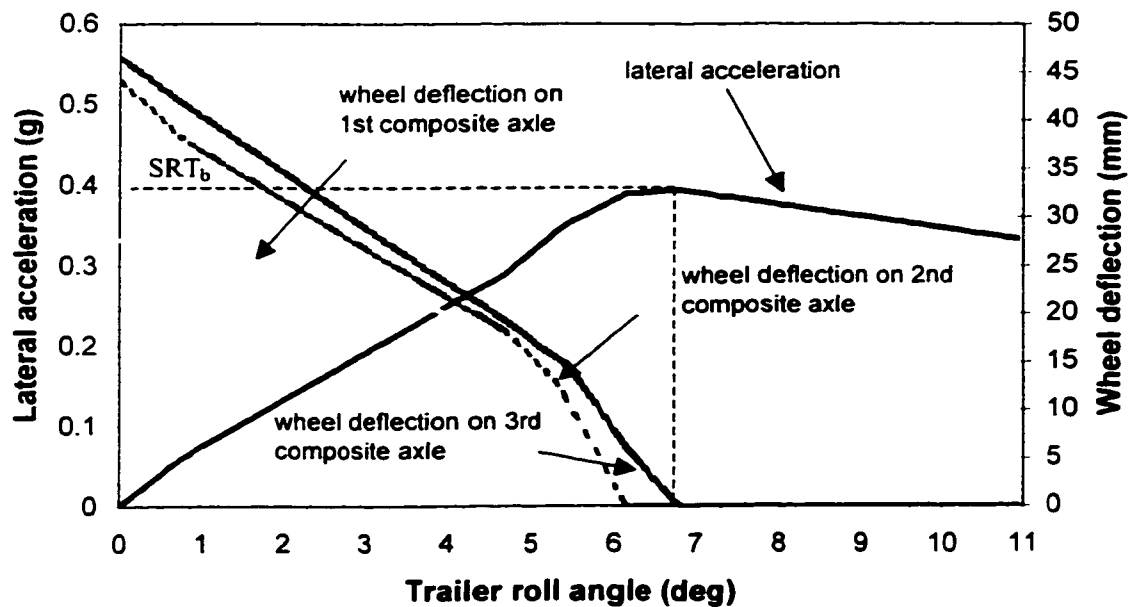


Figure 3.13: Roll performance signature of a tractor semi-trailer combination with reduced suspension rates on tractor rear and trailer axles.

Table 3.6 illustrates parametric study results when auxiliary roll stiffness rates (K_{ϕ_i} , $i=1, 2, 3$), and tractor frame and fifth wheel compliance (KF_1 , KF_2) are varied by $\pm 50\%$ of the baseline values. The static rollover threshold of the baseline vehicle is obtained as 0.417g. Wheels on the 3rd axle lift off at $\phi_{s3}=5.04^0$, following by wheels on the 2nd axle lift off at $\phi_{s3}=5.50^0$. The relative rollover condition of the baseline vehicle is obtained as the moment when wheels on both the 2nd and 3rd axles lift off the road surface. The simulation run is stopped after obtaining relative rollover condition. The exact value of ϕ_{s3} corresponding to wheels lift-off on the 1st axle is thus not attained. As shown in Table 3.6, relative rollover condition is not influenced by parameter variations conducted in this study, and remains the same as that of the baseline vehicle. The tractor frame compliance and auxiliary roll stiffness of the front axle have insignificant influence on *SRT*, while auxiliary roll stiffness of the 2nd and 3rd axles and fifth wheel compliance show relatively large influence on *SRT*. When auxiliary roll stiffness of the 2nd composite axle increases by 50%, wheels on the 2nd composite axle lifts off first, as highlighted in Table 3.6.

The effects of dimensional parameters on static rollover threshold and relative rollover condition are illustrated in Table 3.7. The results reveal that relative rollover condition of the tractor semi-trailer is not influenced by the parameter variations. The parameters which have significant influence on *SRT* are wheel track (T_2 , T_3), and the distance between trailer sprung mass c.g. and trailer suspension roll center (h_{R3}). Simulation runs are also performed when similar parameters for the three composite axles

are varied at the same time, as shown in the last three rows in Table 3.7. When the values of suspension spring spacing (s_1 , s_2 , and s_3) is increased by 30%, SRT is increased by 2%. When half wheel track is increased by 30%, SRT , however, is increased by 24%. A 30% decrease in h_{Ri} ($i=1, 2, 3$) will increase SRT by 29%.

Effects of tire elastic properties on relative rollover condition and SRT are illustrated in Table 3.8. Relative rollover condition is again not influenced by the parameter variations, and remains the same as that of the baseline vehicle. An increase in tire vertical stiffness(KT_y) by 40% will increase SRT by 3%, while the influence of tire overturning and lateral stiffness rates on SRT is insignificant.

Table 3.6: Parametric study: effects of auxiliary roll stiffness and roll compliance.

		φ_{s3} (deg) at lift-off of wheels on			SRT	Relative Rollover Condition (wheels lift on)		
		1 st axle	2 nd axle	3 rd axle		1 st axle	2 nd axle	3 rd axle
Baseline		>5.50	5.50	5.04	0.417	no	yes	yes
K_{a1}	-50%	>5.50	5.50	5.04	0.416	no	yes	yes
	+50%	>5.50	5.50	5.06	0.419	no	yes	yes
K_{a2}	-50%	>6.49	6.49	5.09	0.406	no	yes	yes
	+50%	>5.06	4.80	5.06	0.422	no	yes	yes
K_{a3}	-50%	>5.50	5.50	5.26	0.418	no	yes	yes
	+50%	>5.50	5.50	4.29	0.414	no	yes	yes
KF_1	-50%	>5.50	5.50	5.04	0.417	no	yes	yes
	+50%	>5.50	5.50	5.04	0.417	no	yes	yes
KF_2	-50%	>6.05	6.05	5.08	0.410	no	yes	yes
	+50%	>5.17	5.17	5.08	0.420	no	yes	yes

Table 3.7: Parametric study: effects of vehicle design and operating parameters.

		φ_{s3} (deg) at lift-off of wheels on			SRT	Relative Rollover Condition (wheels lift on)		
		1 st axle	2 nd axle	3 rd axle		1 st axle	2 nd axle	3 rd axle
Baseline		>5.50	5.50	5.04	0.417	no	yes	yes
s_1	-30%	>5.50	5.50	5.05	0.413	no	yes	yes
	+30%	>5.50	5.50	5.02	0.422	no	yes	yes
s_2	-30%	>6.71	6.71	5.11	0.404	no	yes	yes
	+30%	>5.06	4.74	5.06	0.421	no	yes	yes
s_3	-30%	>6.27	5.59	6.27	0.409	no	yes	yes
	+30%	>5.50	5.50	4.24	0.414	no	yes	yes
T_1	-30%	>5.50	5.50	5.04	0.416	no	yes	yes
	+30%	>5.50	5.50	5.04	0.417	no	yes	yes
T_2	-30%	>5.39	5.39	5.15	0.362	no	yes	yes
	+30%	>7.37	7.37	4.94	0.450	no	yes	yes
T_3	-30%	>7.04	7.04	5.06	0.338	no	yes	yes
	+30%	>5.06	5.06	4.79	0.484	no	yes	yes
h_{R1}	-30%	>5.50	5.50	5.03	0.419	no	yes	yes
	+30%	>5.50	5.50	5.04	0.416	no	yes	yes
h_{R2}	-30%	>5.50	5.50	5.04	0.417	no	yes	yes
	+30%	>5.50	5.50	5.04	0.416	no	yes	yes
h_{R3}	-30%	>4.73	4.73	4.61	0.538	no	yes	yes
	+30%	>7.15	7.15	5.17	0.319	no	yes	yes
s_i (i=1, 2,3)	-30%	>6.60	6.60	6.27	0.403	no	yes	yes
	+30%	>4.73	4.73	4.20	0.427	no	yes	yes
T_i (i=1, 2,3)	-30%	>5.72	5.72	5.24	0.295	no	yes	yes
	+30%	>7.04	7.04	4.76	0.515	no	yes	yes
h_{Ri} (i=1, 2,3)	-30%	>4.84	4.84	4.60	0.540	no	yes	yes
	+30%	>7.15	7.15	5.18	0.317	no	yes	yes

Table 3.8: Parametric study: effects of tire elastic properties.

		φ_{s3} (deg) at lift-off of wheels on			SRT	Relative Rollover Condition (wheels lift on)		
		1 st axle	2 nd axle	3 rd axle		1 st axle	2 nd axle	3 rd axle
Baseline		>5.50	5.50	5.04	0.417	no	yes	yes
KT_{η}	-40%	>7.37	7.37	6.74	0.390	no	yes	yes
	+40%	>4.62	4.62	4.31	0.429	no	yes	yes
KOT_{η}	-40%	>5.50	5.50	5.03	0.415	no	yes	yes
	+40%	>5.50	5.50	5.05	0.418	no	yes	yes
KYT_{η}	-40%	>5.50	5.50	5.02	0.411	no	yes	yes
	+40%	>5.50	5.50	5.05	0.419	no	yes	yes

Relative rollover condition and static rollover threshold of the tractor semi-trailer combination are further investigated for an array of heavy vehicle suspension configurations [87]. The deflection-force characteristics of six different suspension configurations are illustrated in Figure 3.14, where *FA* denotes front suspension spring and *RA*, *RB*, *RC* represent three different tractor rear axle suspension springs. *TA* and *TB* denotes trailer axle suspension springs. Table 3.9 illustrates roll center heights and auxiliary roll stiffness rates of the six suspension configurations. Six different combinations are formed based on the front, rear and trailer suspension springs. The simulation results reveal that relative rollover condition of the tractor semi-trailer is approached when wheels on tractor's rear and trailer axles lift off the road surface, irrespective of suspension springs used, as illustrated in Table 3.10. The static roll threshold (*SRT*), however, is strongly dependent on suspension springs. The largest *SRT* of 0.39g is obtained for the combination *FA-RA-TB*, which consists of suspensions with the largest vertical and roll stiffness rates, as shown in Figure 3.14 and Table 3.9. The

lowest *SRT* of 0.324g, on the other hand, is obtained for the combination FA-RC-TA, which comprises the suspensions with the lowest vertical and roll stiffness rates.

Table 3.9: Roll center and auxiliary roll stiffness of different suspension configurations.

	FA	RA	RB	RC	TA	TB
Roll center height (m)	0.465	0.838	0.737	0.686	0.737	0.686
Auxiliary roll stiffness (Nm/deg)	432	6780	3842	1695	2034	13560

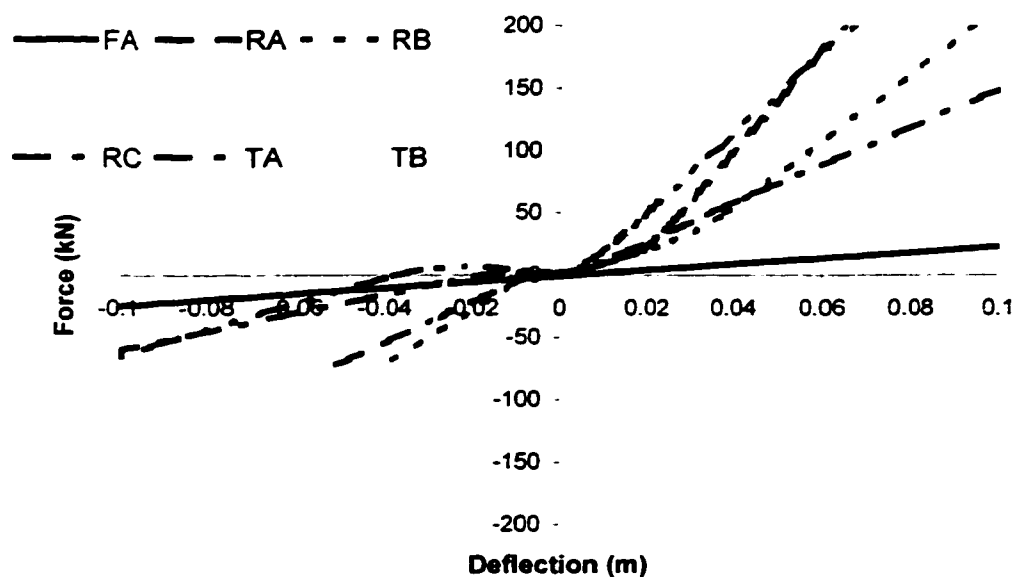


Figure 3.14: Force-deflection characteristics of different suspension springs.

Table 3.10: Parametric study: effects of different combinations of suspension springs.

combinations of suspension springs	φ_{s3} (deg) at lift-off of wheels on			SRT	Relative Rollover Condition (wheels lift on)		
	1 st axle	2 nd axle	3 rd axle		1 st axle	2 nd axle	3 rd axle
(1) FA-RA-TA	>7.37	7.16	7.37	0.378	no	yes	yes
(2) FA_RA_TB	>6.16	6.16	5.13	0.390	no	yes	yes
(3) FA-RB-TA	>8.03	8.03	7.41	0.365	no	yes	yes
(4) FA-RB-TB	>8.14	8.14	5.24	0.363	no	yes	yes
(5) FA-RC-TA	>10.67	10.67	7.58	0.324	no	yes	yes
(6) FA-RC-TB	>7.04	7.04	5.32	0.331	no	yes	yes

3.3.3 B- and C-Train Doubles

The simulation parameters of a typical B-train double, comprising a three-axle tractor, a two-axle semi-trailer and another two-axle semi-trailer with B-dolly, represented by four-axle roll plane model, are illustrated in Table 3.11. Equation 3.42 is solved for small increment of roll angle of the last trailer (φ_{s4}). The roll signature of the B-double is illustrated in Figure 3.15. Tire vertical deflections on each axle are also shown in the figure to help in identifying relative rollover condition of the vehicle combination. The maximum lateral acceleration (or *SRT*) occurs when wheels on the 2nd and 3rd composite axles lift off the ground. Static rollover threshold is observed to be 0.43g. The roll stiffness of the front and rearmost axles are not stiff enough to hold the lateral acceleration after wheels lift-off on the 2nd and 3rd composite axles. Relative rollover condition of the combination is thus identified as the moment when wheels on tractor's rear and the first semi-trailer axles lift off the road surface.

A parametric sensitivity analysis is carried for sprung mass c.g. height and wheel track of the last two composite axles. The simulation results in terms of static rollover threshold and relative rollover condition are summarized in Table 3.12. The c.g. height of the first semi-trailer (h_{R3}) shows significant influence on *SRT*. When h_{R3} is increased by 30%, *SRT* is reduced from baseline value 0.432g to 0.340g. If h_{R3} is reduced by 30%, *SRT* is increased from 0.432g to 0.538g. The c.g. height of the second semitrailer (h_{R4}) shows relatively small effect on *SRT*. Relative rollover condition is reached when wheels on the 2nd and 3rd axles lift off the ground for single parameter variation in h_{R3} or h_{R4} . When h_{R3} is decreased by 30% and h_{R4} is increased by 30%, however, relative rollover condition is obtained as the moment when wheels on the 3rd and 4th composite axles lift off. This relative rollover condition is also obtained when half wheel track on the 4th axle is reduced by 30%. Wheel track of the 3rd composite axle also shows significant influence on *SRT*, while the influence of wheel track of the 4th composite axle is relatively small.

3.3.4 A-Train Doubles

An A-train double is considered as two independent roll units: a tractor semi-trailer, and a full trailer. The methods developed for tractor semi-trailers and full trailers can be used to predict static rollover threshold and relative rollover condition of A-train doubles. Based on the definition of static rollover threshold, *SRT* of an A-train double is chosen from the *SRT* values of the two roll units by “select-low” principle. The roll unit with lower *SRT* value is considered as the dominant unit in terms of roll instability, and

whose *SRT* is taken as *SRT* of the A-train double. Relative rollover condition of A-train double is considered as that of the dominant roll unit. Relative rollover condition and *SRT* of tractor semi-trailers and full trailers have been thoroughly investigated in the previous sections, and the results can be directly interpreted to A-train doubles based on the “select-low” principle.

Table 3.11: Simulation parameters for a B-train double.

	Axle 1	Axle 2	Axle 3	Axle 4
Axle weight (kg)	548 (W_{u1})	2270 (W_{u2})	1362 (W_{u3})	1360 (W_{u4})
Axle load (kg)	4404 ($WAXL_1$)	14365 ($WAXL_2$)	14365 ($WAXL_3$)	14365 ($WAXL_4$)
Distance from roll center to sprung weight c.g. (m)	0.656 (h_{R1})	0.282 (h_{R2})	1.328 (h_{R3})	1.05 (h_{R4})
Auxiliary roll stiffness (kNm/rad)	24.78 (K_{a1})	745.2 (K_{a2})	777.6 (K_{a3})	648 (K_{a4})
Half suspension spacing (m)	0.406 (s_1)	0.483 (s_2)	0.559 (s_3)	0.559 (s_4)
Wheel radius (m)	0.508 (R_1)	0.508 (R_2)	0.508 (R_3)	0.508 (R_4)
Half wheel track (m)	1.016 (T_1)	0.749 (T_2)	0.826 (T_3)	0.826 (T_4)
Dual tire spacing (m)	0 (A_1)	0.33 (A_2)	0.33 (A_3)	0.33 (A_4)
Tire vertical stiffness (kN/m)	847.6 (KT_{1j})	847.6 (KT_{2j})	847.6 (KT_{3j})	847.6 (KT_{4j})
Tire overturning stiffness (Nm/deg)	113 (KOT_{1j})	226 (KOT_{2j})	226 (KOT_{3j})	226 (KOT_{4j})
Tire lateral stiffness (N/m)	876 (KYT_{1j})	1752 (KYT_{2j})	1752 (KYT_{3j})	1752 (KYT_{4j})
Load on the fifth wheel (kg)	13620 (W_5)			
Roll stiffness of tractor frame (kNm/rad)	54.9 (KF_1)			
Roll stiffness of fifth wheel (kNm/rad)	5995 (KF_2)			
Roll stiffness of B-dolly (kN/rad)	1000 (KF_3)			
combinations of suspension springs	FA-RA-TA-RB			

Table 3.12: Parametric study on static rollover threshold and relative rollover condition of a B-train double.

		SRT (g)	Relative Rollover Condition (wheels lift on)			
			1 st axle	2 nd axle	3 rd axle	4 th axle
baseline		0.432	no	yes	yes	no
h_{R3}	-30%	0.538	no	yes	yes	no
	+30%	0.340	no	yes	yes	no
h_{R4}	-30%	0.440	no	yes	yes	no
	+30%	0.428	no	yes	yes	no
h_{R3} -30%		0.500	no	no	yes	yes
h_{R4} +30%						
T_3	-30%	0.372	no	yes	yes	no
	+30%	0.493	no	yes	yes	no
T_4	-30%	0.424	no	no	yes	yes
	+30%	0.438	no	yes	yes	no

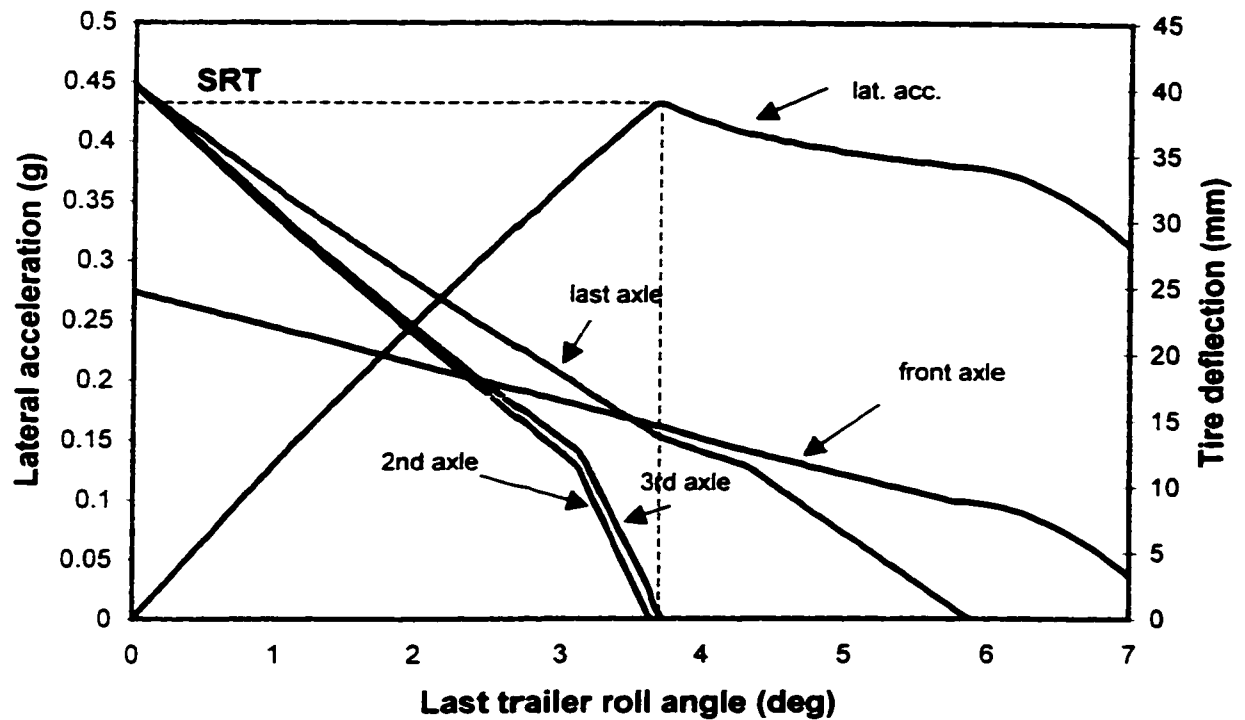


Figure 3.15: Roll performance signature of a B-train double.

3.3.5 Roll Safety Factor

The results presented above reveal that relative rollover condition of heavy freight vehicles does not necessarily require all the wheels on a single track to lose road contact. Relative rollover condition of straight trucks could be approached when wheels on the front and/or rear axles lift off the ground, while that of tractor semitrailer combinations is approached when wheels on tractor rear and trailer axles lift off the road surface. The *LTR* measure defined in Equation 2.9 is based upon the ratio of load transfer on all the axle wheels. *LTR* may thus lead to erroneous prediction of relative rollover condition. Alternatively, a Roll Safety Factor (*RSF*) measure is proposed on the basis of load

transfer ratio of the axles, which experience wheel lift-off. The instantaneous value of RSF of a vehicle subject to a dynamic directional maneuver can thus be derived from:

$$RSF = \frac{\sum_{j=1}^m (FL_j - FR_j)}{\sum_{j=1}^m (FL_j + FR_j)} \quad (3.44)$$

where $m \leq n$ is the number of axles that should experience loss of wheel-road contact in order to approach relative rollover condition. From Equation (3.44) it is apparent that RSF will approach value of ± 1 when relative roll instability condition is reached, irrespective of the vehicle configurations, whereas no such a unique value exists for LTR when relative rollover condition is approached. RSF is thus considered as a reliable rollover indicator, and can be considered as a mathematical representation of relative rollover condition of heavy vehicles.

3.4 SUMMARY

Relative roll instability criterion is employed for investigation of rollover conditions and static rollover threshold of different combinations of heavy vehicles. Two-axle representation of heavy vehicles such as straight trucks and full trailers is realized by grouping the front and the rear axles into their respective single composite axles. An analytical relationship between sprung mass roll angle and lateral acceleration is derived for straight trucks and full trailers. Static roll plane models for tractor semi-trailer combinations and B- or C-train doubles are also developed for the investigation of their respective static rollover threshold and relative rollover conditions. An A-double is considered as two independent roll units comprising a tractor semi-trailer and a full

trailer. Tractor semi-trailer combinations are characterized by a three-composite axle vehicle, while B- or C- doubles are represented by a four-composite-axle vehicle model. The equations of static roll equilibrium are derived upon balancing the roll moments acting on the sprung and unsprung masses, lateral forces acting on the tires, and vertical suspension and tires forces. The equilibrium equations are solved for small perturbation of roll angle of the last sprung weight to derive a relationship between the lateral acceleration and sprung mass roll angle of the last trailer.

A parametric sensitivity study is carried out to investigate the influence of an array of vehicle design parameters and suspension configurations on *SRT* and relative rollover conditions of straight trucks, tractor semi-trailer combinations, and B- /C- doubles. It is concluded that relative rollover condition of straight trucks is strongly influenced by front/rear roll stiffness distribution ratio. Relative rollover condition of straight trucks could be approached when wheels on the front and/or rear axles lift off the ground. Relative rollover condition for tractor semitrailer combinations is approached when wheels on tractor rear and trailer axles lift off the road surface, and is not altered by vehicle and suspension parameter variations explored in this study. Relative rollover condition of B- or C- doubles may be reached when wheels on both tractor's rear and the first semi-trailer axles lift off or when wheels on the first and second semi-trailer axles lift off, depending on vehicle configurations. Relative rollover condition of heavy vehicles is mathematically expressed by a parameter referred to as roll safety factor. Static rollover threshold of the combinations is significantly influenced by sprung mass c.g. height, wheel track, suspension spring spacing, and auxiliary roll stiffness. Tractor frame compliance, however, shows insignificant influence on *SRT*.

CHAPTER 4

DYNAMIC RELATIVE AND ABSOLUTE ROLL STABILITY ANALYSIS

4.1 INTRODUCTION

The rollover propensity of a heavy vehicle, in general, is described quantitatively by its *static rollover threshold (SRT)* [33]. Static rollover threshold, however, is intended to characterize the roll stability of a vehicle subject to a steady lateral acceleration field corresponding to a constant speed steady turning maneuver, in conjunction with certain wheels on a single track of the vehicle losing road contact, referred to as the relative rollover condition. When the lateral acceleration level of the vehicle reaches its *SRT* value in a dynamic maneuver, definite occurrence of an actual rollover of the vehicle may not be assured. An actual rollover occurs only if the sustained level of lateral acceleration is attained for a definite period of time, when the vehicle is in its absolute rollover condition, which is also referred to as tip-over position. The existence of a lateral disturbance or perturbation will then lead to the rollover of the vehicle. In a tip-over situation, the cg height of the vehicle approaches a considerably higher value than that attained when wheels lift off the ground. A considerable amount of work thus must be done to bring the vehicle from the relative rollover position to its tip-over position [89].

Rollover of heavy vehicles in a dynamic directional maneuver, however, may occur at considerably different levels of lateral acceleration, depending on the rollover criteria employed. Moreover, dynamic roll response characteristics of different units of an articulated heavy vehicle are known to be quite different in both amplitude and phase angle [19]. Therefore, under dynamic conditions, the static rollover threshold can not be

simply employed without proper consideration of all the lateral acceleration response parameters.

In this chapter, a constant velocity yaw/roll plane model is derived for relative roll instability analysis of articulated vehicles in dynamic directional maneuvers. Dynamic rollover threshold of articulated heavy vehicles is proposed based on relative rollover criterion, and analyzed using the yaw roll model. A roll plane model for investigation of absolute roll instability of heavy vehicles is further derived. The equations of motion are derived using the energy approach, which are considered valid until the vehicle approaches its tip-over position. Dynamic rollover limits are analyzed using the proposed roll plane model, on the base of the absolute rollover criterion.

4.2 DEVELOPMENT OF A CONSTANT VELOCITY YAW/ROLL MODEL

In developing the vehicle model, it is assumed that the vehicle is travelling at a constant forward speed on a perfectly smooth road [29]. Each of sprung mass is thus characterized as a rigid body with five-degree-of-freedom (*DOF*) (lateral, vertical, roll, pitch and yaw motion), while each axle is considered as a beam axle with two-*DOF* (roll and bounce) motions. The equations of motion for the sprung and unsprung masses can be written with respect to the corresponding body-fixed coordinate system, shown in Figure 4.1. For a five-axle tractor semi-trailer combination, coordinate system attached to the c.g. of sprung masses is denoted as (X_{si}, Y_{si}, Z_{si}) , $i=1, 2$, and that located at the center of each axle is represented by (X_{uj}, Y_{uj}, Z_{uj}) , $j=1, \dots, 5$.

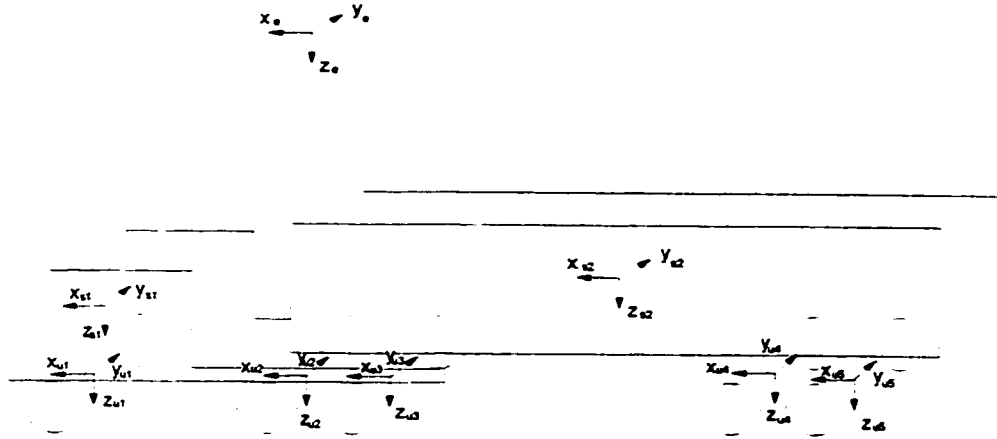


Figure 4.1: Axle system of the yaw/roll plane model.

4.2.1 Equations of Motion

Equations of motion for each sprung mass i

The coupled differential equation of motion for sprung mass i are derived as:

lateral motion:	$m_{si} \dot{v}_{si} - m_{si} (p_{si} w_{si} - r_{si} u_{si}) = \sum Y_{si}$	
vertical motion	$m_{si} \dot{w}_{si} - m_{si} (q_{si} u_{si} - p_{si} v_{si}) = \sum Z_{si}$	
roll motion	$I_{xx_{si}} \dot{p}_{si} - (I_{yy_{si}} - I_{zz_{si}}) q_{si} r_{si} = \sum L_{si}$	
pitch motion	$I_{yy_{si}} \dot{q}_{si} - (I_{zz_{si}} - I_{xx_{si}}) p_{si} r_{si} = \sum M_{si}$	
yaw motion	$I_{zz_{si}} \dot{r}_{si} - (I_{xx_{si}} - I_{yy_{si}}) q_{si} p_{si} = \sum N_{si}$	(4.1)

where m_{si} is the sprung mass, and $I_{xx_{si}}$, $I_{yy_{si}}$ and $I_{zz_{si}}$ are the mass moments of inertia about the fixed (X_{si}, Y_{si}, Z_{si}) axes, respectively. v_{si} and w_{si} are the lateral and vertical velocities of the sprung mass i , respectively. p_{si} , q_{si} and r_{si} respectively are the roll, pitch and yaw velocities of the sprung mass i . The terms on the right side of the equation set (4.1) represent the total external forces and moments acting in the corresponding directions.

Equations of motion for each unsprung mass j

The equations of motion for each unsprung mass are also derived in a similar manner, are expressed as:

$$\begin{array}{ll} \text{vertical motion} & m_{uj} \dot{w}_{uj} = \sum Z_{uj} \\ \text{roll motion} & I_{xx_{uj}} \dot{p}_{uj} = \sum L_{uj} \end{array} \quad (4.2)$$

where m_{uj} and $I_{xx_{uj}}$ are the mass and mass moment of inertia of unsprung mass j . p_{uj} and w_{uj} are the roll rate and bounce velocity of the unsprung mass j . $\sum Z_{uj}$ and $\sum L_{uj}$ are the total external force and moment in vertical and roll directions of the unsprung mass, respectively.

Equations shown in (4.1) and (4.2) are written in the body-fixed coordinate systems. The vehicle attitude and trajectory, however, should be defined with respect to the inertial coordinate system fixed on the ground, referred to as (X_e, Y_e, Z_e) , as shown in Figure 4.1. The relationship between the body-fixed axis system (X_{si}, Y_{si}, Z_{si}) and the inertial axis system X_e, Y_e, Z_e can be expressed using Euler angles in yaw (α_{si}), pitch (β_{si}), roll (ϕ_{si}). The transformation matrix relating the coordinate systems can be expressed as:

$$\begin{aligned}
{}^e R &= R_{z_w}(\alpha_{st}) R_{y_w}(\beta_{st}) R_{x_w}(\varphi_{st}) \\
&= \begin{bmatrix} c\alpha_{st} c\varphi_{st} & c\alpha_{st} s\beta_{st} s\varphi_{st} - s\alpha_{st} c\varphi_{st} & c\alpha_{st} s\beta_{st} c\varphi_{st} + s\alpha_{st} s\varphi_{st} \\ s\alpha_{st} c\beta_{st} & s\alpha_{st} s\beta_{st} s\varphi_{st} + c\alpha_{st} c\varphi_{st} & s\alpha_{st} s\beta_{st} c\varphi_{st} - c\alpha_{st} s\varphi_{st} \\ -s\beta_{st} & c\beta_{st} s\varphi_{st} & c\beta_{st} c\varphi_{st} \end{bmatrix}
\end{aligned}$$

and

$${}^st R = {}^e R^T = \begin{bmatrix} c\alpha_{st} c\varphi_{st} & s\alpha_{st} c\beta_{st} & -s\beta_{st} \\ c\alpha_{st} s\beta_{st} s\varphi_{st} - s\alpha_{st} c\varphi_{st} & s\alpha_{st} s\beta_{st} s\varphi_{st} + c\alpha_{st} c\varphi_{st} & c\beta_{st} s\varphi_{st} \\ c\alpha_{st} s\beta_{st} c\varphi_{st} + s\alpha_{st} s\varphi_{st} & s\alpha_{st} s\beta_{st} c\varphi_{st} - c\alpha_{st} s\varphi_{st} & c\beta_{st} c\varphi_{st} \end{bmatrix} \quad (4.3)$$

where ${}^e R$ is the transformation matrix from the coordinate system (X_{st}, Y_{st}, Z_{st}) to the inertial system (X_e, Y_e, Z_e) , and ${}^st R$ is the transpose of ${}^e R$. c and s denote the *cosine* and *sine* functions of the Euler's angles, respectively. The unit vectors $(\bar{i}_{st}, \bar{j}_{st}, \bar{k}_{st})$ in (X_{st}, Y_{st}, Z_{st}) system is thus related to the unit vectors $(\bar{i}_e, \bar{j}_e, \bar{k}_e)$ in (X_e, Y_e, Z_e) system as:

$$\begin{bmatrix} \bar{i}_{st} \\ \bar{j}_{st} \\ \bar{k}_{st} \end{bmatrix} = {}^st R \begin{bmatrix} \bar{i}_e \\ \bar{j}_e \\ \bar{k}_e \end{bmatrix} \quad (4.4)$$

Thus, the translational velocities (u_e, v_e, w_e) and position coordinates (x_e, y_e, z_e) of the sprung mass i with respect to the inertial axis system can be obtained as:

$$\begin{bmatrix} u_e \\ v_e \\ w_e \end{bmatrix} = {}^e R \begin{bmatrix} u_{st} \\ v_{st} \\ w_{st} \end{bmatrix}$$

and

$$\begin{aligned}
x_e &= x_0 + \int u_e dt \\
y_e &= y_0 + \int v_e dt
\end{aligned}$$

$$z_e = z_0 + \int w_e dt \quad (4.5)$$

where x_0 , y_0 , and z_0 are the initial coordinates of the sprung mass i with respect to the inertial system. Similarly, the rotational velocities ($\dot{\alpha}_{si}$, $\dot{\beta}_{si}$, and $\dot{\varphi}_{si}$) and displacements (α_{si} , β_{si} , and φ_{si}) of the sprung mass i with respect to the inertial axis system are derived as:

$$\begin{bmatrix} \dot{\alpha}_{si} \\ \dot{\beta}_{si} \\ \dot{\varphi}_{si} \end{bmatrix} = \frac{1}{c\beta_{si}} \begin{bmatrix} 0 & s\varphi_{si} & c\varphi_{si} \\ 0 & c\beta_{si}c\varphi_{si} & -c\beta_{si}s\varphi_{si} \\ c\beta_{si} & s\varphi_{si}s\beta_{si} & s\beta_{si}c\varphi_{si} \end{bmatrix} \begin{bmatrix} p_{si} \\ q_{si} \\ r_{si} \end{bmatrix}$$

and

$$\begin{aligned} \alpha_{si} &= \int_0^t \dot{\alpha}_{si} dt \\ \beta_{si} &= \int_0^t \dot{\beta}_{si} dt \\ \varphi_{si} &= \int_0^t \dot{\varphi}_{si} dt \end{aligned} \quad (4.6)$$

The rotation matrix of the unsprung mass j with respect to the inertial axis system can be similarly obtained as:

$${}^e R = R_{z_{uj}}(\alpha_{sj}) R_{y_{uj}}(0) R_{x_{uj}}(\varphi_{uj}) \quad (4.7)$$

where φ_{uj} is the roll angle of axle j . The relationship between the coordinate systems of sprung mass i and unsprung mass j , is derived from Equations (4.3) and (4.7) as:

$$\begin{aligned} {}^{uj} R &= {}^e R^{-1} {}^e R = R_{x_{uj}}^{-1}(\varphi_{uj}) R_{y_{uj}}(\beta_{si}) R_{x_{uj}}(\varphi_{si}) \\ &= \begin{bmatrix} c\beta_{si} & s\beta_{si}s\varphi_{si} & s\beta_{si}c\varphi_{si} \\ -s\varphi_{uj}s\beta_{si} & c\varphi_{uj}c\varphi_{si} + s\varphi_{uj}s\varphi_{si}c\beta_{si} & -s\varphi_{uj}c\varphi_{si} + s\varphi_{uj}c\varphi_{si}c\beta_{si} \\ -c\varphi_{uj}s\beta_{si} & s\varphi_{uj}c\varphi_{si} + c\varphi_{uj}s\varphi_{si}c\beta_{si} & s\varphi_{uj}s\varphi_{si} + c\varphi_{uj}c\varphi_{si}c\beta_{si} \end{bmatrix} \end{aligned} \quad (4.8)$$

Since the pitch angel β_{si} is very small compared to roll and yaw angles, Equation (4.8) can be simplified considering, $\sin \beta_{si} \cong \beta_{si}$ and $\cos \beta_{si} \cong 1$:

$${}_{s1}^{uj}R = \begin{bmatrix} 1 & \beta_{s1} \sin \varphi_{s1} & \beta_{s1} \cos \varphi_{s1} \\ -\beta_{s1} \sin \varphi_{uj} & \cos(\varphi_{s1} - \varphi_{uj}) & -\sin(\varphi_{s1} - \varphi_{uj}) \\ -\beta_{s1} \cos \varphi_{uj} & \sin(\varphi_{s1} - \varphi_{uj}) & \cos(\varphi_{s1} - \varphi_{uj}) \end{bmatrix} \quad (4.9)$$

By assuming small pitch angles, the rotation matrix of the coordinate system (X_{s1}, Y_{s1}, Z_{s1}) with respect to (X_{s2}, Y_{s2}, Z_{s2}) can be derived as:

$${}_{s1}^{s2}R = {}_{s2}^e R^T {}_{s1}^e R = \begin{bmatrix} T_{11} & T_{12} & T_{13} \\ T_{21} & T_{22} & T_{23} \\ T_{31} & T_{32} & T_{33} \end{bmatrix} \quad (4.10)$$

where:

$$\begin{aligned} T_{11} &= \cos(\alpha_{s2} - \alpha_{s1}) \\ T_{12} &= \beta_{s1} \sin \varphi_{s1} \cos(\alpha_{s2} - \alpha_{s1}) + \cos \varphi_{s1} \sin(\alpha_{s2} - \alpha_{s1}) - \beta_{s2} \sin \varphi_{s1} \\ T_{13} &= \beta_{s1} \cos \varphi_{s1} \cos(\alpha_{s2} - \alpha_{s1}) - \sin \varphi_{s1} \sin(\alpha_{s2} - \alpha_{s1}) - \beta_{s2} \cos \varphi_{s1} \\ T_{21} &= \beta_{s2} \sin \varphi_{s2} \cos(\alpha_{s2} - \alpha_{s1}) - \cos \varphi_{s2} \sin(\alpha_{s2} - \alpha_{s1}) - \beta_{s1} \sin \varphi_{s2} \\ T_{22} &= \beta_{s2} \sin \varphi_{s2} \cos \varphi_{s1} \sin(\alpha_{s2} - \alpha_{s1}) - \beta_{s1} \sin \varphi_{s1} \cos \varphi_{s2} \sin(\alpha_{s2} - \alpha_{s1}) \\ &\quad + \cos \varphi_{s1} \cos \varphi_{s2} \cos(\alpha_{s2} - \alpha_{s1}) + \sin \varphi_{s1} \sin \varphi_{s2} \\ T_{23} &= -\beta_{s2} \sin \varphi_{s2} \sin \varphi_{s1} \sin(\alpha_{s2} - \alpha_{s1}) - \beta_{s1} \cos \varphi_{s1} \cos \varphi_{s2} \sin(\alpha_{s2} - \alpha_{s1}) \\ &\quad - \sin \varphi_{s1} \cos \varphi_{s2} \cos(\alpha_{s2} - \alpha_{s1}) + \cos \varphi_{s1} \sin \varphi_{s2} \\ T_{31} &= \beta_{s2} \cos \varphi_{s2} \cos(\alpha_{s2} - \alpha_{s1}) + \sin \varphi_{s2} \sin(\alpha_{s2} - \alpha_{s1}) - \beta_{s1} \cos \varphi_{s2} \\ T_{32} &= \beta_{s2} \cos \varphi_{s2} \cos \varphi_{s1} \sin(\alpha_{s2} - \alpha_{s1}) + \beta_{s1} \sin \varphi_{s1} \sin \varphi_{s2} \sin(\alpha_{s2} - \alpha_{s1}) \\ &\quad - \cos \varphi_{s1} \sin \varphi_{s2} \cos(\alpha_{s2} - \alpha_{s1}) + \sin \varphi_{s1} \cos \varphi_{s2} \\ T_{33} &= -\beta_{s2} \cos \varphi_{s2} \sin \varphi_{s1} \sin(\alpha_{s2} - \alpha_{s1}) - \beta_{s1} \cos \varphi_{s1} \sin \varphi_{s2} \sin(\alpha_{s2} - \alpha_{s1}) \\ &\quad + \sin \varphi_{s1} \sin \varphi_{s2} \cos(\alpha_{s2} - \alpha_{s1}) + \cos \varphi_{s1} \cos \varphi_{s2} \end{aligned}$$

4.2.2 Suspension and Tire Forces

The external forces and moments shown on the right side of the equations of motion of (4.1) and (4.2) involve suspension, tire, roll center and constraint forces. Suspension forces, F_y , comprise of a lateral force F_{Rj} , acting through the suspension roll center, and vertical forces acting perpendicular to the Y_{uj} axis of the unsprung mass j :

$$F_{y_j} = \begin{bmatrix} 0 \\ F_{R_j} \\ -(F_{j1} + F_{j2}) \end{bmatrix}^T \begin{bmatrix} \ddot{i}_{uj} \\ \ddot{j}_{uj} \\ \ddot{k}_{uj} \end{bmatrix} \quad (4.11)$$

where F_{j1} and F_{j2} are the compressive or tensile forces generated by the left and right suspension springs respectively, which can be calculated using force-deflection characteristics of suspension springs. The Equation (4.11) can be written with respect to the coordinate system fixed to the sprung mass i as:

$$F_{y_j} = \begin{bmatrix} 0 \\ F_{R_j} \\ -(F_{j1} + F_{j2}) \end{bmatrix}^T {}^{uj}R_{si} \begin{bmatrix} \ddot{i}_{si} \\ \ddot{j}_{si} \\ \ddot{k}_{si} \end{bmatrix} \quad (4.12)$$

The lateral suspension force F_{R_j} are computed from dynamic equilibrium of the axle forces acting along Y_{uj} direction, such that:

$$F_{R_i} = -m_{uj} a_{uj} \ddot{j}_{uj} + \sum F_{ry} \cos \varphi_{uj} - \sum F_{tz} \sin \varphi_{uj} + m_{uj} g \sin \varphi_{uj} \quad (4.13)$$

where a_{uj} is the lateral acceleration of unsprung mass j . $\sum F_{ry}$ and $\sum F_{tz}$ are the total lateral and vertical forces due to tires on unsprung mass j . The lateral or cornering forces due to tires are derived from the reported measured data, which is provided in a tabular format as a function of tire side-slip angles and vertical loads. The aligning torque due to tires is also extracted from the measured data in a similar manner. The instantaneous lateral force and aligning torque are thus computed from linear interpolation of the tabular tire data, as a function of the tire side-slip angle. The side-slip angle of i^{th} tire of axle j is expressed as:

$$\psi_{ij} = \tan^{-1}(v_{axle-j} / u_{tire-ij}) - \delta_j \quad (4.14)$$

where v_{axle-j} is the lateral velocity of the axle j , and u_{tire-j} is the forward velocity of the i^{th} tire on axle j . δ_j represents the angle made by the wheel plane with respect to the longitudinal axis of the sprung mass coordinate system. The vertical tire forces, $F_{z_{ij}}$, can be calculated from:

$$F_{z_{ij}} = KT_{ij} \Delta_{ij} \quad (4.15)$$

where KT_{ij} and Δ_{ij} are the vertical stiffness and deflection of tire i on axle j , respectively.

4.2.3 Constraint Equations

The differential equations of motion for the sprung masses, Equation set (4.1), contain the constraint forces and moments due to couplings between various sprung masses. Since the commonly used coupling mechanisms are relatively rigid in translation, the forces transmitted through the couplings are determined from kinematic constraints, which state that the acceleration at a coupling point is the same for both the leading and the trailing units of the combination. The constraint moments, on the other hand, are computed by considering the roll compliance due to coupling mechanisms. The transmitted moments are thus derived as a function of the relative roll displacement between the leading and trailing units. Specifically, the fifth wheel and the inverted fifth wheel arrangement permit the leading and the trailing units to yaw and pitch with respect to each other, but are considerably stiff in roll. A kingpin-type connection permits only yaw motion, while a pintle hook connection allows roll, bounce, yaw, and pitch motions between coupled units. Such coupling mechanisms constrain only relative lateral

position, such that the lateral position of the leading coupler is the same as that of the forward end of the drawbar.

The equations of motion of a vehicle with n sprung masses and m unsprung masses can be written in a matrix form as:

$$M\ddot{\underline{x}} + N(\underline{x}, \dot{\underline{x}}) + P(\underline{x})\underline{f}_c = 0 \quad (4.16)$$

where M is the $(k \times k)$ inertia matrix ($k = 5n + 2m$). \underline{x} is a vector of position variables of size k . $N(\underline{x}, \dot{\underline{x}})$ is a $(k \times 1)$ vector of forces and moments, and vehicle dimensions. $P(\underline{x})$ is a $k \times k$ matrix, and \underline{f}_c is a vector of unknown constrain forces. Equation (4.16) can be solved for acceleration vector, $\ddot{\underline{x}}$, such that:

$$\ddot{\underline{x}} = -M^{-1}N(\underline{x}, \dot{\underline{x}}) - M^{-1}P(\underline{x})\underline{f}_c \quad (4.17)$$

The kinematic constrains posed by the various hitch points are written as a set of acceleration constrain equations:

$$B\ddot{\underline{x}} = \underline{c}(\underline{x}) \quad (4.18)$$

An expression for constraint forces can be obtained by substituting (4.17) into (4.18):

$$\underline{f}_c = -[BM^{-1}P(\underline{x})]^{-1}[BM^{-1}N(\underline{x}, \dot{\underline{x}}) + \underline{c}(\underline{x})] \quad (4.19)$$

The constraint moments introduced by the conventional fifth wheel connection can be derived by taking it as a roll coupler. Figure 4.2 illustrates a representation of fifth wheel in the vehicle model. The coordinate system (X_{s1}, Y_{s1}, Z_{s1}) is attached to the leading unit, while (X_{s2}, Y_{s2}, Z_{s2}) is attached to the trailing unit. A reference coordinate system $(X'_{s1}, Y'_{s1}, Z'_{s1})$ has the same yaw and pitch angles as those of the leading unit, but

has a different roll angle φ'_{s1} . The fifth wheel is represented by a roll stiffness rate K_s .

The roll moment (M_{x1}) acting through the fifth wheel can be expressed as:

$$M_{x1} = K_s(\varphi'_{s1} - \varphi_{s1}) \quad (4.20)$$

One constraint in the fifth wheel is that the pitch axis \bar{Y}'_{s1} is always perpendicular to the yaw axis \bar{Z}_{s2} , which yields:

$$\bar{j}'_{s1} \bullet \bar{k}_{s2} = 0 \quad (4.21)$$

where \bar{j}'_{s1} and \bar{k}_{s2} are unit vectors in \bar{Y}'_{s1} and \bar{Z}_{s2} directions, respectively. Substituting (4.4) into (4.21), φ'_{s1} can be derived as:

$$\varphi'_{s1} = \arctan \left[\frac{\sin \varphi_{s2} \cos(\alpha_{s2} - \alpha_{s1}) - \beta_{s2} \cos \varphi_{s2} \sin(\alpha_{s2} - \alpha_{s1})}{\beta_{s1} \sin(\alpha_{s2} - \alpha_{s1}) \sin \varphi_{s2} + \cos \varphi_{s2}} \right] \quad (4.22)$$

The constraining moments acting on the trailing unit in \bar{X}_{s2} and \bar{Y}_{s2} directions can be derived as:

$$M_{x2} = -M_{x1}T_{11} \quad \text{and} \quad M_{y2} = -M_{x1}T_{21} \quad (4.23)$$

where T_{11} and T_{21} are defined in Equation (4.10).

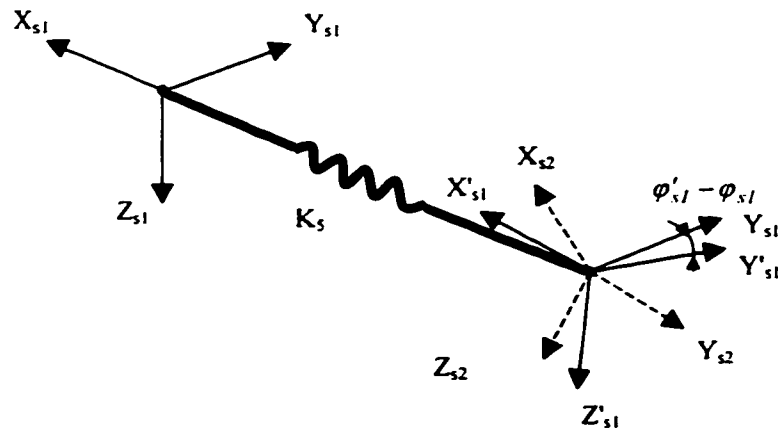


Figure 4.2: Representation of the conventional fifth wheel connection.

4.3 DYNAMIC ROLLOVER THRESHOLD OF ARTICULATED FREIGHT VEHICLES

Dynamic roll properties of articulated freight vehicles are frequently investigated in terms of Load Transfer Ratio (*LTR*) and Rearward Amplification Ratio (*RAR*). Dynamic rollover stability measures based upon load transfer ratio and rearward amplification ratio under a rapid high-speed path change maneuver conducted at 100 km/h have been proposed to assess the relative stability performance of heavy vehicles [45-46]. These measures may be implemented to predict the incipient rollover for development of an open-loop early warning generator for the driver. The detection of dynamic rollover through load transfer ratio, however, involves many measurement complexities, while the rearward amplification ratio is known to be quite sensitive to variations in design and operating conditions. Furthermore, the proposed measures do not permit the study of rollover propensity of heavy vehicles under varying directional maneuvers and speeds. Thus a dynamic rollover measure, characterizing roll property of heavy vehicles in transient steering maneuvers, and its relationship with static rollover threshold need to be investigated.

4.3.1 Definition of Dynamic Rollover Threshold

When a complete roll unit with multiple sprung and unsprung masses is subjected to a steering input, each mass unit experiences a lateral acceleration excitation, as shown in Figure 4.3. The destabilizing moments in the roll plane include those due to the centrifugal forces and the lateral displacement of each sprung mass. The destabilizing moments due to lateral displacements of unsprung masses are considered as insignificant. The vertical load transfer from inside to outside tires yields a stabilizing moment. The

roll moment equilibrium equation of a complete roll unit can be written with respect to point A (midway between the two tire forces FL_j , FR_j) as:

$$\left(\sum_{i=1}^{n_s} m_{si} a_{si} h_{si} + \sum_{j=1}^{n_u} m_{uj} a_{uj} h_{uj} \right) + \sum_{i=1}^{n_s} m_{si} g \Delta_{si} = \sum_{j=1}^{n_u} (FL_j - FR_j) T_j \quad (4.24)$$

where h_{si} and h_{uj} are the instantaneous cg heights of sprung mass i and unsprung mass j , respectively. a_{si} and a_{uj} are the lateral accelerations experienced by sprung mass i and unsprung mass j , respectively. n_s and n_u are the number of sprung and unsprung masses of a complete roll unit. Δ_{si} is the lateral displacement of c.g. of sprung mass i , and T_j is the effective half track width of tires on axle j . The first term in Equation (4.24) represents the total roll moment contributed by the centrifugal forces due to all sprung and unsprung masses, and can be expressed in terms of *Effective Lateral Acceleration (ELA)*:

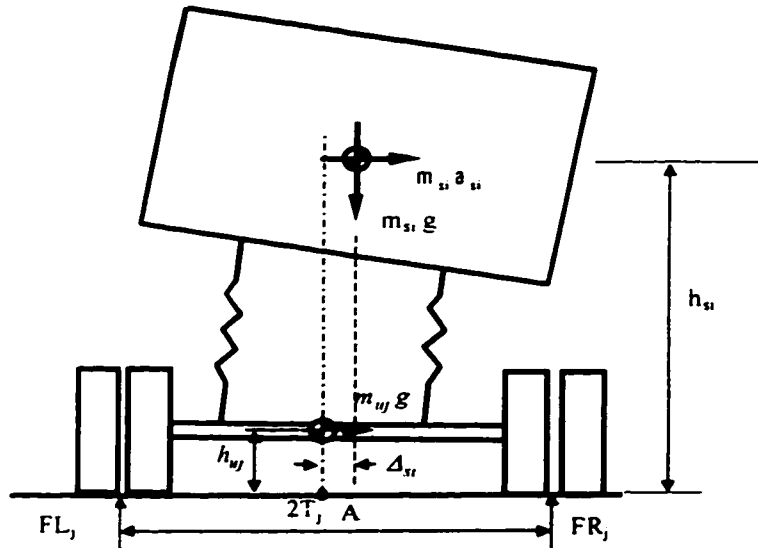


Figure 4.3: Illustration of roll destabilizing moments.

$$\sum_{i=1}^{n_s} m_{si} a_{si} h_{si} + \sum_{j=1}^{n_u} m_{uj} a_{uj} h_{uj} = ELA \left(\sum_{i=1}^{n_s} m_{si} h_{si} + \sum_{j=1}^{n_u} m_{uj} h_{uj} \right) \quad (4.25)$$

Substituting Equation (4.25) into (4.24), the effective lateral acceleration (ELA) of the complete unit can be derived as:

$$ELA = \frac{\sum_{j=1}^{n_u} (FL_j - FR_j) T_j - \sum_{i=1}^{n_s} m_{si} g \Delta_{si}}{\sum_{i=1}^{n_s} m_{si} h_{si} + \sum_{j=1}^{n_u} m_{uj} h_{uj}} \quad (4.26)$$

Equation (4.26) reveals that ELA is a dynamic parameter that depends on the lateral load transfer and track width of each axle, c.g. heights of sprung and unsprung masses, and the lateral displacement Δ_{si} of each sprung mass, which is further related to the suspension properties. ELA can also be evaluated using Equation (4.25), and expressed as:

$$ELA = \frac{\sum_{i=1}^{n_s} m_{si} a_{si} h_{si} + \sum_{j=1}^{n_u} m_{uj} a_{uj} h_{uj}}{\left(\sum_{i=1}^{n_s} m_{si} h_{si} + \sum_{j=1}^{n_u} m_{uj} h_{uj} \right)} \quad (4.27)$$

From Equation (4.27), it is apparent that the ELA represents a moment-weighted average of lateral acceleration response characteristics of the vehicle units. For a single-unit vehicle comprising only one sprung mass, the effective lateral acceleration may be approximated as the vehicle lateral acceleration assuming negligible contributions due to unsprung mass acceleration. For an articulated freight vehicle, however, the dynamic roll response of different mass units may differ considerably in phase and amplitude. The ELA , expressed in Equation (4.27) is thus used to represent the contributions due to the moments caused by all the centrifugal forces.

Based on the above analysis, *dynamic rollover threshold (DRT)* of a heavy vehicle may be defined as the level of effective lateral acceleration (*ELA*), when its *RSF* approaches the unity value in a dynamic steering maneuver.

4.3.2 Analysis of Dynamic Rollover Threshold of Articulated Freight Vehicles

Dynamic rollover of heavy vehicles frequently occurs during low speed cornering and high-speed evasive maneuvers. The dynamic rollover characteristics of heavy vehicles are investigated using the constant velocity yaw/roll model, described in section 4.2. The static rollover threshold of the vehicle is derived from the vehicle response under a ramp steer input applied at a very low rate. Many field measurement studies of heavy vehicles have established that the front wheels steer angle corresponding to lane change and evasive maneuvers can be conveniently approximated by a sinusoidal steer function [90].

The dynamic roll response of the vehicle under low-speed cornering and high-speed lane-change maneuvers can thus be characterized using two simplified steering inputs: ramp-step and sinusoidal. In the present study, the ramp-step steering input is realized by increasing the front-wheel steer angle from 0^0 to 5^0 at a rate of 10 degree/s. The steer angle is then held constant for the entire duration of the maneuver. The vehicle model is analyzed under the steer-input at a constant forward speed, and the speed is gradually increased until a relative roll instability is identified. The vehicle response characteristics corresponding to the final speed are analyzed to derive the dynamic rollover threshold using Equation 4.27. The relative roll instability under high-speed directional maneuver is investigated under sinusoidal steer inputs performed at different

frequencies. Three different values of steering frequencies are selected to yield periods of 2, 3, and 4 seconds. The vehicle forward speed is gradually increased until a relative roll instability is identified under each steer input. The corresponding values of dynamic rollover threshold accelerations are then derived in a similar manner.

The analyses are performed for a 5-axle tractor-semitrailer combination and the simulation parameters are illustrated in Table 4.1. The dynamic roll properties of a vehicle combination are strongly related to various design and operating factors. Analysis of sensitivity of dynamic rollover threshold (*DRT*) to variations in such factors is thus essential to derive a rollover criterion for open-loop early warning generation. The analyses are performed for an array of vehicle configurations realized upon combining a range of currently used tires, suspension, track width and cg heights, as illustrated in Table 4.2. While the c.g. height can vary during day-to-day operation, the tire track width is limited by the maximum permissible vehicle width, which for majority of the current vehicles is either 2.44m or 2.59m. Two different c.g. heights of 1.78m and 2.065m are selected to reflect normal variations in loading condition of tractor semi-trailer combinations. While a leaf spring front axle suspension, referred to as *FA*, is selected, three different rear axle suspension springs are selected for the rear axles. The rear suspension springs, referred to as *RA*, *RB* and *RC*, exhibit considerably different force-deflection characteristics, as shown Figure 3.14 [87]. Two different suspension springs are also selected for the trailer axles, including leaf and air, referred to as *TA* and *TB*, respectively. Roll center heights and auxiliary roll stiffness of the six suspension configurations are illustrated in Table 3.12. Modern heavy vehicles, invariably, employ radial tires, and their profiles may differ slightly. The analyses are thus limited to the

most commonly used radial tires. 11R22.5. The cornering force and aligning torque characteristics of the tires as a function of normal load and side-slip angle are illustrated in Figures 4.4 and 4.5.

Table 4.1: Simulation Parameters of the baseline 5-axle tractor semi-trailer.

	Tractor			semi-trailer	
sprung mass (kg)	6129			19623	
roll mass moment of inertia (kgm^2)	2601			22111	
pitch mass moment inertia (kgm^2)	22055			420941	
yaw mass moment of inertia (kgm^2)	28275			434682	
center of gravity height (m)	1.13			2.065	
	axle 1	axle 2	axle 3	axle 4	axle 5
axle load (kg)	5112	6106	6106	6304	6304
axle roll moment of inertia (kgm^2)	418	577	577	464	464
longitudinal position from c.g (m)	0.65	-2.819	-4.468	-4.60	-6.124
axle center of gravity (m)	0.508	0.508	0.508	0.508	0.508
roll center height (m)	0.46	0.838	0.838	0.686	0.686
half spring spacing	0.406	0.4826	0.4826	0.5588	0.5588
half track -inner tires	1.106	0.9144	0.9144	0.9144	0.9144
dual tire spacing	0	0.33	0.33	0.33	0.33

Table 4.2: Range of variations in the design and operating factors of a tractor-semi trailer.

CG Height (m)	1.78		2.06	
Steering frequency (Hz)	0.25	0.33		0.5
Tires	Radial 11R22.5			
Track width (m)	2.44			
Front Suspension	FA, 53 kN rating (leaf)			
Rear Suspension	RA 97 kN rating (leaf); RB 85 kN rating (leaf) RC 85 kN rating (leaf)			
Trailer Suspension	TA 93 kN rating (leaf); TB 53 kN rating (air)			

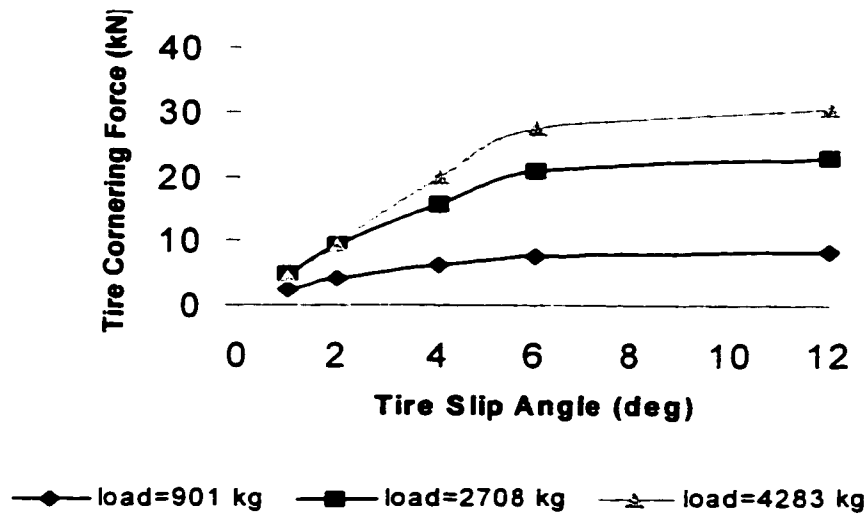


Figure 4.4: Cornering force properties of radial tires as a function of load and side-slip angle.

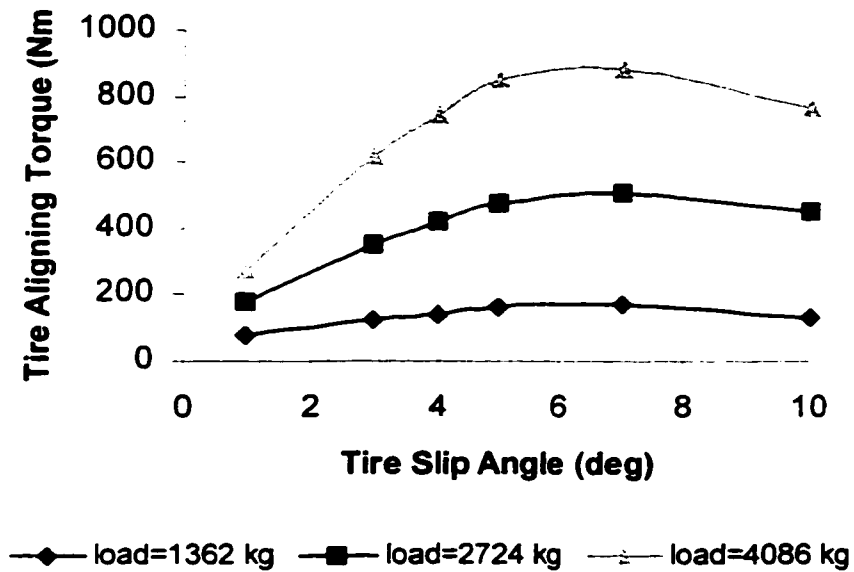


Figure 4.5: Aligning torque property of radial tires as a function of load and side-slip angle.

The yaw-roll analytical model of the vehicle, developed in section 4.2, is solved for ramp-step and sinusoidal steering inputs at the front axle, at a constant forward speed. The dynamic response characteristics of the vehicle in terms of dynamic load transfer are examined to identify, whether the vehicle has approached the condition of relative roll instability. The response characteristics are also analyzed to derive *RSF* and lateral acceleration response of the vehicle. The simulations are initiated at a relatively low speed of 5 km/h. The vehicle speed is gradually increased until a condition of relative roll instability is detected from the response data. The resulting response characteristics are analyzed to establish a relationship between the *RSF* and potential measures of the relative rollover, such as peak lateral acceleration, rearward amplification and effective lateral acceleration. The sensitivity of these measures to variations in design and operating parameters are discussed in the following subsections.

Figure 4.6 illustrates the time histories of lateral acceleration of tractor and trailer sprung weights, when the vehicle is subject to ramp-step and 0.25 Hz sinusoidal steer. The baseline vehicle used in the simulation comprises suspensions *FA*, *RA* and *TA* with total track width of 2.44 m and c.g. height of 2.065m. The results in Figure 4.6 show that lateral acceleration response of the tractor and semitrailer approaches approximately the same steady value during a constant speed turning maneuver, arising from the ramp-step steer input. Both the units approach identical value of lateral acceleration, when *RSF* approaches 1.0. The resulting acceleration response may be considered as the static rollover threshold of the combination. Based on the relative roll instability criterion, the static rollover threshold can thus be considered as the level of lateral acceleration of the vehicle when its *RSF* approaches unity value.

The lateral acceleration response characteristics of the two units of the combination in a lane change maneuver, however, are quite different in both phase and amplitude, as shown in Figure 4.6. For 0.25 Hz sinusoidal steering maneuver, the lateral acceleration response of the tractor approaches a peak value 0.75s prior to that of the trailer acceleration response.

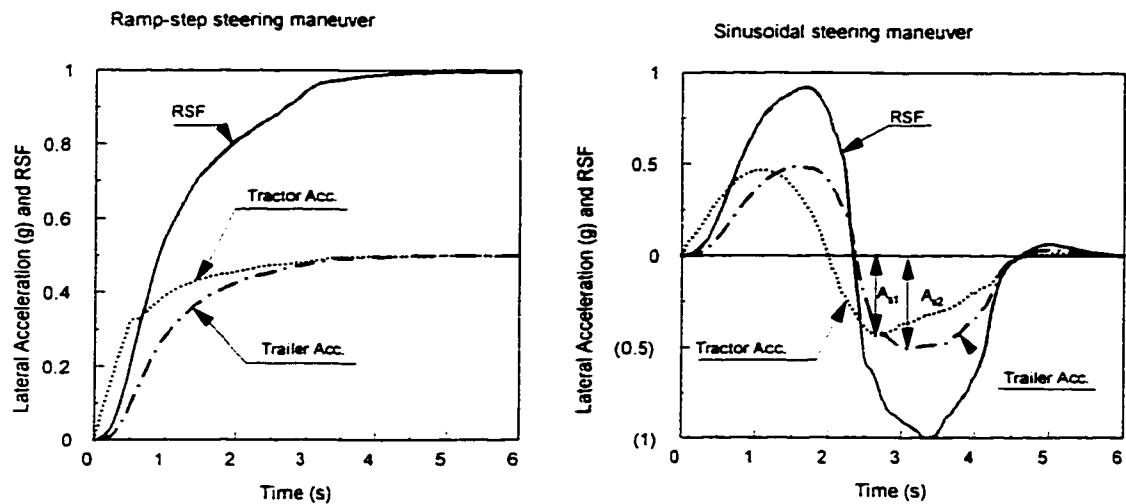


Figure 4.6: Lateral acceleration response and *RSF* of an articulated vehicle subject to two different maneuvers.

Sensitivity of Peak Acceleration and RAR to Variations in Design and Operating Parameters

The *RSF* approaches a value of -1 , when trailer lateral acceleration approaches its negative peak value. The rearward amplification ratio (*RAR*) of the combination corresponding to the relative rollover condition is further evaluated from peak lateral accelerations of the tractor and semitrailer units: $RAR = A_{s2} / A_{s1}$, where A_{s2} and A_{s1} are the peak lateral acceleration response of the trailer and tractor sprung weights, respectively. The relative rollover condition is identified when *RSF* approaches a value of $+1$ or -1 . The peak lateral acceleration of the tractor A_{s1} and *RAR* of the tractor-semitrailer combination, corresponding to relative rollover condition (*RSF*) are derived for different suspensions and steering frequencies to establish their sensitivity to variations in suspension properties and rate of steer input. Table 4.3 summarizes the peak lateral acceleration A_{s1} and *RAR* corresponding to $RSF = \pm 1$, for different combinations of suspension springs, and steering frequencies of 0.25 Hz, 0.33 Hz and 0.5 Hz. The results clearly reveal that both the peak lateral acceleration and the rearward amplification ratio are quite sensitive to the maneuvers performed. For the range of frequencies considered, an increase in the steering frequency tends to decrease the peak lateral acceleration of the tractor, while it leads to noticeable increase in the rearward amplification ratio, irrespective of the suspension configurations. From the results presented in Table 4.3, it can be concluded that characterization of dynamic roll behavior through tractor lateral acceleration threshold and rearward amplification necessitates a thorough knowledge and consideration of the maneuver.

Table 4.3: Tractor rollover limits and rearward amplification factors of a tractor-semitrailer combination.

Front, Rear and Trailer Axle Suspension	Sinusoidal steering frequency					
	0.25 Hz		0.33 Hz		0.5 Hz	
	A_{s1} (g)	RAR	A_{s1} (g)	RAR	A_{s1} (g)	RAR
FA, RA, TA	0.476	1.05	0.437	1.16	0.372	1.41
FA, RA, TB	0.488	1.06	0.465	1.17	0.437	1.19
FA, RB, TA	0.473	1.08	0.415	1.23	0.376	1.35
FA, RB, TB	0.495	1.0	0.468	1.11	0.412	1.34
FA, RC, TA	0.479	1.03	0.413	1.18	0.410	1.20
FA, RC, TB	0.483	1.03	0.468	1.14	0.455	1.17

Sensitivity of ELA to Variations in Design and Operating Parameters

The dynamic rollover threshold of a 5-axle tractor semi-trailer combination with various suspension properties and c.g. heights is evaluated using the Yaw/Roll model, under sinusoidal steering at frequencies of 0.25Hz, 0.33 Hz and 0.50 Hz. The response characteristics of the units are analyzed to derive the effective lateral acceleration (*ELA*) of the combination using Equation (4.27). The *RSF*, computed using Equation (2.10) is also examined to detect the relative roll instability. The analyses are performed for different vehicle configurations and steering inputs, and values of *ELA* are derived corresponding to the relative rollover condition ($RSF = \pm 1$), and summarized in Tables (4.4) and (4.5). The dynamic rollover threshold (*DRT*) expressed in terms of *ELA* is further compared with the static rollover threshold (*SRT*), derived from the ramp-step steer response and *RSF*. The results show that the dynamic rollover threshold of the vehicle, in all cases, is very close to its static rollover threshold. The ratio of *DRT* to *SRT*

is in the range of 0.94 to 1.01 for all the vehicle configurations and maneuvers investigated. The static rollover threshold can thus be employed to attain a reasonable estimation of the dynamic rollover propensity of a tractor-semitrailer combination. A comparison of results presented in Tables (4.3), (4.4) and (4.5) reveals that *DRT* is relatively insensitive to variations considered.

Table 4.4: Dynamic and static rollover threshold values of a tractor-semitrailer at c.g. height of 1.78 m.

Front, Rear and Trailer Axle Suspension	trailer cg height 1.78 m						
	SRT (g)	DRT (g)			DRT/SRT		
		f=0.25 Hz	f=0.33 Hz	f=0.50 Hz	f=0.25 Hz	f=0.33 Hz	f=0.50 Hz
FA, RA, TA	0.596	0.579	0.586	0.571	0.97	0.98	0.96
FA, RA, TB	0.605	0.588	0.580	0.581	0.97	0.96	0.96
FA, RB, TA	0.590	0.570	0.578	0.596	0.97	0.98	1.01
FA, RB, TB	0.595	0.571	0.594	0.576	0.96	1.00	0.97
FA, RC, TA	0.589	0.570	0.582	0.586	0.97	0.99	0.98
FA, RC, TB	0.594	0.570	0.591	0.570	0.96	1.00	0.96

Table 4.5: Dynamic and static rollover threshold values of a tractor-semitrailer at c.g. height of 2.065 m.

Front, Rear and Trailer Axle Suspension	trailer cg height 2.065 m						
	SRT (g)	DRT (g)			DRT/SRT		
		f=0.25 Hz	f=0.33 Hz	f=0.50 Hz	f=0.25 Hz	f=0.33 Hz	f=0.50 Hz
FA, RA, TA	0.510	0.479	0.484	0.490	0.94	0.95	0.96
FA, RA, TB	0.519	0.508	0.519	0.498	0.98	1.00	0.96
FA, RB, TA	0.500	0.498	0.486	0.480	1.00	0.97	0.96
FA, RB, TB	0.507	0.487	0.491	0.512	0.96	0.97	1.01
FA, RC, TA	0.500	0.498	0.498	0.485	1.00	1.00	0.97
FA, RC, TB	0.506	0.498	0.493	0.487	0.98	0.97	0.96

Dynamic Roll Characteristics of Doubles

The dynamic rollover threshold of doubles is further investigated on the basis of proposed *ELA*. The dynamic rollover property of an 8-axle A-train double, comprising a tractor, and two tandem-axle semi-trailers coupled with a single-axle A-type dolly, as shown in Figure 4.7, is further investigated. The suspensions denoted by *FA*, *RA*, and *TA* are used for tractor's front, rear, and semi-trailer axles, respectively. The last trailer uses the suspension denoted by *TA*. The A-train double is modeled as two complete roll units: (i) tractor-semitrailer (roll unit #1), (ii) and the last semitrailer with A-dolly (roll unit #2). The relative rollover condition for each roll unit is analyzed using the roll plane models presented in Chapter 3. For a typical configuration of the A-train double, the relative rollover condition and the *SRT* of different roll units are summarized in Table 4.6. The results show that *SRT* of unit #1 is considerably lower than that of unit #2. The unit #1 of the vehicle thus rolls over first in a steady cornering maneuver, while the roll unit #2 of the vehicle tends to roll over first under a high-speed evasive maneuver due to relatively large lateral acceleration response of the last trailer.

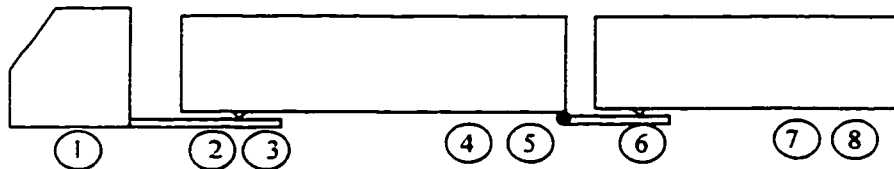


Figure 4.7: Schematic of an eight-axle A-train double.

Table 4.6: Rollover signature of a typical A-train double combination.

		Roll Unit #1	Roll Unit #2
Relative Rollover Condition		Lift-off of wheels on tractor rear & trailer axles	Lift-off of wheels on A-dolly and trailer axles
SRT value		Low (0.47 g)	High (0.61 g)
Rollover Sequence	Cornering maneuvers	First	Second
	Evasive maneuvers	Second	First

The *DRT* of the A-train double with different cg heights of the last trailer is further investigated using the Yaw/Roll model. The simulations are performed under sinusoidal steering maneuvers with steering frequencies of 0.25 Hz, 0.33 Hz, and 0.5 Hz. The *DRT* of the A-train double is taken as the *ELA* of the roll unit approaching the relative rollover condition first in a dynamic steering maneuver. It should be pointed out that the second roll unit of the specified vehicle approaches the rollover condition first under such maneuvers. The sensitivity of *DRT* to variations in c.g. height of the last trailer alone is thus investigated. Figure 4.8 illustrates the ratio of *DRT* to the *SRT* of the second roll unit with three different c.g. heights of the last trailer. An increase in the c.g. height of the last trailer tends to decrease the *DRT* of the vehicle. The ratio of *DRT* to *SRT*, however, varies only slightly with variations in the steering frequency. For the selected vehicle configurations these variations are observed to be within 5%. The variations in c.g. height also result in only slight variation in the ratio of *DRT* to *SRT*. The *DRT* to *SRT* ratio varies by only 2% with variations in c.g. height at steering frequencies of 0.25 Hz and 0.33 Hz. This variation approaches approximately 7% under rapid ($f=0.5$ Hz) steering input.

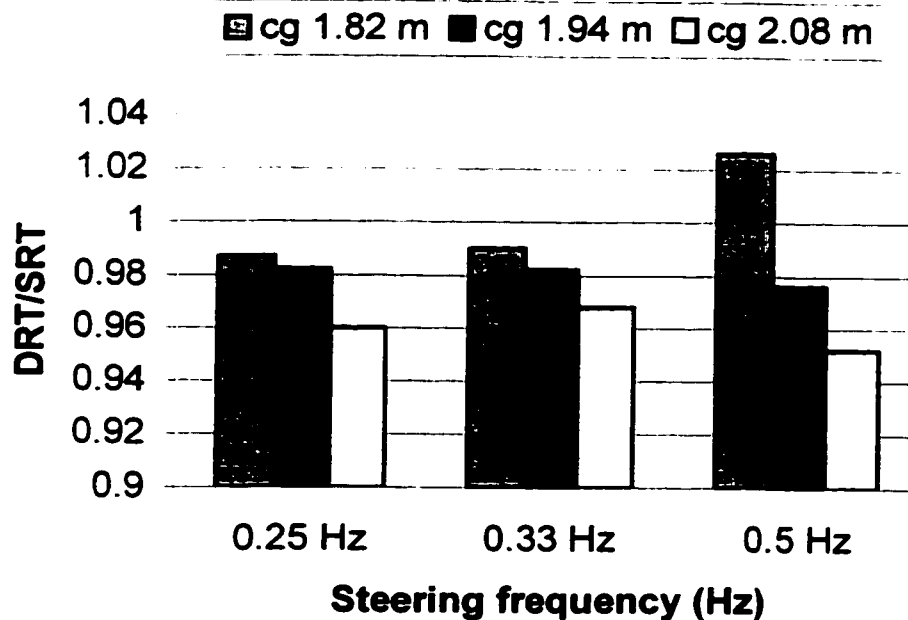


Figure 4.8: The ratio of dynamic rollover threshold to static rollover threshold of a typical A-train double.

4.3.3 Dynamic Rollover Initialization

Rollover of heavy vehicles in directional maneuvers is often initialized on one axle, followed by wheels lift-off on other axles. Identification of dynamic rollover initialization is vital for early warning generation of impending rollover. Rollover initialization is investigated by examining how load transfer ratio occurred on each composite-axle of heavy vehicles in directional maneuvers.

Axle load transfer ratio characteristics of a five-axle tractor semi-trailer combination in sinusoidal steer maneuvers is investigated using the yaw - roll model. Three composite axle load transfer ratios, representing those occurred at tractor front, rear, and trailer axles, are defined as:

$$\text{tractor front axle: } LTR_1 = \frac{FL_1 - FR_1}{FL_1 + FR_1}$$

$$\text{tractor rear axles: } LTR_2 = \frac{FL_2 + FL_3 - FR_2 - FR_3}{FL_2 + FL_3 + FR_2 + FR_3}$$

$$\text{trailer axles: } LTR_3 = \frac{FL_4 + FL_5 - FR_4 - FR_5}{FL_4 + FL_5 + FR_4 + FR_5}$$

where FL_i and FR_i ($i=1, \dots, 5$) are tire vertical forces on the left and right sides of axle i , respectively. A unity value of LTR_i indicates that wheels on composite axle i approach lift-off. Figure 4.9 illustrates the signature of LTR_i ($i=1, 2, 3$) of the five-axle tractor semi-trailer listed in Table 4.1, in a 0.25 Hz sinusoidal steering maneuver with vehicle forward speed 86 km/h. The load transfer ratio of trailer axles (LTR_3) approaches a peak value of 0.69, while LTR_2 of tractor rear axles approaches a relatively small value of 0.48. LTR_1 of tractor front axle demonstrates the smallest variation with peak value of 0.21 during the course of maneuver. When vehicle forward speed is increased, the peak value of LTR_i ($i=1, 2, 3$) is increased towards a unity value, as shown in Figure 4.10. Peak value of load transfer ratio of trailer axles approaches a unity value first, followed by those of tractor rear and front axles. Consequently, wheels on trailer axles lose road contact first in a rollover situation, and rollover of the vehicle is considered to be initialized at the rearmost trailer axles.

Wheels lift-off sequence of the tractor semi-trailer combination is derived for different suspensions and steering frequencies to establish their sensitivity to variations in suspension properties and rate of steer input. Tables 4.7 and 4.8 summarize wheels lift-off sequence for different combinations of suspension springs, semi-trailer c.g. heights,

and steering frequencies of 0.25 Hz and 0.33 Hz. Wheels on tractor's rear and trailer axles lose road contact at the same time when the vehicle is equipped with suspension combination FA-RA-TA in a 0.25 Hz sinusoidal steering maneuver. For all other cases, wheels on trailer axles always lift off first, irrespective of steer frequency and trailer c.g. height considered in this study. Roll instability of the tractor semi-trailer is thus initialized at the rearmost trailer axles.

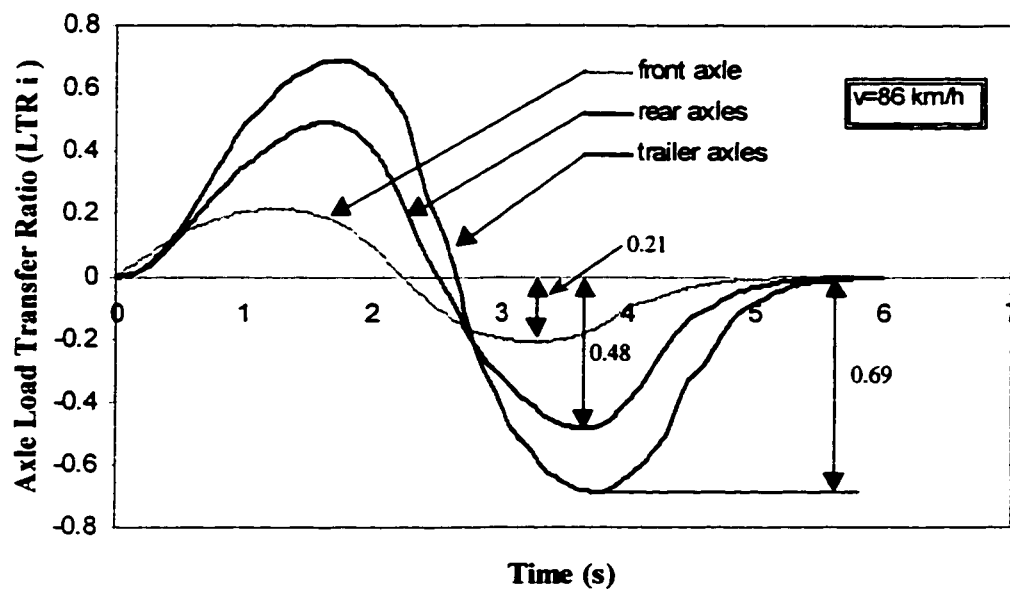


Figure 4.9: Composite axle load transfer ratio of a five-axle tractor semi-trailer during a sinusoidal steering maneuver.

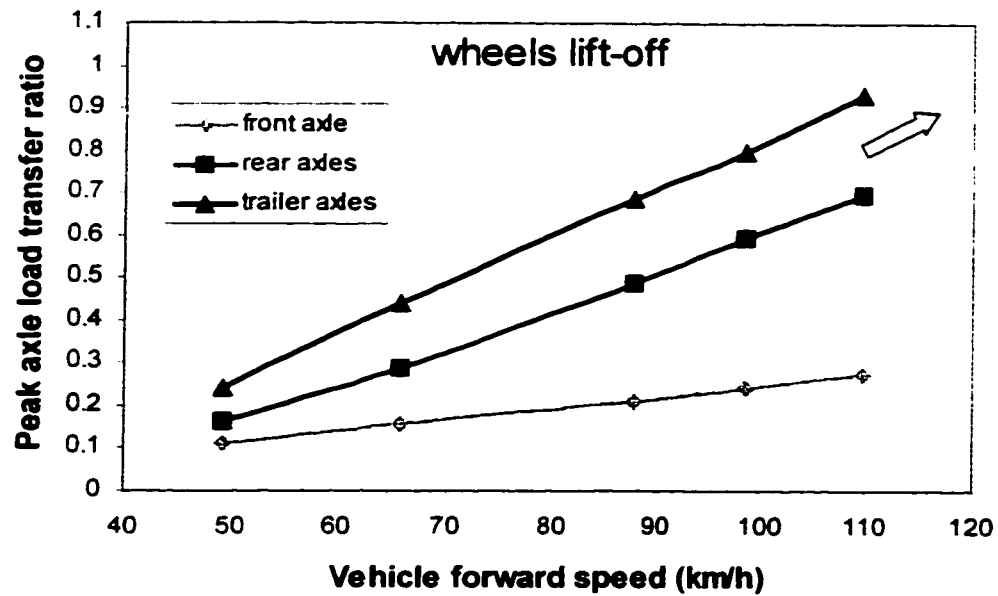


Figure 4.10: Peak axle load transfer ratio of a tractor semi-trailer as a function of vehicle forward speed.

Table 4.7: Wheels lift-off sequence of a tractor semitrailer with different combinations of suspensions: trailer c.g. height 1.78m.

Front, Rear and Trailer Axle Suspension	wheels lift-off sequence (trailer c.g. height 1.78 m)					
	f=0.25 Hz			f=0.33 Hz		
	tractor's front axle	tractor's rear axes	trailer axes	tractor's front axle	tractor's rear axes	trailer axes
FA, RA, TA	②	①	①	③	②	①
FA, RA, TB	③	②	①	③	②	①
FA, RB, TA	③	②	①	③	②	①
FA, RB, TB	③	②	①	③	②	①
FA, RC, TA	③	②	①	③	②	①
FA, RC, TB	③	②	①	③	②	①

Table 4.8: Wheels lift-off sequence of a tractor semi-trailer with different combinations of suspensions: trailer c.g. height 2.06m.

Front, Rear and Trailer Axle Suspension	wheels lift-off sequence (trailer c.g. height 2.06 m)					
	$f=0.25$ Hz			$f=0.33$ Hz		
	tractor's front axle	tractor's rear axles	trailer axles	tractor's front axle	tractor's rear axles	trailer axles
FA, RA, TA	②	①	①	③	②	①
FA, RA, TB	③	②	①	③	②	①
FA, RB, TA	③	②	①	③	②	①
FA, RB, TB	③	②	①	③	②	①
FA, RC, TA	③	②	①	③	②	①
FA, RC, TB	③	②	①	③	②	①

Wheels lift-off sequence of the A-train double, as illustrated in Figure 4.7, is further investigated. The suspensions denoted by *FA*, *RA*, and *TA* are used for tractor's front, rear, and the first semi-trailer axles, respectively, while suspension denoted by *TA* is used for the A-dolly and the second semi-trailer. Load transfer ratios of five composite axles in terms of tractor front, rear, 1st semi-trailer, A-dolly and the 2nd semi-trailer axles are presented in Figure 4.11, where the vehicle is subjected to a sinusoidal steering maneuver at 0.33 Hz. The figure reveals that the maximum load transfer (0.96) occurs at the axles of the second semi-trailer at 3.3 s, indicating that wheels on the axles of the second semi-trailer are very close to lift-off. The peak load transfer ratios for A-dolly axle, axles of the first semi-trailer, and tractor rear axles are 0.80, 0.63 and 0.65, respectively. Roll instability of the A-double will thus be initialized at the axles of the second semi-trailer, or the rearmost axles of the vehicle, when the vehicle is subjected to a similar maneuver in a rollover situation.

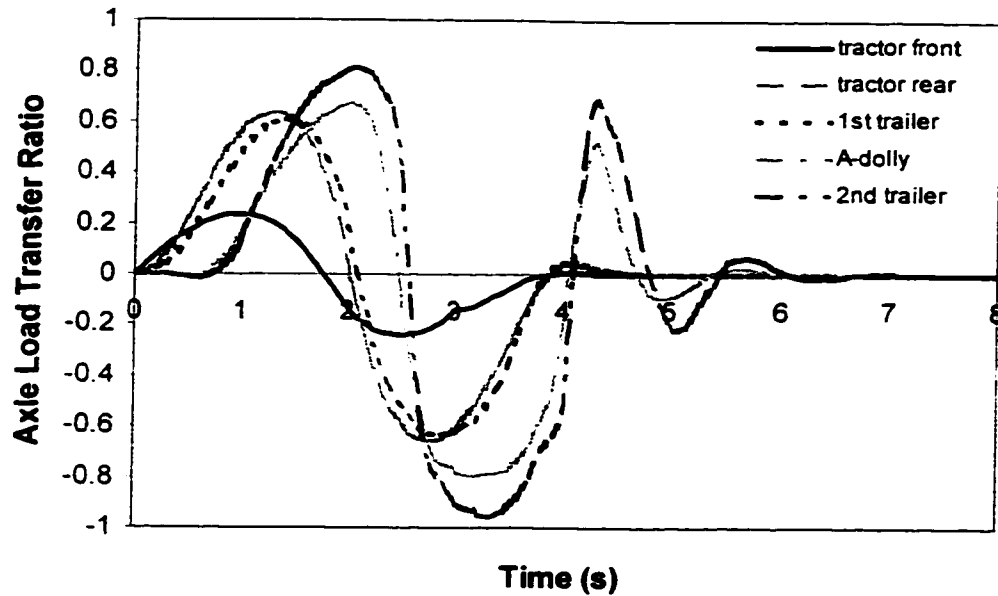


Figure 4.11: Axle load transfer characteristics of an A-train double in a 0.33 Hz sinusoidal steering maneuver.

Parametric sensitivity analysis of wheels lift-off sequence of the A-train double is carried out for three c.g. heights (1.5m , 1.7m and 2.0m) of the last semi-trailer at steering frequencies of 0.25 Hz and 0.33 Hz, while c.g. height of the first semitrailer is kept as constant (1.7m). The results are summarized in Table 4.9. As can be seen, wheels on the axles of the second semi-trailer, or the rearmost axles of the vehicle, lift off first, irrespective of the variations in c.g. height of the second semi-trailer and steering frequency. The subsequent wheels lift-off occurs at A-dolly axle, except for one case where c.g. height of the second semi-trailer is reduced to 1.5m with 0.25 Hz steering frequency. Rollover of A-train doubles is thus considered to be initialized at the rearmost axles of the vehicle.

Table 4.9: Wheels lift-off sequence of an A-train double with variations in c.g. height and steering frequency.

2 nd trailer c.g. height	steering frequency	Wheels lift-off sequence				
		tractor's front axle	tractor's rear axles	1 st trailer axles	A-dolly axle	2 nd trailer axles
1.5 m	$f=0.25$ Hz	5	3	2	4	1
	$f=0.33$ Hz	5	4	3	2	1
1.7 m	$f=0.25$ Hz	5	3	4	2	1
	$f=0.33$ Hz	5	3	4	2	1
2.0 m	$f=0.25$ Hz	5	3	4	2	1
	$f=0.33$ Hz	5	3	4	2	1

4.4 ANALYSIS OF ABSOLUTE ROLLOVER

Although a large number of analytical models have been developed to study the directional dynamics, handling performance and static roll instability of heavy vehicles [4, 7-9], only limited efforts have been reported on their dynamic roll stability. Verma and Gillespie [27] proposed a lumped roll plane model for the analysis of roll dynamics of commercial vehicles. Das et al. [28] employed this model to investigate dynamic rollover threshold of commercial vehicles. The model proposed by Verma and Gillespie [27], however, was developed based on the assumption that none of the wheels lose contact with the road. The application of such a model thus raises many concerns, since a

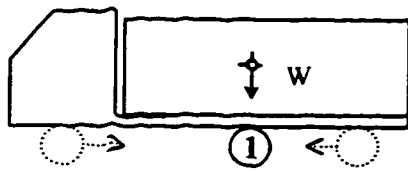
dynamic rollover involves the loss of tire-road contact of the wheels on one track of the vehicle.

A roll plane model incorporating the loss of tire-road contact during a directional maneuver may be considered appropriate for estimation of absolute rollover threshold. Single and multiple roll planes models are thus derived to study the dynamic roll properties of single and multiple units articulated vehicles. A straight truck configuration may be represented by a single-roll-plane model by lumping the front and rear axles into a single composite axle, as illustrated in Figure 4.12(a). A tractor-semitrailer combination can be represented by three composite roll planes, including front axle, a composite drive axle, and a composite trailer axle, coupled by two torsional springs, as shown in Figure 4.12(b). The torsional stiffness of tractor frame is presented by KF_1 , and that of the fifth wheel and semi-trailer structure is characterized by KF_2 . The B-train and C-train doubles are represented in a similar manner by four roll planes coupled by torsional springs, as illustrated in Figure 4.12(c). The torsional stiffness of the last dolly and the trailer structure is represented by KF_3 .

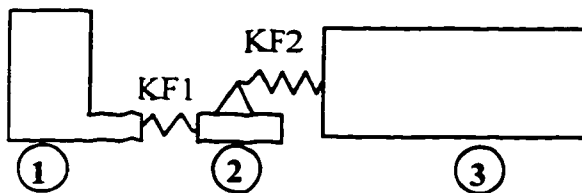
Figure 4.13 illustrates a typical roll plane model comprising the composite axle, lumped tire and suspension properties, and lumped sprung (m_{si}) and unsprung (m_{ui}) masses. Under a severe directional maneuver, the tires on the inside track of the vehicle may experience lift-off, as illustrated in Figure 4.14. In each composite axle roll plane, the unsprung mass consists of a solid beam axle with dual tires. The suspension is characterized by either a linear or nonlinear spring rate, backlash, coulomb friction and a viscous damper. It is assumed that the sprung mass rolls (ϕ_{si}) around its roll center located at a fixed distance (h_{Ri}) from the sprung mass center of gravity (c.g.) in the roll

plane i . The roll center, however, is permitted to translate along a direction normal to the axle (p_i). The unsprung mass i is modeled with three-degrees-of-freedom: vertical (z_{ui}), lateral (y_{ui}) and roll (ϕ_{ui}).

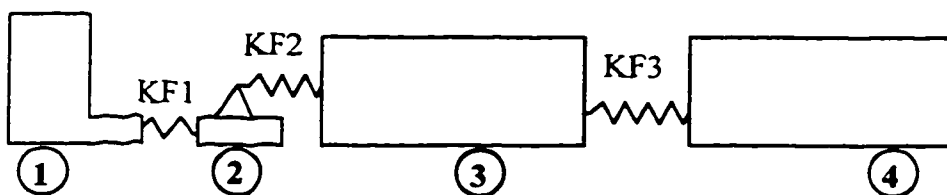
It should be noted that the roll center of the unsprung mass i shifts from c.g. location to the center of contact patch between the outer tire and the road, as the wheels on the inner track lose contact with the road under a directional maneuver. The location of roll center under this condition is indicated by 'A' in Figure 4.14.



(a) Straight trucks



(b) Tractor semi-trailers



(c) B-train and C-train doubles

Figure 4.12: Grouping of axes of different vehicle configurations for the development of roll plane models.

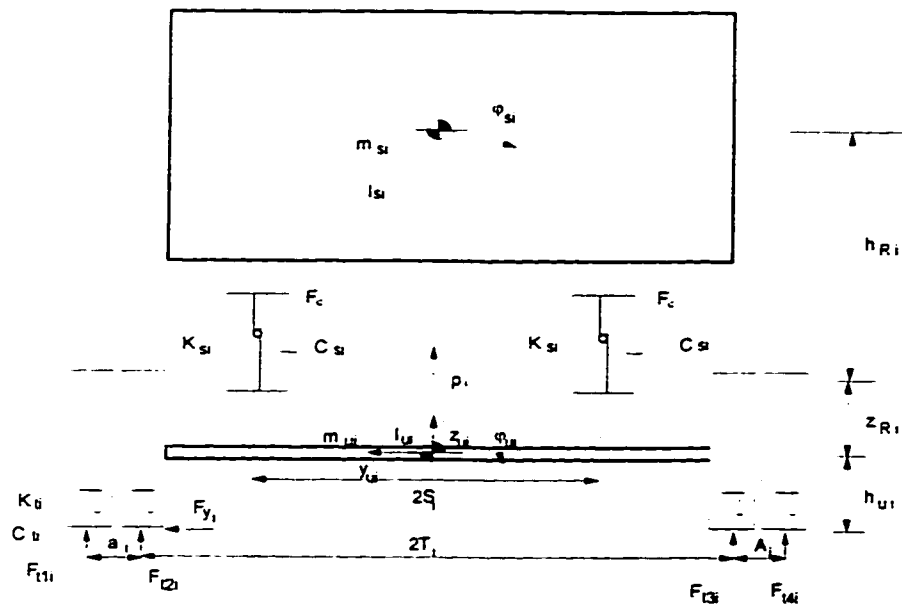


Figure 4.13: Roll plane model of the vehicle prior to loss of tire-road contact.

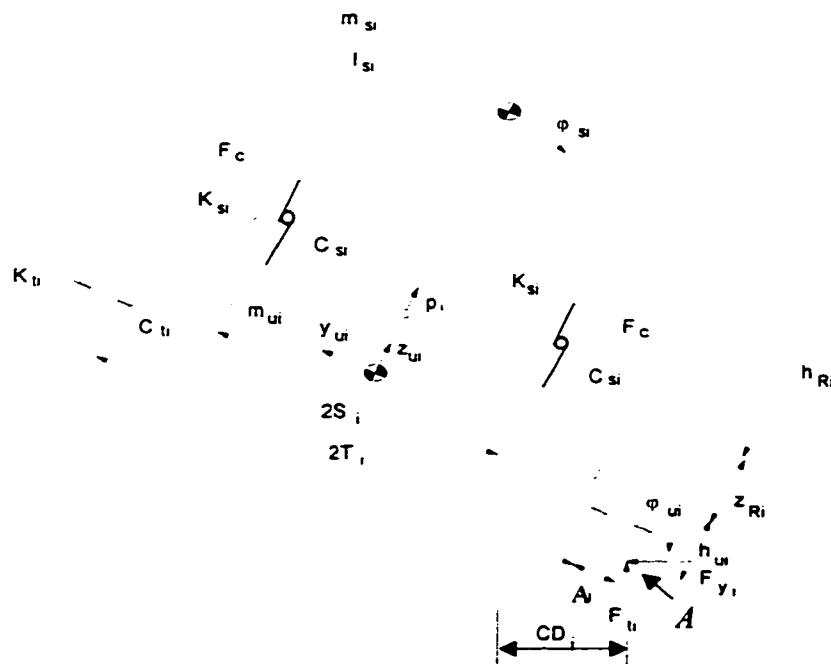


Figure 4.14: Roll plane model after the loss of tire-road contact.

The sprung and unsprung masses thus experience large magnitude translational and angular deflections. The dynamic roll models, reported in the literature, invariably assume small deflections, while the shift in location of the unsprung mass roll center is considered negligible. In view of large magnitude deflection encountered by the sprung and unsprung masses, when loss of wheel-road contact is attained, the validation of such models may be questionable. Such models, however, can be effectively applied to derive relative rollover of the combination based upon loss of wheel-road contact. In a dynamic directional maneuver, however, the vehicle may regain the tire-road contact, when the steering direction is reversed. The dynamic roll indicators derived on the basis of relative rollover may thus lead to false warning.

The analysis of absolute rollover involving large magnitude deflection, is performed upon consideration of the total energy associated with roll plane i , before and after the loss of wheel-road contact. The total kinematic and potential energy of roll plane i , before the wheel lift-off, derived from Figure 4.13, can be expressed as:

Before wheel-liftoff

$$K_i = \frac{1}{2} [m_{ui}(\dot{y}_{ui}^2 + \dot{z}_{ui}^2) + I_{ui}\dot{\phi}_{ui}^2] + \frac{1}{2} m_{si} \{ [\dot{y}_{ui} - (z_{Ri} + p_i)\dot{\phi}_{ui} \cos \phi_{ui} - \dot{p}_i \sin \phi_{ui} - h_{Ri}\dot{\phi}_{si} \cos \phi_{si}]^2 + [\dot{z}_{ui} - (z_{Ri} + p_i)\dot{\phi}_{ui} \sin \phi_{ui} + \dot{p}_i \cos \phi_{ui} - h_{Ri}\dot{\phi}_{si} \sin \phi_{si}]^2 \} + \frac{1}{2} I_{si}\dot{\phi}_{si}^2 \quad (4.28)$$

$$U_i = m_{ui}g(h_{ui} + z_{ui}) + m_{si}g[h_{ui} + z_{ui} + (z_{Ri} + p_i)\cos \phi_{ui} + h_{Ri}\cos \phi_{si}] + UT_i \quad (4.29)$$

where K_i and U_i are the total kinetic and potential energy due to the roll plane i . The datum is considered to be the ground level for computing the potential energy. I_{ui} and I_{si} are the roll mass moments of inertia about the respective cg of the unsprung and

sprung masses. z_{Ri} is the distance between the sprung mass roll center and the unsprung mass cg. UT_i is the potential energy due to the torsional springs coupling the masses m_{si} and $m_{s(i+1)}$. For the multiple roll plane representation, the UT_i can be expressed as:

$$UT_i = \begin{cases} \frac{1}{2}KF_i(\varphi_{s(i+1)} - \varphi_{si})^2 & \text{for } i = 1 \\ \frac{1}{2}KF_{i+1}(\varphi_{s(i+1)} - \varphi_{si})^2 + \frac{1}{2}KF_{i-1}(\varphi_{si} - \varphi_{s(i-1)})^2 & \text{for } 1 < i < n \\ \frac{1}{2}KF_i(\varphi_{si} - \varphi_{s(i-1)})^2 & \text{for } i = n \end{cases} \quad (4.30)$$

After the loss of wheel-road contact, the roll center of the unsprung mass i shifts to the contact patch between the outer tire and the ground, as shown in Figure 4.14 (point A). The total kinetic and potential energy due to the roll plane i , thus, differ from Equations (4.28) and (4.29), and are derived as:

$$\begin{aligned} K_i = & \frac{1}{2}m_{ui}\{\dot{y}_{ui} - T_{ei}\text{sign}(\varphi_{ui})\sin[\varphi_{ui} + \alpha_i\text{sign}(\varphi_{ui})]\dot{\varphi}_{ui}\}^2 \\ & + \frac{1}{2}m_{ui}\{\dot{z}_{ui} + T_{ei}\text{sign}(\varphi_{ui})\cos[\varphi_{ui} + \alpha_i\text{sign}(\varphi_{ui})]\dot{\varphi}_{ui}\}^2 + \frac{1}{2}I_{ui0}\dot{\varphi}_{ui}^2 + \frac{1}{2}I_{si}\dot{\varphi}_{si}^2 \\ & + \frac{1}{2}m_{ui}\{\dot{y}_{ui} - T_{ei}\text{sign}(\varphi_{ui})\sin[\varphi_{ui} + \alpha_i\text{sign}(\varphi_{ui})]\dot{\varphi}_{ui} - (z_{Ri} + p_i)\dot{\varphi}_{ui}\cos\varphi_{ui} - \dot{p}_i\sin\varphi_{ui} - h_{Ri}\dot{\varphi}_{si}\cos\varphi_{si}\}^2 + \\ & + \frac{1}{2}m_{si}\{\dot{z}_{ui} + T_{ei}\text{sign}(\varphi_{ui})\cos[\varphi_{ui} + \alpha_i\text{sign}(\varphi_{ui})]\dot{\varphi}_{ui} - (z_{Ri} + p_i)\dot{\varphi}_{ui}\sin\varphi_{ui} + \dot{p}_i\cos\varphi_{ui} - h_{Ri}\dot{\varphi}_{si}\sin\varphi_{si}\}^2 \end{aligned} \quad (4.31)$$

$$\begin{aligned} U_i = & m_{ui}g\{z_{ui} + T_{ei}\text{sign}(\varphi_{ui})\sin[\varphi_{ui} + \alpha_i\text{sign}(\varphi_{ui})]\} + m_{si}g\{z_{ui} + \\ & T_{ei}\text{sign}(\varphi_{ui})\sin[\varphi_{ui} + \alpha_i\text{sign}(\varphi_{ui})] + (z_{Ri} + p_i)\cos\varphi_{ui} + h_{Ri}\cos\varphi_{si}\} + UT_i \end{aligned} \quad (4.32)$$

where T_{ei} is the distance between the cg and the roll center of the unsprung mass i , given

by $T_{ei} = \sqrt{R_{wi}^2 + (T_i + A_i)^2}$. R_{wi} is the effective wheel radius, and

$\alpha_i = \cos^{-1}[(T_i + A_i)/T_{ei}]$. I_{ui0} is the mass moment inertia of unsprung mass i with respect to the unsprung mass roll center (point A), as show in Figure 4.14. The potential

energy, UT_i , due to the torsional springs is the same as that described by Equation (4.30), and the sign function here describes the direction of roll deflection of the unsprung mass, given by

$$\text{sign}(\varphi_{ui}) = \begin{cases} +1 & \text{if } \varphi_{ui} \geq 0 \\ -1 & \text{if } \varphi_{ui} < 0 \end{cases} \quad (4.33)$$

4.4.1 Development of Absolute Rollover Vehicle Model

The absolute rollover vehicle model is derived upon considering the total energy associated with composite roll plane i . The equations of motion for the roll plane models, before and after the wheels lift off, can be derived using Lagrange's energy approach:

$$\frac{d}{dt} \left(\frac{\partial \mathcal{K}_i}{\partial \dot{q}_i} \right) - \frac{\partial \mathcal{K}_i}{\partial q_i} + \frac{\partial \mathcal{U}_i}{\partial q_i} = Q_i \quad (4.34)$$

where q_i are the generalized coordinates, and Q_i are the generalized external forces. The equations of motion, characterizing the roll dynamics of the vehicle prior to wheels lift-off are derived using Equations (4.28), (4.29) and (4.30) into (4.34), which can not be considered valid when the wheel lift-off is experienced. Alternatively, Equations (4.30), (4.31) and (4.32) can be used to derive the equations of motion for the vehicle with wheel lift-off and relatively large roll deflections. The equations of motion are thus derived and summarized below.

Lateral motion of the unsprung mass (\ddot{y}_{ui})

$$\begin{aligned} & (m_{ui} + m_{si}) \ddot{y}_{ui} - m_{si} (z_{Ri} + p_i) \cos \varphi_{ui} \ddot{\varphi}_{ui} - m_{si} h_{Ri} \cos \varphi_{si} \ddot{\varphi}_{si} - \\ & m_{si} \sin \varphi_{ui} \ddot{p}_i + m_{si} (z_{Ri} + p_i) \sin \varphi_{ui} \dot{\varphi}_{ui}^2 + m_{si} h_{Ri} \sin \varphi_{si} \dot{\varphi}_{si}^2 - \quad \text{for } (F_{y_j} > 0; j = 1, \dots, 4) \quad (4.35) \\ & 2m_{si} \cos \varphi_{ui} \dot{p}_i \dot{\varphi}_{ui} = F_{y_i} \end{aligned}$$

$$\begin{aligned}
& (m_{ui} + m_{si})\ddot{y}_{ui} - \{m_{si}(z_{Ri} + p_i)\cos\varphi_{ui} - (m_{si} + m_{ui})T_{ei}\sin(\varphi_{ui}) \\
& \sin[\varphi_{ui} + \alpha_i\sin(\varphi_{ui})]\}\ddot{\varphi}_{ui} - m_{si}h_{Ri}\cos\varphi_{si}\ddot{\varphi}_{si} - m_{si}\sin\varphi_{ui}\ddot{p}_i + \\
& \{m_{si}(z_{Ri} + p_i)\sin\varphi_{ui} - (m_{si} + m_{ui})T_{ei}\sin(\varphi_{ui})\cos(\varphi_{ui} + \\
& \alpha_i\sin(\varphi_{ui}))\}\dot{\varphi}_{ui}^2 + m_{si}h_{Ri}\sin\varphi_{si}\dot{\varphi}_{si}^2 - 2m_{si}\cos\varphi_{ui}\dot{p}_i\dot{\varphi}_{ui} = F_{yi}
\end{aligned} \quad (F_{yi} = 0; j = 1, 2 \text{ or } 3, 4)$$

(4.36)

where F_{yi} is the total lateral force developed at the tire-road interface of axle i . It should be noted that Equations (4.35) and (4.36) describe the lateral force equilibrium of the unsprung mass i , before ($F_{yi} > 0$; $j = 1, \dots, 4$) and after ($F_{yi} = 0$; $j = 1, 2 \text{ or } 3, 4$) the loss of contact between the wheels and road, respectively. The wheels lift-off is encountered when either $F_{11i}, F_{12i} = 0$ or $F_{13i}, F_{14i} = 0$.

Vertical motion of the unsprung mass (\ddot{z}_{ui})

$$\begin{aligned}
& (m_{ui} + m_{si})\ddot{z}_{ui} - m_{si}(z_{Ri} + p_i)\sin\varphi_{ui}\ddot{\varphi}_{ui} - m_{si}h_{Ri}\sin\varphi_{si}\ddot{\varphi}_{si} + \\
& m_{si}\cos\varphi_{ui}\ddot{p}_i - m_{si}(z_{Ri} + p_i)\cos\varphi_{ui}\dot{\varphi}_{ui}^2 - m_{si}h_{Ri}\cos\varphi_{si}\dot{\varphi}_{si}^2 - \\
& 2m_{si}\sin\varphi_{ui}\dot{p}_i\dot{\varphi}_{ui} = F_{11i} + F_{12i} + F_{13i} + F_{14i} - (m_{ui} + m_{si})g
\end{aligned} \quad (F_{yi} > 0; j = 1, \dots, 4) \quad (4.37)$$

and

$$\begin{aligned}
& (m_{ui} + m_{si})\ddot{z}_{ui} + \{(m_{si} + m_{ui})T_{ei}\sin(\varphi_{ui})\cos[\varphi_{ui} + \alpha_i\sin(\varphi_{ui})] \\
& - m_{si}(z_{Ri} + p_i)\sin\varphi_{ui}\}\ddot{\varphi}_{ui} - m_{si}h_{Ri}\sin\varphi_{si}\ddot{\varphi}_{si} + m_{si}\cos\varphi_{ui}\ddot{p}_i - \\
& \{(m_{si} + m_{ui})T_{ei}\sin(\varphi_{ui})\sin[\varphi_{ui} + \alpha_i\sin(\varphi_{ui})]\} + \\
& m_{si}(z_{Ri} + p_i)\cos\varphi_{ui}\dot{\varphi}_{ui}^2 - m_{si}h_{Ri}\cos\varphi_{si}\dot{\varphi}_{si}^2 - 2m_{si}\sin\varphi_{ui}\dot{p}_i\dot{\varphi}_{ui} \\
& = F_{ii} - (m_{ui} + m_{si})g
\end{aligned} \quad (F_{yi} = 0; j = 1, 2 \text{ or } 3, 4) \quad (4.38)$$

The tire vertical forces before wheels lift-off, F_{yji} ($j = 1, 2, 3, 4$), are derived from the resultant deflections and velocities across the tires. Assuming linear vertical spring rate (k_{ti}) and viscous damping coefficient (c_{ti}) due to the tires, and negligible contribution due to road roughness, the vertical tire forces are derived as:

$$F_{11i} = k_{ti}[\Delta_{10i} - z_{ui} - (T_i + A_i)\sin\varphi_{ui}] + c_{ti}[-\dot{z}_{ui} - (T_i + A_i)\cos\varphi_{ui}\dot{\varphi}_{ui}]$$

$$\begin{aligned}
F_{t2i} &= k_u [\Delta_{t0i} - z_{ui} - T_i \sin \varphi_{ui}] + c_u [-\dot{z}_{ui} - T_i \cos \varphi_{ui} \dot{\varphi}_{ui}] \\
F_{t3i} &= k_u [\Delta_{t0i} - z_{ui} + T_i \sin \varphi_{ui}] + c_u [-\dot{z}_{ui} + T_i \cos \varphi_{ui} \dot{\varphi}_{ui}] \\
F_{t4i} &= k_u [\Delta_{t0i} - z_{ui} + (T_i + A_i) \sin \varphi_{ui}] + c_u [-\dot{z}_{ui} + (T_i + A_i) \cos \varphi_{ui} \dot{\varphi}_{ui}] \quad (4.39)
\end{aligned}$$

where T_i is half track width of the inner tires and a_i is dual tire spacing. Δ_{t0i} is the static tire deflection derived from the axle load distributed over 4 tires of the axle i , given by:

$$\Delta_{t0i} = (m_{si} + m_{ui})g / (4, k_u) \quad (4.40)$$

The total vertical force, developed by the tires on axle i , after the loss of contact of tires, 1 and 2 or 3 and 4, with the road, can be derived as:

$$F_u = (m_{si} + m_{ui})g - 2k_u z_{ui} - 2c_u \dot{z}_{ui} \quad (4.41)$$

Equations (4.35) to (4.41) describe the lateral and vertical force equilibrium for unsprung mass i , before and after the loss of tire-road contact. The application of appropriate equations, however, involves examination of road-wheel contact from the lateral load transfer ratio (LTR_i), defined as:

$$LTR_i = \frac{(F_{t1i} + F_{t2i}) - (F_{t3i} - F_{t4i})}{F_{t1i} + F_{t2i} + F_{t3i} + F_{t4i}} \quad (4.42)$$

The subscripts 1 and 2 denote the tires located on the outer track of the axle, while 3 and 4 denote those located on the inside track. The occurrence of loss of road contact of tires on one-track yields a unity value of the LTR_i .

Roll motion of the unsprung mass ($\ddot{\varphi}_{ui}$)

$$\begin{aligned}
& [I_{ui} + m_{si}(z_{Ri} + p_i)^2] \ddot{\varphi}_{ui} - m_{si}(z_{Ri} + p_i) \sin \varphi_{ui} \ddot{z}_{ui} - m_{si}(z_{Ri} + p_i) \cos \varphi_{ui} \ddot{y}_{ui} \\
& + m_{si} h_{Ri}(z_{Ri} + p_i) \cos(\varphi_{si} - \varphi_{ui}) \ddot{\varphi}_{si} - m_{si} h_{Ri}(z_{Ri} + p_i) \sin(\varphi_{si} - \varphi_{ui}) \dot{\varphi}_{si}^2 + \\
& 2m_{si}(z_{Ri} + p_i) \dot{p}_i \dot{\varphi}_{ui} = m_{si} g(z_{Ri} + p_i) \sin \varphi_{ui} - (F_{t1} - F_{t2}) s_i + \\
& [(F_{t1i} - F_{t4i})(T_i + A_i) + (F_{t2i} - F_{t3i}) T_i] \cos \varphi_{ui} + F_{yi}(h_{ui} + z_{ui}) + k_{\phi}(\varphi_{si} - \varphi_{ui}) \\
& (F_{yi} > 0; \quad j = 1, \dots, 4) \quad (4.43)
\end{aligned}$$

and

$$\begin{aligned}
& \{ [I_{u0i} + m_{si}(z_{Ri} + p_i)^2 + (m_{ui} + m_{si})T_{ei}^2 + 2m_{si}T_{ei}\text{sign}(\varphi_{ui})(z_{Ri} + \\
& p_i)\sin[\alpha_i\text{sign}(\varphi_{ui})]\}\ddot{\varphi}_{ui} - \{m_{si}(z_{Ri} + p_i)\sin\varphi_{ui} - \\
& (m_{ui} + m_{si})T_{ei}\text{sign}(\varphi_{ui})\cos[\varphi_{ui} + \alpha_i\text{sign}(\varphi_{ui})]\}\ddot{z}_{ui} - \\
& \{m_{si}(z_{Ri} + p_i)\cos\varphi_{ui} + (m_{ui} + m_{si})T_{ei}\text{sign}(\varphi_{ui})\sin[\varphi_{ui} + \\
& \alpha_i\text{sign}(\varphi_{ui})]\}\ddot{y}_{ui} + m_{si}T_{ei}\ddot{p}_i + \{m_{si}h_{Ri}(z_{Ri} + p_i)\cos(\varphi_{si} - \varphi_{ui}) \\
& - m_{si}T_{ei}\text{sign}(\varphi_{ui})h_{Ri}\sin[\varphi_{si} - \varphi_{ui} - \alpha_i\text{sign}(\varphi_{ui})]\}\ddot{\varphi}_{si} \quad (F_{yi} = 0; j = 1, 2 \text{ or } 3, 4) \\
& - \{m_{si}h_{Ri}(z_{Ri} + p_i)\sin(\varphi_{si} - \varphi_{ui}) + m_{si}T_{ei}\text{sign}(\varphi_{ui})h_{Ri}\cos[\varphi_{si} \\
& - \varphi_{ui} - \alpha_i\text{sign}(\varphi_{ui})]\}\dot{\varphi}_{si}^2 + m_{si}\{T_{ei}\text{sign}(\varphi_{ui})\sin[\alpha_i\text{sign}(\varphi_{ui})] + \\
& 2(z_{Ri} + p_i)\}\dot{p}_i\dot{\varphi}_{ui} = m_{si}g(z_{Ri} + p_i)\sin\varphi_{ui} - (m_{ui} + m_{si})gT_{ei}\text{sign}(\varphi_{ui}) \\
& \cos[\varphi_{ui} + \alpha_i\text{sign}(\varphi_{ui})] - (F_{1i} - F_{2i})s_i + k_{\phi}(\varphi_{si} - \varphi_{ui})
\end{aligned} \tag{4.44}$$

where F_{1i} and F_{2i} are forces developed by suspension, comprising the restoring and damping force components, and k_{ϕ} is the auxiliary roll stiffness of axle i . Assuming linear spring rate about an operating point and viscous damping, the suspension forces can be expressed as:

$$F_{ji} = \begin{cases} k_{si}\Delta_{ji} + c_{si}\dot{\Delta}_{ji} + F_{ci}\text{sign}(\dot{\Delta}_{ji}) & \text{if } \Delta_{ji} > 0 \\ 0 & \text{if } -\varepsilon_{ji} \leq \Delta_{ji} \leq 0; \\ k_{si}(\Delta_{ji} + \varepsilon_{ji}) + c_{si}\dot{\Delta}_{ji} + F_{ci}\text{sign}(\dot{\Delta}_{ji}) & \text{if } \Delta_{ji} < -\varepsilon_{ji} \end{cases} \quad j=1, 2 \tag{4.45}$$

where k_{si} and c_{si} are suspension stiffness and damping coefficients, respectively, and F_{ci} is the suspension coulomb friction force. ε_{1i} and ε_{2i} are the backlash of the suspension springs 1 and 2, respectively. Δ_{ji} and $\dot{\Delta}_{ji}$ ($j=1, 2$) are the relative deflections and relative velocities of the suspension, respectively, which can be expressed as:

$$\Delta_{ji} = \Delta_{0i} - p_i + (h_{Ri} - b_i)[1 - \cos(\varphi_{si} - \varphi_{ui})] + (-1)^j s_i \sin(\varphi_{si} - \varphi_{ui}); \quad j=1, 2 \tag{4.46}$$

$$\dot{\Delta}_{ji} = -\dot{p}_i + [(h_{Ri} - b_i)\sin(\varphi_{si} - \varphi_{ui}) + (-1)^j s_i \cos(\varphi_{si} - \varphi_{ui})](\dot{\varphi}_{si} - \dot{\varphi}_{ui}); j=1, 2 \tag{4.47}$$

where s_j is the half spring spacing, and b_j is the vertical distance from the sprung mass cg to the spring top attachment point of the spring, when the vehicle is in its static equilibrium position. $\Delta_{0j} = m_{sj}g / (2k_{sj})$ is the static deflection of the suspension springs. The forces developed by nonlinear suspension springs, such as leaf springs and air suspension, are incorporated into the model using force-deflection tables.

The equations of motion for the sprung masses are derived in a similar manner from the vertical and lateral force, and roll moment equilibrium. The coupled differential equations describing the motion of sprung masses before and after the wheel lift-off are presented below.

Vertical motion of the sprung mass (\ddot{p}_i)

$$\begin{aligned} m_{sj} \ddot{p}_i + m_{sj} \cos \varphi_{ui} \ddot{z}_{ui} - m_{sj} \sin \varphi_{ui} \ddot{y}_{ui} - m_{sj} h_{Ri} \sin(\varphi_{si} - \varphi_{ui}) \ddot{\varphi}_{si} \\ - m_{sj} h_{Ri} \cos(\varphi_{si} - \varphi_{ui}) \dot{\varphi}_{si}^2 - m_{sj} (z_{Ri} + p_i) \dot{\varphi}_{ui}^2 \\ = F_{1i} + F_{2i} - m_{sj} g \cos \varphi_{ui} \end{aligned} \quad (F_{yi} > 0; j = 1, \dots, 4) \quad (4.48)$$

and

$$\begin{aligned} m_{sj} \ddot{p}_i + m_{sj} \cos \varphi_{ui} \ddot{z}_{ui} + m_{sj} T_{ei} \text{sign}(\varphi_{ui}) \cos \alpha_i \ddot{\varphi}_{ui} - m_{sj} \sin \varphi_{ui} \ddot{y}_{ui} \\ - m_{sj} h_{Ri} \sin(\varphi_{si} - \varphi_{ui}) \ddot{\varphi}_{si} - m_{sj} h_{Ri} \cos(\varphi_{si} - \varphi_{ui}) \dot{\varphi}_{si}^2 - \\ m_{sj} \{ T_{ei} \text{sign}(\varphi_{ui}) \sin[\alpha_i \text{sign}(\varphi_{ui})] + (z_{Ri} + p_i) \} \dot{\varphi}_{ui}^2 \\ = F_{1i} + F_{2i} - m_{sj} g \cos \varphi_{ui} \end{aligned} \quad (F_{yi} = 0; j = 1, 2 \text{ or } 3, 4) \quad (4.49)$$

Roll motion of the sprung mass ($\ddot{\varphi}_{si}$)

$$\begin{aligned} (I_{sj} + m_{sj} h_{Ri}^2) \ddot{\varphi}_{si} - m_{sj} h_{Ri} \sin \varphi_{si} \ddot{z}_{ui} - m_{sj} h_{Ri} \cos \varphi_{si} \ddot{y}_{ui} + \\ m_{sj} h_{Ri} (z_{Ri} + p_i) \cos(\varphi_{si} - \varphi_{ui}) \ddot{\varphi}_{ui} - m_{sj} h_{Ri} \ddot{p}_i \sin(\varphi_{si} - \varphi_{ui}) \\ + m_{sj} h_{Ri} (z_{Ri} + p_i) \sin(\varphi_{si} - \varphi_{ui}) \dot{\varphi}_{ui}^2 + 2m_{sj} h_{Ri} \cos(\varphi_{si} - \varphi_{ui}) \dot{p}_i \dot{\varphi}_{ui} \quad (F_{yi} > 0; j = 1, \dots, 4) \quad (4.50) \\ = m_{sj} g h_{Ri} \sin \varphi_{si} - (F_{1i} + F_{2i}) (h_{Ri} - b_i) \sin(\varphi_{si} - \varphi_{ui}) + \\ (F_{1i} - F_{2i}) s_i \cos(\varphi_{si} - \varphi_{ui}) - k_{\phi} (\varphi_{si} - \varphi_{ui}) - MT_i \end{aligned}$$

and

$$\begin{aligned}
& (I_{s_i} + m_{s_i} h_{R_i}^2) \ddot{\varphi}_{s_i} - m_{s_i} h_{R_i} \sin \varphi_{s_i} \ddot{z}_{u_i} - m_{s_i} h_{R_i} \cos \varphi_{s_i} \ddot{y}_{u_i} + \\
& \{ m_{s_i} h_{R_i} (z_{R_i} + p_i) \cos(\varphi_{s_i} - \varphi_{u_i}) - m_{s_i} h_{R_i} T_{ei} \text{sign}(\varphi_{u_i}) \times \\
& \sin[\varphi_{s_i} - \varphi_{u_i} - \alpha_i \text{sign}(\varphi_{u_i})] \} \ddot{\varphi}_{u_i} - m_{s_i} h_{R_i} \ddot{p}_i \sin(\varphi_{s_i} - \varphi_{u_i}) + \\
& \{ m_{s_i} h_{R_i} (z_{R_i} + p_i) \sin(\varphi_{s_i} - \varphi_{u_i}) + m_{s_i} h_{R_i} T_{ei} \text{sign}(\varphi_{u_i}) \times \\
& \cos(\varphi_{s_i} - \varphi_{u_i} - \alpha_i \text{sign}(\varphi_{u_i})) \} \dot{\varphi}_{u_i}^2 + 2 m_{s_i} h_{R_i} \cos(\varphi_{s_i} - \varphi_{u_i}) \dot{p}_i \dot{\varphi}_{u_i} \\
& = m_{s_i} g h_{R_i} \sin \varphi_{s_i} - (F_{1i} + F_{2i})(h_{R_i} - b_i) \sin(\varphi_{s_i} - \varphi_{u_i}) + \\
& (F_{1i} - F_{2i}) s_i \cos(\varphi_{s_i} - \varphi_{u_i}) - k_{\phi}(\varphi_{s_i} - \varphi_{u_i}) - MT_i
\end{aligned} \tag{4.51}$$

where MT_i is the moment developed due to torsional compliance of the couplings between the sprung units, which can be expressed as:

$$MT_i = \begin{cases} KF_i(\varphi_{s_i} - \varphi_{s(i+1)}); & i = 1 \\ KF_{i-1}(\varphi_{s_i} - \varphi_{s(i-1)}) + KF_i(\varphi_{s_i} - \varphi_{s(i+1)}); & 1 < i < n \\ KF_{i-1}(\varphi_{s_i} - \varphi_{s(i-1)}); & i = n \end{cases} \tag{4.52}$$

The lateral acceleration response of the sprung mass i , before and after the wheel lift-off, can be derived from derivative of velocity vector of the sprung mass i , and can be expressed as:

$$\begin{aligned}
a_{y_i} &= \ddot{y}_{u_i} - (z_{R_i} + p_i) \cos \varphi_{u_i} \ddot{\varphi}_{u_i} - \sin \varphi_{u_i} \ddot{p}_i - h_{R_i} \cos \varphi_{s_i} \ddot{\varphi}_{s_i} \\
&+ (z_{R_i} + p_i) \sin \varphi_{u_i} \dot{\varphi}_{u_i}^2 - 2 \cos \varphi_{u_i} \dot{p}_i \dot{\varphi}_{u_i} + 2 h_{R_i} \sin \varphi_{s_i} \dot{\varphi}_{s_i}^2 - (F_{y_i} > 0; j = 1, \dots, 4) \\
&\dot{z}_{u_i} \dot{\varphi}_{s_i} + (z_{R_i} + p_i) \sin \varphi_{u_i} \dot{\varphi}_{u_i} \dot{\varphi}_{s_i} - \cos \varphi_{u_i} \dot{p}_i \dot{\varphi}_{s_i}
\end{aligned} \tag{4.53}$$

and

$$\begin{aligned}
a_{y_i} &= \ddot{y}_{u_i} - (z_{R_i} + p_i) \cos \varphi_{u_i} \ddot{\varphi}_{u_i} - \sin \varphi_{u_i} \ddot{p}_i - h_{R_i} \cos \varphi_{s_i} \ddot{\varphi}_{s_i} + \\
&(z_{R_i} + p_i) \sin \varphi_{u_i} \dot{\varphi}_{u_i}^2 - 2 \cos \varphi_{u_i} \dot{p}_i \dot{\varphi}_{u_i} + 2 h_{R_i} \sin \varphi_{s_i} \dot{\varphi}_{s_i}^2 - \dot{z}_{u_i} \dot{\varphi}_{s_i} + \\
&(z_{R_i} + p_i) \sin \varphi_{u_i} \dot{\varphi}_{u_i} \dot{\varphi}_{s_i} - \cos \varphi_{u_i} \dot{p}_i \dot{\varphi}_{s_i} - T_{ei} \text{sign}(\varphi_{u_i}) \cos[\varphi_{u_i} + \\
&\alpha_i \text{sign}(\varphi_{u_i})] \dot{\varphi}_{u_i}^2 - T_{ei} \text{sign}(\varphi_{u_i}) \sin[\varphi_{u_i} + \alpha_i \text{sign}(\varphi_{u_i})] \ddot{\varphi}_{u_i} - \\
&T_{ei} \text{sign}(\varphi_{u_i}) \cos[\varphi_{u_i} + \alpha_i \text{sign}(\varphi_{u_i})] \dot{\varphi}_{u_i} \dot{\varphi}_{s_i}
\end{aligned} \tag{4.54}$$

The equations of motion of the vehicle combination are initially solved under prescribed steering maneuver and vehicle speed, assuming tire-road contact. The vertical

tire forces are examined to identify the loss of road-wheel contact. The response is then evaluated from equations derived corresponding to lift-off conditions. The final state-variable values computed from the equations of motion, applicable before the wheels lift off the ground, are considered as the inertial conditions of the equations of motion after wheel lift-off. The initial condition for the unsprung mass roll rate, however, is derived from conservation of rotational kinetic energy, which can be expressed as:

$$\dot{\phi}_u(0) = \dot{I}_u(T_0) \sqrt{\frac{I_u}{I_{u0}}} \quad (4.55)$$

where $\dot{I}_u(T_0)$ is the unsprung mass roll rate, when LTR_i approaches a unity value, and T_0 is the time corresponding to the wheel lift-off. Equations of motion, derived using Lagrange's energy approach, are solved for lateral force excitations at the tire-road interface arising from different directional maneuvers. The lateral force excitations can be obtained either from the field tests or from a validated more comprehensive vehicle model.

4.4.2 Modeling of Suspension Springs

Heavy vehicles are increasingly employing air springs for their superior load carrying capacity, ride height control, ride comfort and pavement load performance, while leaf springs are still widely used due to their low cost and high durability. The front axles of heavy vehicles and combinations mostly utilize leaf springs. The leaf springs exhibit nonlinear force-deflection and hysteretic properties, as shown in Figure 4.15 [91]. The figure illustrates the envelope force-deflection curves together with those obtained under small amplitude stroking cycles about three operating points. It has been

reported that the force-deflection properties of truck leaf springs are insensitive to frequency of oscillations in the range of 0 to 15 Hz, but depend on the amplitude of motion and the nominal load [91]. Although there exists a variety of configurations of air springs employed in heavy vehicles, most air suspensions exhibit nonlinear force-deflection characteristics and hysteretic loops due to rubber bushings. Since the roll dynamic of heavy vehicle is strongly related to suspension properties, an analytical representation is formulated for force-deflection characteristics of commonly used leaf and air spring suspensions.

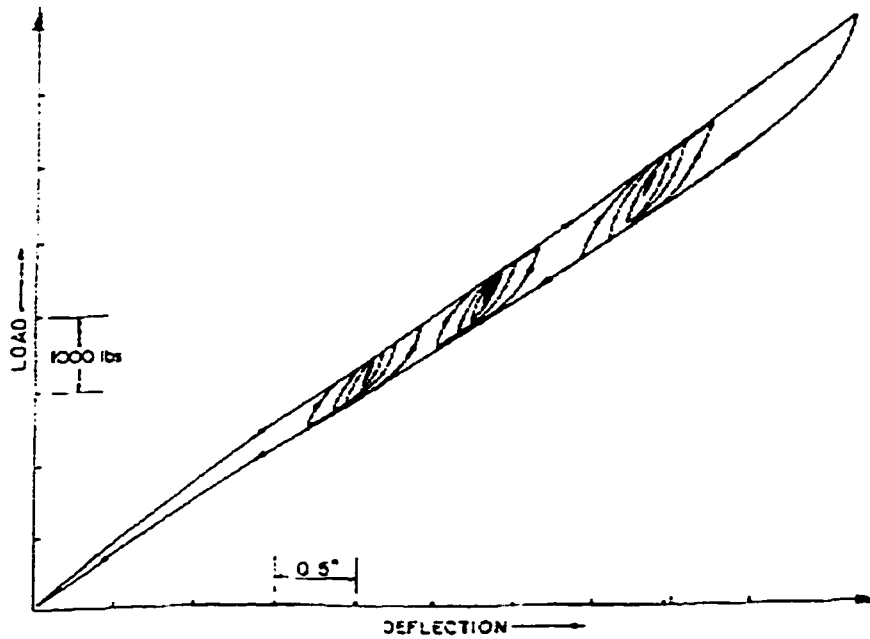


Figure 4.15: Typical tapered-leaf spring envelope with hysteresis loops [91]

The force-deflection characteristics and hysteretic loops of the springs can be approximately represented by the following numerical iteration equation:

$$F_i = F_{Ei} + (F_{i-1} - F_{Ei})e^{-(4-4.1i)^{1/2}} \quad (4.56)$$

where F_i and Δ_i are the suspension force and deflection at the current (i) simulation time step, while F_{i-1} and Δ_{i-1} are the suspension force and deflection at the previous ($i-1$) simulation step. F_{Ei} is the suspension force corresponding to the upper and lower limits of the envelope of the measured spring characteristics at a deflection Δ_i . For $\Delta_i > \Delta_{i-1}$, the F_{Ei} is derived from the upper limit of the envelope, while the lower limit is used for $\Delta_i < \Delta_{i-1}$. λ is a deflection constant, which describes the rate at which the suspension force within a hysteresis loop approach the boundary of the envelope. The value of λ is selected to minimize the error between the measured and estimated force. The lower and upper bounds of the force-deflection characteristics may be represented by linear and nonlinear function in terms of suspension deflection, Δ .

Figure 4.16 illustrates the force-deflection characteristics of the Hendrickson RTE 440 suspension spring, derived from the analysis of the roll plane model under step lateral acceleration excitations. The envelope force F_{Ei} , corresponding to upper and lower bounds, is expressed by the following linear expressions:

For $\Delta_i > \Delta_{i-1}$

$$F_{Ei} = 1773.6 \Delta_i + 4.76 \text{ kN}, \quad (4.57)$$

For $\Delta_i < \Delta_{i-1}$

$$F_{Ei} = 1299.7 \Delta_i + 0.14 \text{ kN}, \quad (4.58)$$

The deflection constants were selected as: $\lambda = 1.65 \times 10^{-3}$ m for $\Delta_i > \Delta_{i-1}$; and $\lambda = 1.27 \times 10^{-3}$ m for $\Delta_i < \Delta_{i-1}$. The results show that both upper and lower limit curves approach their equilibrium positions exponentially corresponding to minimum and

maximum deflections. The rate of approach, however, is dependent upon the deflection constant λ .

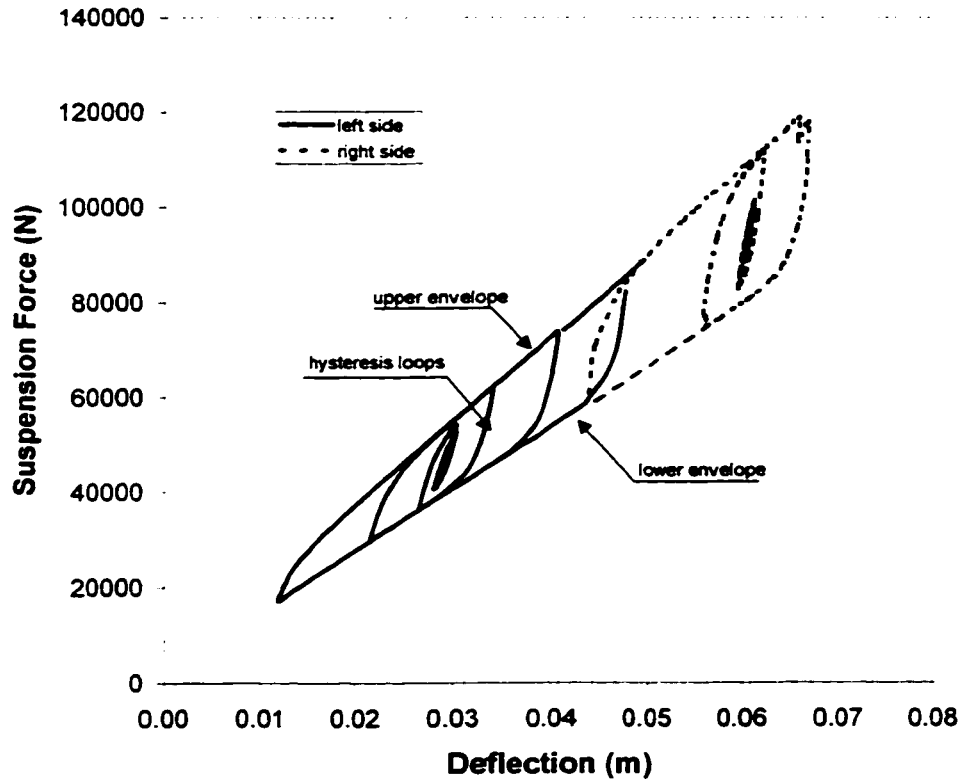


Figure 4.16: Simulation of a leaf spring property using numerical iteration.

4.5 MODEL VALIDATION

The analytical model of suspension springs based upon numerical iteration technique, is integrated within the dynamic roll-plane model. The vehicle model is analyzed under transient steering maneuvers, and its response characteristics are compared with those obtained from comprehensive yaw/roll model. The three-dimensional yaw/roll model has been widely accepted as a valid tool for study of directional behavior of heavy vehicle combinations [92]. The yaw/roll model, however, is

developed upon assuming that the unsprung mass roll center is located at its c.g. [29]. The comprehensive model thus can not be considered valid when loss of tire-road contact occurs, since the roll center shifts to the contact patch of the outer tires. The validation of the proposed roll plane model can thus be examined prior to the loss of wheel-road contact. The yaw/roll model is initially analyzed to determine the lateral force excitations at the tire-road interface under sinusoidal steering inputs. The lateral force excitations together with the simulation parameters, summarized in Table 4.10 are then used to analyze the proposed roll plane model. The sprung weight of the semi-trailer is lumped into two roll planes (#2 and #3), as shown in Figure 4.12 (b). The lateral acceleration of the semi-trailer in the roll plane model (a_{y1}) is derived as the moment-weighted average of lateral acceleration responses of the sprung masses in the 2nd and 3rd roll plane, given by:

$$a_{y1} = (m_{s2}a_{y2}h_{s2} + m_{s3}a_{y3}h_{s3}) / (m_{s2}h_{s2} + m_{s3}h_{s3}) \quad (4.59)$$

where m_{s2} , m_{s3} , a_{s2} and a_{s3} are the sprung masses and lateral acceleration responses in the 2nd and 3rd roll planes, respectively. h_{s2} and h_{s3} are the c.g. heights of the sprung masses in the 2nd and 3rd roll planes, respectively. Figure 4.17 illustrates a comparison of the lateral acceleration response of the trailer sprung mass derived from the proposed model with that obtained from the yaw/roll model. The results show that the proposed model yields excellent agreement with the yaw/roll model in terms of both the magnitude and the phase. The load transfer ratios derived from the proposed and yaw/roll models are further compared in Figure 4.18. It is observed that the load transfer ratios of the tractor and trailer axles, derived from the roll plane model, are quite close to those derived from the yaw/roll model.

Table 4.10: Simulation parameters of a 5-axle tractor-semitrailer combination.

	Tractor front section	Tractor rear section	Trailer section
Sprung mass (kg)	4404.0	14365.0	14365.0
Roll moment of inertia of sprung mass (kgm^2)	2500.0	12000.0	12000.0
Unsprung mass (kg)	548.0	2270.0	1362.0
Roll moment of inertia of unsprung mass (kgm^2)	418.0	1154.0	928.0
Tire vertical stiffness (kN/m)	875	875	875
Suspension viscous damping (Ns/m)	0.0	0.0	17500.0
Coulomb friction (N)	2116	8907	3224
Tire viscous damping coefficient (Ns/m)	0.0	0.0	0.0
Sprung mass cg height (m)	1.120	2.065	2.065
Distance between sprung mass cg and suspension roll center (m)	0.6564	1.2269	1.3284
Distance between the top attachment of the suspension and sprung mass cg (m)	0.6064	1.1469	1.2484
Unsprung mass cg height (m)	0.5080	0.5080	0.5080
Distance between unsprung mass cg and suspension roll center (m)	-0.0444	0.3301	0.2286
Half wheel track (m)	1.0160	0.7493	0.8255
Dual tire separation (m)	0.0000	0.3302	0.3302
Half suspension track (m)	0.4064	0.4826	0.5588
Auxiliary roll stiffness (Nm/rad)	24752.0	745217.0	777618.0
No. of Wheels per axle	2	4	4
No. of axles per section	1	2	2
Tractor frame roll stiffness (Nm/rad)	55000.0		
Fifth wheel roll stiffness (Nm/rad)	6000000.0		

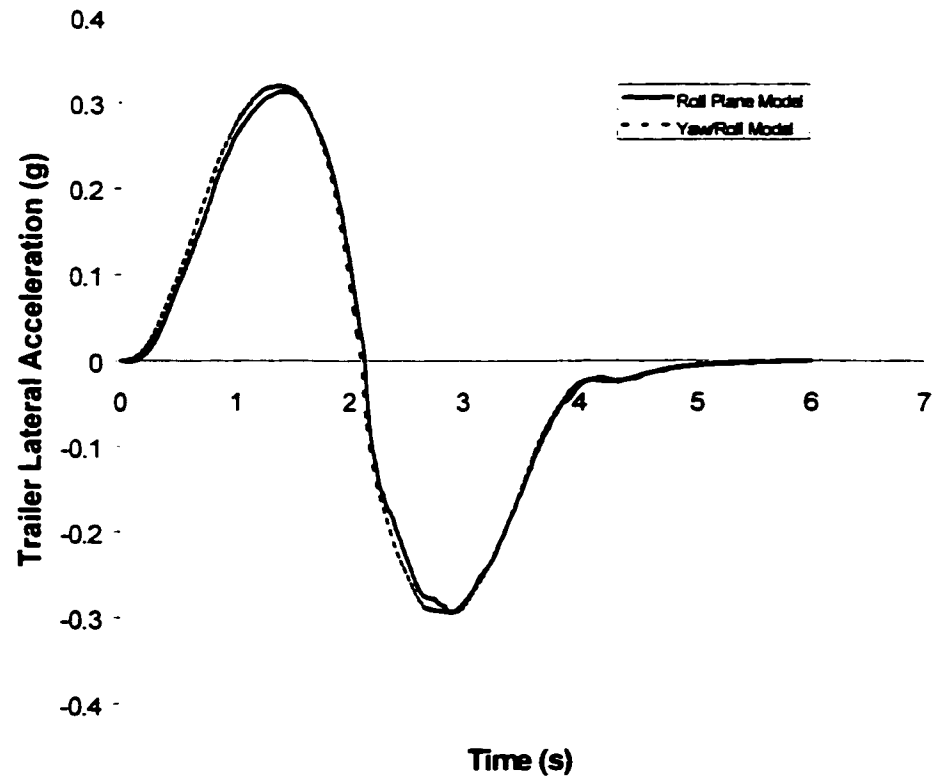
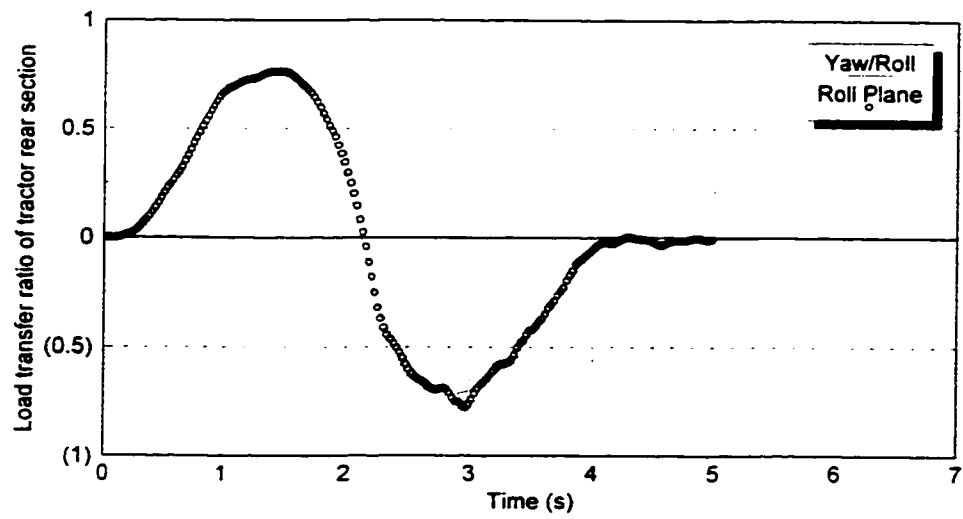
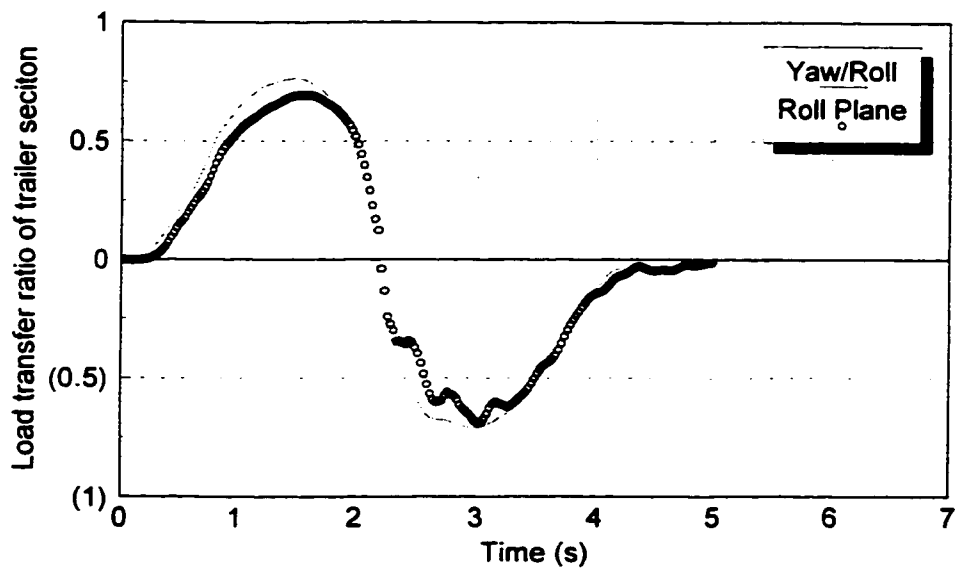


Figure 4.17: Comparison of the trailer lateral acceleration response of the roll plane model with that derived from the yaw/roll model.



(a)



(b)

Figure 4.18: Comparison of load transfer ratio derived from the roll plane and the yaw/roll models.

4.6 ABSOLUTE ROLLOVER THRESHOLD

The roll stability characteristics of heavy vehicles in terms of static rollover threshold (*SRT*) and dynamic rollover threshold (*DRT*) have been thoroughly investigated in previous sections. *SRT* and *DRT*, however, are defined on the basis of relative rollover criterion. Definite occurrence of rollover may not be assured when lateral acceleration response of a vehicle reaches its *SRT* in steady turning maneuvers or *DRT* in directional maneuvers. Absolute rollover threshold (*ART*) of heavy vehicles, on the other hand, is defined based on absolute roll instability criterion. *ART* can thus be taken as a real indication of absolute rollover.

4.6.1 Absolute Roll Instability Indicators

Dynamic roll instability can be quantified by an energy-based function, referred to as *Rollover Prevention Energy Reserve (RPER)*, proposed by Nalecz [42]. The corresponding dimensionless factor *RPERF*, is employed for this study. The *RPERF* is defined as the difference between the potential energy at its tip-over position and the sum of the instantaneous potential and rotational kinetic energies, divided by the difference between the potential energies at its tip-over and static equilibrium positions. *RPERF* function approaches a negative value when rollover occurs, but the function value always remains positive in a non-rollover case. *RPERF* is considered as a conservative dynamic rollover indicator, as the energy dissipated due to non-conservative damping is assumed to be negligible. The *RPERF* can be expressed as:

$$RPERF = \frac{\sum \left[U_{i_{up}} - U_i - K_{i_{roll}} - \frac{1}{2} K F_i (\varphi_{s_{i+1,i}} - \varphi_{s_i})^2 \right]}{\sum (U_{i_{up}} - U_{i_0})} \quad (4.60)$$

where $U_{i_{up}}$ is the potential energy of the vehicle at its tip-over position in the roll plane i . U_i and $K_{i_{roll}}$ are the instantaneous potential and rotational kinetic energy of the vehicle in roll plane i , respectively. U_{i_0} is the potential energy in roll plane i of the vehicle at its static equilibrium position. The instantaneous potential energy of the vehicle U_i , before and after the wheel lift-off, is derived from Equations (4.29) and (4.32), respectively. $U_{i_{up}}$, U_{i_0} and $K_{i_{roll}}$ are further derived as:

$$U_{i_{up}} = m_{ui} g [T_{ci} \sin(\varphi_{\theta_{ui}} + \alpha)] + m_{si} g [T_{ci} \sin(\varphi_{\theta_{ui}} + \alpha) + z_{Ri} \cos \varphi_{\theta_{ui}} + h_{Ri} \cos(\varphi_{\theta_{ui}} + \Delta\varphi_i)] \quad (4.61)$$

$$U_{i_0} = m_{ui} g h_{ui} + m_{si} g (h_{ui} + z_{Ri} + h_{Ri}) \quad (4.62)$$

$$K_{i_{roll}} = \begin{cases} 0.5(I_{ui} \dot{\varphi}_{ui}^2 + I_{si} \dot{\varphi}_{si}^2) & (F_{yi} > 0, i = 1, \dots, 4) \\ 0.5(I_{ui0} \dot{\varphi}_{ui}^2 + I_{si} \dot{\varphi}_{si}^2) & (F_{yi} = 0; j = 1, 2 \text{ or } 3, 4) \end{cases} \quad (4.63)$$

where $\varphi_{\theta_{ui}}$ is the unsprung mass roll angle at the tip-over position, given by:

$$\varphi_{\theta_{ui}} = \tan^{-1} \left[\frac{T_i - h_{Ri} \sin(\Delta\varphi_i)}{h_{Ri} \cos(\Delta\varphi_i) + R_{wi} + z_{Ri}} \right] \quad (4.64)$$

Assuming that the total sprung weight is supported by the suspension springs on one side after wheels lift-off, $\Delta\varphi_i$ can be estimated as, $\Delta\varphi_i = m_{si} g / (2k_{si} s_i)$. The dynamic rollover of a vehicle may also be detected from the lateral distance between the sprung mass cg and the outer tire contact patch with the ground, referred to as *Critical Distance (CD)* shown in Figure 4.14. The critical distance may be computed from:

$$CD_i = |T_{ci} \text{sign}(\varphi_{ui}) \cos[\varphi_{ui} + \text{sign}(\varphi_{ui})\alpha_i] - (h_{ui} + z_{Ri}) \sin \varphi_{ui} - h_{Ri} \sin \varphi_{si}| \quad (4.65)$$

A dimensionless factor, *Critical Distance Ratio* (CDR_i) is defined as:

$$CDR_i = CD_i / (T_{ci} \cos \alpha_i) \quad (4.66)$$

From equations (4.65) and (4.66), it is apparent that the critical distance ratio is at its maximum value, when the vehicle is in its static equilibrium position, and reduces to zero when the vehicle approaches its tip-over position.

4.6.2 Analysis of Absolute Rollover Threshold

Dynamic rollover of heavy vehicles frequently occurs during high-speed evasive maneuvers. Many field measurement studies of heavy vehicles have established that the lateral tire force corresponding to typical evasive maneuvers can be approximated by a sinusoidal function [28, 90]. The roll plane model derived in section 4.4 is used to investigate absolute rollover threshold of heavy vehicles subjected to sinusoidal lateral force excitations at three different frequencies: 0.5Hz, 0.33Hz and 0.25Hz. The simulation parameters of a typical straight vehicle are illustrated in Table 4.11.

Figure 4.19 illustrates the time histories of the dynamic rollover indicators and the roll angles of the sprung and unsprung masses of the vehicle subjected to a sinusoidal lateral excitation at 0.33 Hz. The results show the absolute rollover indicators in terms of $RPERF$ and CDR . The CDR approaches a zero value at $t \approx 1.35s$, which relates to the tip-over position of the vehicle. The roll displacements of the sprung (φ_{si}) and unsprung (φ_{ui}) masses initially increase slowly, when the values of CDR and $RPERF$ are relatively high. The roll angles increase more rapidly as the vehicle approaches its tip-over position, which indicates the occurrence of a definite rollover. The $RPERF$ reduces to a value

below zero prior to the vehicle approaching its tip-over position. The signature of the dynamic rollover indicators and the roll angles of the sprung and unsprung masses of the vehicle subject to a relatively less severe sinusoidal steering maneuver ($f=0.33$ Hz) are illustrated in Figure 4.20. In this case, the roll displacements of the sprung and unsprung masses increase to peak values of 23° and 19° , respectively, and then reduce in a more rapid manner toward the static equilibrium position of the vehicle. An actual rollover of the vehicle thus does not occur even though the *RPERF* approaches zero. The critical distance ratio (*CDR*) approaches a minimum value of 0.33, when the roll angles approach their respective peak values. The *CDR* then tends to increase, as the roll angles decrease, indicating the non-existence of a definite rollover situation. Under such steering inputs, it is apparent that the *RPERF* represents a conservative dynamic rollover indicator, while *CDR* describes the occurrence of a definite rollover more accurately.

Absolute rollover threshold defined as the maximum lateral acceleration level that a vehicle can sustain before the dynamic rollover indicators approach zero values can also be investigated using the proposed roll plane model. Sinusoidal lateral force excitations at the tire-road interface are employed in this study, which approximately represent the lateral forces developed at the tires of a vehicle during obstacle avoidance maneuvers. The roll plane model is analyzed to derive the *RPERF* and *CDR*, which are further examined to predict the absolute rollover threshold of the vehicle at different excitation frequencies. Figure 4.21 illustrates the relationship between the amplitude of lateral acceleration response of the sprung mass, and *RPERF* and *CDR* at an excitation frequency of 0.33 Hz. The results show that the amplitude of lateral acceleration approaches 0.62 g corresponding to zero value of the *RPERF*. The amplitude of lateral

acceleration corresponding to $CDR=0$, however, approaches a higher value of 0.64g, as shown in the figure. Thus two slightly different rollover limits are obtained based on the $RPERF$ and CDR .

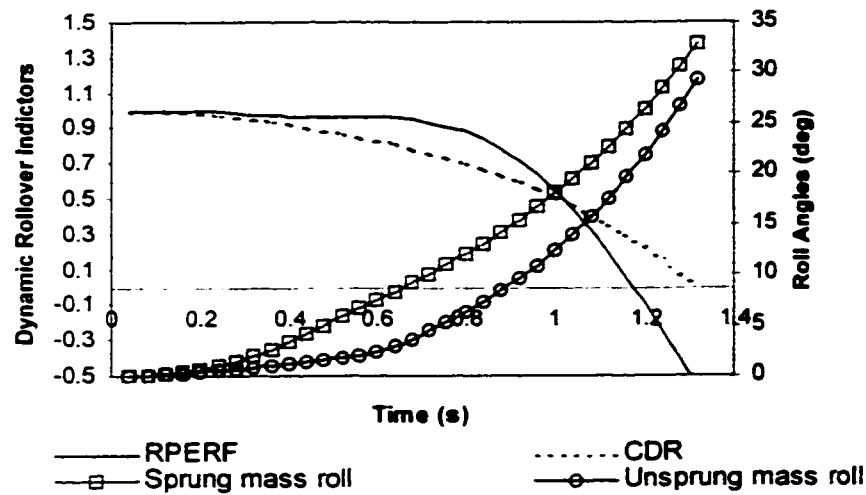


Figure 4.19: Dynamic rollover indicators in a rollover directional maneuver.

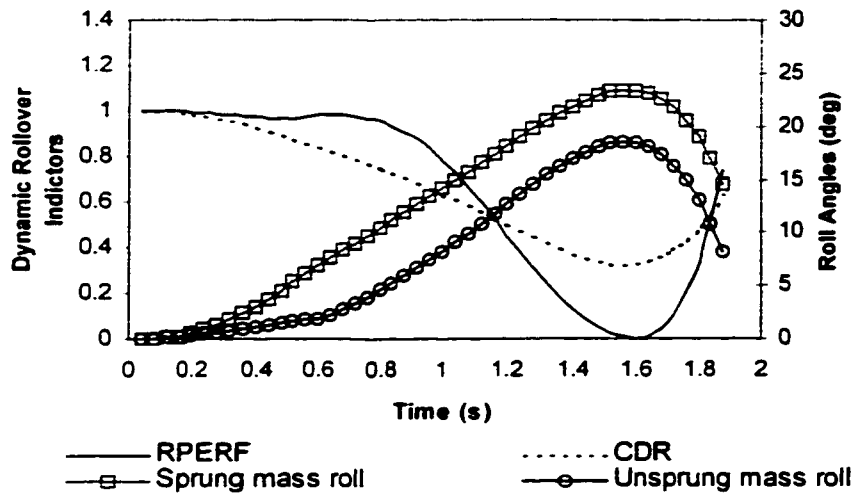


Figure 4.20: Dynamic rollover indicators in a non-rollover directional maneuver.

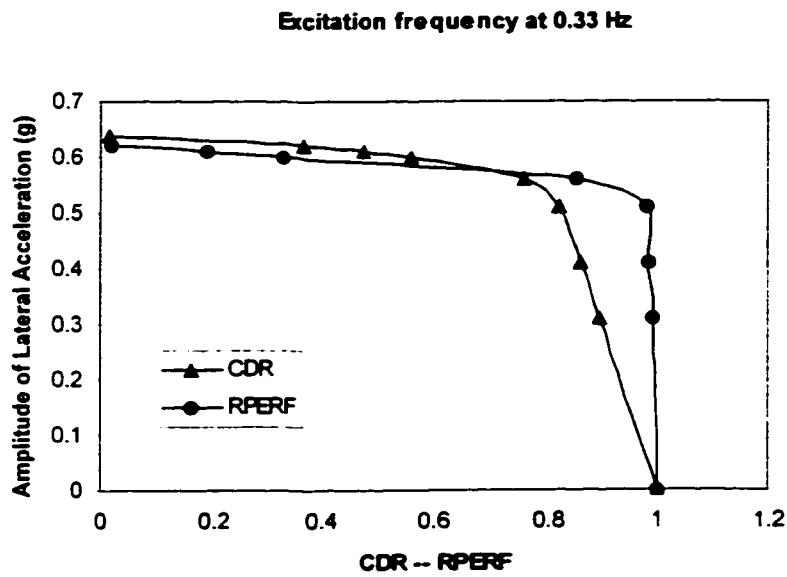


Figure 4.21: Prediction of the dynamic rollover limits using the *CDR* and *RPERF*.

The absolute rollover limits of the vehicle subject to excitations at different frequencies are summarized in Table 4.12. The static rollover threshold (*SRT*) of the vehicle is further evaluated using the roll plane model subject to a ramp-step lateral excitation at a very slow rate. The ratio of absolute rollover threshold (*ART*) to the *SRT* is further derived and presented in the table. The lateral acceleration level when *RSF* approaches 1 is taken as the *SRT* of the vehicle. From the results, it is apparent that excitations at a relatively higher frequency of 0.5 Hz yield dynamic rollover limits considerably higher than the corresponding *SRT*, irrespective of the indicator used. As the excitation frequency decreases, the dynamic rollover limits of the vehicle approach the *SRT* from the upper side. The results of the study thus reveal that the permissible lateral acceleration in a lane change maneuver is higher than that considered safe under a steady maneuver. The *SRT* thus provides an underestimate of the anti-roll ability of the heavy vehicles subject to transient steering maneuvers.

Table 4.11: Simulation parameters of a straight truck.

Parameters	Symbol	Values
sprung mass (kg)	m_{si}	16946
unsprung mass (kg)	m_{ui}	3033
distance between sprung mass cg and its roll center (m)	H_{Ri}	1.2
unsprung mass cg height (m)	H_{ui}	0.508
roll moment of inertia of sprung mass (kg-m^2)	I_{si}	35768
roll moment of inertia of unsprung mass (kg-m^2)	I_{ui}	1410
top of suspension spring to sprung mass cg (m)	b_i	0.3
dual tire separation (m)	A_i	0
half spring track (m)	s_i	0.762
half wheel track (m)	T_i	1.08
tire vertical stiffness (N/m)	k_{ti}	711880
number of tires	N_i	8
suspension spring stiffness (N/m)	k_{si}	1240103
suspension damping coefficient (N-sec/m)	c_{si}	102602
auxiliary roll stiffness (Nm/deg)	k_{ϕ}	20810

Table 4.12: Dynamic rollover threshold of the vehicle at different excitation frequencies.

	Absolute rollover threshold (<i>ART</i>) (g)		<i>SRT</i> (g)	<i>ART/SRT</i>	
	Based on <i>CDR</i>	Based on <i>RPERF</i>		Based on <i>CDR</i>	Based on <i>RPERF</i>
$f=0.25\text{ Hz}$	0.62	0.61	0.60	1.03	1.02
$f=0.33\text{ Hz}$	0.64	0.62		1.07	1.03
$f=0.5\text{ Hz}$	0.76	0.71		1.27	1.18

4.7 SUMMARY

The dynamic roll response characteristics of articulated heavy vehicles are investigated using the yaw/roll model. It was revealed that the roll response characteristics of the tractor and attached trailers are quite different in both amplitude and phase angle. The concept of effective lateral acceleration is thus proposed to characterize all the centrifugal forces of a complete roll unit. Dynamic rollover threshold is proposed based on the effective lateral acceleration and the relative rollover criterion. It is concluded that dynamic rollover threshold of articulated heavy vehicles in most cases are slightly less than or equal to the static rollover threshold of such vehicles, and are relatively insensitive to steering maneuvers. The difference between the static and dynamic rollover thresholds is normally less than five percent. Static rollover threshold can therefore be conveniently employed to estimate the dynamic rollover propensity of heavy vehicles. Wheels lift-off sequence is investigated by examining load transfer ratio

occurred on each composite-axle of heavy vehicles in directional maneuvers. It is concluded that rollover of tractor semi-trailer combinations and A-train doubles is initialized at the rearmost axles of the vehicles.

An analytical nonlinear roll plane model of different heavy vehicle combinations is proposed for investigation of absolute roll instability. The equations of motion derived using Lagrange's energy approach is considered valid until the vehicle approaches its tip-over position. The proposed model differs from the previous reported models in a significant manner, since it can predict the roll dynamics of a vehicle after the wheels lift off the ground, and thus the occurrence of an absolute rollover. The rollover indicators in dynamic maneuvers are proposed in terms of *RPERF* and *CDR*, while *RPERF* is considered as a conservative rollover indicator. The absolute rollover limits predicted by *RPERF* are slightly lower than those predicted by the *CDR*. The simulation results reveal that absolute rollover limits of a straight truck in an obstacle avoidance maneuver are larger than the corresponding *SRT* values, especially for higher excitation frequencies. The *SRT* provides an underestimation of the anti-roll ability of the heavy vehicles subject to transient steering maneuvers.

CHAPTER 5

ANALYSIS OF IMPENDING ROLLOVER INDICATORS FOR OPEN-LOOP ROLLOVER CONTROL

5.1 INTRODUCTION

It has been established in chapter 4 that the dynamic roll instabilities are initiated at the rearmost of articulated freight vehicles, and the driver often remains unaware of the impending instability due to excessive dimensions of the vehicles [38, 93]. It has been recognized that some form of early warning to the driver of the onset of potential vehicle rollover is vital to ensure road safety. Probability of heavy vehicle rollover accidents can be considerably reduced through on-line detection and early warning of impending roll instability, such that a timely corrective maneuver could be performed by the driver to avert the occurrence of a potential instability [94]. Early detection of potential roll instability involves the establishment of a dynamic rollover criterion, and the identification of motion response parameters which are directly related to onset of vehicle rollover. Such vital parameters, however, must be directly measurable and relatively insensitive to variations in vehicle design and operating conditions to realize a reliable early warning system. Furthermore, the warning signals for impending rollover should be generated early enough such that the driver can perform the corrective maneuvers in appropriate time. The design of a dynamic rollover warning device thus necessitates the identification of impending dynamic rollover indicators with high degree of measurability, reliability and available time margin for corrective maneuvers.

Only a few studies have reported on detection of onset of vehicle rollover. Preston-Thomas et al. [95] carried out a feasibility study of a rollover warning device for

heavy vehicles, and concluded that the lateral load transfer ratio (*LTR*) can serve as a reliable indicator for impending rollover. The proposed criteria, however, involves on-line measurement of tire loads in a moving vehicle, which is considered to be quite intricate. Rakheja and Piché [5] investigated the concept of an early warning safety monitor to detect the onset of vehicle rollover and jackknife, and proposed a set of directly measurable response variables, which are directly related to potential roll and yaw instabilities. The study concluded that the onset of vehicle rollover could be detected via on-line acquisition of vehicle lateral acceleration during low speed cornering maneuvers and semi-trailer axle roll angle during high-speed directional maneuvers. The reliability of the indicators proposed in [5, 95] has not been investigated in view of the dynamic rollover of the vehicle and the lead time provided by the indicators.

In this chapter, different potential dynamic rollover indicators are identified through simplified analysis of a lumped two-axle roll plane model. Rollover indicators are evaluated for their reliability to predict roll instability of a five-axle tractor-semitrailer combination. Parametric sensitivity analyses are carried out to study the sensitivity of the indicators to variations in various operating and design factors. Measurability of potential rollover indicators is discussed based on current engineering practice. Phase shift properties of the indicators are investigated to assess their capability to provide an early warning of impending rollover with sufficient lead time for the driver's actions. Different conceptual designs of an early warning roll safety monitor are finally discussed.

5.2 IDENTIFICATION OF POTENTIAL ROLLOVER INDICATORS

Rollover of heavy freight vehicles may occur in low speed cornering maneuvers and in high speed directional maneuvers. Relative rollover condition and rollover threshold of a variety of heavy freight vehicles in steady cornering maneuvers have been investigated and presented in chapter 3. Detection of relative roll instability of heavy vehicles in steady cornering maneuvers can be performed based on static rollover threshold (*SRT*) or lift-off of wheels on certain axles. Relative roll instability of heavy vehicles in transient directional maneuvers, however, can be detected based on dynamic rollover threshold (*DRT*), as analyzed in chapter 4. Since dynamic rollover threshold of a vehicle is nearly equal to its static rollover threshold, *SRT* and the corresponding relative rollover condition can thus be employed to derive relative rollover indicators in directional maneuvers.

As discussed in chapter 3, relative rollover condition of straight vehicles may be approached when wheels on either one axle or two axles lift off the ground, depending on vehicle configurations, roll stiffness distribution between front and rear axles. Relative rollover condition of five-axle tractor semi-trailer combinations is always approached when wheels on tractor rear and trailer axles lift off the road surface. Relative rollover condition of B- or C- doubles may be reached either when wheels on tractor rear axles and on the adjacent semi-trailer axles lift off or when wheels on axles of the first and second semi-trailers lift off, depending on vehicle configurations. Relative rollover conditions of all the vehicle configurations, however, can be synthesized and numerically evaluated by a non-dimensional factor referred to as roll safety factor (*RSF*), as defined in

chapter 3. RSF is proposed on the base of load transfer ratio of the axles which experience wheels lift-off at relative rollover condition, and is expressed as:

$$RSF = \frac{\sum_{j=1}^m (FL_j - FR_j)}{\sum_{j=1}^m (FL_j + FR_j)} \quad (5.1)$$

where m is the number of axles that should experience loss of wheel-road contact in order to approach relative rollover condition. The absolute value of RSF can be used as a rollover indicator. Apparently, $|RSF|$ will approach its maximum value 1 when relative roll instability condition is reached.

The two-axle roll plane model for straight trucks presented in chapter 3 is used to derive an analytical relationship between RSF and vehicle response parameters. Assuming relative rollover condition of a straight truck is reached when wheels on the rear axle lift off the ground, Equation (5.1) can be simplified as:

$$RSF = \frac{FR_2 - FL_2}{FR_2 + FL_2} \quad (5.2)$$

Substituting FR_2 and FL_2 from Equation (3.6) to Equation (5.2), the following linear relationship between RSF and the rear axle roll angle φ_{u2} is obtained as:

$$\varphi_{u2} = \frac{W_2}{2k_{t2}T_2} RSF \quad (5.3)$$

where $W_2 = (m_s q_2 + m_{u2})g$ is the load supported by the rear axle. The unsprung mass roll angle φ_{ui} ($i=1, 2$) is related to the vehicle lateral acceleration a_y and sprung mass roll angle φ_s . The relationship can be derived from Equation (3.7) as:

$$\varphi_{u1} = a_{11}\varphi_s + a_{12}a_y \quad (5.4)$$

$$\varphi_{u2} = a_{21}\varphi_s + a_{22}a_y \quad (5.5)$$

where a_{11} , a_{12} , a_{21} and a_{22} are parameters related to vehicle configurations, suspension and tire stiffness characteristics, as given in Equation (3.7). The lateral acceleration a_y , however, is linearly related to sprung mass roll angle φ_s , as shown in Equation 3.8, and is presented below for clarification as:

$$a_y = C\varphi_s \quad (5.6)$$

where $C = \frac{K_{\varphi 1} + K_{\varphi 2} - m_s g h_R - K_{\varphi 1} a_{11} - K_{\varphi 2} a_{21}}{m_s h_R + K_{\varphi 1} a_{12} + K_{\varphi 2} a_{22}}$ could be taken as a constant for a specified vehicle. Substituting Equations (5.3) and (5.6) to (5.5), the following relationship between φ_s and RSF is obtained:

$$\varphi_s = \frac{W_2}{2k_{t2}T_2(a_{21} + Ca_{22})} RSF \quad (5.7)$$

Substituting (5.7) into (5.6), the relationship between a_y and RSF can be written as:

$$a_y = \frac{CW_2}{2k_{t2}T_2(a_{21} + Ca_{22})} RSF \quad (5.8)$$

The relationship between the front axle roll angle φ_{u1} and RSF can be derived by substituting Equations (5.7) and (5.8) into (5.4), and can be written as:

$$\varphi_{u1} = \frac{W_2}{2k_{t2}T_2(a_{21} + Ca_{22})} (a_{11} + Ca_{12}) RSF \quad (5.9)$$

The relative roll angles between sprung and unsprung masses can be derived as:

$$\Delta\varphi_{u1} = \varphi_s - \varphi_{u1} = \frac{W_2}{2k_{t2}T_2(a_{21} + Ca_{22})} (1 - a_{11} - Ca_{12}) RSF \quad (5.10)$$

$$\Delta\varphi_{u2} = \varphi_s - \varphi_{u2} = \frac{W_2}{2k_{t2}T_2} \left[\frac{l}{(a_{2l} + Ca_{22})} - 1 \right] RSF \quad (5.11)$$

Under a dynamic directional maneuver, the vehicle lateral acceleration a_y describes the lateral dynamic response of vehicle subject to a steering input at the front wheels. For a two-axle vehicle subject to a steady cornering maneuver, the following relationship between the steering angle and lateral acceleration is easily established [21]:

$$\delta_f V^2 = a_y (L + K_{us} V^2 / g) \quad (5.12)$$

where δ_f is the average steer angle of the front wheels, and V is vehicle forward velocity. L is the wheelbase, and K_{us} is the understeer coefficient. $\delta_f V^2$ is referred to as steering-velocity factor (SVF). By defining $SVF = \delta_f V^2$ and substituting (5.8) to (5.12), the following relationship between steering-velocity factor (SVF) and RSF is obtained:

$$SVF = (L + K_{us} V^2 / g) \frac{CW_2}{2k_{t2}T_2(a_{2l} + Ca_{22})} RSF \quad (5.13)$$

Equations (5.3), (5.7) to (5.11) and (5.13) reveal that the vehicle response parameters of straight trucks (φ_{u1} , φ_{u2} , $\Delta\varphi_{u1}$, $\Delta\varphi_{u2}$, φ_s , a_y and SVF) can be directly related to RSF , and thus relative rollover condition of the vehicle. Since RSF is served as a relative rollover indicator, the response parameters of φ_{u1} , φ_{u2} , $\Delta\varphi_{u1}$, $\Delta\varphi_{u2}$, φ_s , a_y and SVF could be taken as potential rollover indicators of straight trucks. Further examination of the above relationships between the response parameters and RSF reveals the following observations. The unsprung mass roll angle (φ_{u2}) shows strong dependency upon the axle load, wheel track and tire stiffness. The lateral acceleration (a_y), sprung mass roll angle (φ_s), relative roll angles ($\Delta\varphi_{u1}$, $\Delta\varphi_{u2}$), and front axle roll angle (φ_{u1})

reveal further dependency upon the c.g. height and suspension properties. The steering-velocity factor parameter (*SVF*) reveals further dependency upon the vehicle handling property, specifically the understeer coefficient.

The potential rollover indicators derived from two-axle roll plane of straight trucks can be classified in six groups: ① roll safety factor (*RSF*); ② unsprung mass roll angles ($\varphi_{u1}, \varphi_{u2}$); ③ relative roll angles ($\Delta\varphi_{u1}, \Delta\varphi_{u2}$); ④ sprung mass roll angle (φ_s); ⑤ vehicle lateral acceleration (a_y); and ⑥ steer-velocity factor (*SVF*). For tractor semi-trailer combinations, B- and C- doubles, however, simple analytical relationships between response parameters and *RSF* could not be derived due to complexity. By similarity, the potential rollover indicators for the articulated vehicles could be picked up from the above five groups of rollover indicators, as illustrated in Table 5.1.

Table 5.1: Potential rollover indicators of different vehicle combinations.

	Straight trucks (2-axle)	Tractor semi-trailer combinations	B- C-doubles
Group 1	<i>RSF</i>	<i>RSF</i>	<i>RSF</i>
Group 2	$\varphi_{u1}, \varphi_{u2}$	$\varphi_{u1}, \varphi_{u2}, \dots, \varphi_{un}^*$	$\varphi_{u1}, \varphi_{u2}, \dots, \varphi_{un}$
Group 3	$\Delta\varphi_{u1}, \Delta\varphi_{u2}$	$\Delta\varphi_{u1}, \Delta\varphi_{u2}, \dots, \Delta\varphi_{un}$	$\Delta\varphi_{u1}, \Delta\varphi_{u2}, \dots, \Delta\varphi_{un}$
Group 4	φ_s	$\varphi_{s1}, \varphi_{s2}, \dots, \varphi_{sm}^{**}$	$\varphi_{s1}, \varphi_{s2}, \dots, \varphi_{sm}$
Group 5	a_y	$a_{y1}, a_{y2}, \dots, a_{ym}$	$a_{y1}, a_{y2}, \dots, a_{ym}$
Group 6	<i>SVF</i>	<i>SVF</i>	<i>SVF</i>

Note: * n is the number of axles of the combination

** m is the number of sprung masses of the combination.

5.3 MEASURABILITY ANALYSIS

As illustrated in Table 5.1, potential rollover indicators are classified into six different groups. Measurability analysis for each group is carried out based on current engineering practice.

Roll Safety Factor - As illustrated in Equation (5.1), roll safety factor involves monitoring dynamic tire vertical forces. Over the years, a variety of techniques has been developed for measuring dynamic tire forces generated by heavy vehicles [96]. A bending moment method was proposed to strain gauge the axle housing between the spring mounting and road wheel mounting [97], based on the proportional relationship between the bending strain and the shear force carried by the axle. Modification of the measured shear forces should be made to compensate the inertia of all wheel and axle components outboard of the load cells. Le Balnc et al [98] noted that the bending moment method became inaccurate in the presence of side forces or roll moment. Attempts to measure dynamic tire force by monitoring tire inside pressure variations have not been successful due to the nonlinear frequency-dependent relationship between tire load and tire inside pressure change [99]. Methods based on measurement of tire vertical and lateral deflections have been proposed [100]. It was assumed that vertical stiffness of the tire is independent of rolling velocity. Practically, this assumption is not correct [100], and considerable errors may result in when the tire is rolling with side-slip. Strain gauged hubs are also developed for measurement of dynamic tire forces [101]. The tire forces and moments are transferred from wheel rim to wheel hub by eight specially designed flex-members with 56 strain gauges. It is claimed that this system can accurately measure dynamic tire forces and moments. A rotating wheel dynamometer system is developed by

Kistler [102], which incorporates piezoelectric quartz force sensors for measurement of dynamic wheel forces and moments.

The dynamic tire force measurement systems, however, are very expensive. The current price for the systems illustrated in [101, 102], for example, is more than \$200,000 for one axle. They are thus economically unrealistic to serve as a detector of impending rollover of heavy vehicles. A simple and inexpensive vertical tire force sensor needs to be developed. Since wheels with small vertical load due to load transfer can easily be locked up, one potential method is to apply a small braking effort and measure the longitudinal slip ratio of the wheel. This method, however, needs to be thoroughly explored for its effectiveness and cost. The measurability of *RSF* is therefore rated as poor, as illustrated in Table 5.2.

Roll Angles of Unsprung and Sprung Masses - Roll angles of sprung and unsprung masses are defined as roll displacements of vehicle body and axle with respect to road surface, respectively. One method of obtaining axle roll angle is to measure wheel deflection on each side of the axle with height sensors. Unsprung mass roll angle can be obtained as the ratio of the difference between the left and right wheel deflections divided by the wheel track. The measurement of sprung mass roll angle can also be made in the same manner. Highly accurate height sensors, however, are considerably expensive for a rollover-warning device. Another method is to use gyroscopes, which also appears to be an expensive solution. The measurement of roll angles of sprung and unsprung masses are thus rated as good but costly.

Relative Roll Angle - Relative roll angle of sprung mass with respect to unsprung mass can be easily measured using Linearly Variable Displacement Transducer (*LVDT*).

Two laterally spaced *LVDT* transducers are needed to attach across sprung and unsprung masses of a vehicle. The relative roll angle between sprung and unsprung masses is derived from the relative displacement of the two transducers.

Lateral Acceleration - Lateral acceleration of heavy vehicle can be easily measured using inexpensive accelerometers. The measurement of lateral acceleration is considered as good and cheap.

Table 5.2: Measurability of different rollover indicators.

Indicators	Measurability
<i>Roll Safety Factor</i>	poor, costly
Roll Angles of Sprung and Unsprung Masses	good, costly
Relative Roll Angles	good, cheap
Lateral Acceleration	good, cheap
Steer-Velocity Factor	good, cheap

Steer Velocity Factor (SVF) - *SVF* involves vehicle forward velocity and average steer angle of front wheels. Since speedometers are normally equipped in heavy vehicles, no additional sensor is needed to measure vehicle forward speed. There are several methods of measuring front wheel steer angles. One is to measure the steer angle of hand-wheel (or steering wheel). Steer angle of road wheels is derived approximately as the hand-wheel steer angle divided by the gear ratio of the steering system. Considerable errors may result in due to unknown compliance of the steering system. The second method is to measure the sweep angle of the pitman arm of the steering system. Static calibration is needed to correlate the sweep angle to the steer angles of the inside (δ_i) and outside (δ_o) wheels. The average steer angle of the front wheels is calculated as: $\delta_f = \arctan[2 \tan \delta_o \tan \delta_i / (\tan \delta_o + \tan \delta_i)]$. Dynamic factors such as roll steer, bump steer and wrap steer are not considered in this approach. The third method is to directly

measure the steer angles of front wheels, which involves relatively expensive instrumentation devices. The measurement of SVF is considered as good and cheap.

5.4 RELIABILITY ANALYSIS

Detection of impending rollover involves two important steps: (1) on-line measurement of a rollover indicator; and (2) comparison of the obtained instantaneous value with a preset threshold value of the indicator for generation of a rollover warning to the driver. False warning of impending rollover may occur if the threshold value varies with vehicle operating parameters and maneuvers performed such that its exact value can not be known. A rollover indicator is considered reliable if its threshold value has little variations in daily operation of the vehicle or its threshold can be predicted with little estimation errors for various operating conditions. Reliability analysis of potential rollover indicators is carried out in terms of estimation errors due to uncertainty of dependent parameters and correlation properties with RSF .

5.4.1 Estimation Error Analysis

Reliability analysis of the proposed rollover indicators could be carried out using the analytical equations derived in section 5.2. Generally speaking, an indicator is said to be less reliable if it depends on more vehicle parameters whose values are not exactly known. Table 5.3 illustrates the order of reliability of rollover indicators in terms of dependent variables. Since RSF is a mathematical expression of relative rollover condition, RSF is considered as the most reliable impending rollover indicator irrespective of the vehicle configurations. The roll angle of the rear axle (ϕ_{u2}), whose

wheels experience lift-off at relative rollover condition, reveal strong dependency upon the axle load, wheel track and tire stiffness. While wheel track can be reasonably established, dynamic wheel load and tire stiffness may involve certain estimation errors. The lateral acceleration (a_y), sprung mass roll angle (ϕ_s) and the relative roll angles ($\Delta\phi_{u1}$, $\Delta\phi_{u2}$) reveal further dependency upon sprung mass c.g. height and suspension properties. These response parameters are thus considered as relatively less reliable indicators. The steering factor parameter (SVF) reveals further dependency upon the vehicle handling property, specifically the understeer coefficient. The steering factor is thus considered the least reliable indicator.

Table 5.3 Classification of rollover indicators in terms of dependent parameters.

Indicators	Dependency factors	Reliability
Roll Safety Factor RSF	No	①
Axle roll angle ϕ_{u2}	Axle load, wheel track and tire properties	②
Lateral acceleration a_y Sprung mass roll angle ϕ_s Unsprung mass roll angle ϕ_{u1} Relative roll angle $\Delta\phi_{u1}$, $\Delta\phi_{u2}$	All those in ② and c.g height, suspension properties	③
Steer-velocity factor SVF	All those in ③ and vehicle handling properties	④

Reliability analysis of different rollover indicators is also numerically carried out for a straight truck, whose parameters vary from baseline values to certain percentages, as illustrated in Table 5.4. It is assumed that $\pm 5\%$ variations exist in sprung weight, sprung mass c.g. height, suspension roll center heights, roll stiffness rates and tire vertical

stiffness rates, while $\pm 50\%$ variations exist in understeer coefficient. Equations (5.2), (5.3), (5.6) to (5.11) and (5.13) are used to derive estimation errors of the rollover indicators due to the variations in vehicle parameters. As shown in Table 5.4, *RSF* is not influenced by the vehicle parameter variations. The rear axle roll angle (φ_{u2}) varies from -7% to 8% over its baseline value, while sprung mass roll angle (φ_s) changes from -12% to 13% over the baseline value. Estimation error for lateral acceleration a_y is in the range of $\pm 8\%$, while that for front axle roll angle (φ_{u1}) ranges from -16% to 21%. Errors in relative roll angles ($\Delta\varphi_{u1}$, $\Delta\varphi_{u2}$) range from -13% to 14%. Steer-velocity factor (*SVF*) experiences the largest estimation error, which ranges from -28% to 32%.

RSF is thus taken as the most reliable rollover indicator, while *SVF* is the least reliable. Surprisingly, the rear axle roll angle and lateral acceleration errors are in the same order for the typical straight truck, although previous analysis shows that there are more dependent parameters for the lateral acceleration. Estimation errors for the sprung mass roll angle and relative roll angles are in the same order, while the roll angle of the front axle reveals relatively large error. It should be pointed out that large error for front axle roll angle comes from the assumption that relative rollover condition of the straight truck is approached when wheels on the rear axle lift off the ground. A comment from this observation is as follows. If unsprung mass roll angles are selected to serve as impending rollover indicators, the roll angles of the axles whose wheels are not subjected to lift-off in relative rollover condition are less reliable than those of the axles whose wheels experience lift-off.

Table 5.4: Reliability analysis results in terms of estimation errors.

Vehicle parameters		Response vector	
baseline value	variation	rollover indicator	estimation error
a: 2.14 m	0%	RSF	0%
L: 4.03 m	0%		
H_{u1} : 0.381 m	0%	φ_{u2}	-8% ~ 9%
H_{u2} : 0.394 m	0%		
T_1 : 0.991 m	0%	φ_s	-12% ~ 13%
T_2 : 0.845 m	0%		
m_{u1} : 513 kg	0%	a_y	-8% ~ 8%
m_{u2} : 731 kg	0%		
m_s : 4690 kg	$\pm 5\%$	φ_{u1}	-16% ~ 21%
h_R : 0.92 m	$\pm 5\%$		
h_{c1} : 0.405 m	$\pm 5\%$	$\Delta\varphi_{u1}$	-13% ~ 14%
h_{c2} : 0.686 m	$\pm 5\%$		
$K_{\varphi1}$: 49832 Nm/rad	$\pm 5\%$	$\Delta\varphi_{u2}$	-13% ~ 14%
$K_{\varphi2}$: 295776 Nm/rad	$\pm 5\%$		
k_{t1} : 604157 N/m	$\pm 5\%$	SVF	-28% ~ 32%
k_{t2} : 1208314 N/m	$\pm 5\%$		
K_{us} : 2 deg/g	$\pm 50\%$		

5.4.2 Correlation Analysis with RSF

The effectiveness and reliability of the proposed roll instability indicators are discussed in the previous section using the roll-plane model for straight trucks. The roll plane model, however, does not adequately describe the transient roll dynamics of a multi-axle vehicle with different suspension properties. The effectiveness and reliability of the proposed indicators are thus further investigated through analysis of a comprehensive directional dynamic model described in chapter 4. The equations of motion are solved in the time domain, while steering input is described either by the path coordinates or by the steering angle of front wheels. Two different steering inputs are considered, namely, *trapezoidal steering* and *sinusoidal steering*, to characterize low speed cornering maneuvers and high speed obstacle avoidance maneuvers to study the effectiveness of the indicators. In trapezoidal steering, the front steering wheels are turned from 0^0 to a certain angle at a rate of 10 deg/s and held constant for the duration of the maneuver. The vehicle model is analyzed at increasing vehicle speeds until relative roll instability is observed. Sinusoidal steering is performed such that the steering angle of front wheels varies in the form of a sinusoid, which lasts for only one period. The vehicle forward speed is increased in successive increments until relative roll instability is detected.

While vehicle design parameters could be considered as constant for a specific vehicle, operating conditions vary considerably in daily operation. Reliability analysis of various rollover indicators are thus performed for a typical 5-axle tractor semi-trailer combination under different operating conditions, summarized in Table 5.5 together with the rollover indicators. A total of seven relative roll instability indicators are considered,

which include: *RSF*, lateral acceleration of the tractor and semi-trailer, roll angles of the tractor and trailer sprung masses, unsprung mass roll angles, and the steering velocity factor. The reliability and effectiveness of each roll indicator is investigated with respect to *RSF* under three directional maneuvers: steady turning, trapezoidal steering, and sinusoidal steering. The simulation parameters of the baseline tractor semi-trailer are presented in Table 5.6. A correlation between the different indicators and *RSF* is established to study the effectiveness of each indicator in predicting the relative roll dynamic instability. The results of the study are discussed in the following section.

Linear Correlation: The correlation between the lateral acceleration response of the tractor and the semi-trailer units and the *RSF* of the articulated heavy vehicle at nominal load is illustrated in Figure 5.1, for steady and transient directional maneuvers. Poor correlation is observed between the tractor lateral acceleration response and the *RSF* under transient directional maneuvers. The results show that during a sinusoidal steering maneuver one *RSF* value corresponds to two considerably different values of lateral acceleration of the tractor. For instance, when *RSF* approaches a value of 0.8, the lateral acceleration of the tractor reaches 0.43g and 0.01g, respectively. Thus monitoring the tractor lateral acceleration can not instantaneously determine how close the vehicle is to rollover. The results further reveal existence of a phase shift between the tractor lateral acceleration and the roll safety factor. The lateral acceleration response of the semi-trailer, however, correlates very well with the *RSF* and thus the onset of the vehicle rollover in dynamic maneuvers. The high degree of correlation between the trailer lateral acceleration and the *RSF* is most likely attributed to its high inertia and center of gravity,

and the fact that the semi-trailer lateral acceleration response is nearly in phase with that of the *RSF*.

Table 5.5: Specifications of simulation vehicles and rollover indicators.


Vehicle Configuration			
Semitrailer c.g. Heights (m)	1.6	1.85	2.05
Gross Vehicle Weight (% of Nominal Load)	70%	100%	
Tires	Radial 11R22.5		
Front Suspension	International Harvester (leaf)		
Tractor Rear Suspension	Hendrickson Walking Beam RTE 440 (leaf)		
Semi-trailer Suspension	Neway AR 95-17 Rating 10896 kg (air)		
Rollover Indicators	<ul style="list-style-type: none"> ① <i>RSF</i>; ② Tractor lateral acceleration (a_{y1}) ③ Semi-trailer lateral acceleration (a_{y2}); ④ Tractor roll angle (ϕ_{x1}) ⑤ Semi-trailer roll angle (ϕ_{x2}); ⑥ Unsprung mass roll angles ϕ_{ui} ($i=1\sim5$) ⑦ Steering Velocity Factor (<i>SVF</i>) 		

Table 5.6: Nominal simulation parameters of the baseline 5-axle tractor semi-trailer.

	tractor			semi-trailer	
sprung mass (kg)	4404			28730	
roll mass moment of inertia (kgm^2)	1697			24000	
pitch mass moment inertia (kgm^2)	8483			431196	
yaw mass moment of inertia (kgm^2)	8483			435444	
center of gravity height (m)	1.13			2.06	
	axle 1	axle 2	axle 3	axle 4	axle 5
axle load (kN)	48804	81507	81507	77057	77057
axle roll moment of inertia (kgm^2)	418	577	577	464	464
longitudinal position from c.g (m)	0.73	-2.31	-3.54	-4.83	-6.05
axle center of gravity (m)	0.508	0.508	0.508	0.508	0.508
roll center height (m)	0.46	0.84	0.84	0.74	0.74
half spring spacing (m)	0.406	0.483	0.483	0.559	0.559
half track - inner tires (m)	1.106	0.749	0.749	0.826	0.826
dual tire spacing (m)	0	0.33	0.33	0.33	0.33

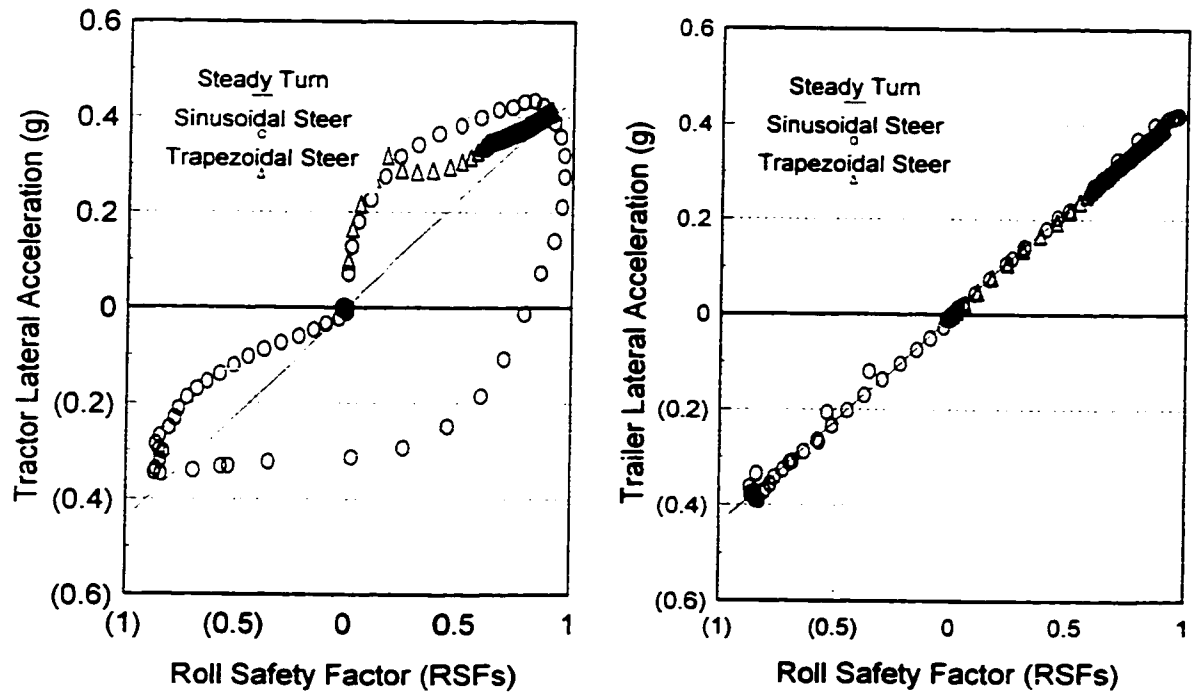


Figure 5.1: The relationship between the lateral acceleration response and the roll safety factor during different dynamic maneuvers.

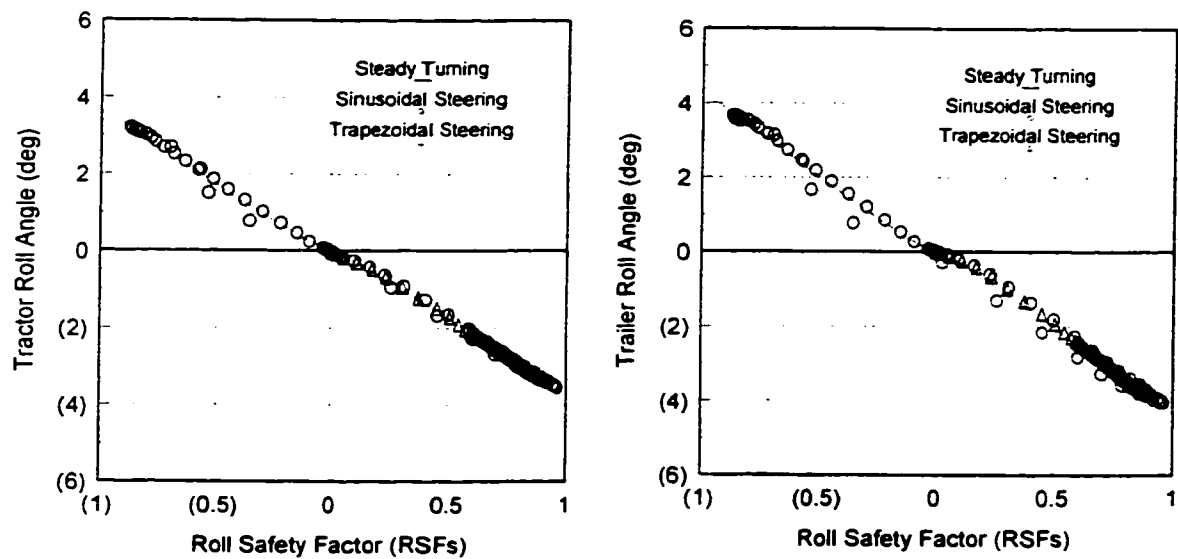


Figure 5.2: The relationship between the sprung mass roll responses and the roll safety factor.

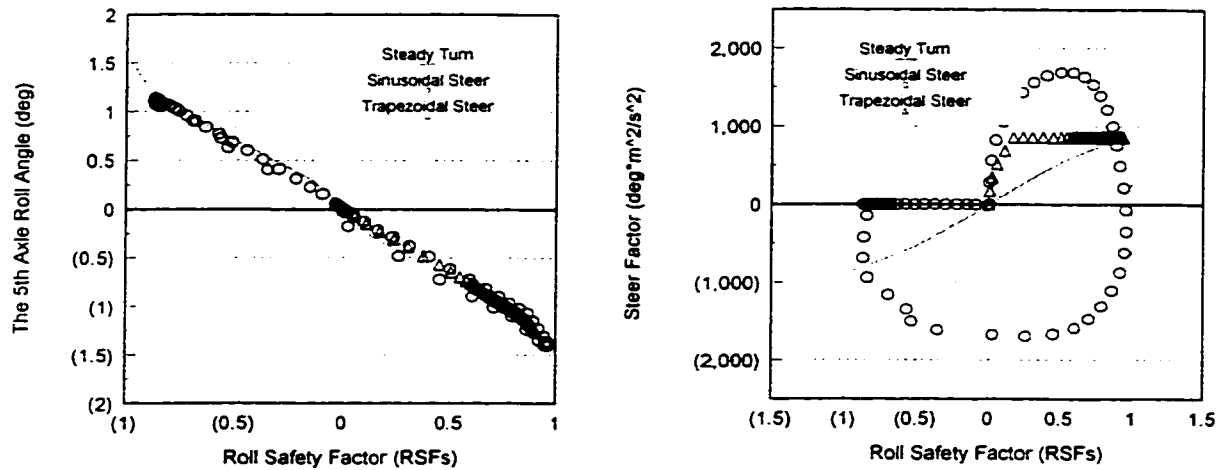


Figure 5.3: The relationship between the 5th axle roll angle, the steering velocity factor and the roll safety factor.

The relationship between sprung mass roll angle response characteristics of the vehicle and the *RSF* are presented in Figure 5.2. It is revealed that the roll safety factor is directly related to roll angle response of both the tractor and the semi-trailer. Good linear correlation is observed between roll response of the last axle (ϕ_{u5}) and the *RSF*, as shown in Figure 5.3. However there exists poor linear relationship between the steering velocity factor and *RSF* of the tractor semi-trailer. Larger value of steering factor thus does not instantaneously indicate larger roll safety factor.

Sensitivity to Operating Conditions: The operating conditions of heavy vehicles may vary considerably due to different distributions of payload and cg heights. A good rollover indicator should be insensitive to such variations in vehicle operating parameters and maneuvers performed. Such insensitivity implies that rollover threshold of an indicator should not be significantly influenced by variations in operating conditions and

maneuvers. The reliability of the rollover indicators is thus evaluated by examining variations in their limiting values, when RSF approaches 95% for different vehicle operating conditions. The rollover limits in terms of lateral accelerations of the tractor (a_{y1}) and the semi-trailer (a_{y2}), and steer-velocity factor (SVF) reveal strong dependence upon c.g. height of the semi-trailer. The three rollover limits are considerably reduced by increase of the c.g. height, as illustrated in Figure 5.4. The roll angle limits of the semi-trailer axles (φ_{u4} , φ_{u5}), however, are insensitive to the c.g. height, as shown in Figure 5.5. The roll angle threshold of the semi-trailer slightly decreases as the semi-trailer c.g. height increases. The effects of payload variation on rollover limits of different indicators are illustrated in Figures 5.6 and 5.7. Compared to nominal load condition, reduced payload (70% nominal load) tends to slightly increase lateral acceleration rollover limits and SVF . Roll angle limits of unsprung masses (φ_{u4} , φ_{u5}) and sprung mass (φ_{s2}), however, are significantly reduced when the vehicle carries only 70% of its nominal load. The effects of maneuvers on rollover limits of different indicators are represented in Figures 5.8 and 5.9. The steering velocity factor is maneuver-dependent. The limit value of the steering factor is much higher in the sinusoidal steering maneuver than in the steady turning maneuver, while other factors (a_{y1} , a_{y2} , φ_{s2} , φ_{u4} and φ_{u5}) are relatively insensitive to different maneuvers.

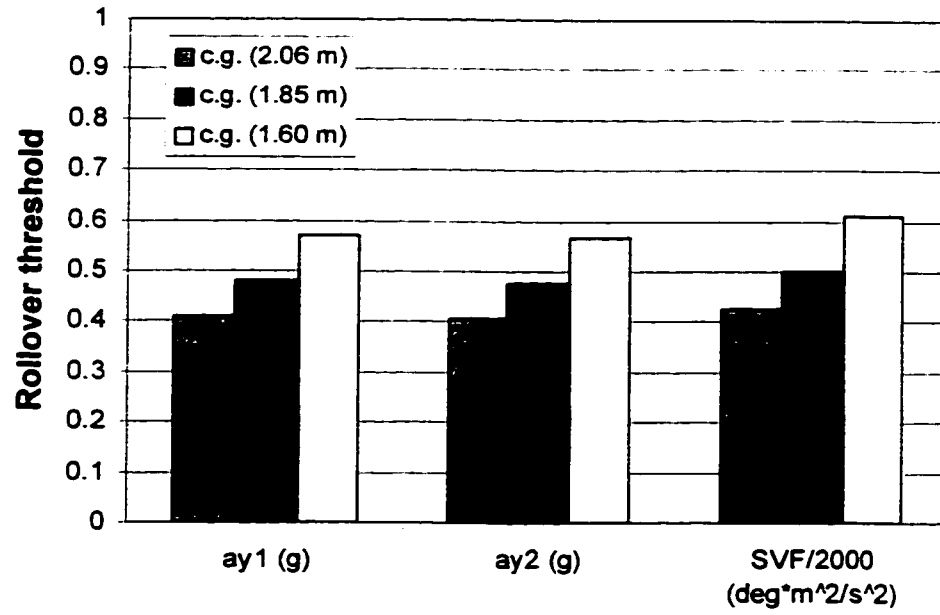


Figure 5.4: Effects of semi-trailer c.g. height on rollover threshold of a_{y1} , a_{y2} and SVF .

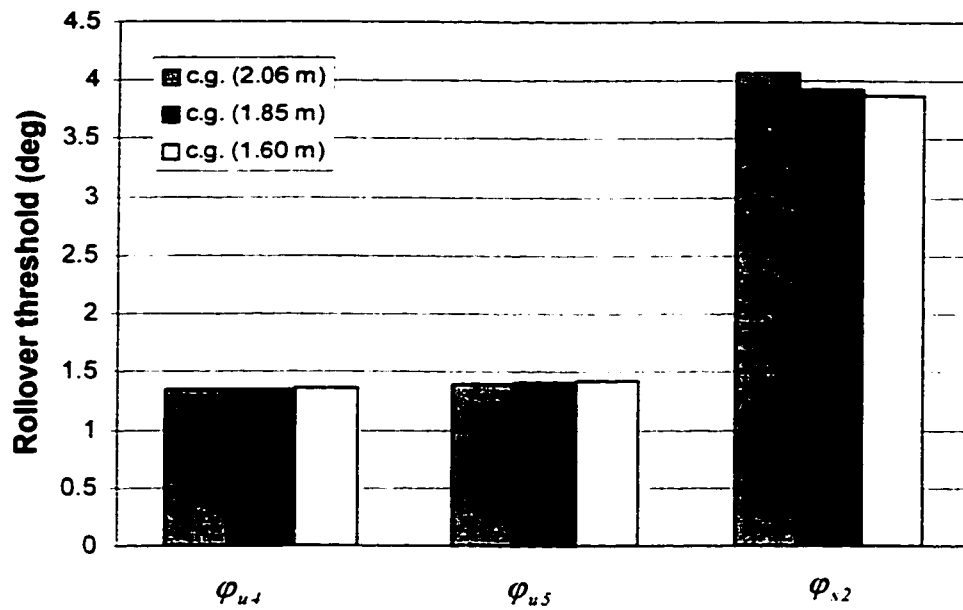


Figure 5.5: Effects of semi-trailer c.g. height on rollover threshold of φ_{u4} , φ_{u5} and φ_{s2} .

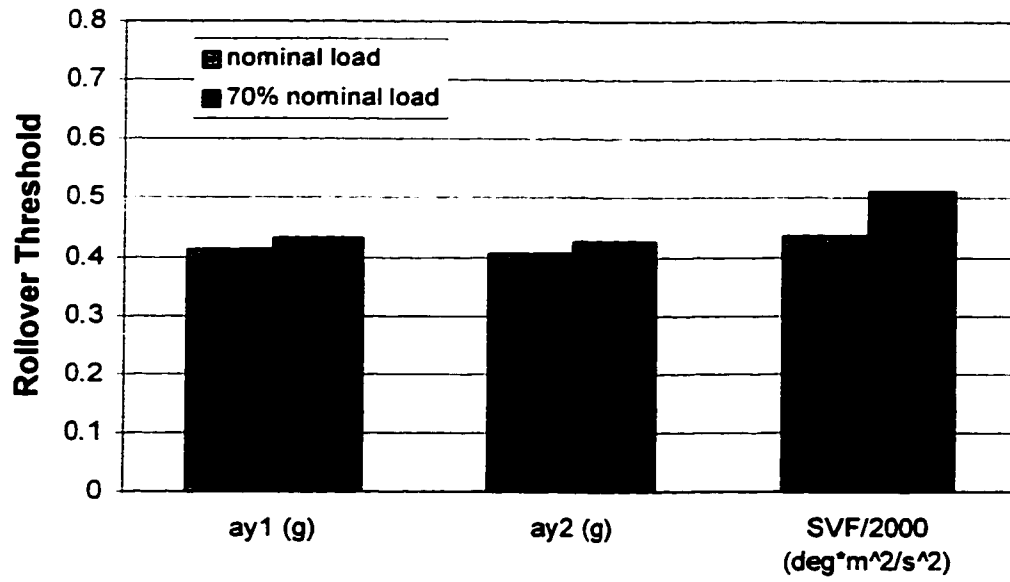


Figure 5.6: Effects of payload variation on rollover threshold of a_{y1} , a_{y2} and SVF .

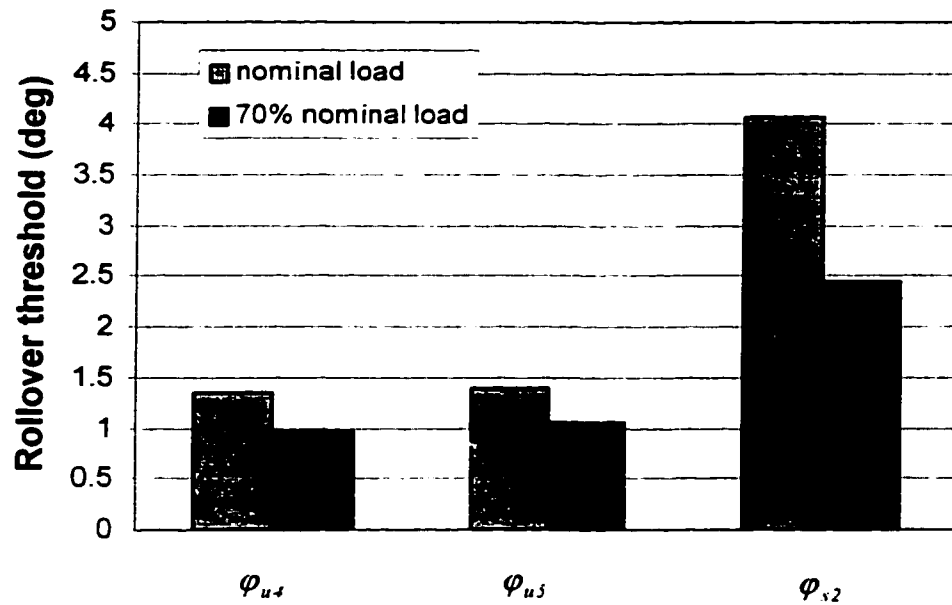


Figure 5.7: Effects of payload variation on rollover threshold of φ_{u4} , φ_{u5} and φ_{s2} .

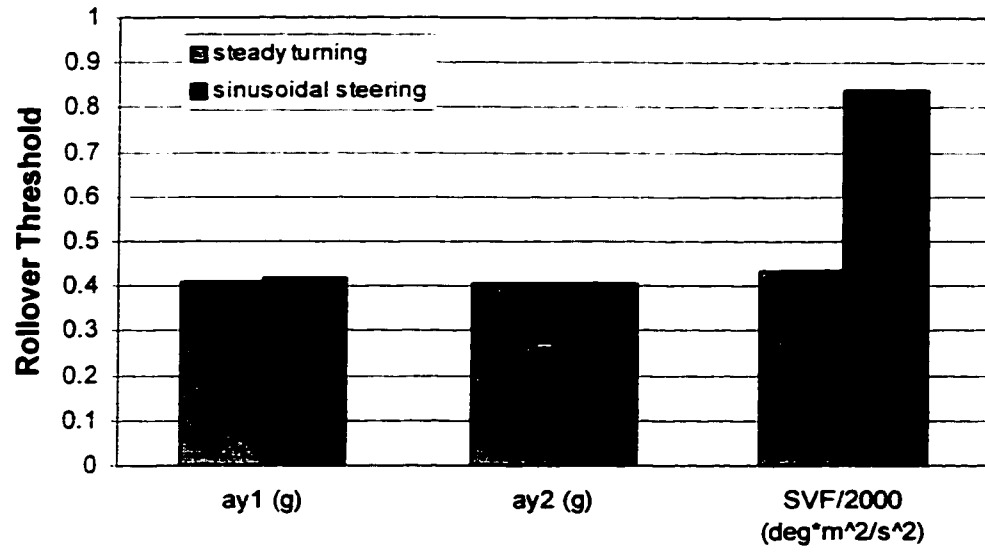


Figure 5.8: Effects of different maneuvers on rollover threshold of a_{y1} , a_{y2} and SVF .

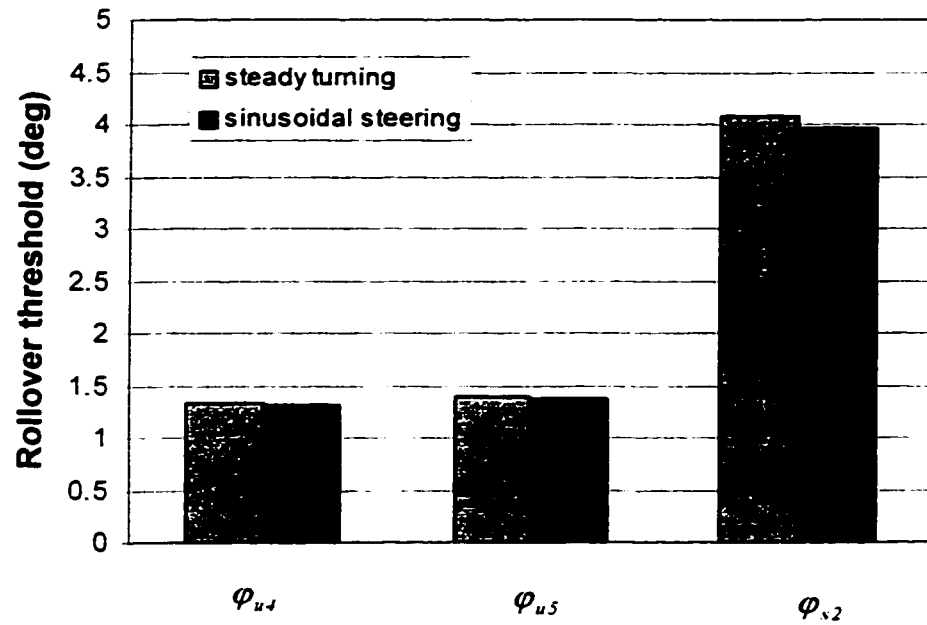


Figure 5.9: Effects of different maneuvers on rollover threshold of φ_{u4} , φ_{u5} and φ_{s2} .

5.5 EARLY WARNING EVALUATION OF ROLLOVER INDICATORS

Early warning to the driver about impending roll instability of heavy vehicles is vital for the driver to undertake corrective maneuvers so as to avert the occurrence of a potential rollover. Thus a good rollover indicator should be not only measurable and reliable but also capable of giving an early warning. Since the roll safety factor is the most reliable rollover indicator regardless of vehicle configurations and operational conditions, other indicators are further analyzed in the time domain in terms of correlation coefficient and time delay in comparison with the *RSF*.

Figure 5.10 illustrates sample rollover indicators in the time domain as the vehicle is subjected to a sinusoidal steering maneuver. It is revealed that there exist phase shifts among these signals. The steering factor is ahead of the roll safety factor by about 0.7 s, followed by tractor lateral acceleration which is ahead of *RSF* by nearly 0.4 s. Thus these signals have a capability of providing an early warning if they are well correlated with *RSF*. The correlation coefficient and time delay characteristics of an array of rollover indicators are illustrated in Table 5.7, when the vehicle is subjected to a sinusoidal steering maneuver. The results further include the effects of different vehicle forward velocity and steering frequency. It is revealed that all the indicators except for the steering factor demonstrate high correlation with *RSF* if the phase shift in the time domain is compensated. The steering factor provides the largest time margin: 0.43s to 0.87s ahead of *RSF*, with small penalty of correlation coefficient. The smaller the steering frequency, the longer time delay between steering factor and *RSF*. The higher vehicle speed also generates larger time delay. The tractor lateral acceleration, however, provides a time margin between 0.37 s to 0.40 s, which is less sensitive to vehicle speed and steering

frequency. The first axle roll angle response is ahead of *RSF* by 0.23 s to 0.28 s. Other indicators are approximately in-phase with *RSF*, and thus cannot provide an early warning of impending rollover.

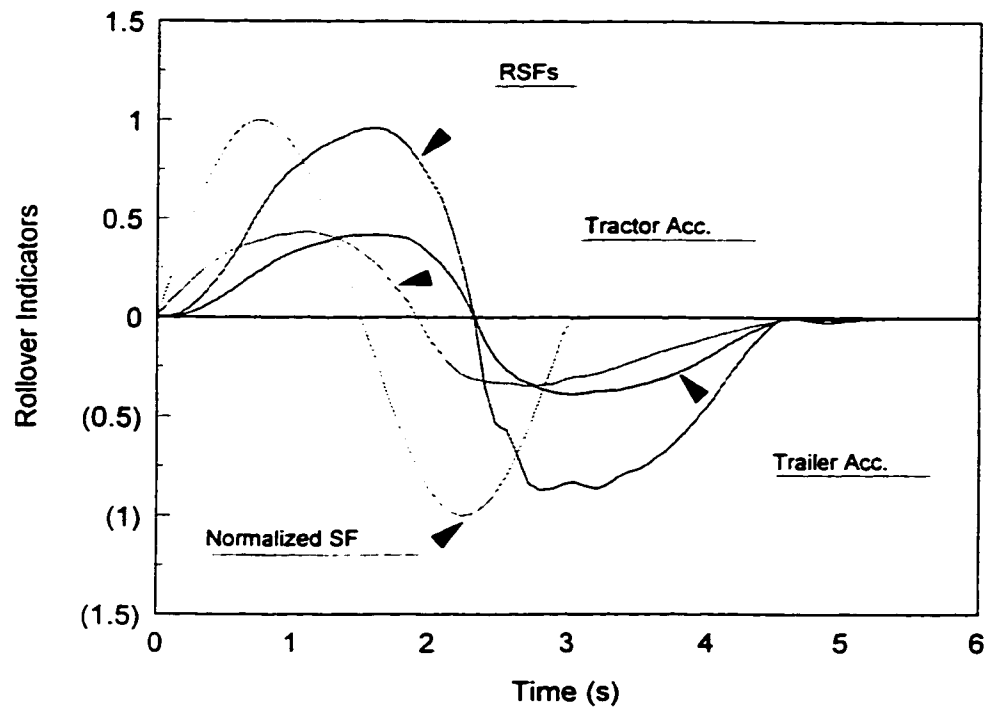


Figure 5.10: Rollover indicators in the time domain during a sinusoidal steering maneuver.

Table 5.7: Correlation coefficient and time delay between *RSF* and various rollover indicators.

Indicators		v=65 km/h			v=80 km/h		
		f=0.25 Hz	f=0.33 Hz	f=0.5 Hz	f=0.25 Hz	f=0.33 Hz	f=0.5 Hz
<i>RSF</i>	correl coef.	1.0	1.0	1.0	1.0	1.0	1.0
	time delay (s)	0	0	0	0	0	0
a_{y1}	correl coef.	0.994	0.992	0.986	0.985	0.993	0.987
	time delay (s)	-0.40	-0.38	-0.37	-0.40	-0.39	-0.39
a_{y2}	correl coef.	0.998	0.998	0.998	0.997	0.998	0.997
	time delay (s)	0.01	0.01	0.01	0.02	0.01	0.01
φ_{s1}	correl coef.	0.997	0.997	0.996	0.995	0.997	0.996
	time delay (s)	0.01	0.01	0.01	0.01	0.01	0.01
φ_{s2}	correl coef.	0.996	0.996	0.995	0.995	0.997	0.996
	time delay (s)	0.03	0.03	0.03	0.03	0.03	0.03
φ_{u1}	correl coef.	0.996	0.995	0.991	0.994	0.994	0.993
	time delay (s)	-0.28	-0.27	-0.26	-0.23	-0.26	-0.26
φ_{u2}	correl coef.	0.997	0.997	0.996	0.997	0.997	0.996
	time delay (s)	-0.01	-0.01	-0.01	-0.02	-0.02	-0.02
φ_{u3}	correl coef.	0.998	0.997	0.997	0.986	0.997	0.997
	time delay (s)	-0.04	-0.04	-0.03	-0.03	-0.04	-0.03
φ_{u4}	correl coef.	0.998	0.998	0.997	0.967	0.999	0.997
	time delay (s)	0.03	0.02	0.02	0.03	0.03	0.03
φ_{u5}	correl coef.	0.998	0.997	0.997	0.968	0.998	0.997
	time delay (s)	0.03	0.03	0.02	0.03	0.03	0.03
<i>SVF</i>	correl coef.	0.984	0.980	0.973	0.946	0.946	0.943
	time delay (s)	-0.56	-0.50	-0.43	-0.87	-0.71	-0.54

5.6 FEASIBILITY OF ROLLOVER EARLY WARNING DEVICE

The above analysis reveals that no single measure will serve as an appropriate indicator of impending dynamic rollover in terms of measurability, reliability and time margin for corrective maneuvers. While the rollover safety factor is the most reliable impending rollover indicator regardless of the vehicle payload, cg height and maneuvers, the evaluation of the *RSF* necessitates on-line measurement of wheel loads, which is considered to be more difficult than measurement of other response parameters such as lateral accelerations. Furthermore the *RSF* does not have the capability to provide an early

warning of impending rollover. All other indicators are considered as less reliable measures since their limits depend on vehicle design and/or operating conditions.

If all the necessary information about vehicle design and vehicle operating conditions, however, is known, the indicators other than *RSF* can be reliably employed to detect onset of roll instability of the vehicle. Thus the onset of vehicle rollover can be detected via monitoring roll angles of tractor rear and trailer axles, provided wheel track, axle load, and tire elastic property for each axle are known. The measurement of axle load in this case may not be as complex as that in *RSF*, since static measurement of axle load is acceptable. To employ trailer lateral acceleration or roll angle as a rollover indicator, further information such as the c.g height and axle roll stiffness, as a minimum, must be provided. However the c.g height is normally quite difficult to measure.

The steering factor and tractor lateral acceleration provide good “preview” time of a potential impending rollover for the driver to undertake corrective maneuvers. The information can be used to generate an early warning of impending roll instability. Since the steering factor is very sensitive to vehicle maneuvers, the tractor lateral acceleration is considered to be more suitable as an early warning indicator.

In view of the difficulties in finding a single satisfactory impending rollover indicator with desirable measurability, reliability and available time margin for corrective maneuvers, certain combinations of several indicators may be considered. Three different designs of a rollover early warning device based upon manipulation of different indicators are proposed in Table 5.8. Neural network algorithms can be conveniently employed to perform the necessary manipulations. The first design adopts the rollover safety factor as the impending roll instability indicator, combined with the signal of tractor lateral

acceleration for early warning generation. This design involves complex and costly on-line measurement of the dynamic wheel loads. However, possibility exists to modify the current on-board weigh scale systems to perform the additional function of on-line evaluation of the *RSF* with a relatively small incremental cost [95]. The second approach uses unsprung mass roll angles as a rollover indicator, which necessitates the predetermination of axle loads. The third design, based upon lateral accelerations of the tractor and semi-trailer, can be used in special application vehicles such as tank trucks operating at a few specific loading conditions where the c.g height can be easily estimated. Such a design offers a reliable and least expensive option for realizing an early warning device. The reliability of this design, however, will depend upon the degree of accuracy of the estimated c.g. height.

Table 5.8: Proposal of a rollover early warning device.

	Rollover Indicator	Early Warning Signal	Minimum Parameters	Remarks
Design #1	Roll safety factor	Tractor lateral acceleration	① tractor lateral acceleration; ② dynamic wheel load	Costly
Design #2	Axle roll angle	Tractor lateral acceleration	① tractor lateral acceleration; ② axle roll angle; ③ axle load; ④ wheel track	Involves static axle load measurement
Design #3	Trailer lateral acceleration	Tractor lateral acceleration	① tractor lateral acceleration, ② trailer lateral acceleration; ③ cg height; ④ wheel track	Difficult to measure cg height

5.7 SUMMARY

Potential rollover indicators are identified through simplified analysis of a lumped roll plane model, and classified into six groups. The potential rollover indicators are assessed in terms of their measurability, reliability, and the lead time available for driver's action. Measurability analysis is performed in terms of easiness of measurement and

subsequent costs. Reliability analysis of potential rollover indicators is carried out in terms of estimation errors due to uncertainty of dependent parameters and correlation characteristics with roll safety factor (*RSF*). Parametric sensitivity analyses are conducted to study sensitivity of the indicators to variations in operating conditions.

It is concluded that *RSF* has poor measurability but high reliability, while steer velocity factor (*SVF*) has good measurability and large time margin for early warning but poor reliability. Unsprung mass roll angles demonstrate good linear correlation with *RSF*, and are relatively insensitive to vehicle c.g. height and maneuvers performed. The threshold values of unsprung mass roll angles, however, are very sensitive to vehicle load conditions. Lateral acceleration response of the semi-trailer of a 5-axle tractor semi-trailer combination correlates very well with the *RSF*, while its threshold value is strongly dependent upon vehicle c.g. height. Sprung mass roll angles are the same as the lateral acceleration of the semi-trailer in terms of reliability. Lateral acceleration response of the tractor of the combination demonstrates good capacity for early warning generation of impending rollover in directional maneuvers, but poor linear correlation with *RSF*. How early the warning should be generated to the driver is addressed in the next chapter.

CHAPTER 6

EFFECTIVENESS ANALYSIS OF IMPENDING ROLLOVER INDICATORS FOR OPEN-LOOP ROLLOVER CONTROL

6.1 INTRODUCTION

The drivers of heavy vehicles often remain unaware of the impending roll instability, which is mostly initialized at the rearmost axles. The potential vehicle rollovers may be evaded through timely detection of an impending instability and by providing an early warning to the drivers. The development of such a rollover prevention mechanism necessitates identification of reliable indicators of impending rollover. From the dynamic roll analysis of vehicle combinations, presented in chapter 5, it was established that a set of rollover indicators based on measurability, reliability and lead time may be identified towards an early warning rollover prevention device, such that the driver can be warned to undertake corrective maneuvers to avert the occurrence of a potential roll instability. Such a rollover prevention system, in its simplest form, can be considered as an open-loop rollover control, as illustrated in Figure 6.1. The warning signals are generated for the driver via monitoring and interpreting the key vehicle motion parameters related to onset of a roll instability. Upon receiving the warning signal, the driver may perform the braking and/or steering actions to avert the potential roll instability. The warning signal, however, must be generated to provide sufficient lead time for the driver's actions.

The results presented in chapter 5 revealed that the impending rollover of a heavy vehicle can be detected via monitoring the roll angles of sprung and unsprung masses, lateral accelerations, the steering factor (δ, v^2) and the roll safety factor (RSF). The

reliability analyses of the potential indicators further showed that the *RSF* is most reliable impending rollover indicator, irrespective of the vehicle configurations, while the other indicators are relatively sensitive to variations in vehicle design parameters and operational conditions. The assessment of early warning based upon the rollover indicators, performed using the dynamic yaw/roll model, further revealed that the steering factor and tractor lateral acceleration of a tractor-semitrailer combination can provide good preview time for a potential impending rollover, while a unity value of *RSF* indicates a near occurrence of vehicle rollover. The *RSF*, however, can be effectively employed to generate an early warning of a potential impending rollover, by selecting its threshold value to be less than unity.

It is further recognized that a warning signal for an impending rollover should be generated early enough such that the driver can perform a corrective maneuver in appropriate time. The corrective maneuver that the driver can perform, in most cases, is limited to application of braking and/or variations in steering to avert the development of roll instability. There exists time delay between the moment when the warning is sent to the driver and the moment when braking force is established on road wheels. The vehicle may approach its roll instability condition, in the event that the lead time provided by the warning signal is inadequate to develop braking forces. The feasibility and effectiveness of a roll instability early warning device thus depend on: (i) the lead-time provided by the warning signal, and (ii) the ability of impending rollover indicators to provide such a early warning. The effectiveness of an early warning should be investigated through directional dynamic response of the vehicle under application of braking and/or steering inputs.

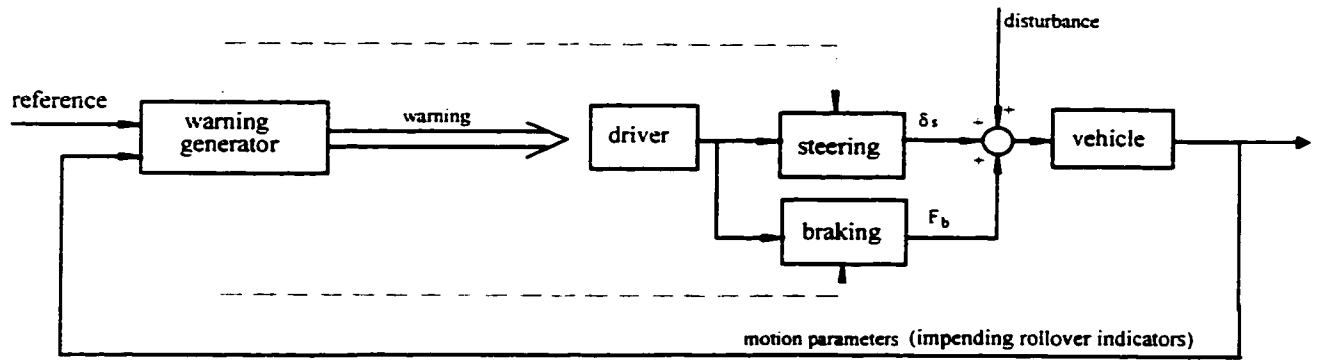


Figure 6.1 Schematic diagram of an open-loop rollover control.

A three-dimensional directional dynamic model of heavy vehicle combinations, incorporating braking dynamics, is thus developed to investigate the feasibility of an open-loop roll instability control. A comprehensive steering system model incorporating steering system compliance, roll steer, bump steer, ackerman steer and wrap steer is further developed and integrated into the vehicle model. The nonlinear cornering and braking forces and moments due to the tires are derived using the magic formula tire model [103]. An *ABS* algorithm is also incorporated to enhance the braking efficiency of the vehicle. The rollover indicators are investigated for their effectiveness for open-loop roll stability control in various maneuvers, road conditions and braking efforts.

6.2 THREE-DIMENSIONAL VEHICLE MODEL

The yaw/roll model described in chapter 4 is based on the assumption of constant vehicle forward speed, and can not be used to predict the dynamic characteristics and roll stability of heavy vehicles in response to steering and braking inputs. A comprehensive three-dimensional vehicle model incorporating vehicle longitudinal motion is therefore

developed for the study. The sprung mass of the straight truck or the tractor is characterized as a rigid body with six *DOF* (longitudinal, lateral, vertical, roll, pitch and yaw) motions. Each unsprung mass is treated as a beam axle with two *DOF* (roll and bounce) with respect to the sprung mass on which the unsprung mass is attached. For a tractor semi-trailer combination, the hitch connection between the lead and towed units is modeled kinematically as a ball joint, which has three-rotational degrees of freedom [92]. A schematic of the model for a tractor semi-trailer combination is shown in Figure 6.2. The trailing unit sprung mass (body S_2) is attached to the leading unit sprung mass (body S_1) via the ball joint. The origin of the reference frame for S_2 is defined at the hitch point. S_2 thus has three rotational *DOF* relative to S_1 . For the fifth wheel connection, the roll motion of S_2 about the hitch is retarded by a torsional spring. A three-axle straight truck can be represented by a 12-*DOF* vehicle system, while a five-axle tractor semi-trailer is represented by a 19 degrees-of-freedom dynamical system.

6.2.1 Equations of Motion

Equations of motion for the three-dimensional vehicle model described above can be easily derived after assigning proper body-centered coordinate systems. Figure 6.2 illustrates motion parameters and the assigned coordinate system for a five-axle tractor semi-trailer combination. The coordinate system for the tractor body is attached to the center of gravity of the tractor sprung mass. The six motion variables for the tractor sprung mass are represented by three translational variables: u_{s1} , v_{s1} , w_{s1} ; and three rotational velocities: p_{s1} , q_{s1} , r_{s1} . The coordinate system for the semi-trailer is attached to the fifth wheel and its motion variables are represented by three rotational velocities:

p_{s2} , q_{s2} , r_{s2} . The coordinate systems for unsprung masses are located at the center of each axle. The equations of motion, derived from the force and moments equilibrium, are described below.

Equations of Motion for Tractor Sprung Mass

$$\begin{aligned}
\text{longitudinal motion: } & m_{s1} \dot{u}_{s1} - m_{s1} (r_{s1} v_{s1} - q_{s1} w_{s1}) = \sum X_{s1} \\
\text{lateral motion: } & m_{s1} \dot{v}_{s1} - m_{s1} (p_{s1} w_{s1} - r_{s1} u_{s1}) = \sum Y_{s1} \\
\text{vertical motion: } & m_{s1} \dot{w}_{s1} - m_{s1} (q_{s1} u_{s1} - p_{s1} v_{s1}) = \sum Z_{s1} \\
\text{roll motion: } & I_{xx1} \dot{p}_{s1} - (I_{yy1} - I_{zz1}) q_{s1} r_{s1} = \sum L_{s1} \\
\text{pitch motion: } & I_{yy1} \dot{q}_{s1} - (I_{zz1} - I_{xx1}) p_{s1} r_{s1} = \sum M_{s1} \\
\text{yaw motion: } & I_{zz1} \dot{r}_{s1} - (I_{xx1} - I_{yy1}) q_{s1} p_{s1} = \sum N_{s1}
\end{aligned} \tag{6.1}$$

where m_{s1} is the tractor sprung mass, and I_{xx1} , I_{yy1} and I_{zz1} are its mass moments of inertia about the three translational axes. The components on the right side of the equation set (6.1) are the total external forces and moments acting along the corresponding directions.

Equations of Motion for Semi-Trailer Sprung Mass

$$\begin{aligned}
\text{roll motion: } & I_{xx2} \dot{p}_{s2} - (I_{yy2} - I_{zz2}) q_{s2} r_{s2} = \sum L_{s2} \\
\text{pitch motion: } & I_{yy2} \dot{q}_{s2} - (I_{zz2} - I_{xx2}) p_{s2} r_{s2} = \sum M_{s2} \\
\text{yaw motion: } & I_{zz2} \dot{r}_{s2} - (I_{xx2} - I_{yy2}) q_{s2} p_{s2} = \sum N_{s2}
\end{aligned} \tag{6.2}$$

where I_{xx2} , I_{yy2} and I_{zz2} are the mass moments of inertia of the semi-trailer about the fifth wheel. $\sum L_{s2}$, $\sum M_{s2}$ and $\sum N_{s2}$ are external moments due to suspension forces and hitch roll stiffness.

Equations of Motion for Each Unsprung Mass j

$$\text{vertical motion: } \quad m_{uj} \dot{w}_{uj} = \sum Z_{uj}$$

$$\text{roll motion:} \quad I_{xx_j} \dot{p}_{uj} = \sum L_{uj} \quad (6.3)$$

where m_{uj} and I_{xx_j} are the unsprung mass and roll mass moment of inertia of axle j ($j=1, \dots, 5$). p_{uj} and w_{uj} are the roll rate and bounce velocity of the unsprung mass j . $\sum Z_{uj}$ and $\sum L_{uj}$ are the total external force and moment along the vertical and roll directions along the unsprung mass j . The external forces and moments in Equations (6.1) to (6.3) are due to suspensions, tires, compliance due to articulation, structure compliance etc. The modeling considerations for the suspension and tire forces are discussed in the following sub-sections.

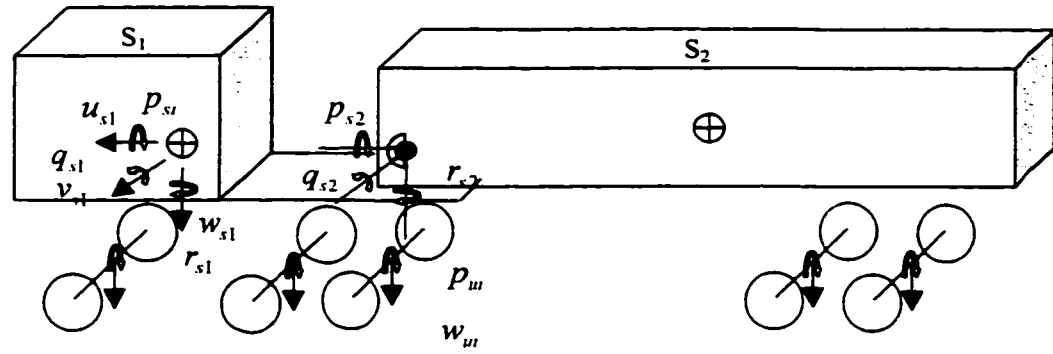


Figure 6.2: Schematic of *DOF* of a tractor semi-trailer combination.

6.2.2 Suspension forces

Leaf and air springs in conjunction with hydraulic dampers are most commonly employed in modern heavy vehicles. The sprung and unsprung masses are subjected to forces and moments due to suspension springs, hydraulic dampers, and auxiliary roll stiffness. The spring force developed by a leaf or air spring is derived using the iterative

algorithm, and the lower and upper envelope force (F_{Ei}) curves, as described in Equation (4.56):

$$F_i = F_{Ei} + (F_{i-1} - F_{Ei})e^{-|4-4_{-i}| \lambda} \quad (6.4)$$

The computation of vertical force from the above equation requires description of: (i) upper and lower force limits either through a polynomial or tabular function; and (ii) a characteristic deflection constant λ . Due to strong nonlinearity, integration time step should be adjusted to a new smaller step if the calculated forces are not stable. Test values of deflection that are in error should not be used as the reference “old” values in the spring model.

Although leaf springs provide considerable energy dissipation due to hysteresis, additional hydraulic dampers may be employed to enhance the ride and road load performance. In such a case, the hydraulic dampers are modeled assuming linear damping characteristics. The roll stiffness due to anti-sway bars and linkages is represented by auxiliary roll stiffness between the sprung and unsprung masses for each axle. Total suspension roll stiffness can be measured on a suspension rig. The auxiliary roll stiffness is determined by subtracting the total measured axle roll stiffness by that due to the vertical springs at their spacing. Auxiliary roll stiffness may be negative if the frame has considerable compliance in twist.

6.2.3 Modeling of Tires

Vehicle motions are primarily caused by forces and moments developed at the tire-road interface. These forces arise from powertrain, braking, and steering inputs, and directly influence the handling and braking performance of the vehicle. The braking and

cornering forces, developed by a pneumatic tire, are strong nonlinear function of normal load, road surface characteristics, side-slip, longitudinal deformation slip, etc. A large number of empirical and analytical models have been developed and reported in the literature [103-106]. Tire models, reported in the literature, in general, can be grouped into two categories: physical models and black box models [103]. In physical models, the tire forces and moments are derived from a mathematical description of the tire structure and its deformation mechanisms. Such tire models, however, are usually not employed in dynamic analysis of vehicles due to their complexity and poor computational efficiency. Black box models, on the other hand, are derived directly from the experimental data, and can be easily incorporated into directional dynamic model of vehicles. The inputs to the black box models are usually tire vertical load, lateral and longitudinal slip ratios, and camber angle, derived from vehicle response parameters, while the outputs of the black box models are tire forces and moments [106].

The tire forces and moments developed at the contact patch are represented by longitudinal traction/braking force (F_x), lateral cornering force (F_y), vertical force (F_z), aligning moment (M_z), overturning moment (M_x) and rolling resistance moment (M_y), as shown in Figure 6.3. The pneumatic tires exhibit nearly linear force-deflection characteristics in the vicinity of the operating point with considerably low dissipative force component. The vertical force F_z is determined by considering the tire as a linear spring model, and expressed as:

$$F_u = \begin{cases} k_u \Delta_u + c_u \dot{\Delta}_u ; & \Delta_u \geq 0 \\ 0 & ; \Delta_u < 0 \end{cases} \quad (6.5)$$

where Δ_u and $\dot{\Delta}_u$ are the vertical deflection and velocity of the tire, respectively. While the overturning and rolling resistance moments (M_x and M_y) have only insignificant influence on directional dynamics of vehicles, the braking/traction and cornering forces (F_x and F_y), and aligning moment (M_z) affect the directional performance most significantly. The computation of F_x , F_y and M_z due to a pneumatic tire under simultaneous application of braking and steering, however, is known to be extremely complex due to nonlinear behavior of the tire. Pacejka [106] proposed semi-empirical relationships referred to as the 'magic formula' to describe the traction/braking and cornering characteristics of tires. The formula has been extensively used to characterize the properties of heavy vehicle tires.

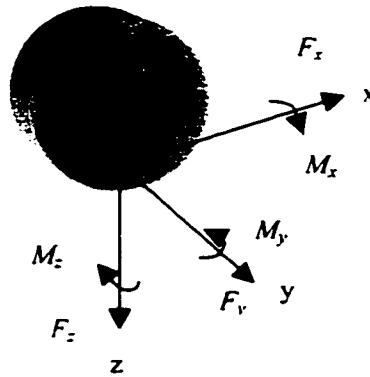


Figure 6.3: A schematic representation of tire forces and moments at the contact patch.

The magic formula yields an output variable $Y(x)$ which may be F_x , F_y or M_z in the following form [107]:

$$Y(x) = D \sin\{C \arctan[B(x + S_h) - E_x[B(x + S_h) - \arctan(B(x + S_h))]]\} + S_v \quad (6.6)$$

where S_h and S_v are referred to as the horizontal and vertical shifts, respectively. x represents input variable such as slip angle (α) or longitudinal slip ratio (κ). B , C , D and E are constants identified from the measured data, and referred to as stiffness factor, shape factor, peak value, and curvature factor, respectively. The application of magic formula under the application of braking and/or steering yields expressions for F_x , F_y and M_z .

Longitudinal Force (pure longitudinal slip)

The longitudinal force developed by the tire in the absence of cornering ($\alpha = 0$), can thus be derived as:

$$F_{x0} = D_x \sin\{C_x \arctan[B_x \kappa_x - E_x[B_x \kappa_x - \arctan(B_x \kappa_x)]]\} + S_{vx} \quad (6.7)$$

where κ_x is the input variable, derived from longitudinal slip ratio (κ) and horizontal shift S_{hx} : $\kappa_x = \kappa + S_{hx}$. The horizontal and vertical shift factors (S_{hx} , S_{vx}) together with B_x , C_x , D_x and E_x are functions of normal load F_z .

Lateral Force and Aligning Moment (pure lateral slip)

The lateral force F_{y0} and aligning moment M_{z0} developed by the pneumatic tire in the absence of traction/braking force ($\kappa = 0$), can be derived from:

$$F_{y0} = D_y \sin\{C_y \arctan[B_y \alpha_y - E_y[B_y \alpha_y - \arctan(B_y \alpha_y)]]\} + S_{vy} \quad (6.8)$$

$$M_{z0} = D_t \sin\{C_t \arctan[B_t \alpha_t - E_t[B_t \alpha_t - \arctan(B_t \alpha_t)]]\} + S_{vt} \quad (6.9)$$

where α_y and α_l are input parameters, derived from side slip angle α and horizontal shifts S_{hy} and S_{hl} : $\alpha_y = \alpha + S_{hy}$, $\alpha_l = \alpha + S_{hl}$. All other parameters are expressed in function of side slip angle (α), normal load (F_z) and camber angle γ .

Combined Cornering and Braking Forces and Moments

The longitudinal and lateral forces and moments developed by the tire under simultaneous application of braking and steering inputs can also be derived based on Equation (6.6), when the measured forces and moments for combined longitudinal and lateral slips are available. The measurement of tire forces and moments in combined braking and steering maneuvers, however, is very intricate. Alternatively, forces from pure longitudinal and lateral slips can be manipulated to derive the forces in the combined braking and steering maneuvers [106]. The similarity method based on the observation that the pure slip curves remain approximately similar in shape when the tire runs at road conditions different from the reference conditions (or tire test conditions), is also employed to derive the tire forces and moments on different road friction conditions.

The total theoretical slip σ_t can be expressed in terms of longitudinal and lateral slips as [92]:

$$\sigma_t = \sqrt{\sigma_x^2 + \sigma_y^2} \quad (6.10)$$

where

$$\sigma_x = -\frac{\kappa}{l + \kappa} \quad \text{and} \quad \sigma_y = -\frac{l \tan \alpha}{l + \kappa} \quad (6.11)$$

The theoretical slip is normalized by peak slip values, $\sigma_{x \max}$, $\sigma_{y \max}$, which yields peak forces F_{x0} and F_{y0} . The resultant normalized slip σ_i^* is then expressed using the friction ellipse concept:

$$\sigma_i^* = \sqrt{\sigma_x^{*2} + \sigma_y^{*2}} \quad (6.12)$$

where σ_x^* and σ_y^* are normalized slip ratios, given by:

$$\sigma_x^* = \frac{\sigma_x}{\sigma_{x \max}}; \quad \sigma_y^* = \frac{\sigma_y}{\sigma_{y \max}} \quad (6.13)$$

The equivalent longitudinal and lateral slips (κ' and α') are derived from the normalized total theoretical slip, and expressed as:

$$\kappa' = \frac{\sigma_i^* \sigma_{x \max} \text{sign}(\sigma_x)}{1 + \sigma_i^* \sigma_{x \max} \text{sign}(\sigma_x)} \frac{\mu_0}{\mu} \quad (6.14)$$

$$\alpha' = \arctan[\sigma_i^* \sigma_{y \max} \text{sign}(\sigma_y)] \frac{\mu_0}{\mu} \quad (6.15)$$

where μ_0 is the friction coefficient of the reference road on which tire forces and moments characteristics are measured, and μ is the friction coefficient of the road surface considered. Upon substituting for κ' and α' into Equations (6.7) and (6.8), the equivalent forces are obtained as functions of normal load and equivalent slips, as:

$$F_{x0} = F_{x0}(F_z, \kappa') \quad \text{and} \quad F_{y0} = F_{y0}(F_z, \alpha', \gamma) \quad (6.16)$$

The lateral and longitudinal forces developed by tires may approach their respective saturation limits corresponding to large slips. The saturation levels for F_{x0} and F_{y0} may differ considerably. The expressions for the forces are modified to account for the anisotropic property:

$$F_{x0}^* = F_{x0} - \varepsilon(F_{x0} - F_{y0}) \left(\frac{\sigma_y^*}{\sigma_t^*} \right)^2 \quad (6.17)$$

$$F_{y0}^* = F_{y0} - \varepsilon(F_{y0} - F_{x0}) \left(\frac{\sigma_x^*}{\sigma_t^*} \right)^2 \quad (6.18)$$

where F_{x0}^* and F_{y0}^* are modified longitudinal and lateral forces, respectively, incorporating the respective saturation limits. ε assumes a value of normalized resultant slip, when $\sigma_t^* \leq 1$, and a unity value for $\sigma_t^* > 1$. The longitudinal and lateral tire forces, and aligning moment due to a pneumatic tire subject to combined braking and steering maneuvers are then derived as follows:

$$F_x = \frac{\mu}{\mu_0} F_{x0}^* \frac{\sigma_x}{\sigma_t} \quad (6.19)$$

$$F_y = \frac{\mu}{\mu_0} F_{y0}^* \frac{\sigma_y}{\sigma_t} \quad (6.20)$$

$$M_z = M_{z0}(F_z, \alpha', \gamma) \frac{|F_y|}{F_{y0}} \quad (6.21)$$

The validity of the magic formula is examined by computing the forces and moment, derived from Equations (6.7) to (6.9), with the raw data obtained through measurements. The results of the magic formula modeling for a heavy truck tire are illustrated in Figures 6.4 to 6.6. The longitudinal force F_{x0} in the absence of steering input is globally fitted in terms of longitudinal slip ratio (κ) and tire vertical load (F_z), while the cornering force F_{y0} and aligning moment M_{z0} in the absence of traction/braking force ($\kappa=0$) are represented in terms of side-slip angle (α), camber angle (γ) and tire

vertical load (F_z). The results reveal that the measured forces are closely modeled by the magic formula.

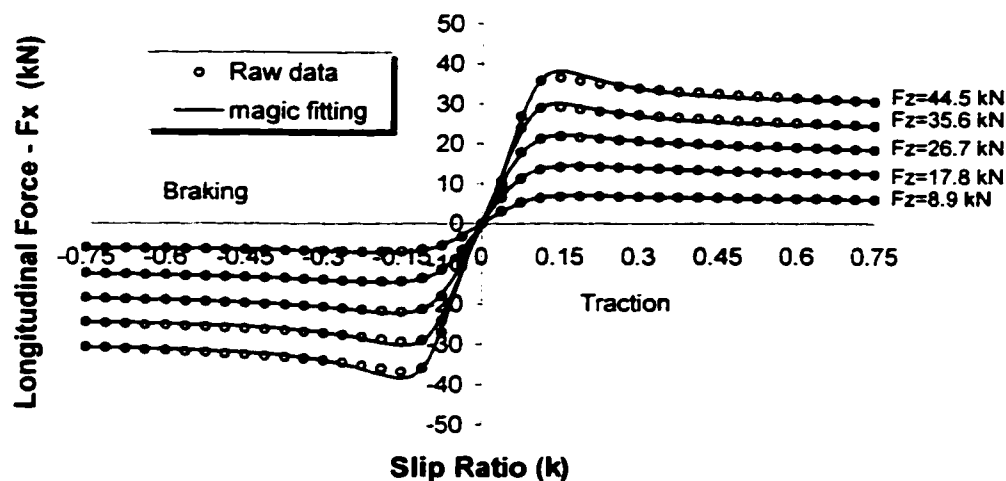


Figure 6.4: Magic formula simulation of longitudinal force of a truck tire as a function of slip ratio for five different loads.

Tire Relaxation

The magic formula and the measurements, in general, provide the forces and moment under steady state conditions. The tire forces, however, are developed in a transient manner with considerable time delay and consequently the distance delay due to tire rolling [108]. The phenomenon is typically characterized by tire relaxation lengths. A method described in [109] is used to account for the lag in tire response. In this method, the lag is introduced into the side slip angle which yields the lagged side force and aligning moment. The lateral slip angle α is defined as the arc tangent of an auxiliary state variable η , which is derived from a first-order differential equation.

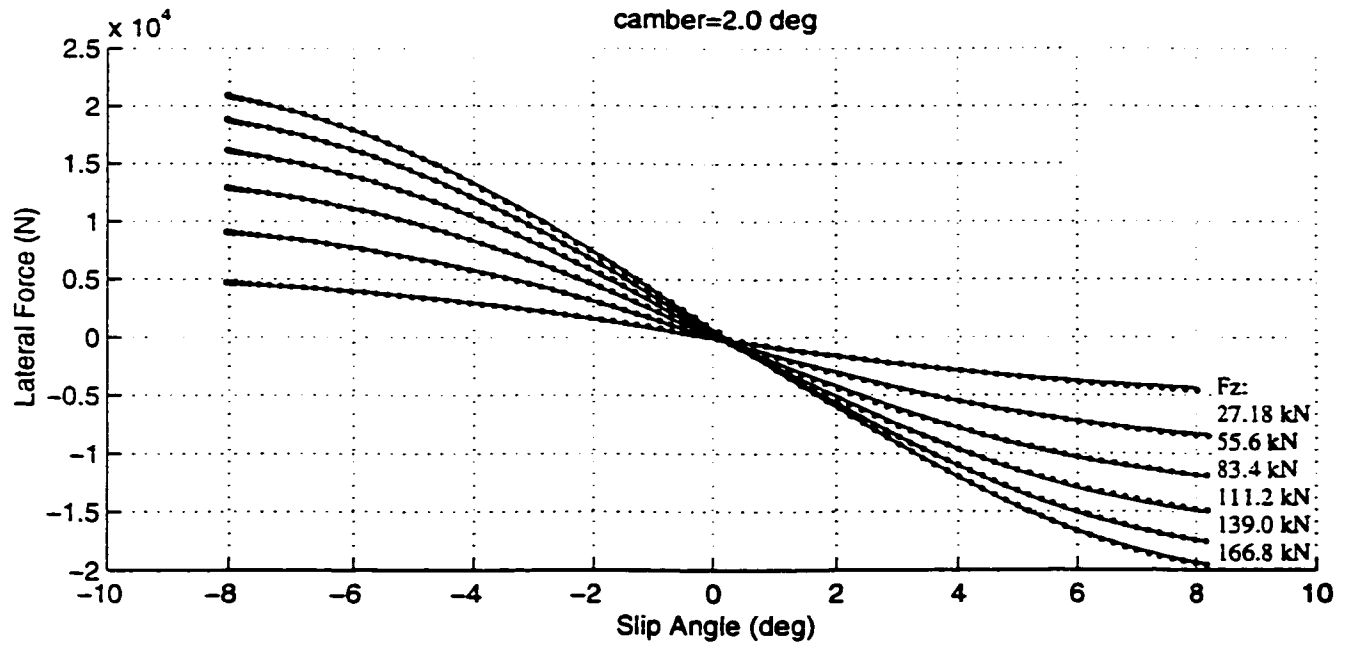


Figure 6.5: Magic formula simulation of lateral force of a truck tire as a function of side-slip angle for six different loads.

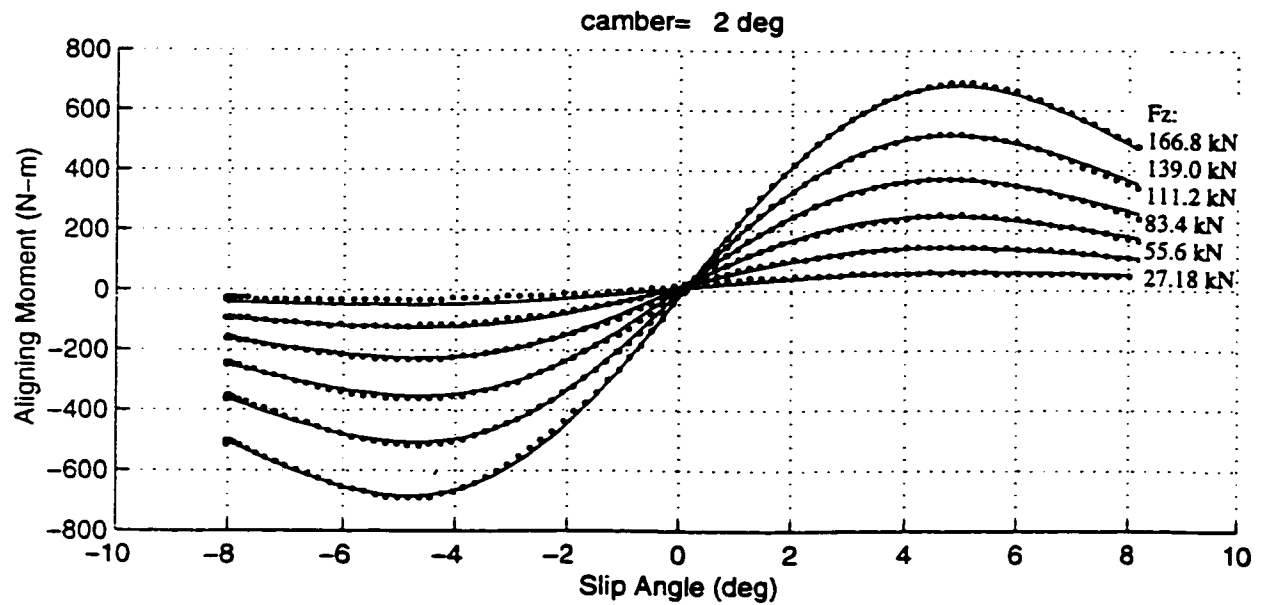


Figure 6.6: Magic formula simulation of aligning torque of a truck tire as a function of side-slip angle for six different loads.

$$\alpha = \arctan(\eta) \quad (6.22)$$

$$\frac{d\eta}{dt} = \frac{l}{L_r} (V_{ty} - |V_{tx}| \eta) \quad (6.23)$$

where L_r is the tire relaxation length, and V_{tx} and V_{ty} are tire lateral and longitudinal speeds, respectively.

ABS Braking

As discussed earlier, the driver's action to control the roll behavior of the vehicle is limited to application of braking and steering, when onset of vehicle rollover is detected. The effectiveness of the onset of rollover detection and driver's actions for control of rollover can be analyzed from analysis of directional response of the vehicle under application of steering and braking. Applications of sudden and severe braking can cause lockup of certain wheels, which may lead to yaw instabilities. Most modern heavy vehicles, thus, employ anti-lock braking system (*ABS*) to minimize the potentials for wheel lockup, and ideally to keep the skid of the tire within a desired range. This will ensure that the tire can develop a sufficiently high braking force for stopping the vehicle, and at the same time to retain an adequate cornering force for directional control and stability. In order to account for *ABS* braking, the wheel spin velocity ω_w can be described with a differential equation as:

$$\dot{\omega}_w = \frac{M_{yBK} \text{sign}(\omega_w) + F_x (R_w - \Delta_l)}{I_w} \quad (6.24)$$

where R_w is the tire radius under static condition, and Δ_l is the dynamic deflection variation of the tire. M_{yBK} is the braking torque applied at the wheel, and I_w is the polar moment of inertia of the spinning wheel. The longitudinal slip ratio κ is defined as:

$$\kappa = \frac{\omega_w R_w - V_{ix}}{V_{ix}} \quad (6.25)$$

The *ABS* braking is modeled on the basis of instantaneous longitudinal slip ratio, using the following algorithm:

$$braking = \begin{cases} on & \text{if } \kappa < \kappa_{on} \\ off & \text{if } \kappa \geq \kappa_{off} \end{cases} \quad (6.26)$$

where κ_{on} and κ_{off} are threshold values of the longitudinal slip ratio κ . When the longitudinal slip ratio κ is greater than κ_{off} , the braking system is turned off. As the slip ratio drops to κ_{on} , the braking system is turned on again. The threshold values κ_{on} and κ_{off} are chosen to ensure the skid of the tire in a desired range. Most pneumatic tires demonstrate peak braking forces on hard surface somewhere between 0.15 to 0.30 slip. In this investigation, κ_{on} is set to 0.2, and κ_{off} is set to 0.3 to reflect a reasonable braking effort of an anti-lock braking system.

6.2.4 Steering System

The directional dynamics of the vehicle subject to braking and steering inputs is further related to the compliance of the steering system, and its roll, bump and wrap steer characteristics. Figure 6.7 illustrates a schematic of a truck steering system. The steering system compliance plays a very significant role in determining the relation between steering wheel angle and road wheel steer, which is represented by the compliance due to steering column (C_{SW}) and tie rod (C_{TR}). The left and right steer angles of road wheels due to a steering wheel input can be established using a quasi-static moment balance of the two wheels, and expressed as:

$$\delta_{cL} = C_{SW} [M_{zL} + M_{zR} - L_{MT} (F_{yL} + F_{yR})]$$

$$\delta_{cR} = \delta_{cL} + C_{TR} (M_{zR} - L_{MT} F_{yR}) \quad (6.27)$$

where δ_{cL} and δ_{cR} are the steer angles of the left and right wheels due to steering system compliance, respectively. F_{yi} and M_{zi} ($i = L, R$) are the lateral force and aligning moment developed at the left and right wheels, respectively. L_{MT} denotes the mechanical trail, which is a function of unsprung mass cg height, wheel caster angle and body pitch angle [92].

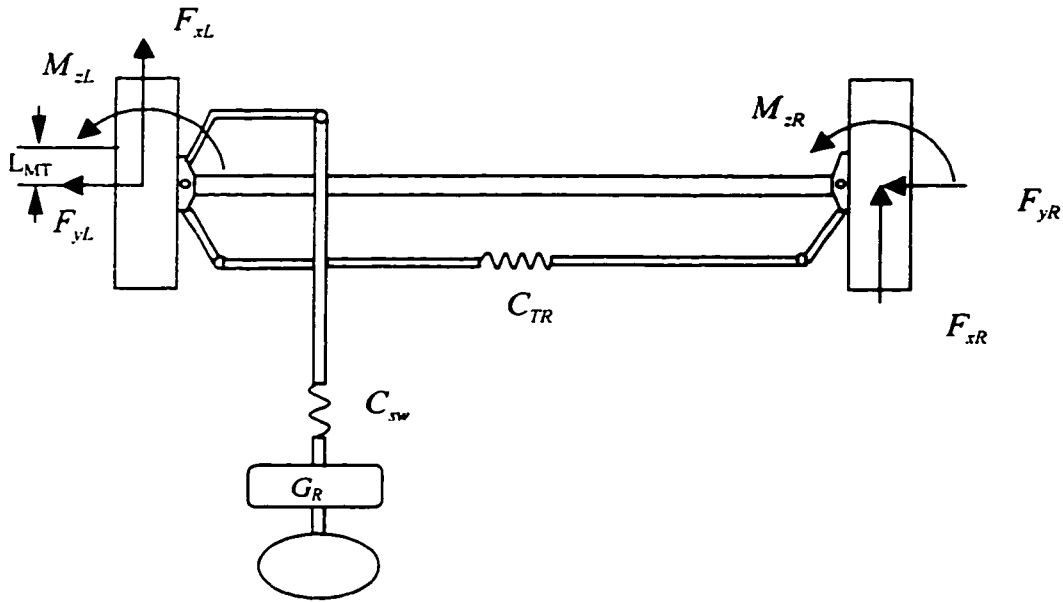


Figure 6.7: Steering system model of heavy vehicles.

The steer angle, developed at right and left wheels, may differ considerably depending upon the steering system designs. The relationship between the left and right wheel steering angles is known to be complex function of kinematics of the steering

mechanisms, which may vary considerably in heavy vehicles. The kinematic steer for both wheels is thus conveniently derived using a lookup table function of the steering wheel angle δ_{sw} . The Ackerman steer angles developed at the left (δ_{aL}) and right (δ_{aR}) wheels are then computed from the gear ratio of the steering system (G_R):

$$\delta_{aL} = f(\delta_{sw} / G_R) \quad \delta_{aR} = g(\delta_{sw} / G_R) \quad (6.28)$$

Apart from the kinematic steer, the road wheels undergo additional steering effects due to vehicle roll (roll-steer), vertical motion of the axle (bump-steer), and wrapping of the axle (wrap steer). These steering effects are briefly described below.

The roll steer characteristics of a vehicle relate to steering motion of the front or rear wheels (δ_{roll}) caused by relative roll motion of the sprung mass with respect to the unsprung mass ($\Delta\phi_u$). The roll steer is frequently characterized as a function of the relative roll angle and the roll steer coefficient R_{roll} , and given by [92]

$$\delta_{roll} = R_{roll} \Delta\phi_u \quad (6.29)$$

The roll steer is considered positive when the axle steers to the left in a left turn.

When an axle translates vertically, the geometry of the steering linkages can introduce some steering effect, known as bump-steer. The bump-steer (δ_b) is assumed to be identical for left and right wheels, and is modeled using a bump-steer coefficient (R_{bump}) as:

$$\delta_b = R_{bump} \Delta z_u \quad (6.30)$$

where Δz_u is the vertical deflection of the front axle with respect to vehicle body.

When the vehicle accelerates or decelerates longitudinally, the axles tend to twist about Y axis (called wrap), and consequently introduce a steering effect on the front axle,

referred to as 'wrap steer'. The wrap steer (δ_w) is linearly related to axle wrap angle through a wrap-steer coefficient (R_{wrap}):

$$\delta_w = R_{wrap} \mathcal{G}_{wrap} \quad (6.31)$$

where \mathcal{G}_{wrap} is the axle wrap angle due to tractive or braking torque, and can be derived from:

$$\mathcal{G}_{wrap} = C_{wr} [(h_u - \Delta_{iL}) F_{xL} + (h_u - \Delta_{iR}) F_{xR}] \quad (6.32)$$

where $(h_u - \Delta_{iL})$ and $(h_u - \Delta_{iR})$ are the instantaneous left and right front tire radii, respectively. F_{xL} and F_{xR} are the longitudinal forces, respectively, developed at the left and right tires of the front axle. C_{wr} is the wrap compliance of the axle.

The effective steer angles developed at the left and right wheels are then derived upon combining Equations (6.27) to (6.32), and expressed as:

$$\begin{aligned} \delta_l &= \delta_{roll} + \delta_{cL} + \delta_b + \delta_{aL} + \delta_w \\ \delta_r &= \delta_{roll} + \delta_{cR} + \delta_b + \delta_{aR} + \delta_w \end{aligned} \quad (6.33)$$

where δ_l and δ_r are the total steer angles developed at left and right front wheels, respectively.

6.3 DESCRIPTION OF INPUT VARIABLES

A typical 5-axle tractor semi-trailer combination is used to investigate the effectiveness of open-loop rollover control, which is strongly dependent upon the time delays associated with driver's reaction and braking system, and the lead time provided by the detection variables. The driver's reaction time and braking system delay are thus considered as vital parameters for the assessment of open-loop rollover control. The road

adhesion limits and braking effort intensity are considered as additional important input parameters to study directional stability characteristics of the vehicle. The vehicle maneuvers are characterized by both open-loop steer inputs and close-loop path trajectories for typical cornering and lane change maneuvers.

6.3.1 Time Delay due to Driver and Braking Systems

When an impending rollover signal is generated for the driver, the driver can not immediately perceive it until the time τ_1' is elapsed. The driver then applies braking by depressing the pedal, which involves another delay of τ_1'' . The total delay $\tau_1 = \tau_1' + \tau_1''$, is referred to as the reaction time of the driver, which may range from 0.2 s to 1.0 s [110]. The brake actuation, however, may initiate after a τ_2' due to latches and 'plumbing' of the air braking system. Initial transient response time τ_2'' is also related to the speed of sound and dynamics of the tubing connecting the air supply to the braking chambers. The elapsed time τ_2'' between the instant when the braking force takes effect and the instant when the force approaches 95% of its final value is called build-up time. For air brakes, τ_2'' depends charging rate of the air chamber, which can be characterized by a time constant TC . The instantaneous pressure in the air chamber can be expressed as:

$$P = P_0(1 - e^{-t/TC}) \quad (6.34)$$

where P_0 is air supply pressure, and P is the instantaneous pressure in the chamber, and $TC = \tau_2''/3$. The sum of the initial response time and the build-up time is generally referred to as the lag time (τ_2) of air braking system, which ranges from 0.5 to 1.5 s for typical air brake systems of commercial vehicles [111]. After the braking force is fully

developed, the driver maintains the braking for a period τ_3 before releasing the brake pedal.

The elapsed time between the instant at which a warning signal is generated to the instant when the braking force is fully developed may thus range from 0.7 s to 2.5s. This period, referred to as the total delay time ($\tau_0 = \tau_1 + \tau_2$), is characterized by driver's reaction time and the lag time of braking system, and is very critical for the effectiveness of open-loop rollover control. To ensure that the driver's corrective action takes effect before the vehicle reaches its rollover condition, the warning signal should be generated early enough to account for the total delay time.

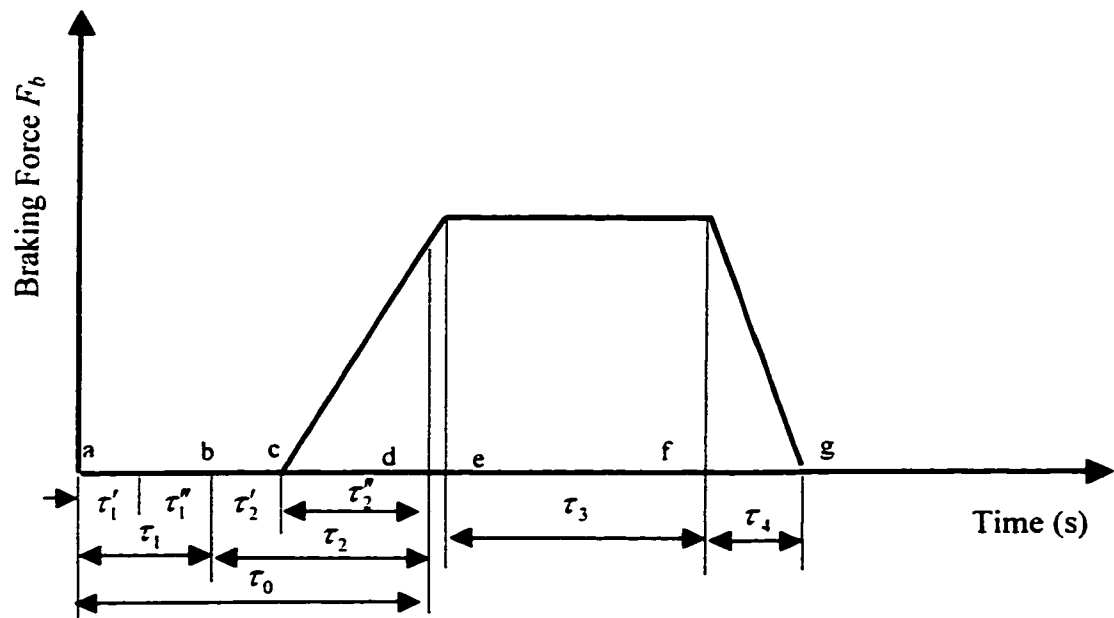


Figure 6.8: A Schematic diagram of the elapsed time in braking sequence.

The components of the total delay time (τ_0) are regrouped as:

$$\tau_0 = (\tau'_1 + \tau''_1 + \tau'_2) + \tau''_2 = \tau'_0 + \tau''_2 \quad (6.35)$$

where $\tau'_0 = \tau'_1 + \tau''_1 + \tau'_2$, referred to as the reaction delay, is the sum of the driver reaction time and the initial response time of the braking system. τ'_0 is taken as a variable in this investigation, while τ''_2 is characterized by the time constant TC , as illustrated in Equation (6.34). The time constant TC of the air braking system is selected as 0.3s [111], while three different reaction delays ($\tau'_0=0.6s$, 1.2s and 1.8s) are considered to investigate the feasibility of open-loop rollover control and the effectiveness of the rollover indicators.

6.3.2 Vehicle Maneuvers

Rollover accidents of heavy vehicles typically occur during cornering and high-speed evasive maneuvers. These maneuvers may be defined in an open-loop manner by characterizing the time history of steering angle of the steering wheel, or in a close-loop manner by providing coordinates of the path trajectory.

Cornering Maneuvers

The cornering maneuvers in an open-loop mode are often characterized by a ramp-step steer input. The steer angle is initially increased as a ramp function until it approaches the desired steer angle, which is then held constant over the simulation period. In this study, the open-loop maneuver is defined by a ramp function alone at a constant forward speed until onset of vehicle rollover is identified. The vehicle response is evaluated under various ramp-steer inputs performed at different rates, as shown in Figure 6.9, while the steering gear ratio is assumed to be 30.

The cornering maneuver in a closed-loop mode is characterized by a spiral trajectory with constant rate of radius reduction per degree. The trajectory radius of the spiral trajectory is given by:

$$R = R_o(\theta_f - \theta) \quad (\theta \leq \theta_f) \quad (6.36)$$

where R is the path radius, and θ is the rotation angle, as shown in Figure 6.10. R_o and θ_f are control parameters. The X-Y coordinates of the trajectory can be obtained from:

$$x = R \cos(\theta); \quad y = R \sin(\theta); \quad \text{and} \quad \frac{dR}{d\theta} = -R_o \quad (6.37)$$

The effect of radius reduction rate on the path radius as a function of rotation angle is illustrated in Figure 6.11.

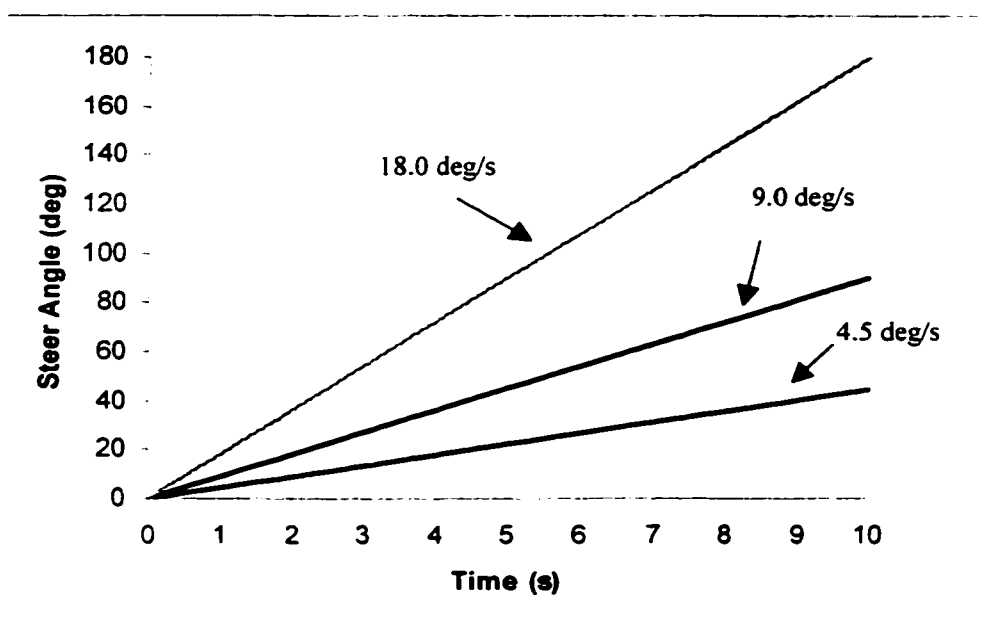


Figure 6.9: Ramp steering inputs for cornering maneuvers.

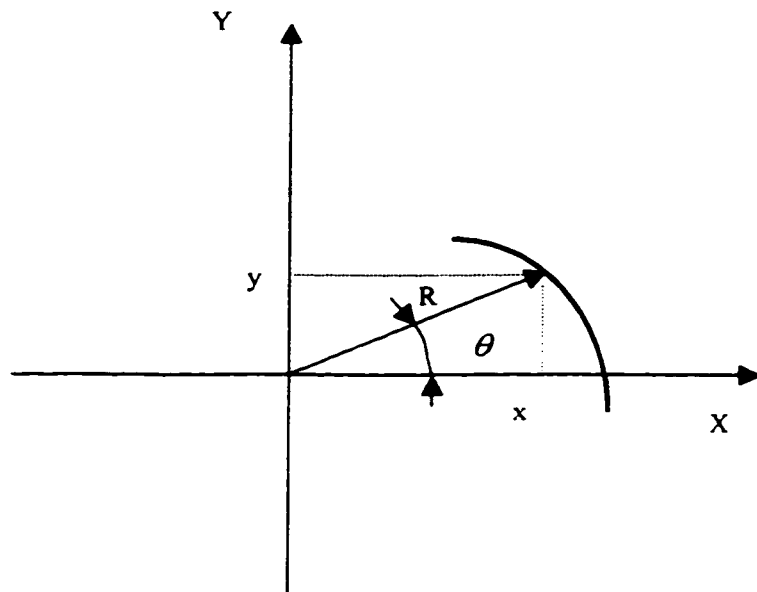


Figure 6.10: Definition of path trajectory for cornering maneuvers.

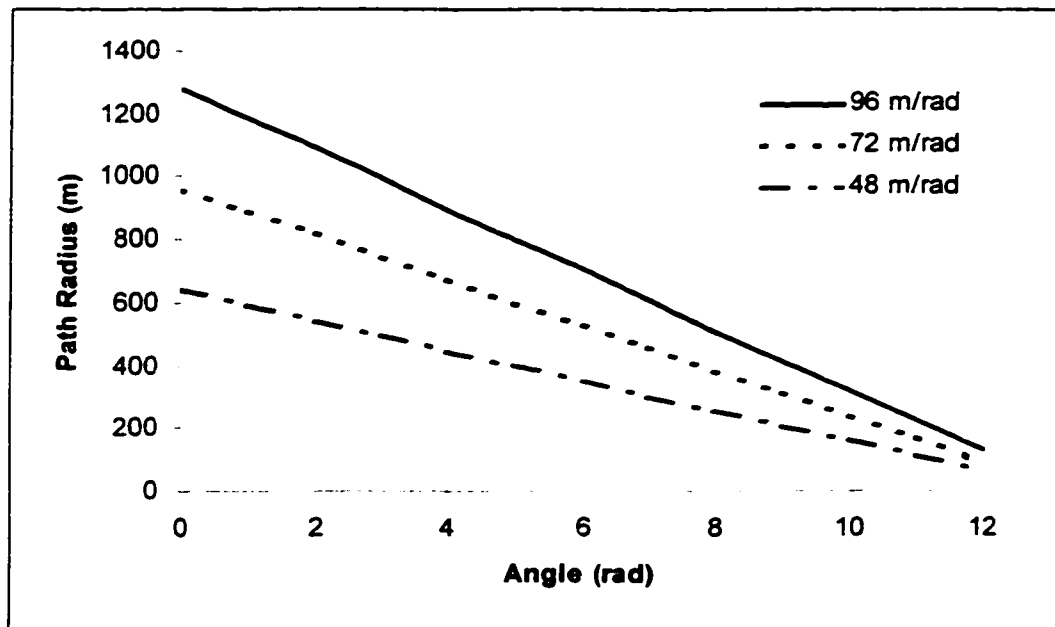


Figure 6.11: Radius of path trajectories with different rates of path radius reduction.

Lane Change Maneuvers

Obstacle evasion maneuvers are characterized by either a single- or a double- lane change maneuver with varying gate lengths. Figure 6.12 illustrates the trajectory of a single-lane change maneuver. The single-lane change maneuvers can be further characterized by sinusoidal steering maneuvers with different steering frequencies [28]. A lane change maneuver in an open-loop mode can thus be expressed as:

$$\delta_{sw} = \delta_0 \sin(2\pi ft) \quad 0 \leq t \leq 1/f \quad (6.38)$$

where δ_{sw} is the steering wheel angle, δ_0 is its amplitude, and f is the steering frequency. In this study, different steering frequencies (0.25Hz, 0.33Hz and 0.5 Hz) are considered to examine the effectiveness of rollover indicators, while δ_0 is held constant.

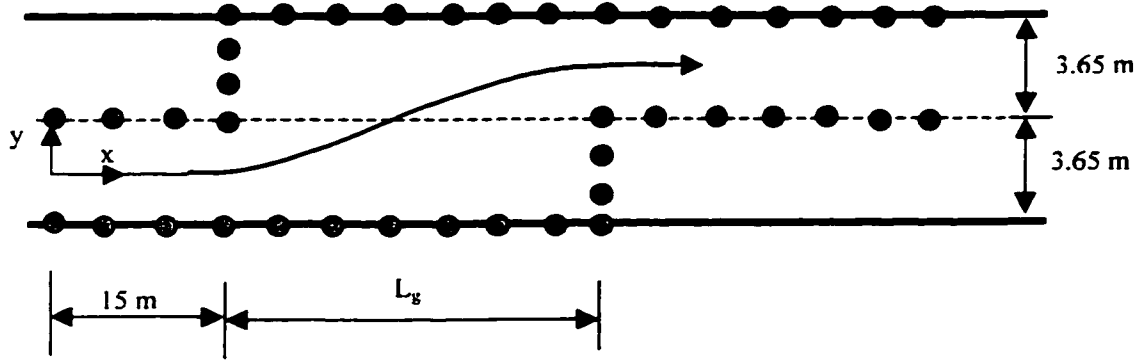


Figure 6.12: Schematic of typical single lane change maneuvers.

A single lane change maneuver in a closed-loop mode is characterized by a path trajectory defined as:

$$y = \begin{cases} 0 & x \leq 15 \text{ m} \\ 1.825 \left[1 + \sin \left(\frac{\pi}{L_g} (x - 15) + \frac{3\pi}{2} \right) \right] & 15 \text{ m} < x < (15 + L_g) \text{ m} \\ 3.65 & x \geq (15 + L_g) \text{ m} \end{cases} \quad (6.39)$$

where x and y are the coordinates of the path trajectory in meters along the longitudinal and lateral directions of the vehicle, respectively. L_g is the gate length for the path. In this study, two different gate lengths (20m and 30m) are selected to evaluate the effectiveness of open-loop rollover control.

6.3.3 Road Adhesion Limit and Braking Intensity

In response to an impending rollover warning, the driver may choose to slow down the vehicle through application of braking. The maximum braking effort, however, depends upon the adhesion limits of the road surface. Although the coefficient of road adhesion is influenced by tire construction, inflation pressure, speed and normal load, the most significant factor is road surface condition. The average road adhesion coefficient may vary from a low value of 0.1 for an icy surface to 0.8 - 0.9 for dry asphalt or concrete roads [21]. In this investigation, two different road adhesion coefficients (0.80 and 0.5) are chosen to represent typical dry and wet road conditions. Snow or icy roads are not considered since such surfaces can initiate lateral skid before the vehicle approaches its roll instability condition.

The braking force developed also depends upon its intensity. Application of sudden and intense braking upon the perception of an impending rollover signal, may cause yaw instabilities leading to potential jackknife. Alternatively, the driver may adopt a modulated braking to avert the impending roll instability. The influence of braking

intensity adopted by the driver on avoidance of a potential rollover thus needs to be investigated to assess the effectiveness of the open-loop rollover control. The study is thus performed for two different intensities of braking effort: 100%, 50%, and the results are discussed to quantify the contributions of braking intensity. Table 6.1 summarizes the simulation parameters of the tractor semi-trailer vehicle considered in this study.

Table 6.1: Simulation parameters for a 5-axle tractor semi-trailer combination.

ABS parameter: slip ratio to turn brake off (k_{off})	0.3
ABS parameter: slip ratio to turn brake back on (k_{on})	0.2
ABS parameter: minimum speed for ABS control (km/h)	6.0
Torsional steering system complinace due to tie rods (C_{ir} , deg/Nm)	0.00042
Steering shaft compliance (C_{sw} , deg/Nm)	0.00222
Wrap-up compliance of front axle (C_{rw} , deg/Nm)	0.000186
Wrap-up coefficient (R_{wrap})	0.1
Bump-steer ratio: steer/jounce (R_{hump} , deg/mm)	0.00404
Roll mass moment of inertia for sprung mass of tractor (kg-m^2)	6967.79
Pitch and yaw mass moments of inertia for sprung mass of tractor (kg-m^2)	19943.9, 19943.0
Roll mass moment of inertia for sprung mass of semi-trailer (kg-m^2)	24700.9
Pitch and yaw mass moments of inertia for sprung mass of semi-trailer (kg-m^2)	357412.0, 367084.0
Longitudinal tandem axle spacing for tractor (mm)	1219.2
Longitudinal tandem axle spacing for semitrailer (mm)	1321.0
Wheelbase of tractor (mm)	4789
Wheelbase of semitrailer (mm)	14000
Tire relaxation length (L_r , mm)	600.0
Tire spring rate (N/mm)	875
Hitch roll torsional stiffness (N-m/deg)	650000
Hitch pitch torsional stiffness (N-m/deg)	0
Hitch articulation torsional stiffness (N-m/deg)	0
Tractor sprung mass CG height (mm)	1050.38
Semi-trailer sprung mass CG height (mm)	2123.98
Height of fifth wheel above ground (mm)	1120.0
Tire/ground adhesion coefficient	0.8

	Axle 1	Axle 2	Axle 3	Axle 4	Axle 5
Unsprung mass (kg)	624.5	1068	1068	750	750
Height of axle CG above ground (mm)	480	480	480	546	546
Height of axle roll center above ground (mm)	427.0	695.0	695.0	673.0	673.0
Axle yaw and roll mass moments of inertia (kg-m ²)	490.0	540.0	540.0	600.0	600.0
Wheel spin inertia	30.8	60.0	60.0	50.7	50.7
Tire track width (to center of dual tires) (mm)	2110	1810	1810	1943	1943
Dual tire spacing (mm)	0	330.0	330.0	330.0	330.0
Suspension spring spacing (mm)	823	1030	1030	1030	1030
Axle load (kN)	53.45	71.28	71.28	71.28	71.28
Auxiliary roll stiffness (Nm/deg)	1045	1356	1356	2260	2260
Damping coefficient (N/mm/s)	2.8	6.3	6.3	6.3	6.3
Roll-steer coefficient	-0.2	0.1	0.1	-0.2	-0.2
Time constant for air brake chambers (s)	0.3	0.3	0.3	0.3	0.3

6.4 ROLLOVER METRIC

As discussed in Chapter 2, the roll instability criteria can be expressed in two categories in terms of the rollover severity: relative and absolute. The relative roll instability criterion characterized by a dimensionless parameter referred to as *Roll Safety Factor (RSF)*, is initially used to investigate the static rollover propensity of heavy vehicles. A relative rollover condition is identified, when *RSF* approaches a unity value. The absolute roll instability, however, is defined in conjunction with vehicle tip-over position. A dynamic parameter referred to as *Rollover Prevention Energy Reserve Factor* and discussed in section 4.6, is used to characterize the absolute roll instability.

The primary objective of open-loop rollover control is to inform the driver of the impending roll instability of the vehicle. The driver then performs corrective maneuvers to retain vehicle stability by averting the occurrence of potential instability. A contact between the tires and the road, however, should be maintained for the driver to undertake appropriate efforts. The absolute roll instability criterion thus can not be employed to

assess the open-loop rollover control, since the driver has little control of the vehicle after all the wheels on a single track lift off the ground. The effectiveness of the open-loop rollover control is thus assessed on the basis of relative roll instability as a measure of impending rollover and early warning. Based on the relative roll instability criterion, the rollover metric for the open-loop control is proposed as $RSF \geq 0.99$. In the event, the RSF during a maneuver is detected beyond this limit, the open-loop rollover control is considered to be failed.

6.5 ROLLOVER WARNING THRESHOLD OF VARIOUS INDICATORS

As illustrated in Figure 6.1, the generation of an early warning on impending rollover to the driver necessitates identification of a reference signal (or threshold). A warning signal is generated when the magnitude of a rollover indicator exceeds the preset threshold. The directional dynamic response of a 5-axle tractor semi-trailer vehicle is analyzed to identify the threshold values of various indicators. The analyses are performed for selected indicators, described in section 5.4, which include: roll safety factor (RSF); tractor lateral acceleration (a_{y1}); trailer lateral acceleration (a_{y2}); tractor roll angle (ϕ_{x1}); trailer roll angle (ϕ_{x2}); and the rearmost axle roll angle (ϕ_{u5}). The steer-velocity factor is not selected as a candidate indicator due to its poor reliability, as illustrated in section 5.4.

The equations of motion, (4.1) to (4.2), describing the directional dynamics of the articulated vehicle in the yaw and roll planes under constant forward speed are solved for ramp steer input. The response characteristics are analyzed to identify the static rollover of the tractor semi-trailer combination during a low rate ramp steer (0.02 deg/s) maneuver

at 100 km/h, in terms of each of the selected indicators. Table 6.2 illustrates the rollover limits for the selected indicators, where the limits are presented with a superscript '0'. The rollover warning thresholds are then established as percentage of the identified rollover limits. The effectiveness of the open-loop rollover control is examined for each warning threshold under a range of directional maneuvers, delay time (τ'_d), road adhesion limits and braking intensities. The three-dimensional vehicle model, described in section 6.2, is analyzed under the application of braking and steering. A braking effort, however, is incorporated when an impending roll instability is identified. The directional dynamics of the vehicle is evaluated upon incorporating: tire forces and moments, *ABS* braking model, derived in section 6.2.3; steering system compliance, derived in section 6.2.4; and driver and brake system delays, derived in section 6.3.1.

The relative rollover condition corresponding to each threshold value is examined to identify a more reliable threshold value that can be considered valid under varying road and vehicle variables. In the event that a relative rollover condition is reached, the open-loop control based on that warning threshold value is considered to be failed, and a lower percentage value is assigned as a new rollover warning threshold. The results of the systematic analyses are presented in the following subsections.

Table 6.2: Static rollover limits in terms of different indicators.

Indicator	Rollover Limit
RSF	$RSF^0=99\%$
a_{y1}	$a_{y1}^0=0.42 \text{ g}$
a_{y2}	$a_{y2}^0=0.42\text{g}$
φ_{r1}	$\varphi_{r1}^0=6.57 \text{ deg}$
φ_{r2}	$\varphi_{r2}^0=6.67 \text{ deg}$
φ_{u5}	$\varphi_{u5}^0=1.50 \text{ deg}$

6.5.1 Rollover Warning Threshold in Cornering Maneuvers

The effectiveness of the open-loop rollover control is initially investigated under cornering maneuvers, described in section 6.3.2. The vehicle model is analyzed under a ramp-steer input at a rate of 9 degrees/s and a speed of 100 km/h, while the reaction delay is held at 0.6 s. The analyses are performed for two different values of thresholds of RSF ($0.85 \text{ } RSF^0$ and $0.70 \text{ } RSF^0$), to investigate the effectiveness of the driver's efforts undertaken to avert the occurrence of potential rollover. Figure 6.13 illustrates the RSF response of the vehicle corresponding to two values of warning threshold. The rollover boundary line represents the relative rollover condition of the vehicle. The results clearly show that the open-loop roll control fails, when the warning threshold is selected as $0.85 \text{ } RSF^0$. The warning based upon this threshold is considered to be too late for the driver to undertake corrective action in terms of braking. The warning based upon $0.70 \text{ } RSF^0$, however, yields an effective open-loop roll control, as shown in the Figure. The resulting warning, generated near $t=20 \text{ s}$, yields sufficient lead time for the driver's reaction and brake force development. The results further show that under application of braking ($t=20 \text{ s}$), the RSF increases rapidly to approximately 0.88 at $t=20.9 \text{ s}$, until the braking force is fully developed. The RSF , then rapidly decreases to zero, as the vehicle slows down. The sudden increase in RSF response when braking force is applied, is mainly due to steering system compliance, which is discussed in the following sections.

The influence of variations in the reaction delay and steer rates on the RSF are further investigated for various threshold values, ranging from $0.65 \text{ } RSF^0$ to $0.9 \text{ } RSF^0$. The results are examined to assess the effectiveness of open-loop roll control and to establish a reliable value of the warning threshold. The analyses are performed for

different cornering maneuvers, involving hand wheel steer rates of 4.5 deg/s, 9.0 deg/s and 18.0 deg/s, in conjunction with different reaction delays $\tau'_0 = 0.6$ s, 1.2 s and 1.8 s. The simulations are performed for road adhesion limit of $\mu = 0.8$ and braking pressure of 700 kPa. The results of the analysis, in terms of success or failure of the open-loop control corresponding to various warning thresholds, are summarized in Table 6.3. The results show that the steering rates and reaction delays influence the control of vehicle roll instability in a significant manner. A roll instability initiated by a low-rate steer input can be effectively controlled, even if the warning is generated corresponding to a relatively higher value of RSF , provided that the reaction time is relatively low. For a 4.5 degree/s steer rate, the roll control based upon warning threshold of $0.85RSF^0$ is considered to be successful for $\tau'_0 = 0.6$ s. The open-loop control, however, fails, when both the reaction time τ'_0 and steer rate increase. A slow reaction time and/or rapid steer rate require that a lower warning threshold should be selected to provide the driver and brake system with sufficient lead time. In a rapid steer maneuver (18 degree/s) coupled with slow reaction time ($\tau'_0 = 1.8$ s), an effective open-loop roll control can be realized by relaxing the warning threshold to $0.65 RSF^0$.

Figures 6.14 and 6.15 illustrate the results of the assessment studies in terms of other rollover indicators (a_{y1} , φ_{s1} , φ_{u5} , a_{y2} and φ_{s2}). The results show nearly linear relationship between the rollover indicators and the RSF in ramp steer maneuvers. It can thus be deduced that early warning signals can also be generated on the basis of lateral acceleration (a_{y1}) and/or roll angle (φ_{s1}) response of the tractor, lateral acceleration

($a_{y,2}$) and/or roll angle ($\varphi_{,2}$) response of the trailer, and roll angle (φ_{us}) response of the rearmost axle, in conjunction with certain percentage of RSF^0 , as illustrated in Table 6.3.

Table 6.3: Assessment of open-loop control in ramp steer maneuvers ($\mu = 0.8$, braking pressure: 700 kpa).

Steer rate (deg/s)	τ'_0 (s)	90% RSF^0	85% RSF^0	80% RSF^0	75% RSF^0	70% RSF^0	65% RSF^0
4.5	0.6	Failed	Success	Success	Success	Success	Success
	1.2	Failed	Failed	Success	Success	Success	Success
	1.8	Failed	Failed	Success	Success	Success	Success
9.0	0.6	Failed	Failed	Success	Success	Success	Success
	1.2	Failed	Failed	Failed	Success	Success	Success
	1.8	Failed	Failed	Failed	Success	Success	Success
18.0	0.6	Failed	Failed	Failed	Success	Success	Success
	1.2	Failed	Failed	Failed	Failed	Success	Success
	1.8	Failed	Failed	Failed	Failed	Failed	Success

The effectiveness of the open-loop roll control is further assessed under cornering maneuvers using closed-loop path following spiral trajectories, described in section 6.3.2. The vehicle model is analyzed for three different trajectories with radius reduction rate of 48 m/rad, 72 m/rad and 96 m/rad. The simulations are performed for the range of reaction time delays, considered earlier, and $\mu = 0.8$. The simulation results are assessed in view of the warning threshold, expressed as percentage of RSF^0 , ranging from 0.65 RSF^0 to 0.90 RSF^0 . The results, in terms of success or failure of the open-loop control as a function of reaction delay and radius reduction rates, are summarized in Table 6.4. The

results show trends similar to those observed for open-loop ramp steer inputs. An open-loop roll control is observed to be successful, when early warning is generated based upon $0.75 \text{ } RSF^0$, irrespective of the reaction delay, and rate of radius change. Slower radius change, however, can yield an effective roll control with warning threshold of $0.80 \text{ } RSF^0$ for $\tau'_o = 0.6 \text{ s}$ and 1.2 s . From the results, it can be concluded that an effective open-loop roll control can be realized on the basis of warning threshold of $0.75 \text{ } RSF^0$, for cornering maneuvers performed either in a closed-loop path following mode for in an open-loop ramp steer up to a rate of 9 degree/s .

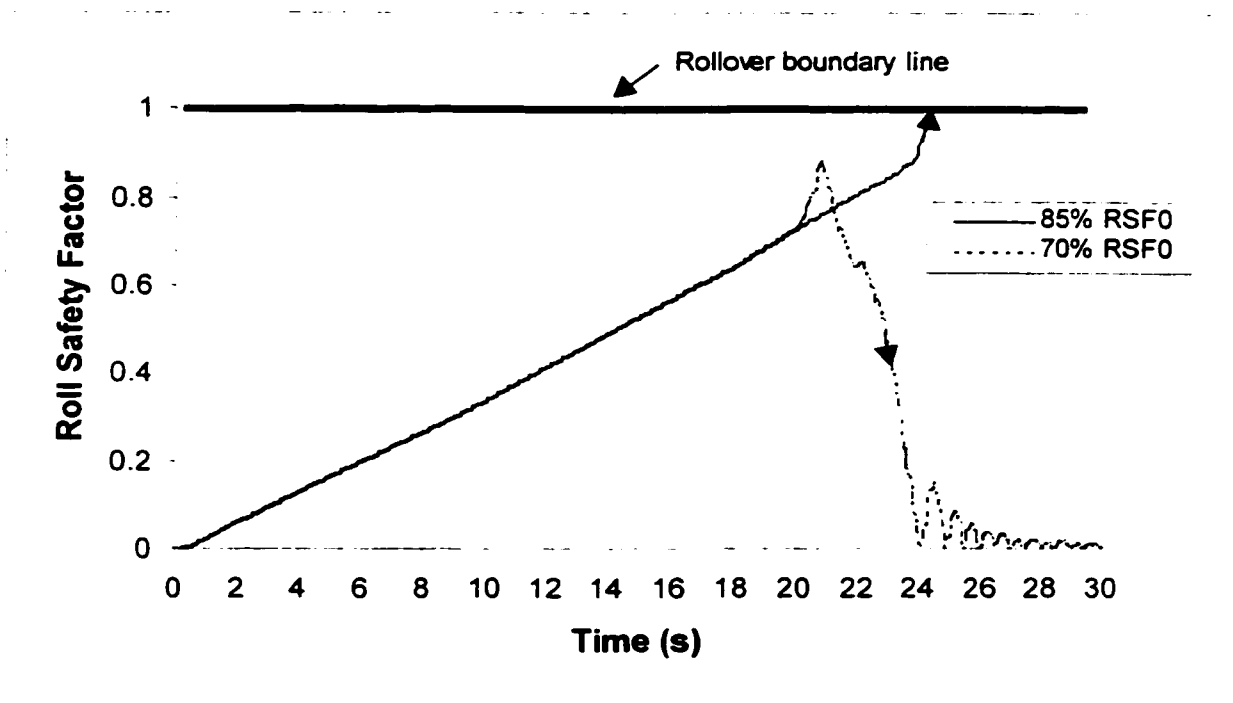


Figure 6.13: Rollover warning given at different percentages of RSF^0 .

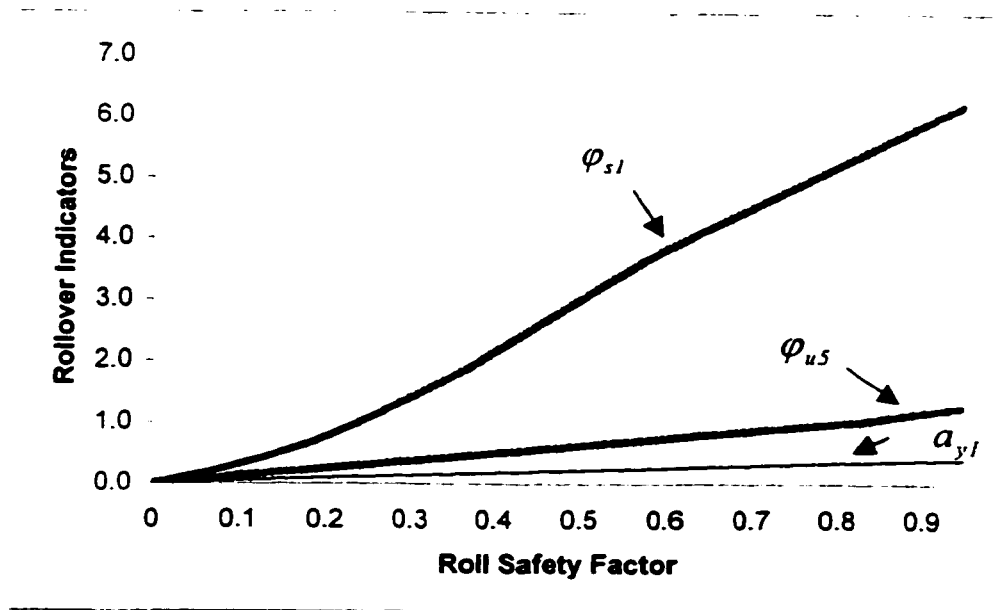


Figure 6.14: Relationship between RSF , a_{y1} , ϕ_{s1} and ϕ_{u5} .

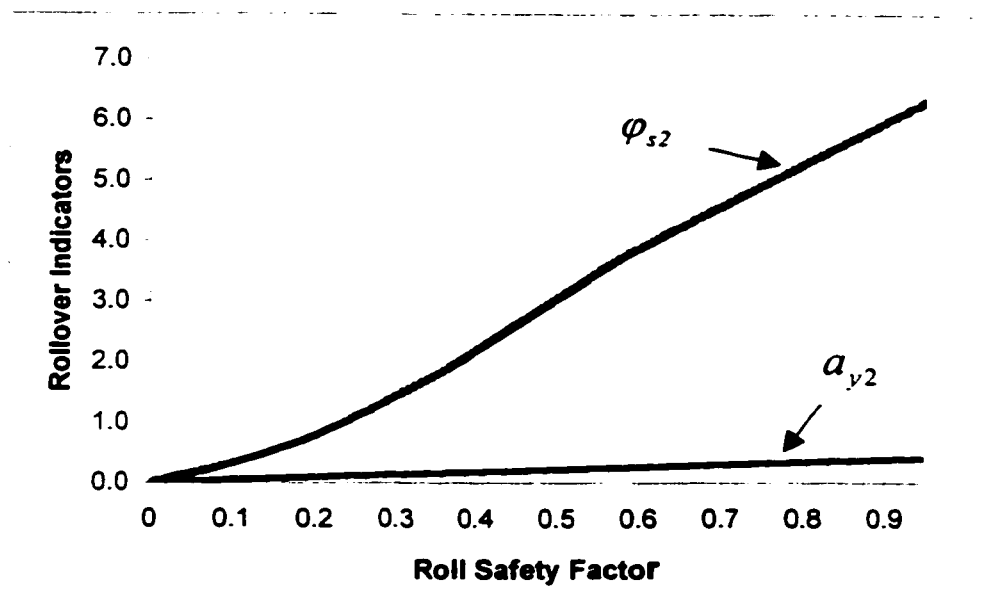


Figure 6.15: Relationship between RSF , a_{y2} and ϕ_{s2} .

Table 6.4: Open-loop rollover control on spiral paths with constant radius reduction rate ($\mu = 0.8$).

	τ'_0 (s)	90%RSF ⁰	85%RSF ⁰	80%RSF ⁰	75%RSF ⁰	70%RSF ⁰	65%RSF ⁰
48 m/rad	0.6	Failed	Failed	Success	Success	Success	Success
	1.2	Failed	Failed	Success	Success	Success	Success
	1.8	Failed	Failed	Failed	Success	Success	Success
72 m/rad	0.6	Failed	Failed	Success	Success	Success	Success
	1.2	Failed	Failed	Failed	Success	Success	Success
	1.8	Failed	Failed	Failed	Success	Success	Success
96 m/rad	0.6	Failed	Failed	Failed	Success	Success	Success
	1.2	Failed	Failed	Failed	Success	Success	Success
	1.8	Failed	Failed	Failed	Success	Success	Success

6.5.2 Rollover Warning Threshold in Lane Change Maneuvers

The effectiveness of the open-loop roll control is assessed under transient directional maneuvers, performed either in an open-loop or in a closed-loop path following mode. The directional dynamics of the vehicle model, described in section 6.2, is analyzed for different lane-change maneuvers. The response characteristics of the vehicle are analyzed to derive the ratio of *RSF* peaks obtained during turning and correction phases of the maneuver. In lane change maneuvers, the vehicle response parameters, such as lateral acceleration and roll safety factor demonstrate two peaks, as illustrated in Figures 6.16 and 6.17. The ratio of the second peak ($A_{s,12}$ or $A_{s,22}$) to the first peak ($A_{s,11}$ or $A_{s,21}$) represents the amplification tendencies of the vehicle system

during a lane change maneuver. The amplification ratios for lateral acceleration response of the tractor and semi-trailer units, and the *RSF* are defined as:

$$G_{As1} = \frac{A_{s12}}{A_{s11}} \quad ; \quad G_{As2} = \frac{A_{s22}}{A_{s21}} \quad ; \quad \text{and} \quad G_{RSF} = \frac{RSF_2}{RSF_1} \quad (6.40)$$

where G_{As1} , G_{As2} and G_{RSF} are the amplification factors for the tractor lateral acceleration, semi-trailer lateral acceleration and the roll safety factor, respectively. In the event, the *RSF* ratio (G_{RSF}) exceeds a unity value, the vehicle may roll over during second part (correcting phase) of the maneuver, while it may safely perform the first part of the maneuver. It should be noted that G_{As1} and G_{As2} are different from the rearward amplification ratio (*RAR*) defined in section 4.3.2. While *RAR* is introduced to study the lateral acceleration response characteristics of different units of a combination, G_{As1} and G_{As2} are used to characterize the response of the same unit in different phases during a lane change maneuver. Since lateral acceleration response of the tractor and the semi-trailer is highly correlated with *RSF*, as shown in Table 5.7, G_{As1} or G_{As2} could be interpreted the same as G_{RSF} . Specifically, if G_{As1} or G_{As2} is greater than a unity value, the vehicle may approach the relative rollover condition during the second part of the maneuver even though it can safely perform the first part of the maneuver.

The vehicle response is evaluated under sinusoidal steering maneuvers, performed at frequencies of 0.25 Hz, 0.33 Hz and 0.50 Hz at different vehicle forward speeds. Two different values of gate length (20 m and 30 m) are also selected for the maneuvers. The response characteristics are analyzed to evaluate peak *RSF* and G_{RSF} , and to establish an appropriate range of warning generation threshold. Figure 6.18 illustrates the *RSF*

amplification factor as a function of RSF_2 for the 5-axle tractor semi-trailer combination during typical sinusoidal steering maneuvers at 0.25Hz, 0.33 Hz and 0.5 Hz. The results show that the RSF amplification factor (G_{RSF}), increases with increase in RSF_2 , irrespective of the steering frequency. The magnitude of G_{RSF} obtained at a frequency of 0.33 Hz, however, is larger than that obtained at a lower frequency of 0.25 Hz, over the entire range of RSF_2 . When the steer frequency is increased to 0.5 Hz, the G_{RSF} increases further at lower values of RSF_2 , but reaches a relatively smaller value than that obtained at 0.33 Hz at higher values of RSF_2 . G_{RSF} approaches approximately 1.29 as the vehicle approaches its rollover condition. Figure 6.19 illustrates the influence of gate length on the relationship between G_{RSF} and RSF_2 . The results show that G_{RSF} increases with increase in the gate length. The maximum values G_{RSF} approaches 1.19 and 1.22, respectively, for gate lengths of 20m and 30m, corresponding to relative rollover condition of the vehicle.

The results, shown in Figures 6.18 and 6.19, illustrate that G_{RSF} may exceed the unity value for $RSF \leq 1.0$. This implies that an early warning for the open-loop roll control must be generated at a relatively earlier stage. Assuming linear relationship between G_{RSF} and RSF_2 , it is suggested that the warning signal should be generated when RSF approaches $0.99/(G_{RSF})_{\text{peak}}$. For a peak value of $G_{RSF} = 1.3$, the warning may be generated near a threshold value of $0.76 RSF''$.

Similar to G_{RSF} , the lateral acceleration amplification factors for the tractor and semi-trailer units ($G_{A\lambda 1}$ and $G_{A\lambda 2}$) are evaluated to examine their relationship with RSF_2 . Figures 6.20 and 6.21 illustrate the variations in $G_{A\lambda 1}$ and $G_{A\lambda 2}$ as a function of RSF_2 for

the three steering maneuvers. For lower steering frequencies (0.25 Hz and 0.33 Hz), the G_{As1} varies only slightly over the entire range of $RSF_2 \leq 1$, while the corresponding G_{As2} increases with increase in RSF_2 . The peak value of G_{As2} approaches 1.25 corresponding to relative rollover condition ($RSF_2=1.0$). For a relatively rapid maneuver (steering frequency=0.5 Hz), G_{As1} increases considerably with RSF_2 , while G_{As2} decreases with RSF_2 . G_{As1} approaches a peak value of approximately 1.24 corresponding to rollover condition. Figures 6.22 and 6.23 illustrate the influence of gate length on the relationship between lateral acceleration amplification factors and RSF_2 . In both cases, the amplification factors initially increase and then decrease with increase in RSF_2 . Corresponding to the relative rollover condition, the G_{As1} approaches values of 1.08 and 1.05 for the 20m and 30m gate lane change maneuvers, respectively. The corresponding values of G_{As2} are observed to approach approximately 1.11 and 1.07 for the 20m and 30m gate lane change maneuvers.

The vehicle model is further analyzed to derive amplification factors of roll angles of tractor ($G_{\varphi 1} = \Phi_{s12} / \Phi_{s11}$), semi-trailer ($G_{\varphi 2} = \Phi_{s22} / \Phi_{s21}$) and rearmost axle ($G_{\varphi 3} = \Phi_{u52} / \Phi_{u51}$), where Φ_{ij} represents the peak values obtained during turning and correction phases of the maneuver. The relationship between each amplification factor and RSF_2 is examined to derive an appropriate value of the warning signal threshold. Table 6.5 summarizes the amplification factors of the six rollover indicators corresponding to relative rollover condition under lane change maneuvers performed at different frequencies and gate lengths. The maneuver performed at a frequency of 0.5 Hz is highlighted since it yields considerably large variations in the amplification factors.

Furthermore, the maneuver corresponding to 0.5 Hz sinusoidal steering is considered to be quite severe and may not be encountered in practice for heavy articulated vehicles. It is therefore excluded in the following analyses. The results show a maximum value of amplification factors of 1.29, with the exception of $G_{\varphi u5}$, which approaches 1.66. An upper limit of 1.3 is thus selected for G_{RSF} , G_{As2} , $G_{\varphi u1}$ and $G_{\varphi u2}$, while the upper limit for $G_{\varphi u5}$ is selected as 1.7. The limiting value of G_{As1} is identified as 1.1. The corresponding values of threshold for generation of rollover warning signals are then computed as 75% for G_{RSF} , G_{As2} , $G_{\varphi u1}$ and $G_{\varphi u2}$; 91% for G_{As1} and 59% for $G_{\varphi u5}$. These threshold values are proposed to ensure sufficient lead time to account for delays associated with the driver's reaction and braking system.

Table 6.5: Amplification factors of various rollover indicators in sinusoidal steer and lane change maneuvers.

Maneuver	Amplification factor					
	G_{RSF}	G_{As1}	G_{As2}	$G_{\varphi u1}$	$G_{\varphi u2}$	$G_{\varphi u5}$
0.25 Hz	1.22	1.05	1.23	1.24	1.25	1.52
0.33 Hz	1.29	1.00	1.27	1.29	1.29	1.66
0.50 Hz**	1.20	1.23	0.83	1.32	1.32	2.53
20 m gate	1.19	1.08	1.11	1.16	1.15	1.33
30 m gate	1.22	1.05	1.07	1.22	1.22	1.44
Range	1.19 - 1.29	1.0 - 1.23	0.83 - 1.27	1.16 - 1.32	1.15 - 1.32	1.33 - 2.53
Range (0.5 Hz maneuver excluded)	1.19 - 1.29	1.0 - 1.08	1.07 - 1.27	1.16 - 1.29	1.15 - 1.29	1.33 - 1.66
Selected upper limit	1.3	1.1	1.3	1.3	1.3	1.7
Warning given at limit %	77%	91%	77%	77%	77%	59%

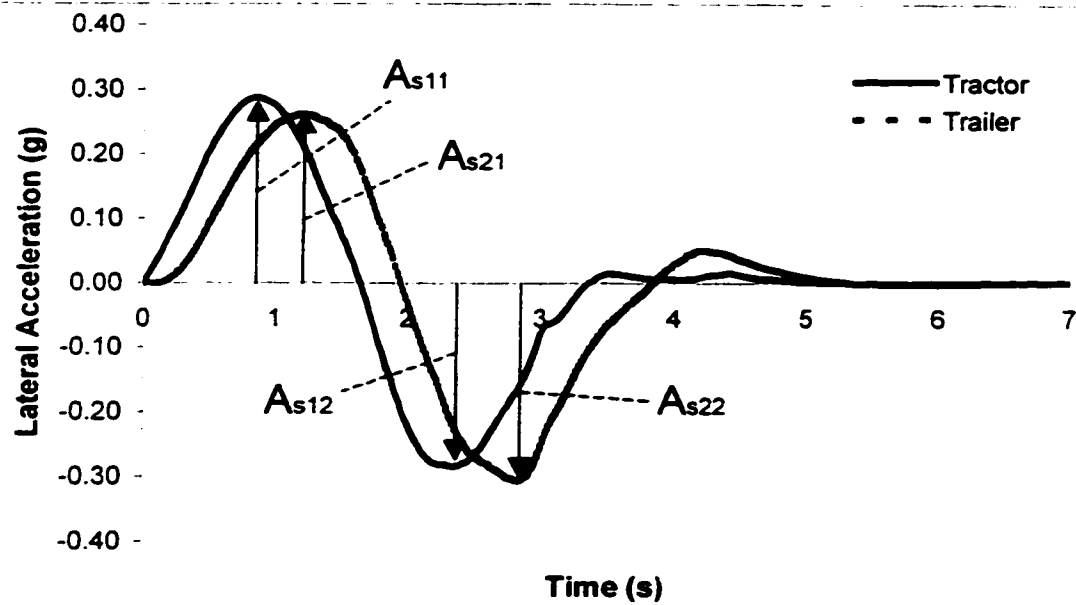


Figure 6.16: Time history of lateral acceleration response of an articulated vehicle during a lane change maneuver.

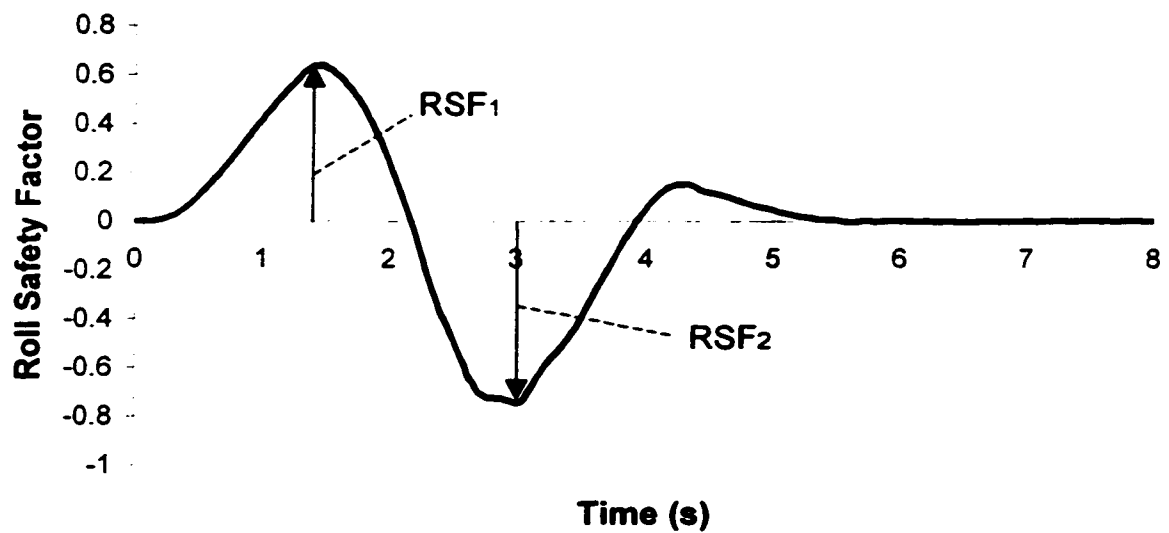


Figure 6.17: Time history of *RSF* amplification of an articulated vehicle during a lane change maneuver.

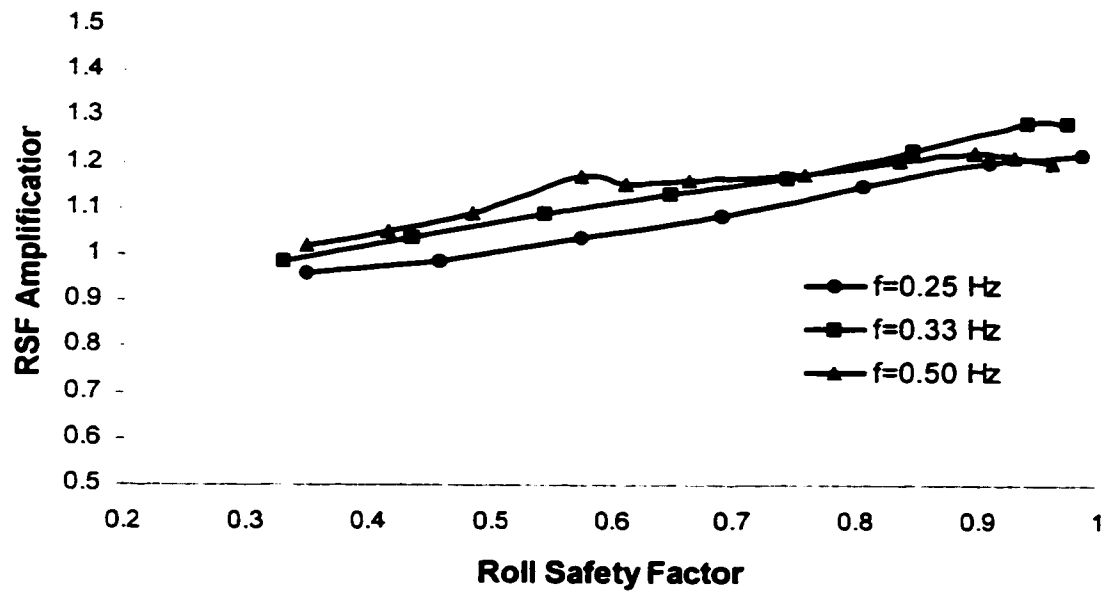


Figure 6.18: RSF amplification factor G_{RSF} during sinusoidal steer maneuvers.

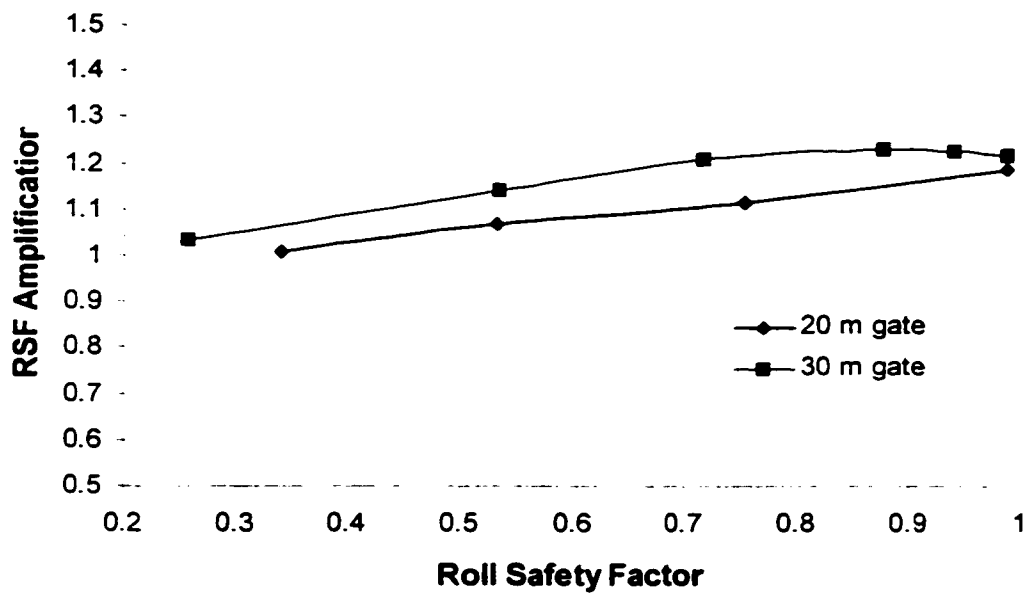


Figure 6.19: RSF amplification factor G_{RSF} during a single lane change maneuver of different gate lengths.

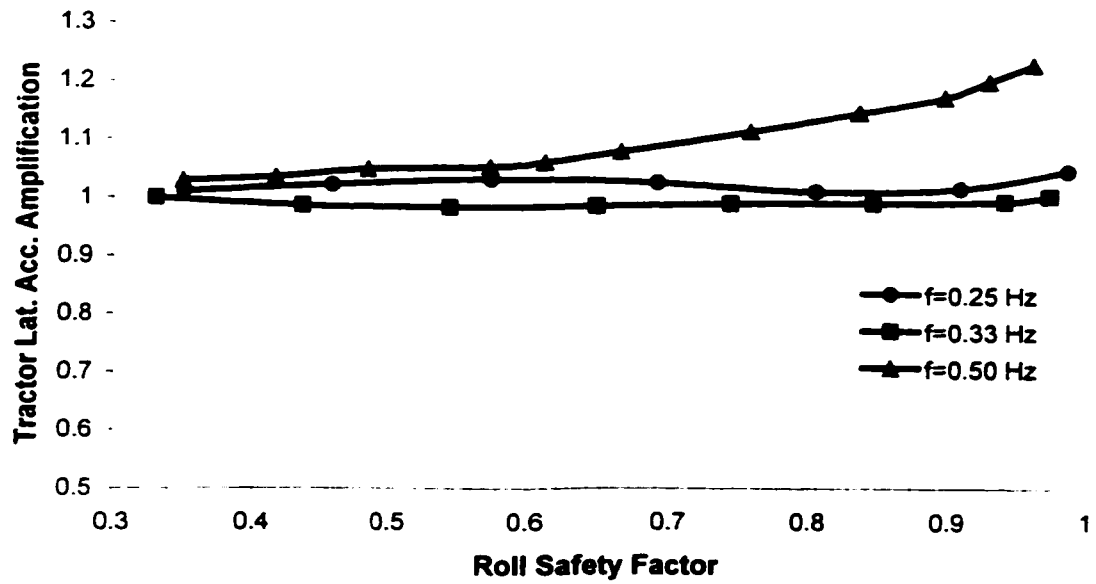


Figure 6.20: Tractor lateral acceleration amplification G_{As1} during sinusoidal steer maneuvers.

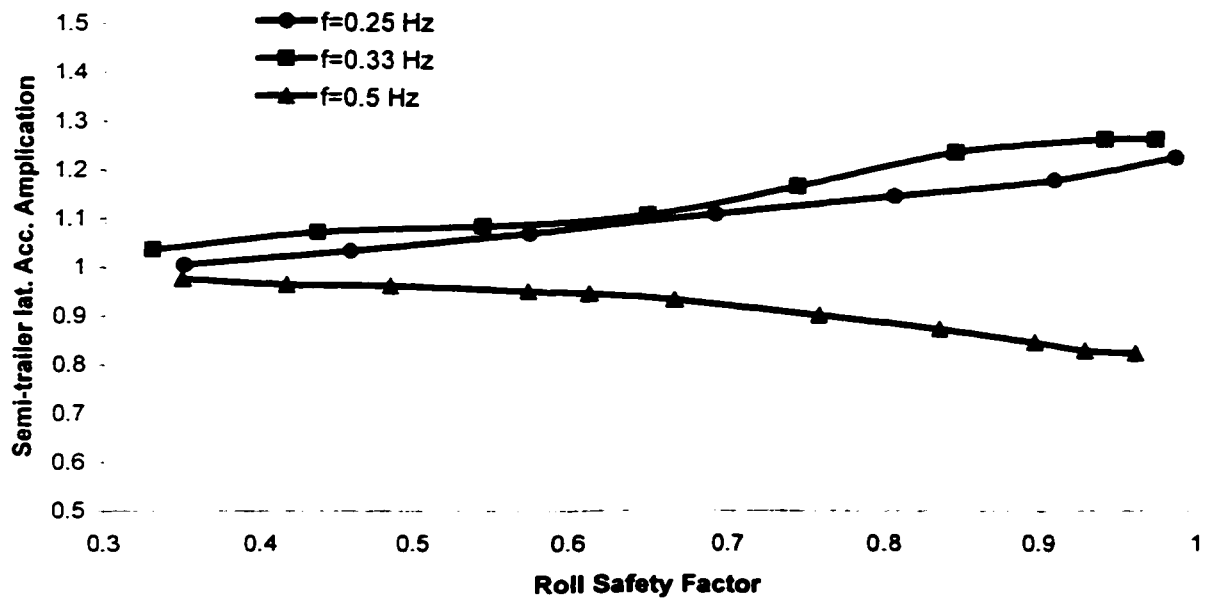


Figure 6.21: Semi-trailer lateral acceleration amplification G_{As2} during sinusoidal steer maneuvers.

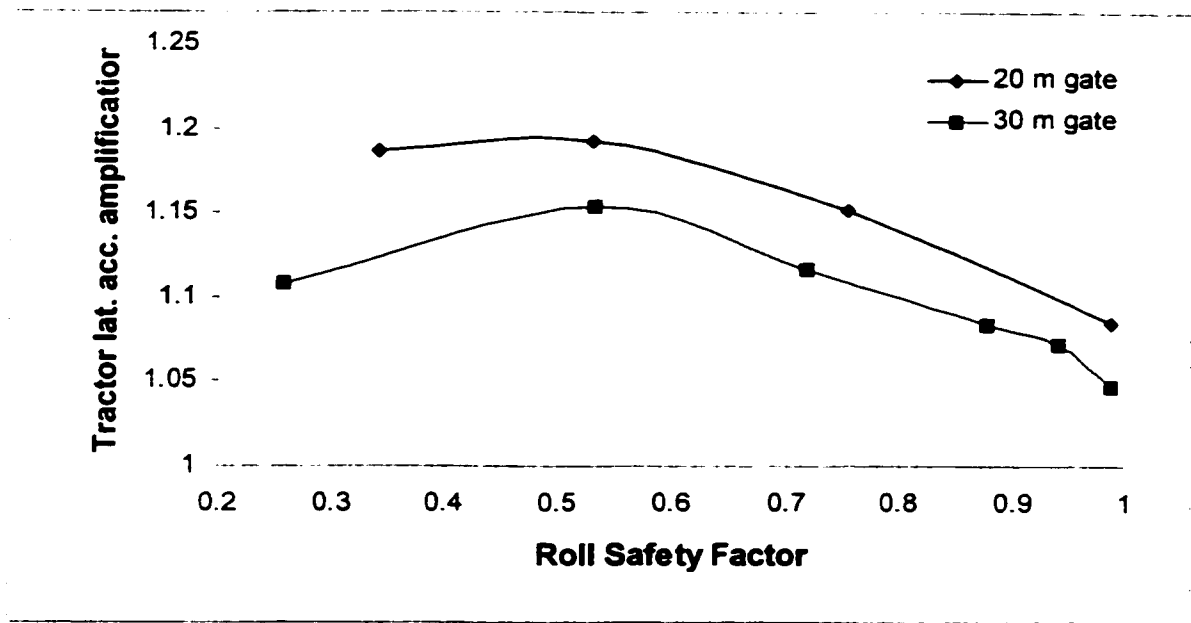


Figure 6.22: Tractor lateral acceleration amplification G_{Ast1} during a single lane change maneuver of different gate lengths.

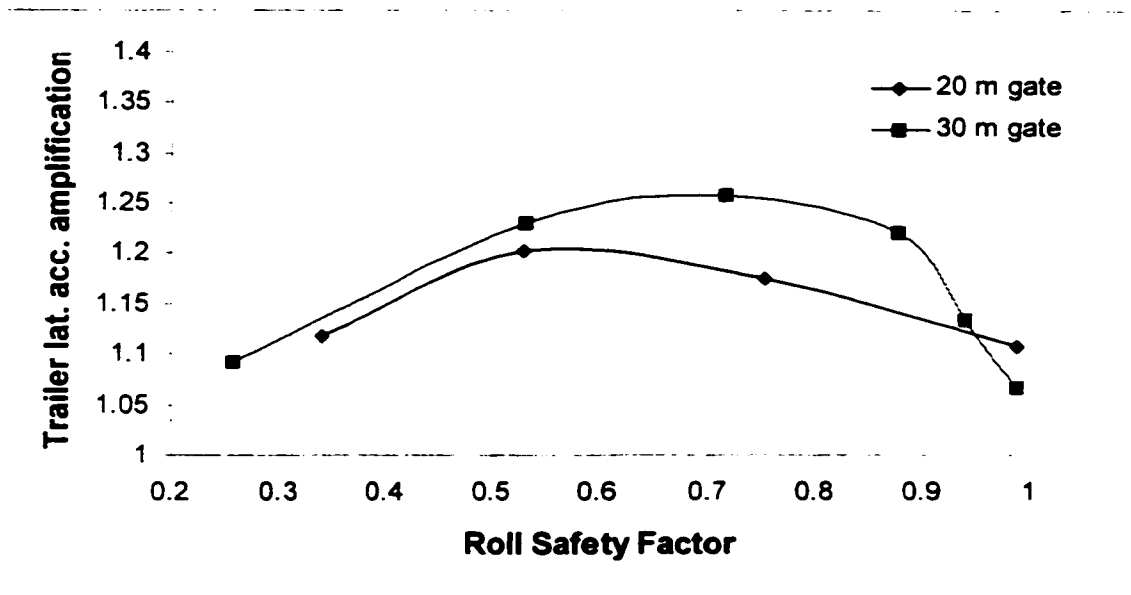


Figure 6.23: Semi-trailer lateral acceleration amplification G_{Ast2} during a single lane change maneuver of different gate lengths.

6.5.3 Influence of Road Adhesion Limit and Braking Intensity on Open-loop Rollover Control

The previous analyses of the effectiveness of the open-loop rollover control is conducted at road adhesion limit of 0.8 and braking pressure of 700 kPa, (referred to as 100% braking effort), which are considered to be upper limits of these parameters. The effectiveness of the open-loop rollover control is further examined by varying the braking intensity and road adhesion limits. Two different values of braking intensity are considered by selecting the brake pressure as 100% and 50% of the nominal pressure (700 kPa), while adhesion coefficients of 0.5 and 0.8 are selected to represent wet and dry surfaces.

Figures 6.24 and 6.25 illustrate the wheel braking pressures at the left- and right-side wheels, respectively, at 100% braking effort, when the vehicle negotiates a ramp steer at 4.5 deg/s. Since an *ABS* algorithm is incorporated in the vehicle model, wheel-braking pressures are adjusted to avoid wheel lockup, as shown in Figure 6.24. Figures 6.26 and 6.27 illustrate the resulting wheel braking pressures corresponding to 50% braking effort (350 kPa control pressure). It should be noted that the *ABS* is not activated at the right side wheels due to insufficient braking effort, as shown in Figure 6.27. The variations in the vehicle forward speed during braking at different braking efforts are illustrated in Figure 6.28. Higher braking effort (700 kPa braking pressure) yields higher longitudinal deceleration of the vehicle, which does not necessarily indicate higher rollover control ability, as observed from the *RSF* response illustrated in Figure 6.29.

Figure 6.29 illustrates that *RSF* approaches close to unity value under application of higher braking pressure (700 kPa), while the lower braking pressure yields a lower value of peak *RSF*. The vehicle may thus approach its relative rollover condition at

relatively high braking pressure, while a moderate braking effort may reduce the risk of rollover. The *RSF* response reveals a rapid increase, when the braking effort is applied. This increase is mostly attributed to the steering system compliance, which introduces a sudden increase in road wheel steer angle when braking is engaged, as shown in Figure 6.30. The theoretical explanation is that the tire cornering force is considerably reduced when braking force is introduced, which in turn increases the steer angle of the road wheels, as shown in Equation (6.27). The results further show that a greater braking effort yields a larger increase in the steer angle of the road wheels.

The road adhesion limit determines the maximum braking efforts that the vehicle can achieve. In straight-line braking maneuvers, it is widely accepted that braking on a road surface with higher adhesion coefficient, yield shorter braking distance [112]. In cornering maneuvers the vehicle may reach yaw instability prior to developing a roll instability, when braking is performed on low friction road. The influence of braking effort and road adhesion limit on the directional performance of the vehicle subject to a ramp steer (4.5 deg/s) is thus investigated. The response characteristics are analyzed to derive the threshold of early warning based upon RSF'' . The results, summarized in Table 6.6, reveal that rollover warning should be generated when *RSF* approaches 85% RSF'' on high friction road ($\mu = 0.8$) with 100% braking effort. If 50% braking effort is applied, rollover warning threshold can be relaxed to 89% RSF'' . A moderate braking on high friction road ($\mu = 0.8$) is thus more efficient to bring the vehicle to the roll stability condition. On low friction road ($\mu = 0.5$), warning thresholds are obtained as 81% RSF'' and 82% RSF'' under 100% and 50% braking efforts, respectively. On low friction road, the impending rollover signal should thus be generated earlier than on high friction road.

Table 6.6: Minimum warning threshold for different road friction and braking efforts.

		$\mu = 0.8$	$\mu = 0.5$
4.5 deg/s	100% Braking	85% RSF^0	81% RSF^0
	50% Braking	89% RSF^0	82% RSF^0

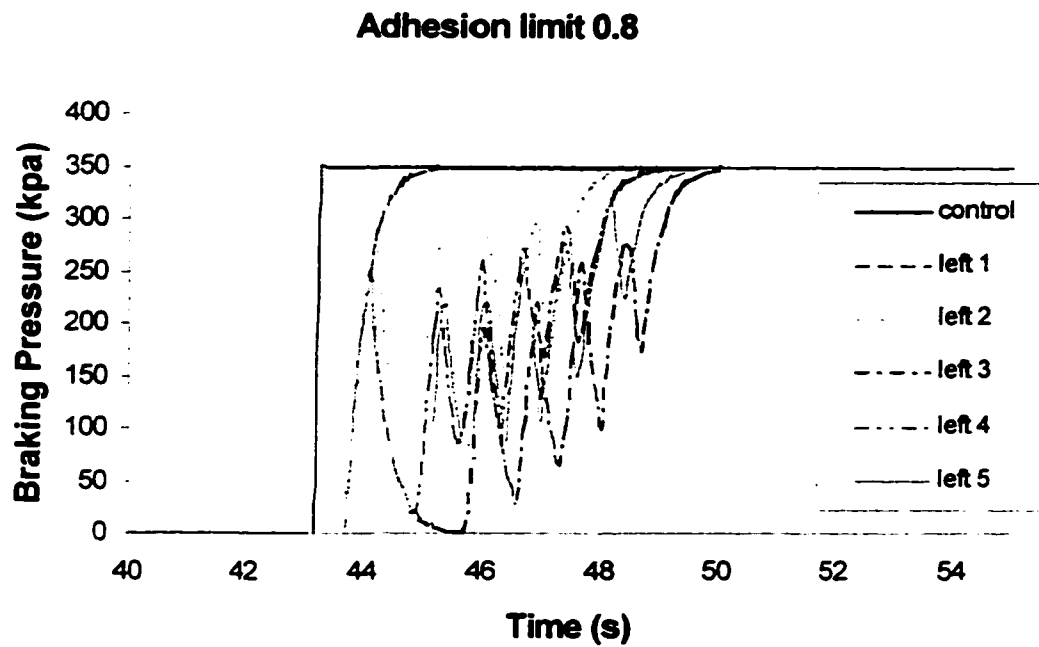


Figure 6.24: Braking pressure on the left side wheels at 100% braking effort.

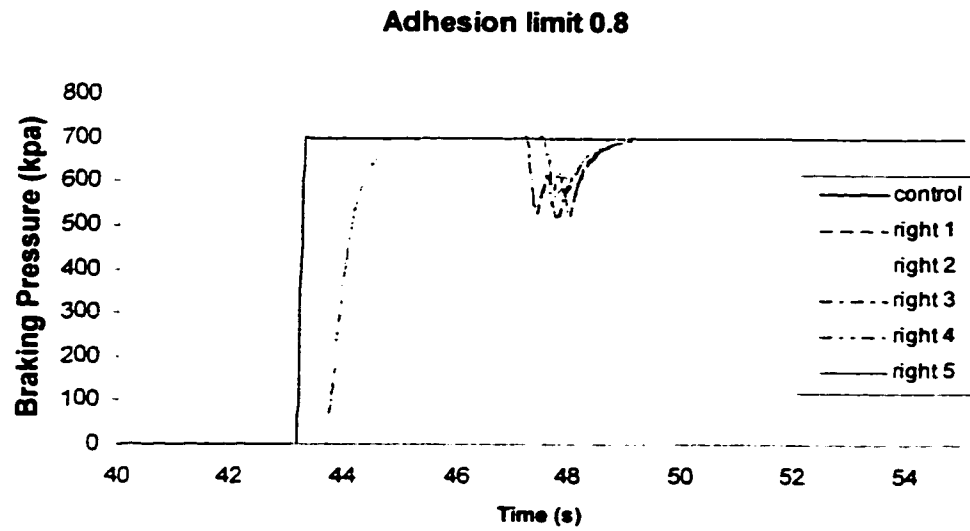


Figure 6.25: Braking pressure on the right side wheels at 100% braking effort.

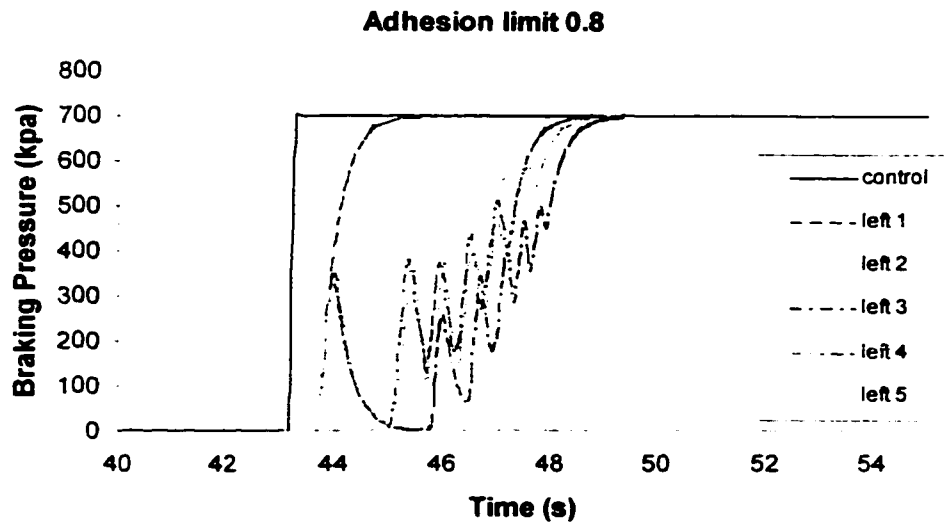


Figure 6.26 Braking pressure on the left side wheels at 50% braking effort.

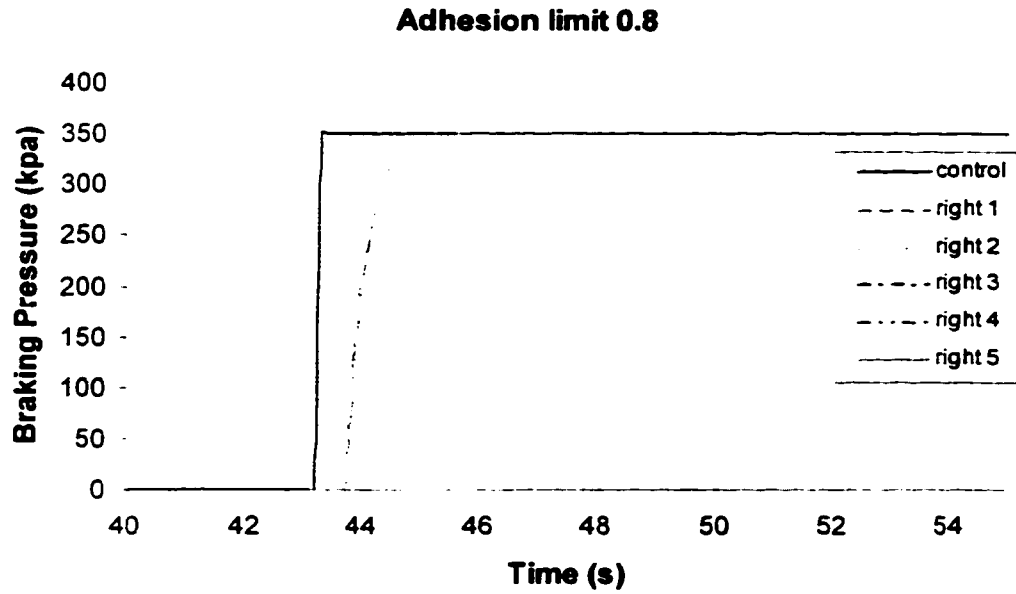


Figure 6.27: Braking pressure on the right side wheels at 50% braking effort.

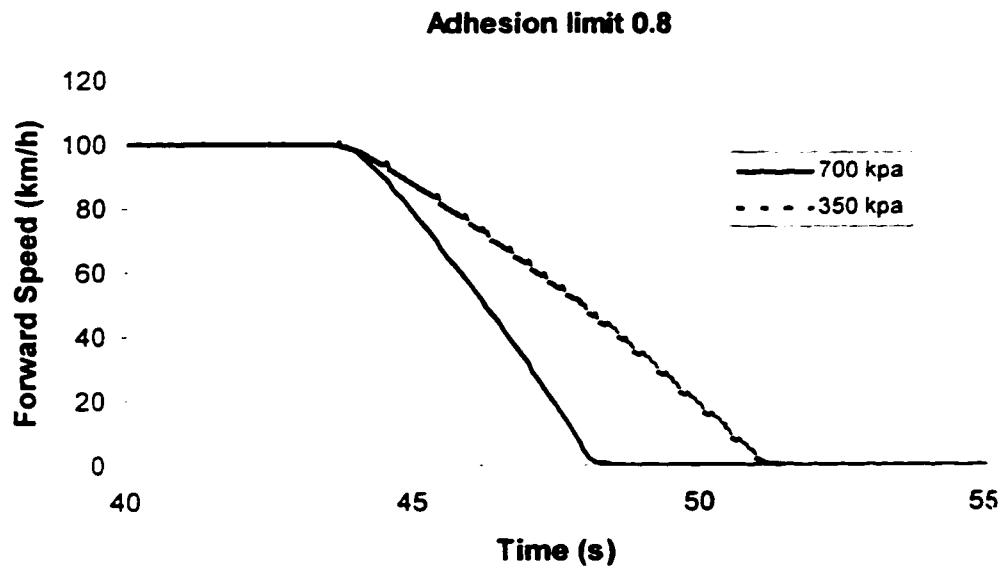


Figure 6.28: Changes of vehicle forward speed during braking at different braking efforts.

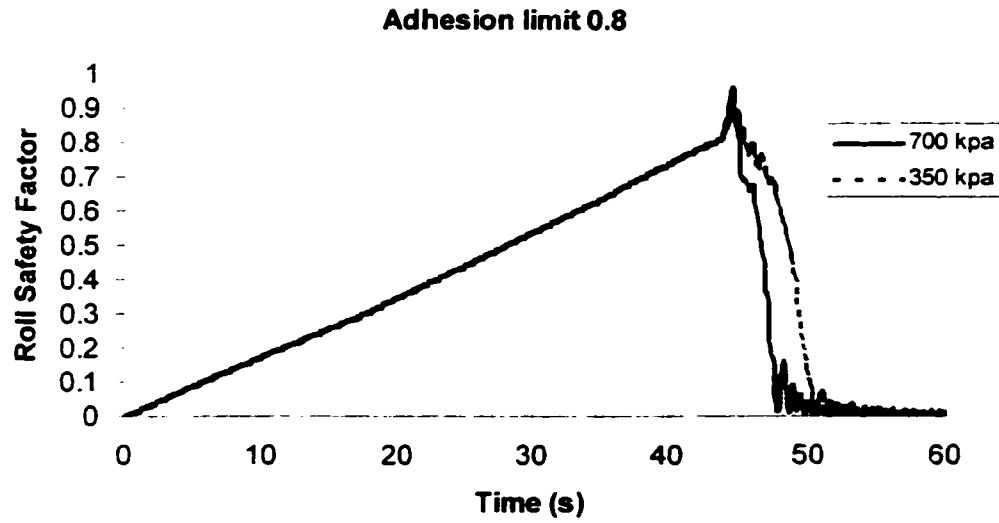


Figure 6.29: *RSF* signature at different braking efforts.

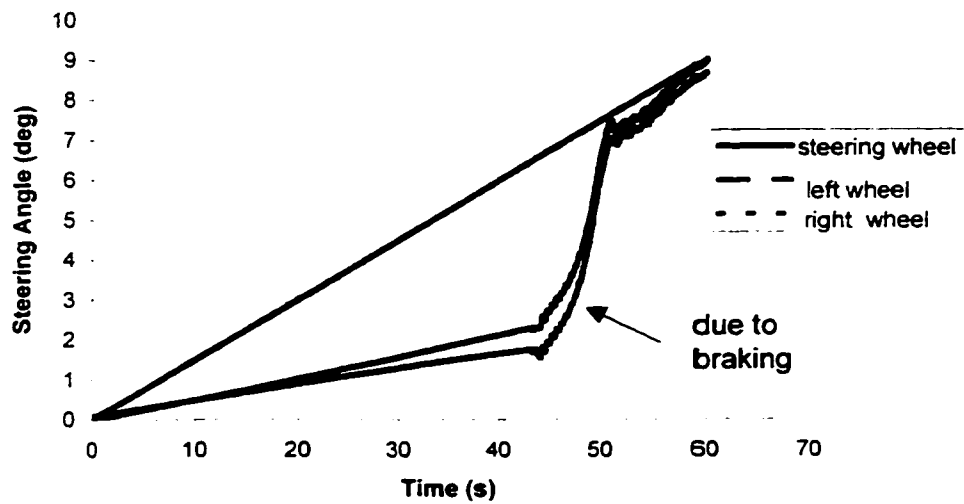


Figure 6.30: Influence of braking on road-wheel steer angles.

6.6 SUMMARY

In this chapter, a comprehensive three-dimensional heavy vehicle model is developed to investigate the effectiveness of open-loop roll instability control. The steering system compliance, roll steer, bump steer, ackerman steer and wrap steer are incorporated in the vehicle model, along with comprehensive tire model and *ABS* algorithm. Time delays due to driver's reaction and the transportation lag of the braking system are characterized by a variable called reaction delay. The rollover indicators in terms of roll safety factor, tractor and trailer lateral accelerations and roll angles, and the rearmost axle roll angle are investigated for their effectiveness for open-loop roll stability control in various cornering and evasive maneuvers, road conditions, braking efforts, and different reaction delays.

It is concluded that warning signal should be generated when *RSF* reaches 65% to 85% in ramp steering maneuvers for different steering rates and reaction delays. The range of threshold values for warning generation reduces to 75% - 80% in the spinal path maneuvers. In lane change maneuvers, the warning thresholds are mainly dependent on amplification mechanism of the vehicle response. An upper limit of amplification factor is identified as 1.3 for *RSF*, semi-trailer lateral acceleration, tractor and semi-trailer roll angles for all the lane change maneuvers, while the limiting values for tractor lateral acceleration and rearmost axle roll angle amplification factors are identified as 1.1 and 1.7, respectively. Larger amplification factor at the relative rollover condition requires the generation of the early warning signal at an earlier stage. While larger braking effort can reduce vehicle forward speed more quickly, the vehicle exhibits violent transient roll response under larger braking effort. Consequently, a moderate braking effort can yield

improved performance for rollover control. Operation on road surface with lower adhesion limits requires earlier warning generation of impending rollover.

CHAPTER 7

CONCLUSIONS AND RECOMMENDATIONS

7.1 HIGHLIGHTS OF THE INVESTIGATION

In this dissertation, a systematic study of static and dynamic roll characteristics of heavy vehicles is conducted to identify measures related to onset of roll instability, such that a design of an open-loop early warning roll control device may be conceived. The study involves: establishment of roll instability criteria; identification of rollover conditions through analysis of static and dynamic rollover characteristics; identification of dynamic response vector directly related to onset of vehicle roll instabilities; evaluation of the response vector in terms of measurability, reliability, and early warning capability; and effectiveness of the proposed open-loop rollover control methodologies. Some of the results attained from the dissertation research have been published in [113, 114, 115, 116]. The major highlights of various aspects of the study are summarized in the following subsections.

7.1.1 Development of Relative and Absolute Roll Instability Criteria

Development of a definite roll instability criterion forms the most important issue in assessing the dynamic rollover characteristics of heavy vehicles. Although the roll stability of heavy vehicles has been extensively addressed in the literature, a roll instability criterion has not been defined clearly. In this dissertation, two roll instability criteria are defined based upon fundamental analysis of rollover mechanics of heavy vehicles in terms of severity of the rollover: *Relative Roll Instability*; and *Absolute Roll Instability*. Relative roll instability is approached when vehicle wheels on one or more

axles lose road contact such that the vehicle can not remain stable under the action of a constant level of lateral force. The corresponding maximum lateral acceleration response of the vehicle, realized during a steady turn maneuver, is referred to as the static rollover threshold. Absolute roll instability of the vehicle occurs at tip-over with zero tolerance of lateral disturbance, when center of mass of the vehicle aligns vertically above the effective contact region of the outer tires with the road. The rollover measures reported in the literature are categorized based on the proposed roll instability criteria. Relative roll instability criterion is employed to derive relative rollover conditions, and static and dynamic rollover threshold of heavy vehicles. The proposed relative roll instability criterion is employed to detect an impending roll instability and to assess the effectiveness of open-loop rollover control. The absolute roll instability criterion is employed to study the absolute rollover limits of heavy vehicles subject to directional maneuvers.

7.1.2 Development of Relative Rollover Condition and Roll Safety Factor

Freight vehicle combinations comprise different numbers of multi-axle units, where the suspension properties and loading conditions for each axle may differ considerably. Under a severe directional maneuver, the loss of tire-road contact may initially occur with wheels on one of the axles, which may be followed by loss of road contact of wheels on the other axles. The relative roll instability criterion does not necessarily imply that all the wheels on a single-track lift off the road surface. For detection of impending roll instability of heavy vehicles, it is necessary to identify the relative rollover conditions, which may vary with variations in the vehicle configurations.

Furthermore, static rollover threshold of heavy vehicles can also be evaluated when a vehicle approaches its relative rollover condition. In this dissertation, relative rollover condition for heavy freight vehicles is mathematically represented by a variable referred to as roll safety factor (*RSF*). The *RSF* approaches a unity value when relative rollover condition is reached, irrespective of the vehicle configuration. The proposed *RSF* thus serves as a reliable impending rollover indicator.

The relative rollover conditions for straight trucks, full trailers, tractor semitrailer combinations, and B- or C- train doubles are analyzed through development of static roll plane models. An A-train double combination is considered as two independent roll units: a tractor semitrailer and a full trailer. The proposed models developed for tractor semitrailers and full trailers are thus analyzed to predict *SRT* and relative rollover condition for the A-train doubles. A parametric study is conducted to derive the influence of an array of vehicle design parameters and suspension configurations on *SRT* and relative rollover condition for various vehicle combinations. Wheels lift-off sequence of various vehicle configurations in dynamic steering maneuvers is also investigated in order to derive rollover initialization and subsequent relative rollover condition. The results of the parametric study are further analyzed to derive the sensitivity of proposed criterion to variations in vehicle design and operating variables.

7.1.3 Dynamic Rollover Threshold Analysis

While the static rollover of heavy vehicles has been extensively investigated in many reported studies, only few studies have attempted to analyze the vehicle rollover in a dynamic maneuver. Since dynamic lateral acceleration response characteristics of

different units of an articulated heavy vehicle differ considerably in both amplitude and phase angle, a concept referred to as effective lateral acceleration (*ELA*) is introduced. The *ELA* represents a moment-weighted average lateral acceleration response characteristic of all the units of a vehicle combination. Dynamic rollover threshold (*DRT*) of a heavy vehicle is defined as the level of effective lateral acceleration, when its *RSF* approaches a unity value in a dynamic steering maneuver. Dynamic rollover threshold values of tractor semitrailer combinations and A-train doubles are investigated for various operating conditions and steering frequencies, and compared with the corresponding static rollover threshold values. The dynamic roll characteristics are further assessed in terms of rearward amplification gains. The effectiveness of *DRT* and rearward amplification gain in predicating a dynamic rollover is evaluated in terms of their sensitivity to variations in vehicle design and operating parameters.

7.1.4 Development of a Roll Plane Model for Absolute Rollover Analysis

Although a large number of analytical models have been developed to study the directional dynamics, handling performance and static roll instability of heavy vehicles, only limited efforts have been reported on study of maneuver-induced dynamic roll instability. The reported roll plane models for dynamic roll stability analysis were developed based on the assumption that none of the wheels lose contact with the road. The application of such a model thus raises many concerns, since a dynamic rollover involves the loss of tire-road contact of the wheels on one track of the vehicle.

A roll plane model incorporating the loss of tire-road contact during a directional maneuver is thus developed in this dissertation to study the dynamic roll properties of

single and multiple units articulated vehicles. A straight truck configuration is represented by a single-roll-plane model, while a tractor-semitrailer combination is represented by three composite roll planes, including front axle, a composite drive axle, and a composite trailer axle, coupled by two torsional springs. The B- and C-train doubles are represented in a similar manner by four roll planes coupled by three torsional springs. Each roll plane is characterized by five degrees-of-freedom motions. Equations of motion are derived using Lagrange's energy approach, which are considered valid until the vehicle approaches its tip-over position. The proposed model differs from the previous reported models in a significant manner, since it can predict the roll dynamics of a vehicle after the wheels lift off the ground, and thus the occurrence of an absolute rollover. The absolute rollover indicators in terms of Rollover Prevention Energy Reserve Factor (*RPERF*) and Critical Distance Ratio (*CDR*) are employed to investigate absolute rollover threshold of heavy vehicles.

7.1.5 Analysis of Potential Rollover Indicators

The design of a dynamic rollover warning device necessitates the identification of impending dynamic rollover indicators with high degree of measurability, reliability and available time margin for corrective maneuvers. Although few studies have attempted to identify vehicle response variables related to onset of vehicle rollover, analysis of such variables in terms of measurability, reliability and lead time for driver's actions has not yet be reported.

In this dissertation, potential rollover indicators are identified through analytical analysis of a lumped roll plane model, and evaluated in terms of measurability, reliability

and early warning capacity for driver's action. Measurability analysis is carried out based on current engineering practice in terms of ease of measurement. Reliability analysis of potential rollover indicators is conducted in terms of estimation errors due to uncertainty of dependent parameters, linear correlation characteristics with roll safety factor (*RSF*), and sensitivity to variations in operating conditions of the vehicle. Early warning evaluation of the indicators is performed in terms of lead time for driver's corrective efforts in dynamic directional maneuvers.

7.1.6 Feasibility Analysis of Open-Loop Rollover Control

In an open-loop rollover control, a warning signal is generated for the driver through monitoring and interpretation of the impending rollover indicators. Upon recognizing the warning signal, the driver may undertake braking and/or steering actions to avert the potential roll instability. In view of the time delays associated with driver's perception and reaction, and buildup of the braking force, a warning signal for an impending rollover should be generated early enough for the driver to perform a corrective maneuver in appropriate time. The vehicle may approach its roll instability condition, in the event that the lead time provided by the warning signal is inadequate to develop necessary braking forces.

In this dissertation research, the feasibility and effectiveness of the open-loop rollover control is investigated through development and analysis of a comprehensive three-dimensional vehicle model. The model is formulated upon incorporating nonlinear forces and moments due to tires, *ABS* braking, steering system kinematics and compliance, and driver and braking system delays. The proposed model for a five-axle

tractor semitrailer combination is analyzed under various cornering and evasive maneuvers, road conditions, braking efforts, and reaction delays. The results are analyzed to derive impending rollover warning threshold and effectiveness of the open-loop rollover control.

7.2 CONCLUSIONS

The following specific conclusions are drawn from the dissertation research.

- Complete roll units of articulated vehicles can be identified on the basis of roll coupling mechanisms, while the towing and trailing units coupled by a hitch with weak roll stiffness can be treated as independent roll units.
- The rollover and tip-over of heavy vehicles can be accurately described by relative and absolute roll instability criteria, respectively. The limiting value of lateral acceleration of vehicle corresponding to its relative rollover condition directly relates to the static rollover threshold of the vehicle.
- The analytical relationship between sprung mass roll angle and lateral acceleration, derived from static roll analysis of various vehicle configurations, yields relative rollover condition and static rollover threshold of the combination.
- The straight trucks or full trailers may approach their relative rollover conditions when wheels on the front and/or rear axles lift off the ground, while the tractor semitrailer combinations approach relative rollover condition when wheels on tractor rear and trailer axles lift off the road surface. The relative rollover for B- or C-doubles is described by one of the two conditions: (i) when wheels on both tractor's

rear axles and the axles of the first semitrailer lift off; or (ii) when wheels on the axles of the first and second semitrailers lift off.

- While the relative rollover condition for straight trucks and full trailers is strongly dependent upon the suspension roll stiffness and vehicle configurations, the relative rollover condition for tractor semitrailer combinations is independent of variations in suspension and vehicle parameters considered in this study.
- Relative rollover condition for all the heavy vehicle combinations can be mathematically expressed by the roll safety factor, which approaches a unity value when relative rollover condition is reached, irrespective of the vehicle configuration.
- Static rollover threshold of the combinations is significantly influenced by center of gravity heights of the sprung masses, wheel track widths, track width and force-deflection characteristics of suspension springs, auxiliary roll stiffness rates, but insignificantly influenced by tractor frame compliance.
- Dynamic rollover threshold (*DRT*) of the articulated vehicles can be described in terms of an effective lateral acceleration response of the combination subject to dynamic maneuvers. The effective lateral acceleration (*ELA*) response of articulated vehicles under dynamic directional maneuvers correlates very well with unity value of *RSF* thus describes the dynamic rollover threshold.
- A comparison of dynamic and static rollover threshold accelerations of different articulated vehicles revealed that *DRT* in most cases is slightly less than or equal to the *SRT*. The difference between the static and dynamic rollover threshold values is normally less than five percent. The static rollover threshold can thus be effectively employed to estimate the dynamic rollover propensity of heavy vehicles.

- The rearward amplification ratio response of articulated vehicles, derived from constant-velocity three-dimensional model developed for large roll angles, revealed extreme sensitivity to variations in maneuvers performed. An analysis of the *DRT* response, however, revealed that *DRT* is relatively insensitive to directional maneuvers.
- An analysis of the load transfer ratio response of different axles of a heavy vehicle combination, yields wheel lift-off sequence in directional maneuvers. The analysis further revealed that rollover of tractor semitrailer combinations and A-train doubles is initiated at the rearmost axles of the vehicles.
- The roll dynamics analysis of a vehicle combination after the loss of road contact of certain wheels, and thus the occurrence of an absolute rollover, necessitates the shift in the coordinates of the roll center to the contact patch of the outboard tires. The absolute rollover of vehicles in dynamic maneuvers can be effectively predicted from the Rollover Prevention Energy Reserve Factor (*RPERF*) and Critical Distance Ratio (*CDR*). The absolute rollover limits predicted by *RPERF*, in general, are slightly lower than those derived from the *CDR*.
- Absolute rollover limits of straight trucks in an obstacle avoidance maneuver are larger than the corresponding *SRT* values, especially for higher frequency maneuvers. The *SRT* thus provides an underestimation of the anti-roll ability of heavy vehicles under transient steering maneuvers.
- Potential relative rollover indicators can be identified through development of their explicit relationships with the roll safety factor. While roll safety factor is the most reliable impending rollover indicator, irrespective of the vehicle configuration, its

measurability is relatively poor. The steer velocity factor (*SVF*) yields superior measurability and large time margin for early warning but it exhibits considerable sensitivity to variations in operating conditions and the maneuvers performed. The indicators based upon unsprung mass roll angles demonstrate excellent linear correlation with the *RSF*, and are relatively insensitive to variations in vehicle c.g. height and maneuvers performed. The threshold values of unsprung mass roll angles, however, are observed to be quite sensitive to variations in axle loads.

- The indicators based upon lateral acceleration response of the semitrailer and sprung mass roll angles of a 5-axle tractor semitrailer combination revealed excellent correlation with the *RSF*, while their threshold values were observed to be strongly dependent upon the variations in vehicle c.g. height. The lateral acceleration response of the tractor demonstrates excellent capability for early warning generation of impending rollover in directional maneuvers, but poor linear correlation with *RSF*.
- The effectiveness of the roll instability indicators and the open-loop roll instability control must be evaluated through analysis of a three-dimensional heavy vehicle model, incorporating braking dynamics and driver's reaction delays.
- The design requirements for an early warning based open-loop roll instability control, derived from the analysis of the nonlinear three-dimensional vehicle model, revealed that:
 - In ramp steering type maneuvers, the warning signal should be generated for the driver to avert impending roll instability, when *RSF* approaches 65% to 85%.
 - In spiral path maneuvers, the warning signal should be generated when *RSF* reaches 75% to 80%.

- In lane change maneuvers, the warning thresholds are primarily dependent on amplification mechanism of the vehicle response. The warning threshold values in lane change maneuvers should not be greater than 77% of static rollover limits in terms of *RSF*, semitrailer lateral acceleration, tractor and semitrailer roll angles. The warning threshold values in terms of tractor lateral acceleration and rearmost axle roll angle should not be greater than 91% and 59% of their respective static rollover limits.
- Analysis of the open-loop roll instability control further revealed that a moderate braking effort may yield improved performance for rollover control, and vehicle operation on road surfaces with lower adhesion limits requires earlier warning generation of the impending rollover.

7.3 RECOMMENDATIONS FOR FUTURE WORK

In this study, the warning thresholds of different indicators are obtained for a specific 5-axle tractor-semitrailer combination under a range of specific steering maneuvers. These maneuvers are characterized qualitatively to represent typical cornering and lane-change maneuvers, and do not necessarily represent vehicle's maneuvers in daily operation. Based on this investigation, the rollover warning threshold can be selected from a wide range of 60% to 85% of the static rollover limit. The simulation results presented in this dissertation can only be interpreted for the specific maneuvers and reaction delays, although they provide significant insight into the feasibility and methodology for prototype development. The effectiveness of open-loop

rollover warning system should be examined through implementation of a warning system and instrumentation of a test vehicle.

The open-loop rollover control, in general, must be useful to the driver and must not interfere with normal driving tasks. The warnings generated by the system should result in a minimum demand on the driver's attention. The effectiveness of the open-loop control further depends upon how often the early warning is generated. Frequent warnings may lead to reduced sensitivity of the driver to the signals, and may cause the driver to ignore them. Occasional or rare warnings, on the other hand, may cause panic and distract the driver during critical situations. Therefore, the method of warning and the frequency at which warnings are given must be chosen carefully. Nevertheless, the preset warning threshold determines how often a warning occurs. The preset value should be identified based on the vehicle duty cycle to ensure that warnings occur at an acceptable frequency level.

Other aspects of feasibility are the ease of installation and reliability of the warning signal. Although *RSF* is the most reliable rollover indicator, the measurement of *RSF* requires dynamic vertical load information on tractor rear and trailer axles, which is quite complex. One reasonable way is to monitor the wheel loads for only one axle. Since rollover of heavy freight vehicles mostly initiates at the rearmost axle, it may be appropriate to monitor only the rearmost axle load. For tractor semitrailer or trailer combinations, the rearmost axle is the axle on a semitrailer or full trailer. Since tractors and trailers are made by different manufactures and normally owned and maintained by different companies, the instrumentation of a trailer axle needs an additional power

supply and signal transmission between tractor and trailer, which may also pose certain difficulties. Another choice is to monitor the wheel loads of tractor drive axles.

From the point of view of rollover warning, a precise measurement of wheel load is not necessary. A qualitative estimation of how close a wheel approaches lift-off condition is sufficient to generate a warning. One feasible method is to apply a small braking pressure and measure the slip ratio of the wheel. Wheels with small vertical load due to load transfer can easily be locked up. Figure 7.1 illustrates a possible flow chart for the generation of rollover warning. The lateral acceleration level is initially examined by comparing it with the preset value e.g. 0.25 g. A small test braking pressure is released to the wheels on the drive axle, when lateral acceleration exceeds the preset value. If the wheel longitudinal slip ratio is greater than a preset value (for example 0.2), a warning signal is generated to the driver, or a braking effort is automatically applied to slow down the vehicle in a close-loop manner. Otherwise, the system continues to re-examine the condition after a certain elapsed time. The proper selection of test braking pressure for different vehicles is very important for the effectiveness of such a warning algorithm.

In view of the difficulties in finding a single satisfactory impending rollover indicator with desirable measurability, reliability and available time margin for corrective maneuvers, certain combinations of several indicators may be considered for generation of an early warning of impending rollover. Neural network algorithms may be explored for such a purpose.

The methods for effective presentation of the warning signal to the driver should also be explored. Instead of an audio warning signal, the warning can also be provided to

the driver by constant visual feedback in the form of graduated light displays representing how close the vehicle approaches rollover condition.

Further studies can also be carried out on possible closed-loop rollover control systems. Upon detection of impending rollover, corrective actions may be directly applied by control mechanisms, which include electric braking to slow down the vehicle and to avert potential yaw instability, application of counter-roll moment to reduce roll displacement of the vehicle and thus improve roll stability.

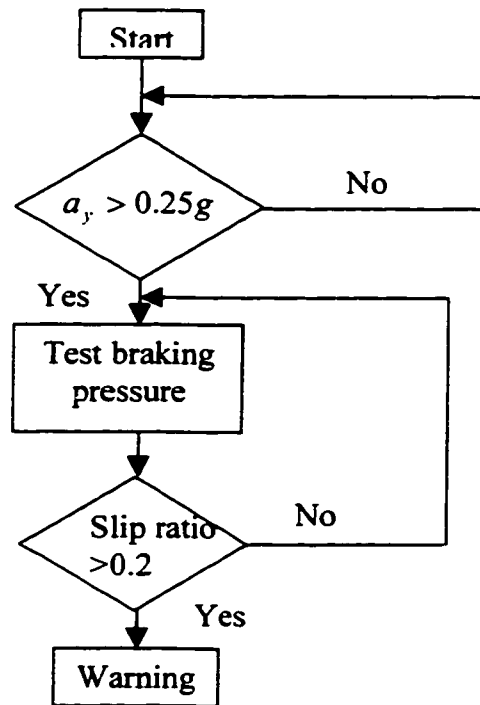


Figure 7.1: Flow chart of impending rollover warning generator based on monitoring of wheel loads.

REFERENCES

1. Heglund, Robert E., "Truck Safety - An Agenda for the Future," SAE Publication No. P-181, 1986, p.154-159.
2. Seiff, H. E., "Status Report on Large-Truck Safety", Transportation Quarterly, vol. 44, no.1, pp. 37-50.
3. Uffelmann, F., "Automotive Stability and Handling Dynamics in Cornering and Braking Maneuvers," Vehicle System Dynamics, 1983, vol. 12, pp. 203-223.
4. Ervin, R.D., "The Dependence of Truck Roll Stability on Size and Weight Variables," Int. J. of Vehicle Design, Special Issue on Vehicle Safety, 1986, pp. 192-208.
5. Rakheja, S., and Piche, A., "Development of Directional Stability Criteria for an Early Warning Safety Device," SAE paper no. 902265, SP-843, 1990, pp. 1-13.
6. Dorion, S. L., and Pickard, J. G., "Feasibility of Anti-Jackknifing Systems for Tractor Semitrailers," SAE 891631.
7. Rakheja, S., Sankar, S., and Ranganathan, R., "Roll Plane Analysis of Articulated Tank Vehicles During Steady Turning", Vehicle System Dynamics, vol. 17, 1988, pp. 81-104.
8. Fancher, P.S., "Directional Dynamics Considerations for Multi-Articulated, Multi-Axled Heavy Vehicles", SAE 892499.
9. Vlk, F., "Handling Performance of Truck-Trailer Vehicles: a state-of-the-art survey", Int. J. of Vehicle Design, vol. 6, no. 3, 1985, pp. 323-361.
10. Piché, A., "Detection of Onset of Instabilities for an Early Warning Safety Monitor for Articulated Freight Vehicles", M. Thesis, Concordia University 1990.
11. Dugoff, H. and Murphy, R. W. (1971), "The dynamic performance of articulated highway vehicles - A review of the state-of-the-art", SAE paper 710223.
12. Vlk, F. (1982), "Lateral Dynamics of Commercial Vehicle Combinations - A Literature Survey", Vehicle System Dynamics 11 (1982) pp. 305-324.
13. Fancher, P. S., "The Static Stability of Articulated Commercial Vehicles", Vehicle System Dynamics, 14(1985) pp. 201-227.
14. Jindra, F., "Tractor and Semi-Trailer Handling", Automotive Engineering, Vol. 53, (1963), pp. 438-446.
15. Jindra, F., "Handling Characteristics of Tractor-Trailer Combinations", SAE Paper 650720.

16. Ellis, J.R., "The Ride and Handling of Semi-trailer Articulated Vehicles", *Automotive Engineer*, vol. 56, pp. 523-529.
17. Schmid, I., "Engineering Approach to Truck and Tractor Train Stability", SAE Paper 670006.
18. Strandberg, L., Nordström, O., and Nordmand, S., "Safety Problems in Commercial Vehicle Handling", Symposium on Commercial Vehicle Braking and Handling, May 5-7, Ann Arbor, Michigan, USA.
19. Mallikarjunarao, C. and Fancher, P., "Analysis of the Directional Response Characteristics of Double Tankers", SAE paper 781064.
20. Leucht, P. M., "The Direction Dynamics of the Commercial Tractor-Semitrailer Vehicle During Braking", SAE paper 700371.
21. Wong, J. Y., "Theory of Ground Vehicles", John Wiley & Sons, Inc., 2nd Edition, 1993.
22. Bernard, J. E., "A Digital Computer Method for the Prediction of the Directional Response of Trucks and Tractor-Trailers", SAE paper 740138.
23. Shapley, C. G., "The Rolling Motions of Road Vehicles", *Vehicle System Dynamics*, Vol. 4, no.1, 1975.
24. Miller, D. W. G., and Barter, N. F., "Rollover of Articulated Vehicles, Vehicle Safety Legislation - Its Engineering and Social Implications", The Institution of Mechanical Engineers, Great Britain, 1975.
25. Mallikarjunarao et al., "Roll Response of Articulated Motor Trucks during Steady-Turning Maneuvers", Computational Method in Ground Transportation Vehicles, ASME Winter Annual Meeting, Nov. 1982, pp. 133-152.
26. El-Gindy, M., and Hosamel-deen, Y.H., "Sensitivity Parametric Analysis of UMTRI Static Roll Model", *Int. J. of Vehicle Design*, 1989, vol. 10, no. 2, pp.187-189.
27. Verma, M.K., and Gillespie, T.D., "Roll Dynamics of Commercial Vehicles", *Vehicle System Dynamics*, 9(1980), pp. 1-17.
28. Das, N.S. et al., "Estimation of Dynamic Rollover Threshold of Commercial Vehicles Using Low Speed Experimental Data", SAE 932949.
29. Gillespie, T. D., and MacAdam, C. C., "Constant Velocity Yaw/Roll Program", User's Manual, The University of Michigan Transportation Research Institute, Oct. 1982.

30. Wong, J. Y., and El-Gindy, M., "Computer Simulation of Heavy Vehicle Dynamic Behavior. User's Guide to the UMTRI Models", Technical Report 3, Vehicle Weights and Dimensions Study, Road and Transportation Association of Canada, June 1985.
31. El-Gindy, M., and Wong, J.Y., "A Comparison of Various Computer Simulation Models for Predicting the Directional Responses of Articulated Vehicles", Vehicle System Dynamics, 16(1987), pp. 249-268.
32. Ervin, R. D. et al., "Future configuration of tank vehicles hauling flammable liquids in Michigan", Highway Safety Research Institute, University of Michigan, Report No. UM-HSRI-80-73-2.
33. Preston-Thomos, J., and El-Gindy, M., "Static Rollover Thresholds of Heavy Vehicles" Proceedings of CSME Forum , Montreal, 1992, p. 946-951.
34. Ervin, R. D., "The Influence of Size and Weight Variables on the Roll Stability of Heavy Duty Trucks" SAE paper 831163.
35. Winkler, C. B., et al., "Repeatability of the Tilt-Table Test Method", SAE paper 930832.
36. Chrstos, J.P., Guenther, D.A, "The Measurement of Static Rollover Metrics", SAE 920528.
37. Fancher, P. S., and Mathew, A., "Safety Implications of Trucks Designed to Weigh Over 80,000 Pounds." SAE paper 891632.
38. Miller, D. W. G., and Barter, N. F., "Roll-Over of Articulated Vehicles", Proceedings of the Institute of Mechanical Engineers, c203/73.
39. Rakheja, S. et al. "Study on Liquid Tanker Stability: Steady Turning Stability of Partially Filled Tank Vehicles", Interim Report, CONCAVE Research Center, Dept. of Mech. Engr., Concordia University, 1987.
40. Jones, I. S., and Penny, M. B., "Engineering Parameters Related to Rollover Frequency", SAE paper 900104.
41. Klein, T. M., "A Statistical Analysis of Vehicle Rollover Propensity and Vehicle Stability", SAE Paper 920584.
42. Nalecz, A.G., "Influence of Vehicle and Roadway Factors on the Dynamics of Tripped Rollover", Int. J. of Vehicle Design, Vol. 10, no. 3, 1989, pp. 321-345.
43. Hinch, J., et al., "NHTSA's Rollover Rulemaking Program-Results of Testing and analysis". SAE 920581.

44. Lund, Y. I., and Bernard, J. E., "Analysis of Simple Rollover Metrics", SAE paper 950306.
45. El Gindy, M., "An Overview of Performance Measures for Heavy Commercial Vehicles in North America", *Int. J. of Vehicle Design*, 1995, Vol. 16, Nos 4/5, pp. 441-463.
46. Winkler, C. B., and Fancher P. S., "Scenarios for Regulation of Commercial Vehicle Stability in the US", 4th int. Heavy Vehicle Seminar Inst. Road and Dimensions, Cambridge UK, June 28-July 2.
47. Macdam, C. C., "A Computer-Based Study of the Yaw/Roll Stability of Heavy Trucks Characterized by High Centers for Gravity", SAE paper 821260.
48. Collins, T. D., and Wong, J. Y., "Stability of Car Trailer Systems with Special Regard to Trailer Design", *J. of Dyn. Sys., Meas., and Control*, Transactions ASME, 1974, pp. 236-243.
49. Troger, H., and Zeman, K., "A Non-linear Analysis of the Generic Types of Loss of Stability of the Steady State Motion of a Tractor-Semitrailer", *Vehicle System Dynamics*, vol. 13, pp. 161-172, 1984.
50. Crolla, D. A., and Hales, F. D., "The Lateral Stability of Tractor and Trailer Combinations", *J. of Terramechanics*, vol. 16, no. 1, 1979, pp 1-22.
51. Mikulcik, E. C., "Stability Criteria for Automobile-Trailer Combinations", *Vehicle System Dynamics*, vol. 9, 1980, pp. 281-289.
52. Ervin, R. D., and Mallikarjunarao, C., "A Study of the Yaw Stability of Tractor-Semitrailer Combinations", *Proc. 7th IAVSD Symp. on Dyn. of Veh. on Rds and Tracks*, Swets and Zeitlinger, 1982.
53. El-Gindy, M., and Wong, J. Y., "Steering Response of Articulated Vehicles in Steady State Turns", SAE paper 852235.
54. El-Gindy, M., and Wong, J. Y., "Steady-State Steering Response of an Articulated Vehicle with a Multi-Axle Steering Dolly", SAE Paper 850537.
55. Vlk, F., "A Linear Study of the Transient and Steady Turning Behavior of Articulated Buses", *Int. J. of Vehicle Design*, vol. 5, no. 1/2, 1984, pp. 171-196.
56. Rakheja, S., R.K. Vallumpalli, & Woodrooffe, J., "Influence of Articulated Dampers on the Yaw and Lateral Response of Heavy Vehicles", *Int. J. of Vehicle Design, Heavy Vehicle Systems*, 2(2), 1995, pp105 – 123.
57. Vlk, F., "Lateral stability of articulated buses", *Int. J. of Vehicle Design*, vol. 9, no. 1, 1988, pp. 35-51.

58. Nordström, O., "Stability, Steerability and Braking Performance of Heavy Vehicles: A Review of Experimental and Theoretical Research and Regulation Proposals by VTI in Sweden". Heavy Vehicle Systems, Int. J. of Vehicle Design, vol. 1, no. 1, 1993, pp. 34-61.
59. El-Gindy, M., "Directional Response of a Tractor Towing a Semitrailer", Int. J. of Vehicle Design", vol. 10, no. 2, 1989, pp. 210-226.
60. Mashadi, B., and Crolla, B. M., "Theoretical Relationship Between Steady State and Transient Response Properties of Vehicles", Proceedings of CSME Forum, 1996, Hamildon, Ontario, pp. 186-195.
61. Radlinski. R. W., "Braking Performance of Heavy U.S. Vehicles", SAE paper 870492.
62. Sankar, S. et al., "Effect of Wheel Slip on the Stability and Stopping Ability of a Road Vehicle", Int. J. of Vehicle Design, vol. 3, no. 1, 1982, pp. 77-89.
63. Huston, J. C., and Johnson, D. B., "Effect of the Normal Force Dependence of Cornering Stiffness on the Lateral Stability of Recreational Vehicles", SAE paper 800161.
64. Segel, L., and Ervin, R. D., "The Influence of Tire Factors on the Stability of Trucks and Tractor Trailers", Vehicle System Dynamics, vol. 10, 1981, pp. 39-59.
65. Essers, U., and Glasner, E. C., "The Braking Performance of Commercial Vehicle while Cornering with and without an Anti-Lock System", SAE paper 881823.
66. Decker, H., and Stock, R., "BOSH-ABS-Designed for the User", SAE paper 861977.
67. Göhring, E., et al., "The impact of different ABS-philosophies on the directional behavior of commercial vehicles", SAE paper 892500.
68. Larocque, G. R., et al, "Feasibility Study of a System Safety Monitor for Hazardous Material Trucking". SAE paper 852357.
69. Susemihl, E. A., and Krauter, A. I., "Jackknifing of Tractor-Semitrailer Trucks - Detection and Corrective Action", Transactions of the ASME, June 1974, pp. 244-252.
70. Susemihl, E. A., and Krauter, A. I., "Automatic Stabilization of Tractor Jackknifing in Tractor-Semitrailer Trucks", SAE paper 740551.
71. Croce, P. A., et al "A Feasibility Study of a Sealed Safety Monitor for Trucks Carrying LNG and other Hazardous Materials", U. S. Dept. of Energy Report DOE/EV/10502-1, Dec. 1982.

72. Allen, R. W., and Rosenthal, T. J., "A Computer Simulation Analysis of Safety Critical Maneuvers for Assessing Ground Vehicle Dynamic Stability", SAE paper 930760.
73. Sneigrove, F. B., et al. "Performance Evaluation of Several Jackknife Control Devices", Ontario Ministry of Transp. and Comm. Report CVOS-TR-80-03, 1980.
74. Dunwoody, A. B., and Froese, S., "Active Roll Control of a Semi-Trailer", SAE paper 933045.
75. Glasner, E. G., et al., "Analysis of Intelligent Suspension Systems for Commercial Vehicles", SAE paper 933008.
76. Darling, J., et al., "A Low Cost Active Anti-Roll Suspension for Passenger Cars", ASME J. of Dynamic Systems, Measurements and Control, Vol. 114, 1992, pp. 599-605.
77. Constantine, C. J., and Law, E. H., "The Effect of Roll Control for Passenger Cars during Emergency Maneuvers", SAE paper 940224.
78. Hwang, S. M., and Park, Y., "Active Roll Moment Distribution Based on Predictive Control", Int. J. of Vehicle Design, vol. 16, no. 1, 1995, pp. 15-29.
79. Furleigh, D. D., et al., "Multiple Steered Axles for Reducing the Rollover Risks of Heavy Articulated Trucks", "SAE paper 881866.
80. Aurell, J., and Edlund, S., "The Influence of Steered Axles on the Dynamic Stability of Heavy Vehicles", SAE paper 892498.
81. Sankar, S., Rakheja, S., and Piché, A., "Directional Dynamics of a Tractor-Semitrailer with Self- and Forced-Steering Axles", SAE paper 912686.
82. Watanabe, Y., et al., "Effect of Rear-Axle Steering on Vehicle Controllability and Stability of a Medium-Duty Truck", SAE paper 93307.
83. Palkovics, L., and El-Gindy, M., "Examination of Different Control Strategies of Heavy-Vehicle Performance", DSC-vol. 52, Advanced Automotive Technologies, ASME 1993, pp. 349-362.
84. Winkler, C. B., et al "Heavy Vehicle Size and Weight - Test Procedures for Minimum Safety Performance Standards", DOT HS 807-855, Final Report, National Highway Traffic Safety Administration US, April, 1992.
85. Wolkowicz, M., "On-the-Scene Study of Commercial Vehicle Accidents", Proc. of Int. Symposium on Heavy Veh. Weights and Dimensions, June 8-13, 1986, Kelowna, BC, Canada, pp.171-186.

86. Winkler, C.B., "Innovative Dollies: Improving the Dynamic Performance of Multi-Trailer Vehicles", Proc. of Int. Symposium on Heavy Vehicle Weights, and Dimensions, pp. 289-313, June 1986, Kelowna, British Columbia, Canada.
87. Ervin, R.D. et al "The Influence of Weights and Dimensions on the Stability and Control of Heavy Duty Trucks in Canada", UMTRI report, 1986.
88. Nalecz, A. G., Lu, Zhengyu, and d'Entremont, K. L., "An Investigation into Dynamic Measures of Vehicle Rollover Propensity", SAE paper 930831.
89. Tamny, S., "Operating Vehicle Roll Stability", SAE paper 932945.
90. Lam, C.P., "Comparison of Simulation and Test Results for Various Truck Combination Configurations", Proc. of Int. Symposium on Heavy Vehicle Weights, and Dimensions, pp. 315-335, June 1986, Kelowna, British Columbia, Canada.
91. Fancher, P.S., et al., "Measurement and Representation of the Mechanical Properties of Truck Leaf Springs", SAE Technical Paper 800905.
92. Sayers, Michael W, and Riley, Stephen M., "Modeling Assumptions for Realistic Multibody Simulation of the Yaw and Roll Behavior of Heavy Trucks", SAE paper 960173.
93. Sankar, S., S. Rakheja and R. Ranganathan, "Directional Response of Partially Filled Tank Vehicles", SAE paper No. 892481, SAE Truck and Bus Meet, North Carolina, Nov. 1989.
94. Sparks, G. A. and Berthelot, C. "The Cost/Benefit Analysis of a Rollover Warning Device for Large Trucks", June 1989, Clayton, Sparks and Associates Ltd., Saskatoon, Saskatchewan.
95. Preston-Thomas, J., and Woodroffe, J.H.F., "A Feasibility Study of a Rollover Warning Device for Heavy Trucks", Technical Report, TP 10610E, National Research Council Canada, 1990/09.
96. Cebon, D., "Interaction Between Heavy Vehicles and Roads", SAE paper 930001.
97. Cebon, D., "Heavy Vehicle Vibration - a Case Study", Proc. 9th IAVSD Symposium on the Dynamics of Vehicles on Roads and on Tracks, Linkoping, Swets and Zeitlinger, 1985.
98. Le Blanc, P.A. et al, "A Comparison of Two Types of Instrumentation for Measuring Vertical Wheel Load", 3rd Int. Symposium on Heavy Vehicle Weights and Dimensions, Cambridge, UK, Thomas Telford, 1992.

99. Hahn, W.D., "Measurements of Road Loadings by HGV Suspensions - Survey of the German Research Program". ImechE Conference on Road Wear, London, 1991.
100. Clark, S.K., "Mechanics of Pneumatic Tires", NBS, Washington D.C., 1971.
101. Rupp, A., and Grubisic, V., "Reliable Determination of Multi-Axle Road Loads and Tire Deformations on Buses and Heavy Trucks for the Design and Proof Out", SAE paper 973189.
102. Kistler, "The Rotating Wheel Dynamometer System for Vehicles", Type 9298, Kistler, Switzerland.
103. Schuring, D.J., Pelz, W., and Pottinger, M.G., "The BNPS Model – An Automated Implementation of the "Magic Formula" Concept", SAE paper 931909.
104. Dugoff, H., Fancher, P.S., and Segel, L., "An Analysis of Tire Traction Properties and Their Influence on Vehicle Dynamic Performance", SAE paper 700377.
105. Bakker, E., Pacejka, H.B., and Lidner, L., "A New Tire Model with an Application in Vehicle Dynamics Studies", SAE paper 890087.
106. Pacejka, H.B., and Sharp, R.S., "Shear Force Development by Pneumatic Tires in Steady State Conditions A Review of Modeling Aspects", Vehicle System Dynamics, vol. 20, Nos. 3-4, pp. 121 – 176, 1991.
107. Pacejka, H.B., "The Tire as a Vehicle Component", XXV FISITA congress, Prague, June 16-23, 1996.
108. Loeb, J.S., et al. "Lateral Stiffness, Cornering Stiffness, and Relaxation Length of the Pneumatic Tires." SAE paper No. 900129, 1990.
109. Bernard, J.E., and Clover, C.L., "Tire Modeling for Low-Speed and High-Speed Calculations", SAE paper No. 950311, 1995.
110. Yu, Z., "The Theory of Ground Vehicles", Mechanical Industrial Publishing Co. of China, 1981, (in Chinese).
111. Fancher, P.S, Ervin, R.D. et al., "The Mechanics of Heavy Vehicle Systems", UMTRI, 1998.
112. Gillespie, T. D., "Fundamentals of Vehicle Dynamics", Published by Society of Automotive Engineers, Inc., 400 Commonwealth Drive, Warrendale, PA 15096-0001.

113. Liu, P. J., Rakheja, S., and A.K.W., Ahmed, "Detection of Dynamic Roll Instability of Heavy Vehicles for Open-Loop Rollover Control", SAE paper 973263.
114. Liu, P. J., Rakheja, S., and Ahmed, A.K.W., "Dynamic Roll Instability Analysis of Heavy Vehicles Using Energy Approach", Proceedings CSME FORUM 1998, Ryerson Polytechnic University, Toronto, Ontario, Canada May 19-22, 1998, pp. 392-400.
115. Liu, P. J., Rakheja, S., and Ahmed, A.K.W., "Dynamic Rollover Properties of Articulated Heavy Vehicles", Proceedings of the 16th Canadian Congress of Applied Mechanics, Quebec, June 1-8, 1997, pp.191-192.
116. Liu, P. J., Rakheja, S., and Ahmed, A.K.W., "Dynamic Rollover Threshold of Articulated Freight Vehicles", to be published in *Heavy Vehicle Systems*, Special Series, Int. J. of Vehicle Design.